Novel Silicon(IV) Phthalocyanines as Efficient Photosensitizers for Targeted Photodynamic Therapy

JIANG, Xiongjie

A Thesis Submitted in Partial Fulfillment

of the Requirements for the Degree of

Doctor of Philosophy

in

Chemistry

The Chinese University of Hong Kong

March 2010

Thesis Committee:

Professor XIE, Zuowei (Chair)

Professor NG, Kee Pui Dennis (Supervisor)

Professor LEE, Hung Kay (Committee Member)

Professor LO, Kam Wing Kenneth (External Examiner)

Professor ZHENG, Gang (External Examiner)

ABSTRACT

This thesis reports the synthesis, spectroscopic characterization, and photophysical and biological properties of several series of novel silicon(IV) phthalocyanines which are specially designed as efficient and selective photosensitizers for photodynamic therapy.

Chapter 1 presents an overview of photodynamic therapy, including its historical development, photophysial and biological mechanisms, and current clinical situation. A brief review of second-generation photosensitizers and the different approaches for targeted photodynamic therapy are also given.

Chapter 2 reports the synthesis and characterization of a silicon(IV) phthalocyanine which is substituted axially with two diamino moieties, together with its di- and tetramethylated derivatives. The non-methylated analogue shows a high photocytotoxicity toward HT29 human colorectal adenocarcinoma and HepG2 human hepatocarcinoma cells with IC_{50} values down to 0.01 μM. Interestingly, this compound also exhibits a pH-dependent behavior. The fluorescence quantum yield increases by four folds and the singlet oxygen quantum yield increases by three folds in water when the pH decreases from 7.0 to 5.0. The preliminary results suggest that this compound is a promising photosensitizer of which the photodynamic activity can be modulated by changing the pH of the environment. Furthermore, this compound can be used as a near-infrared fluorescence probe for optical imaging of intracellular acidic level.

Chapter 3 reports a novel series of aminophenyl-substituted silicon(IV) phthalocyanines. The aminophenyl moieties in these conjugates can also modulate the photophysical and photosensitizing properties of the phthalocyanine core through changing the pH of the environment. These phthalocyanines exhibit a low photocytotoxicity under physiological conditions (pH 7.4). It is likely that the amino groups, in the free amine form, can quench the singlet excited state of phthalocyanine by a photoinduced electron transfer (PET) mechanism, and reduce the chance of intersystem crossing and the efficiency in generating singlet oxygen. The strong aggregation tendency of these compounds in this pH environment is another major reason for the low photocytotoxicity. When the pH is lower to 6.4-6.9, the amino groups are protonated so that they are no longer electron donors, and the compounds become less aggregated. These changes lead to an increase in photocytotoxicity. The results of this study are reported in this Chapter.

Chapter 4 describes a new series of silicon(IV) phthalocyanines conjugated axially with various polyamine derivatives. Polyamines are naturally occurring compounds which are involved in a number of cell processes including cell proliferation and differentiation. Their biosynthetic activity and polyamine levels in some tumor cells are significantly higher than those in normal cells. Conjugation of polyamine analogues is therefore one of the promising approaches to improve the tumor-targeting property of photosensitizers. This Chapter describes the synthesis, spectroscopic characterization, and photophysical properties of these compounds. Their photodynamic activities toward HT29 and Chinese hamster ovary (CHO) cells

have also been studied in detail. Their cellular uptake, subcellular localization, cell death mechanism, and in vivo photocytotoxicity have also been studied.

In **Chapter 5**, we report a series of silicon(IV) phthalocyanines containing one or two cholesterol unit(s) at the axial position(s), including their synthesis, spectroscopic characterization, photophysical properties, and in vitro photodynamic activities. These cholesterol-containing photosensitizers can form stable conjugates with low-density lipoprotein (LDL), which is the major lipoprotein carrier for cholesterol in human plasma. On the basis that cancer cells generally express significantly more LDL receptors than normal cells, these cholesterol-conjugated phthalocyanines are designed with a view to enhancing their selectivity toward tumor. Unfortunately, conjugation of cholesterol reduces the photodynamic activity of the silicon(IV) phthalocyanines as a result of their higher aggregation tendency.

At the end of this thesis, ^{1}H and $^{13}C\{^{1}H\}$ NMR spectra for all the new compounds and the crystallographic details for the X-ray structure are given as Appendices.

摘要

本論文闡述了一系列新型硅酞菁配合物的合成、光譜表徵、光物理及光生物性質。這些化合物的結構被特別設計希望得到高效和有選擇性的光敏劑應用在光動力療法中。

第一章概述了光動力療法，包括它的歷史發展，光物理和生物機理，現今的臨床應用。簡單的介紹了第二代光敏劑和一些靶向性光動力治療的方法。

第二章闡述了一個軸向包含兩個二氨基取得的硅酞菁及其二甲基化和四甲基化的衍生物的合成、光譜表徵及光物理性質。這無甲基化的配合物展現很高的光動力活性對人肝癌細胞 HepG2 和人腸腺癌細胞 HT29，它們的 IC_{50} 值可低於 0.01 μM。有趣的是這個配合物顯現出 pH 依賴特性。當水的 pH 值從 7.0 降到 5.0， 它的螢光量子產率增加 4 倍，單線態氧量子產率增加 3 倍。這初步的實驗結果表明這個配合物是一個光動力活性能被環境的 pH 調控的光敏劑。另外，這個配合物也能用來作爲 pH 探針檢查細胞內的 pH 值。

第三章報導了一系列氨苯基取代的硅酞菁配合物。這些配合物中的氨苯基基團也能調控酞菁環的光物理和光化學性質通過環境 pH 的改變。這些配合物展現低的光動力活性在生理環境下（pH 7.4）。這可能是氨基的孤對電子淬滅了酞菁激發態通過光誘導電子轉移過程，減少了系間串越幾率，降到了單線態氧的產生效率。在這個 pH 環境下酞菁配合物強的聚集行爲可能是光動力活性低下的另外一個原因。當 pH 值低到 6.4-6.9，氨基被質子化，孤對電子不在存在，酞菁配合物的聚集行爲減少。這些變化導致光動力活性增強。這些研究結果將會在本章中報導。

第四章論述了一系列聚氨取代的硅酞菁配合物。聚氨是細胞增殖和分裂中所需的天然化合物。一些癌細胞聚氨的生物合成活性和聚氨的濃度比正常細胞高很多。把聚氨衍生物引入酞菁配合物中可以提高酞菁配合物的靶向性。本章介紹了這些配合物的合成、光譜表徵、光物理及光化學性質和它們對 HT29 細胞和中國鼠卵巢細胞 CHO 體外光動力活性。它們的細胞攝取、亞細胞定位、細胞死亡機理和體內光動力活性也被研究。

在第五章中，我們報導了一系列軸向單膽固醇取代和二膽固醇取代的硅酞菁配合物。它們的合成、光譜表徵、光物理性質和體外光動力活性也被研究。低密度脂蛋白是一個膽固醇的主要載體在血液中。膽固醇取代酞菁可與低密度脂蛋白形成穩定的配合物。由於癌細胞表面有比正常細胞多的低密度脂蛋白受體，膽固醇取代的硅酞菁被設計希望可以提高光敏劑的靶向性。不幸的是軸向配位膽固醇後，硅酞菁配合物的光動力活性大大降低，由於它們很強的聚集特性。

在這本論文的結尾列出了所以新化合物的核磁共振質譜和碳譜圖，X-ray 晶體結果測定資料也被提供。

Acknowledgment

My deepest gratitude goes first and foremost to Prof. Dennis K. P. Ng, my supervisor, for his constant encouragement and guidance during my postgraduate studies. He has taught me a lot in various aspects. He taught me how to design a novel and feasible project about photodynamic therapy and how to organize and present data in a scientific way. The impressive three-year study in Hong Kong has been a very important period in my life and pave a more solid foundation for my future career development. Prof. Ng also gave me the opportunities to attend international conferences in Hong Kong and Singapore to widen my horizon. He also provided a huge assistance during the preparation of my seminars and this thesis. I really appreciate his unfailing support and kindness.

I would also like to thank Prof. Gigi P. C. Lo for her great help and encouragement when I encountered many troubles during my research. She taught me the basic of in vitro studies and provided a great assistance to me during the preparation of my seminars and this thesis. My thanks should also go to my group members, past and present, including Dr. Bill C. F. Choi, Dr. Xuebing Leng, Dr. Ming Bai, Dr. Hu Xu, Dr. Jiangyong Liu, Janet, T. F. Lau, Yingsi Huang, Hui He, Qunling Fang, Meirong Ke, and Wenjing Shi for their help, stimulating discussions, and friendship.

Thanks are also given to Prof. Wing-Ping Fong, Elaine Y. M. Chan, Crystal M. H. Chan, Yee-Man Tsang, and Sin-Lui Yeung of the Biochemistry Department for their help in in vitro and in vivo studies reported in this thesis.

Finally, I would like to give my thanks to my parents and my wife for their continuous care, support, and understanding during these years.

TABLE OF CONTENTS

LIST OF FIGURES

LIST OF SCHEMES

LIST OF TABLES

ABBREVIATIONS

General:

λ_{max}	Absorption maximum
ca.	Coarse approximation
Calcd.	Calculated
DMF	*N,N*-Dimethylformamide
THF	Tetrahydrofuran
equiv.	Equivalent
min	Minutes
h	Hours
Me	Methyl
Et	Ethyl
r.t.	Room temperature
UV	Ultraviolet
Vis	Visible
v/v	Volume to volume ratio
w/v	Weight to volume ratio

Nuclear Magnetic Resonance (NMR) data:

$\{^1H\}$	Proton decouple
δ	Chemical shift

J	Coupling constant in Hz
ppm	Part per million
s	Singlet
d	Doublet
t	Triplet
m	Multiplet

Mass Spectrometric (MS) data:

M^+	Molecular ion
ESI	Electronspray ionization
FAB	Fast atom bombardment
HRMS	High resolution mass spectroscopy

CHARPTER 1

Introduction

1.1 Historical Development of Photodynamic Therapy

The concept of cell death being induced by the interaction of light and chemicals has been recognized for a century.[1] This was first reported by a German medical student Oscar Raab in 1900.[2] During the course of his study on the effects of acridine on malaria-causing protozoa, he discovered that the combination of acridine red and light had a lethal effect on infusoria. A few years later, von Tappeiner and Jodlbauer used topical administration of eosin combined with sunlight to treat skin tumor patients.[3] They went on to demonstrate the requirement of oxygen in photosensitization reaction and in 1904 introduced the term "phododynamic action" to describe this phenomenon.[4] This marked the beginning of photodynamic therapy (PDT). The treatment involves three individually non-toxic components namely a photosensitizer, light, and oxygen, which are combined to cause cellular and tissue damage.[5] Photosensitizers are generally given intravenously and preferably can be localized in neoplastic tissue. Upon activation by visible light in an appropriate wavelength region in which the drug has a strong absorption, the excited photosensitizer reacts directly with organic substrates to produce free radicals or reacts with ground-state triplet oxygen to generate reactive oxygen species (ROS).[6] This photodynamic process causes irreversible oxidation of one or more critical cellular components, including plasma membranes, mitochondria, and lysosomes, inducing necrosis and/or apoptosis of the treated tissue. PDT also induces oxidative damage to the microvasculature, contributing to ischemic tumor death.[5] In the mid-

1950s, Liposn et al. found that hematoporphyrin derivatives (HpD) were useful photosensitizing agents.[7] The clinical therapeutic application of PDT took a long time to develop. In 1983, Dougherty discovered that the HpD contain a complex mixture of porphyrin derivatives. He partially isolated and identified the active components of HpD and named the active components as Photofrin@.[8] PDT was first approved in 1993 in Canada using Photofrin@ as the photosensitizer for the treatment of bladder cancer. Nowadays, a number of photodynamic drugs have been approved for clinical use and several photosensitizers are in clinical trials. Selected examples are presented in Table 1 and Table 2, respectively.[9] The chemical structures of these photosensitizers are shown in Figure 1.1.

Table 1.1. List of clinically approved photosensitizers.[9]

Photosensitizer	Commercial Name	Cancer Type
Polyhematoporphrin ether/ester (**1.1**)	Photofrin	Cervial cancer Endobronchial Cancer Bladder cancer Esophageal cancer Gastric cancer
meta-Tetrahydroxyphenylchlorin (**1.2**)	Foscan	Head and neck cancer Prostate and pancreatic tumors
5-Aminolevulinic acid (**1.3**)	Levulan	Actinic keratoses Basal cell carcinoma
5-Aminolevulinic acid methyl ester (**1.4**)	Metvix	Basal cell carcinoma Non-melanoma skin cancers
Mono-L-aspartyl-chlorin e6 (**1.5**)	Laserphyrin Talaporfin Sodium	Lung cancer
Benzoporphyrin derivative monoacid ring A (**1.6**)	Verteporfin or Visudyne	Basal cell carcinoma
Sulphonated Aluminium Phthalocyanine (**1.7**)	Photosense	Lung cancer Head and neck cancer Skin cancer Breast cancer

Table 1.2. List of photosensitizers in clinical trials.[9]

Photosensitizer	Commercial Name	Cancer Type
Hexyl aminolevulinate (**1.8**)	Hexvix	Diagnosis of bladder tumors
Benzyl aminolevulinate (**1.9**)	Benzvix	Gastrointestinal cancers
Silicon phthalocyanine (**1.10**)	Pc4	Cutaneous and subcutaneous lesions from diverse solid tumor origins
Lutetium (III) texaphyrin (**1.11**)	Antrin Lutex or Motexafin Lutetium	Cervical cancers Prostate cancers Brain tumors Recurrent breast cancer
Tin ethyl etiopupurin (**1.12**)	Photrex	Cutaneous metastatic Breast cancer Basal cell carcinoma
2-[1-Hexyloxyethyl]-2-divinyl pyropheophorbide-a(**1.13**)	Photochlor	Basal cell carcinoma
Pd-bacteriopheohorbide (**1.14**)	Tookad	Prostate cancers Diseases involving proliferation of neovessels

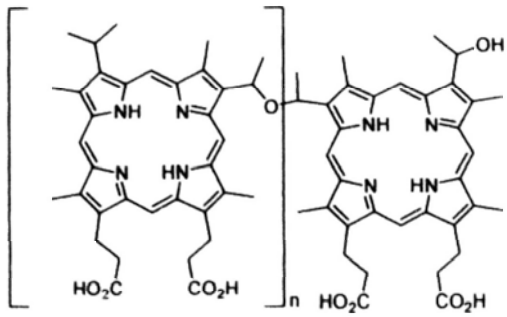

1.1 (Photofrin contains ether-linked oligomers)

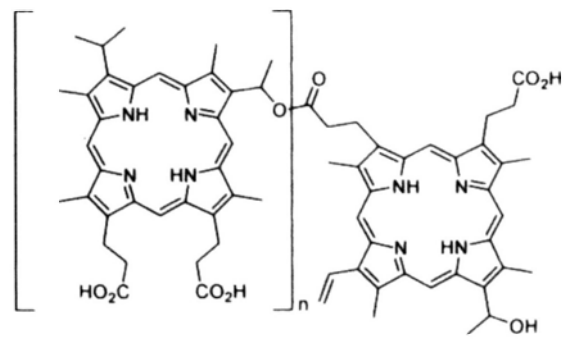

1.1 (Photofrin contains esterr-linked oligomers)

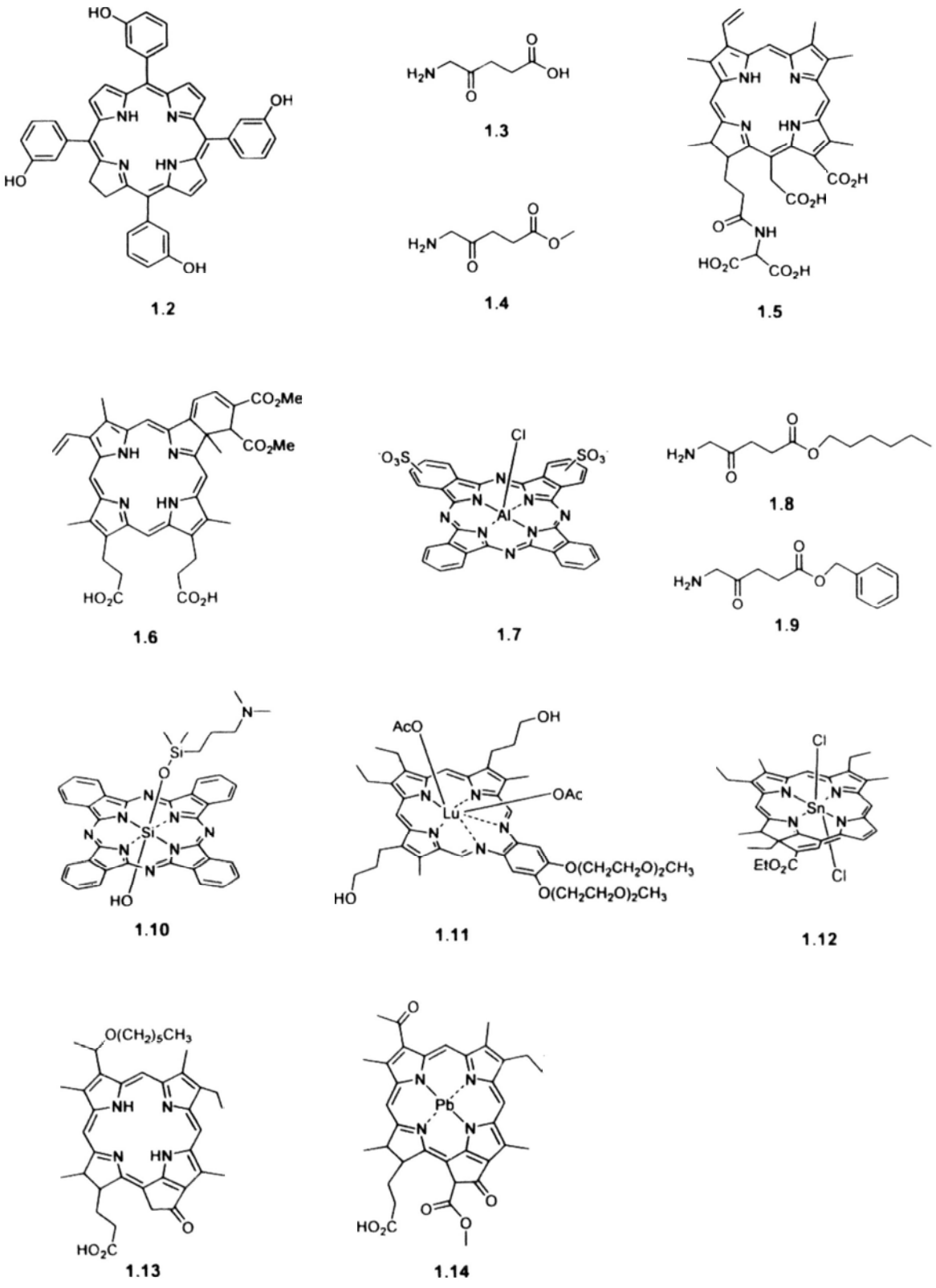

Figure 1.1. Structures of the photosensitizers listed in Table 1 and Table 2.

PDT has several potential advantages over traditional cancer therapeutic methods.[10-12] First of all, it is comparatively non-invasive and can be targeted

accurately mainly through the precise application of light. In addition, repeated doses can be given to the patients without the total-dose limitations associated with radiotherapy. It also does not have the multidrug resistant problem which is common for chemotherapy. Furthermore, PDT can usually be done in an outpatient or day-care setting, which is convenient to patients. Finally, this method does not have significant and long-term side-effects. Notwithstanding the many positive results with PDT, both preclinical and clinical protocols are still being optimized to address the major reasons that PDT sometimes fails to eradicate the targeted tumor. Failure generally results from (a) minimal differential in photosensitizer level between tumor and surrounding normal tissue; (b) poor penetration of light to some parts of the tumor; and (c) inability to ensure that the entire tumor remains sufficiently well oxygenated during the full photoirradiation period.[13] The next phase of development of PDT will aim to resolve these problems and develop more efficient and selective photosensitizers.

1.2 Mechanisms of Photodynamic Therapy

1.2.1 Photophysical Mechanisms

The photochemical and photophysical principles of PDT involve the following processes.[14] Firstly, upon illumination, the photosensitizer is excited from the ground state (S_0) to the first excited singlet state (S_1), followed by conversion to the triplet state (T_1) via intersystem crossing. The longer lifetime of the triplet state enables the interaction of the excited photosensitizer with the surrounding molecules, and it is generally accepted that the generation of the cytotoxic species during PDT occurs in this state. The excited triplet state can react in two ways, defined as Type I and Type II mechanisms. The Type I mechanism involves hydrogen-atom abstraction or electron-transfer reactions between the excited state of the sensitizer and a biological

substrate to yield free radicals and/or radical ions. These species are generally highly reactive and can readily interact with molecular oxygen to generate ROS such as superoxide anions and hydroxyl radicals causing irreparable biological damage. These reactions produce oxidative damage that is eventually expressed as biological lesions. By contrast, the Type II mechanism involves an energy transfer between the excited triplet state of the sensitizer and the ground state molecular oxygen, generating the first excited state of oxygen, singlet oxygen. Singlet oxygen is a highly reactive oxygen species that can react rapidly with numerous biologically important substrates, resulting in oxidative damage and ultimately cell death. It is generally accepted that the Type II process predominates during PDT and that singlet oxygen is the primary cytotoxic agent responsible for the biological effects.[15] The overall photophysical processes of PDT are summarized in Figure 1.2.

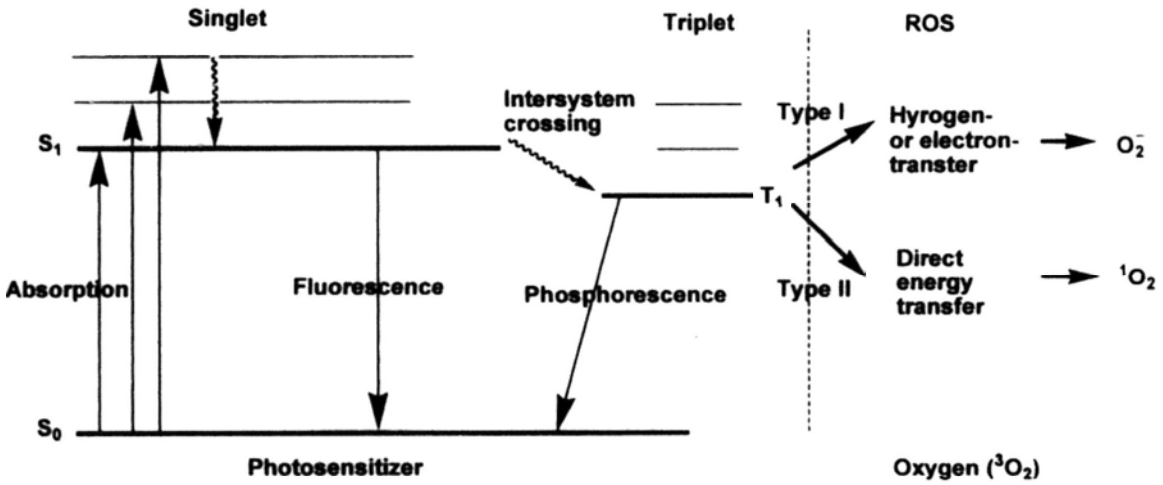

Figure 1.2. Photophysical mechanism of photodynamic therapy.

1.2.2 Cellular Mechanisms

Significant effort has been directed toward understanding the cellular mechanisms of PDT in recent years. Cell death in a necrotic fashion can be induced following organelle damage, such as membrane lipid peroxidation, disruption of lysosomal membrane, membrane enzyme inhibition or damage to nuclear components.[16] Apoptosis is a major type of programmed cell death.[17] It is a process of deliberate suicide by unwanted cells. In contrast to necrosis, apoptosis results in acute tissue injury, which is carried out in an ordered process. The cell genotype and the PDT dose have been found to determine whether cell death occurs by apoptosis or necrosis.[18] For instance, apoptosis was the predominant mode of cell death when murine leukemia P388 cells were treated with chloroaluminum phthalocyanine (AlPcCl), under low light doses, whereas necrosis was observed for high light doses.[18]

1.2.3 In Vivo Mechanisms

There are three main ways to induce tumor destruction in vivo by PDT. Firstly, PDT can damage the tumor-associated vasculature, leading to tumor infarction. The viability of tumor cells depends on the amount of nutrients supplied by the blood vessels. It was reported that a greater percentage of tumor cells in vivo die after PDT treatment because vascular shutdown starves them of oxygen and nutrients.[19] Secondly, PDT can generate ROS which can kill tumor cells directly when the photosensitizer concentration is high within the tumor cells at the time of illumination. In vivo studies showed that PDT can reduce the number of tumor cells through direct photodamage.[20] Finally, several studies showed that PDT induces immune modulation, either immune stimulating mediated by natural killer cells and macrophages or

immune suppressing. It was suggested that the modulation of immune effects may play a role in PDT-induced destruction of tumors.[21]

1.3 Photosensitizers for Photodynamic Therapy

Photosensitizers are compounds that are capable of absorbing light of a specific wavelength and transforming it into useful energy. In the case of PDT, this would involve the production of lethal cytotoxic agents. There are hundreds of natural and synthetic dyes that can function as photosensitizers for PDT, ranging from plant extracts to complex synthetic macrocycles.[22] The key characteristic of any photosensitizer is its ability to preferentially accumulate in diseased tissue and to then generate cytotoxic agents to induce the desired biological effects. In general, for solid tumors an ideal photosensitizer should meet at least some of the following criteria:[23]

(1) low dark toxicity but strong photocytotoxicity;

(2) high selectivity toward tumor in order to reduce side effects in peritumoral tissues;

(3) long wavelength (e.g. 600–800 nm) absorption allowing a deeper light penetration;

(4) high extinction coefficient (ε) at a long wavelength position where tissue penetration of light is at a maximum while the energy is high enough to produce singlet oxygen;

(5) rapid removal from the body, thus inducing a low systemic toxicity;

(6) desirable physical properties including high triplet state yield ($\Phi_T > 0.4$) and long triplet state lifetime ($\tau_T > 20$ μs) and be able to effectively produce singlet oxygen and other ROS.

1.3.1 The First Generation Photosensitizers

The first generation photosensitizers are haematoporphyrin derivatives (HpD) such as Photofrin® (**1.1**).[24] HpD were originally synthesized by treating haematoporphyrin with 5% H_2SO_4 in acetic acid at room temperature. In order to prepare solutions for injection, HpD were treated with an aqueous base and then neutralized. HpD consist of a mixture of several monomeric and oligomeric compounds. Partial purification of the most active oligomers by high-performance liquid chromatography or size-exclusion gel chromatography leads to the isolation of Photofrin@. It is the most commonly used photosensitizer in clinic to date. However, this drug has a number of disadvantages.[24] Firstly, the longest-wavelength absorption band appears at 630 nm with a low extinction coefficient (~ 1170 M^{-1} cm^{-1}). The biological effects after irradiation at this wavelength occur only to a tissue depth of ~5 mm. Secondly, the non-selective accumulation in the tumor results in distribution of drug between the tumor and the skin, with a tumor/skin ratio of ~ 2:1. Only 0.1-3% of the injected photosensitizer amount is found in the tumor tissue. Most importantly, the sensitizer is retained in cutaneous tissues for 2-3 months, which requires that the patients avoid bright light. Lastly, it consists of about 60 compounds and therefore it is difficult to reproduce its composition.[25]

1.3.2 The Second Generation Photosensitizers

The second generation photosensitizers have been developed with the goal of overcoming some of the shortcomings of photofrin@ and take advantage of their more ideal properties. These photosensitizers have absorption mainly in 650-800 nm. Light with this wavelength penetrates into tissues to a depth of up to 2-3 cm. The

interpretation of dose-response relationships for these photosensitizers is easier because their chemical composition is well defined.[26]

The first group of second generation of photosensitizers is porphyrin derivatives. *meso*-Tetraphenyl porphyrin (H_2TPP) (**1.15**), tetrasulfonated porphyrin H_2TPPS_4 (**1.16**),[27] and the *o*-, *m*- and *p*-isomers of tetra(hydroxyphenyl)porphyrins (**1.17-1.19**)[28] are some of the representative examples. The second group consists of chlorins and bacteriochlorins, like chlorin e6 **1.5**,[29] benzoporphyrin derivative **1.6**,[30] Sn etiopurpurin **1.12**,[31] and *meso*-tetra(hydroxyphenyl) chlorin **1.2**.[32] The third group of potential candidates is expanded porphyrin such as lutetium texaporphyrin **1.11**. The fourth group is phthalocyanine-based photosensitizers such as the disulfonated aluminium phthalocyanine Photosense (**1.7**)[33] and silicon phthalocyanine Pc4 (**1.10**).[34]

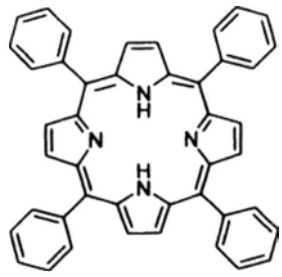

1.15

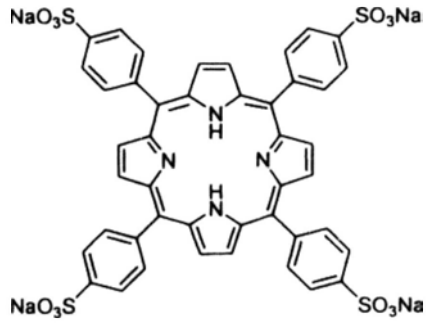

1.16

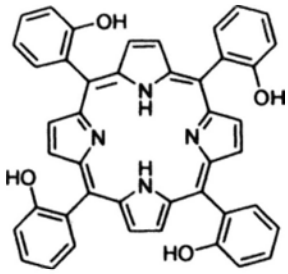

1.17

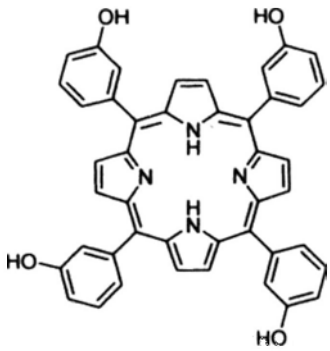

1.18

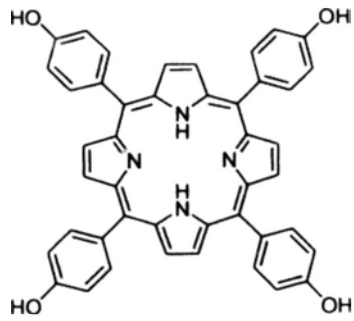

1.19

1.3.3 Phthalocyanines as Efficient Photosensitizers

Phthalocyanines are porphyrin analogues that have an additional benzo ring on each of the four subunits, which are linked by nitrogen atoms. These modifications result in a red-shift of the absorption and a higher molar absorptivity (2×10^5 M^{-1} cm^{-1} at 670 nm), and therefore allow a deeper light penetration into tissue. These compounds also possess favorable photophysical and chemical properties which can be altered through incorporation of appropriate substituents either on the periphery of the macrocyles or at the axial positions linked to the metal center.[35] The photophysical properties of phthalocyanines are strongly influenced by the central metal ion. Complextion of phthalocyanines with an open shell or paramagnetic metal ion such as Cu^{2+}, Co^{2+}, and Ni^{2+} results in shortening the excited state lifetimes due to the effects of the unpaired electrons, which in turn makes the compounds photoinactive. Phthalocyanines containing a closed *d* shell or diamagnetic metal ion such as Zn^{2+} and Al^{3+} generally have high triplet state quantum yields with long triplet state lifetimes. The triplet state of these metallophthalocyanines varies in energy from 110 to 126 KJ mol^{-1}, which is sufficient to trigger the formation of singlet oxygen (94 KJ mol^{-1}). As a result, these metallophthalocyanines usually also have a high singlet oxygen quantum yield.[36] Phthalocyanines with a group IV metal center can be modified readily via the attachment of axial substituents. Axially substituted silicon phthalocyanines have advantage over other peripherally substituted phthalocyanines. Firstly, these derivatives usually are free from structural isomers. Additionally, the axial ligands can prevent aggregation of the phthalocyanines and enhance their stability. Aggregation of phthalocyanines results in quenching of the excited state, thus preventing both fluorescence emission and singlet oxygen formation.[37]

1.4 Targeting Delivery Systems for Photodynamic Therapy

1.4.1 Passive Targeting Systems

Due to the fast angiogenesis in malignant tissue, tumor vessel walls show an enhanced vascular permeability with fenestra of a pore size of 100 to 1200 nm.[38] Furthermore, as tumor tissue lacks a functional lymphatic system, extravasated macromolecules do not return efficiently to the central circulation.[39] Liposomes, oil dispersions, and polymeric micelles and nanoparticles are considered as passive targeting systems due to the phenomenon known as enhanced permeability and retention (EPR) effect.[40]

1.4.1.1 Liposomes

Liposomes are uni- or multi-lamellar phospholipidic submicroscopic vesicles. Their components (phospholipids and cholesterol) are materials also existing in the body in high amounts and may provide a good biocompatibility. For PDT, liposomal preparations are currently used as effective delivery systems in experimental studies and in clinical trials.[41] The preparation involves simple aqueous dispersions of the drugs.[42] Using the benzoporphyrin derivative monoacid ring A (BPD-MA) (**1.6**) as photosensitizer, Richter et al. compared the biodistribution and clearance of an unilamellar liposomal formulation (L-BPD-MA) with a dimethyl sulfoxide solution (DMSO-BPD-MA) and a PBS solution (PBS-BPD-MA).[43] The in vivo study in M1 rhabdomyosarcoma-bearing DAB/2 male mice showed that L-BPD-MA was rapidly and significantly accumulated in the tumor tissue and the efficiency was significantly higher than that of both DMSO-BPD-MA and PBS-BPD-MA formulations.

1.4.1.2 Polymeric Micelles

Most photosensitizers easily form aggregates in aqueous media through their π-π stacking and hydrophobic interactions. Such aggregate formation severely decreases ROS formation due to the self-quenching of the excited state.[43] Encapsulation of photosensitizers into nanocarriers such as polymeric micelles might reduce their aggregation, resulting in enhancement of PDT efficacy.[44a] However, it is generally difficult to incorporate such very hydrophobic compounds into nanocarriers. To solve this problem, some ionic dendritic photosensitizers were prepared.[45] Li et al. reported a polyion complex formed via electrostatic interactions between a negatively charged poly(benzyl ether) dendritic porphyrin (DP) (**1.20**) and positively charged poly(ethylene glycol)-*block*-poly(L-lysine) (PEG-*b*-PLL) (**1.21**).[46] Dynamic light scattering (DLS) measurements and transmission electron microscopy (TEM) showed that DP-PEG-*b*-PLL complex formed a core-shell-type nanocarrier micelle. DP-loaded micelle exhibited almost comparable fluorescence lifetimes and oxygen consumption abilities to the free DP. The incorporation of DP into micelle resulted in an appreciable increase in the cellular uptake. The photocytotoxicity was also enhanced greatly compared to that of the free DP.

Jang et al. reported another polymeric micellar system in which the anionic dendritic zinc(II) phthalocyanine (DPcZn) (**1.22**) complexes with the polymer PEG-*b*-PLL (**1.21**) via electrostatic interactions.[47] This polymeric micelle (DPcZn/m) exhibited a strong Q-band absorption around 650 nm. Dynamic light scattering (DLS) studies indicated that the DPcZn/m system has a relevant size of 50 nm for intravenous administration. Under light irradiation, either DPcZn or DPcZn/m exhibited efficient consumption of dissolved oxygen in a medium to generate ROS. The photocytotoxicity of DPcZn was drastically improved by incorporation into the polymeric micelles (by ca. 100 times).

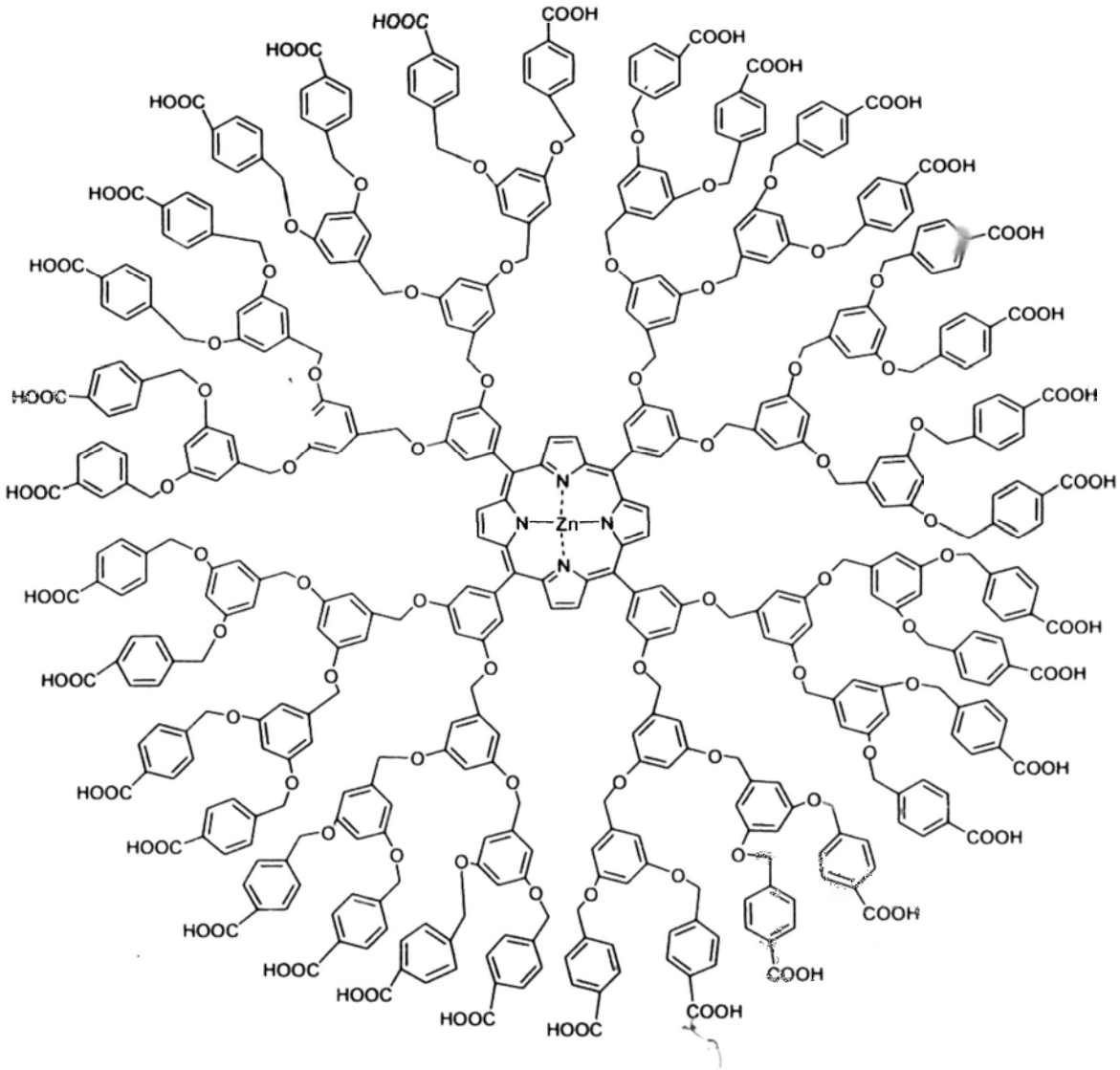

1.20

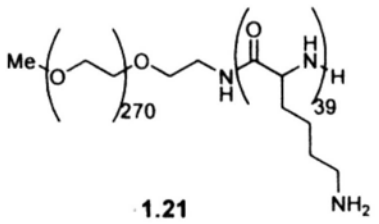

1.21

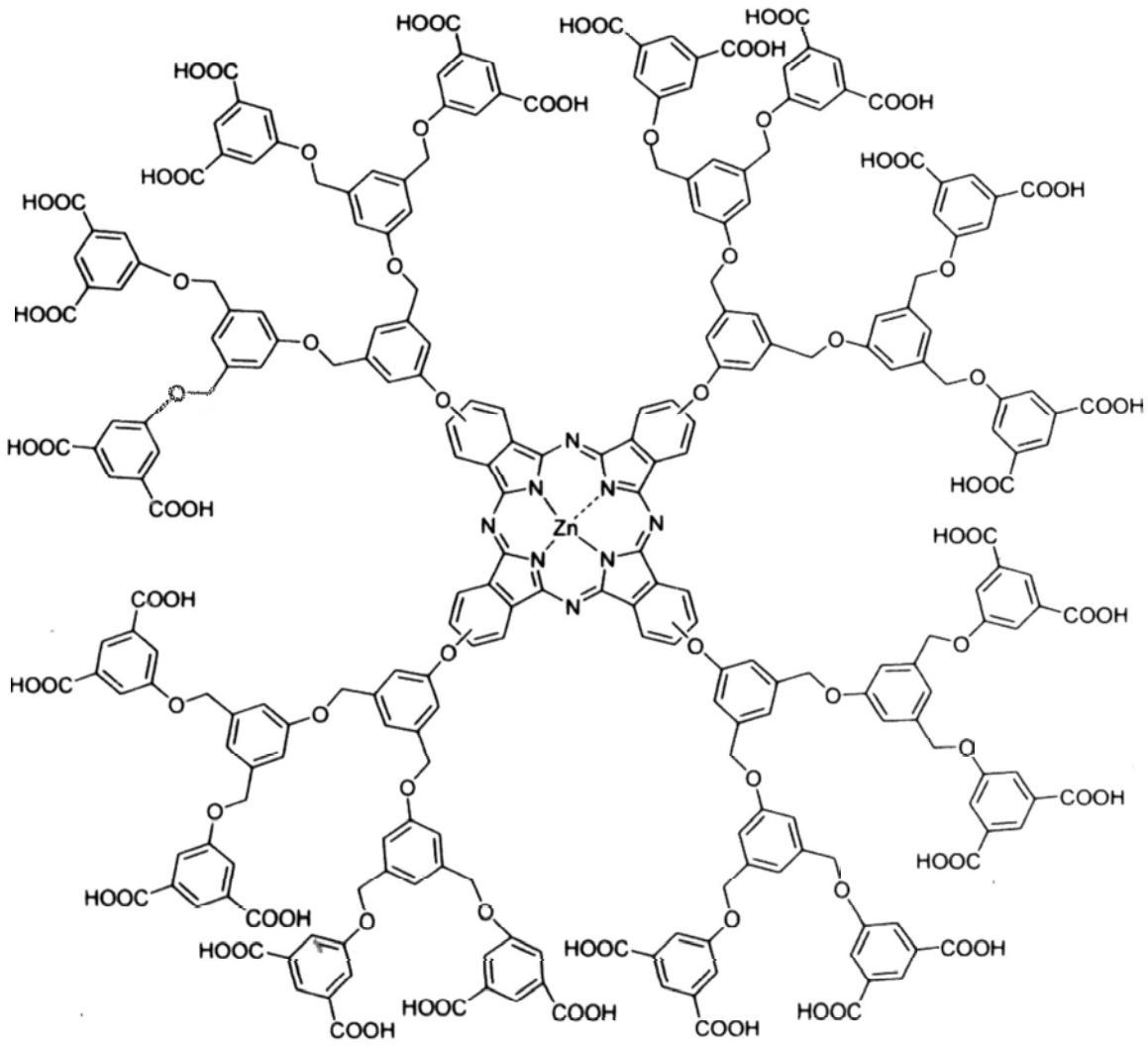

1.22

1.4.1.3 Polymeric Nanoparticles

Biodegradable polymeric nanoparticles, perceived as an alternative to liposomes, have received tremendous attention as a possible means of delivering antineoplastic agents.[48] Their main advantages lie in high drug loading, the possibility of controlling the drug release, and the existence of a large variety of materials and manufacturing processes.[49] The chemical composition and architecture of polymers

can be readily designed to accommodate drugs with varying degrees of hydrophobicity, molecular weight, and charge. In addition, the surface properties, morphologies, and composition of polymer matrices can be easily optimized for controlled polymer degradation and drug release kinetics. For example, modifying the surface of nanoparticles with polymers like poly(ethylene glycol) and poly (ethylene oxide) increases the circulation times.[50] Ricci-Junior et al. reported the preparation, characterization, and results of the photocytotoxicity of Poly (D, L latic-co-glycolic acid) (PLGA) nanoparticles containing zinc(II) phthalocyanine (ZnPc).[51] These ZnPc-loaded nanoparticles were prepared by a spontaneous emulsion-diffusion method. Their photophysical behavior was maintained after the encapsulation process and the in vitro photodynamic activity of ZnPc-loaded PLGA nanoparticles was enhanced suggesting that it is a promising drug delivery system for PDT.

1.4.2 Active Targeting Systems

Active targeting encompasses the strategy of coupling a specific targeting entity to photosensitizers, enhancing their selective interaction with cells or tissues through binding with specific membrane-located markers. The objective of active targeting is to enhance tumor-selective accumulation through target binding, thereby increasing the photodynamic effect.[38] In this way, active targeting aims at minimizing undesired side-effects related to non-specific photosensitizer accumulation.

1.4.2.1 Lipoprotein-Mediated Delivery

Cholesterols, triacylglycerols, and other lipids are transported in the serum by lipoproteins classified according to their density, namely chylomicrons, chylomicron remnants, very low density lipoproteins (VLDLs), intermediate density lipoproteins,

low density lipoproteins (LDLs) and high density lipoproteins (HDLs).[52] Basically, a lipoprotein is a particle consisting of a central core of hydrophobic lipids surrounded by a shell of hydrophilic polar lipids and apoproteins. These serum particles have two important biological functions. They solubilize highly hydrophobic lipids and allow the transportation of these important molecules throughout the body. They also contain signals that regulate the movement of the particular lipid into and out of specific cells and tissues. Of these lipoproteins, the most important in terms of drug delivery are the LDLs. LDLs are the major carriers of cholesterol in the blood.[53] Having a diameter of 22 nm and a mass of approximately 3 million Da, these LDL particles contain a core of about 1500 esterified cholesterol molecules surrounded by a shell of phospholipids and unesterified cholesterols. This outer shell also contains a single copy of the very large (514 kDa) B-100 apolipoprotein. It is this apolipoprotein that is responsible for recognition and binding by the LDL receptor and leads to receptor-mediated endocytosis of the LDL particles.[53] As cholesterol is a key component of all eukaryotic plasma membranes and is thus essential for the growth and viability of cells in higher organisms, it is natural that tumor cells and tumor vascular endothelial cells over express the LDL receptor.[54] This makes LDL particles extremely attractive vehicles for drug delivery and targeting. It has been found that photosensitizers mixed non-covalently with LDL before administration leads to an increase in photodynamic efficiency in comparison with the administration of photosensitizer alone.[55] Allison et al. noted that at 3 h post-injection, an increased level of BPD-MA (**1.6**) was delivered to M-1 tumor when the drug was mixed with LDL or HDL.[56] Furthermore, in vivo cytotoxicity assays also showed a higher photodynamic efficiency. Schmidt-Erfurth et al. covalently linked Chlorin (Ce6) (**1.5**) to LDL by a peptide linkage.[57] The optimal binding ratio, which provides the maximal

cellular uptake efficiency, was 50:1 (Ce6: LDL). At this optimal ratio, the in vitro uptake of Ce6-LDL conjugate by fibrosarcoma and retinoblastoma cells was 3- to 4-fold higher than the dye alone. After irradiation of light at 10 J cm^{-2}, Ce6-LDL conjugate provided 20% survival of retinoblastoma cells against 80-90 % with a mixture of Ce6 and LDL or ca. 100% with free dye.

1.4.2.2 Antibody-Targeted Delivery

Monoclonal antibody (MAb)-based drug delivery is another approach to improve the specificity of PDT and to overcome side effects associated with this therapy.[58] The strategy consists of linking photosensitizers with Mabs against specific antigens of malignant cells. To date, the American Food and Drug Administration (FDA) has approved 11 MAbs/MAb conjugates for therapy (and several others for diagnosis).[59] At least 400 other MAbs/MAb conjugates are in clinical trials worldwide, among which several are in phase III trials for treating cancer.[59b] Some in vitro and in vivo investigations of MAb-conjugated photosensitizers have given encouraging results, particularly for small tumors and ascite tumors which are suitable for this type of treatment. It has been established that the linkage of MAb to molecules including photosensitizers and cytotoxic agents does not significantly reduce the drug activity and MAb specificity. The results of these investigations have also shown that a lower effective dose of MAb-conjugated photosensitizer is necessary to produce higher selective phototoxicity effect over drug or MAb alone. Vrouenraets et al. investigated the photodynamic activities of the MAb 425 conjugate of tetrasulfonated aluminum phthalocyanine ($AlPcS_4$)-MAb 425 (**1.23**) and *meso*-tetra(hydroxyphenyl) chlorin (*m*THPC)-MAb (**1.24**).[60] Preliminary in vitro data showed that $AlPcS_4$-MAb 425 conjugate was highly toxic to A431 cells. This conjugate was 7500 times more toxic

than the free photosensitizer (IC_{50}: 0.12 vs. 900 nM), and about 60 times more toxic than *m*THPC-MAb 425 (**1.24**) in the same model. In an extended in vitro evaluation, *m*THPC- and $AlPcS_4$-MAb conjugates with three Mabs (BIWA4, E48 and 425) were directly compared using 5 squamous cell carcinoma (SCC) cell lines as the targets.[61] In contrast to free $AlPcS_4$ (IC_{50} > 700 nM), MAb-conjugated $AlPcS_4$ was found to be highly photocytotoxic in all the 5 cell lines. $AlPcS_4$-BIWA4 was most consistently effective with IC_{50} values ranging from 0.06 to 5.4 nM. *m*THPC-MAb conjugates were in general ineffective. These results showed that $AlPcS_4$-MAb conjugates have a high potential than *m*THPC-MAb conjugates for use in PDT.

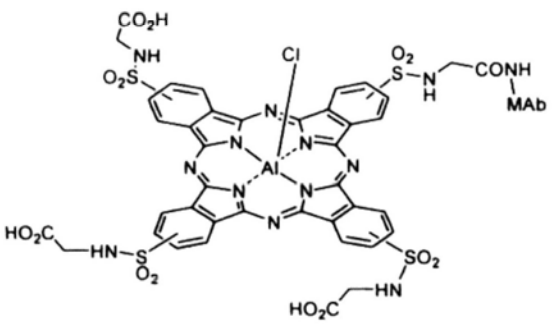

1.23

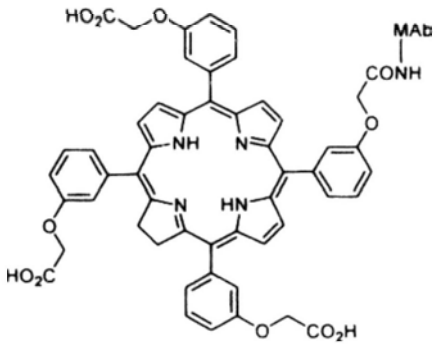

1.24

Recently, Malatesti et al. have reported a series of cationic isothiocyanato diphenyl porphyrins (**1.25-1.27**) which can be conjugated to anti-EpCAM and anti-CD104 Mabs.[62] Their photocytotoxicities toward both LoVo human colon adenocarcinoma and CORL23 human lung large cell carcinoma cell lines have also been evaluated. In contrast to the free porphyrins of which the IC_{50} values range from 3.23 to 9.95 μM, the MAb-conjugated photosensitizers show a high photocytotoxicity (IC_{50} = 0.17-1.11 μM).

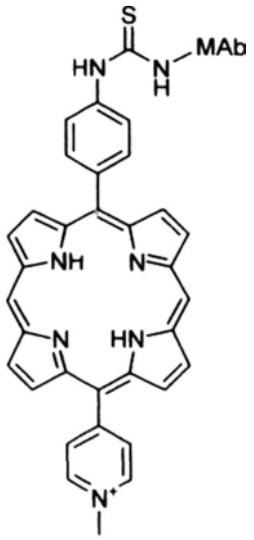

1.25

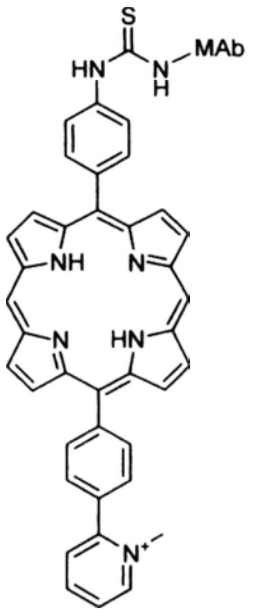

1.26

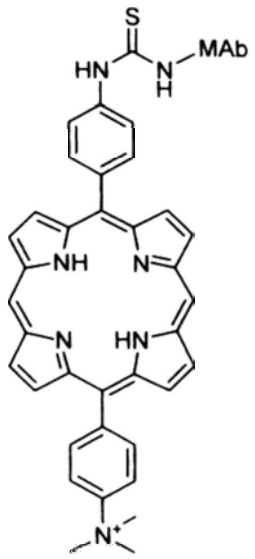

1.27

1.4.3 Photosensitizers Covalently Bound to Biomolecules

Many attempts have been made to increase the uptake of the dyes by the target cells and tissues and to improve subcellular localization so as to deliver the dyes to photosensitive sites within the cells.[63] The following sections give an overview of the development of photosensitizers covalently conjugated with biomolecules that may serve these properties.

1.4.3.1 Photosensitizers Conjugated with Glucose

Malignant cells are known to have accelerated metabolism which requires a high glucose uptake. Transport of glucose across the plasma membrane of mammalian cells is the first rate-limiting step for glucose metabolism and is mediated by facilitative glucose transporter (GLUT) proteins. Increased glucose transport in malignant cells has been associated with increased and deregulated expression of

glucose transporter proteins. Hence overexpression of GLUT1 and/or GLUT3 is a characteristic identified in many cancerous cells.[64]

Zheng et al. used near-infrared confocal microscopy to show that glycosylated pyropheophorbide **1.24** was selectively taken up by 9L glioma cells.[65] In the presence of 50 mM α-D-glucose, the fluorescence of **1.24** was drastically decreased. This competitive experiment showed that the glycosylated species **1.24** is taken up via GLUT proteins.

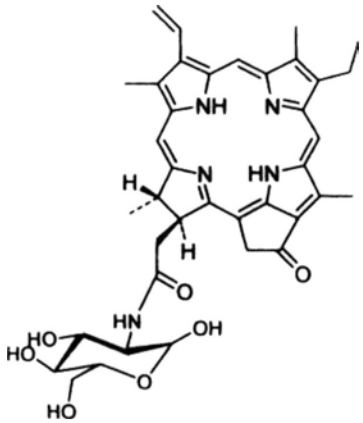

1.24

Lo et al. reported the preparation, photophysical properties, and photodynamic activities of two glucoconjugated silicon(IV) phthalocyanines **1.25** and **1.26**.[66] With two axial 1,2:5,6-di-*O*-isopropylidene-α-D-glucofuranose substituents linked to the silicon center through tetraethylene glycol chains, both compounds are highly photocytotoxic against HT29 and HepG2 cells, particularly the non-chlorinated phthalocyanine **1.25**, of which the IC_{50} values are as low as 5.5 nM. The lower photodynamic activity of the chlorinated derivative (IC_{50} = 17.2-21.3 nM) can be attributed to its higher aggregation tendency in the biological media, leading to a lower efficiency to generate ROS inside the cells. Fluorescence microscopic studies

also revealed that compound **1.25** has a high and selective affinity to the lysosomes, but not the mitochondria, of HT29 cells.

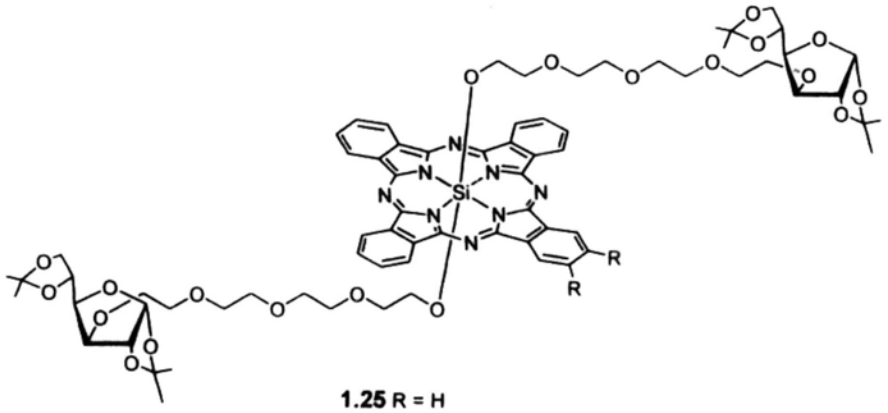

1.25 R = H

1.26 R = Cl

Liu et al. described the preparation and in vitro photodynamic activities of a series of tetraethylene-glycol-linked glucosylated zinc(II) phthalocyanines (**1.27-1.32**).[67] The number and position of the substituents have a great influence on the in vitro photocytotoxicity. Their photocytotoxicity follows the order: di-α-substituted > di-β-substituted > mono-α-substituted > tetra-β-substituted derivatives. The di-α-substituted analogue **1.28** shows the highest photocytotoxicity against HT29 and HepG2 cells with IC_{50} values down to 0.03-0.04 μM. Removal of the isopropylidene protection groups leads to an adverse effect on the photocytotoxicity. The IC_{50} values of **1.29** increase to 2.5-3.0 μM. The different photodynamic activities of these compounds can be explained by their different extent of cellular uptake and aggregation tendency.

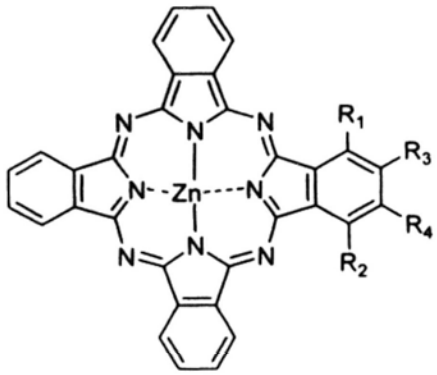

1.27 $R_1 = R_2 = R_3 = H$, R_4 =

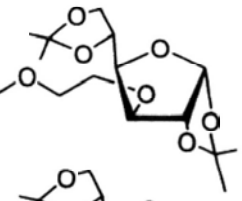

1.28 $R_3 = R_4 = H$, $R_1 = R_2$ =

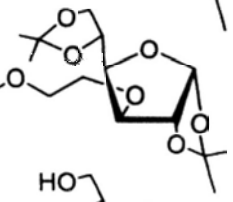

1.29 $R_3 = R_4 = H$, $R_1 = R_2$ =

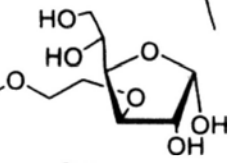

1.30 $R_1 = R_2 = H$, $R_3 = R_4$ =

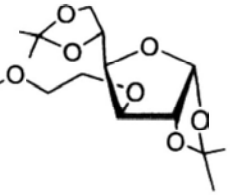

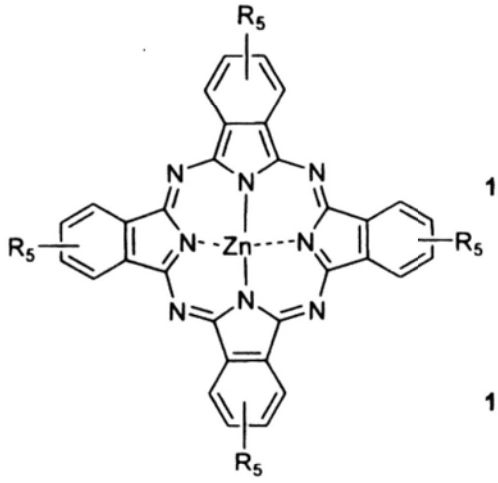

1.31 R_5 =

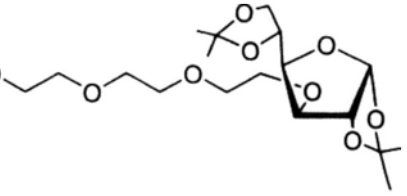

1.32 R_5 =

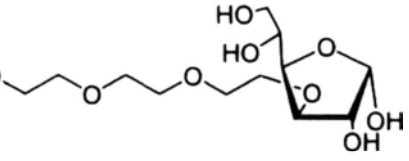

1.4.3.2 Photosensitizers Conjugated with Steroid Hormones

Steroid hormones are all derived from cholesterol. They are an interesting class of biomolecules that can target cancer cells. In particular, cholesterol is a vital

component of eukaryotic cell membranes and can be taken up quickly by cancer cells.[68] It thus appears that covalent coupling of cholesterol to a photosensitizer could favor its association with LDL and increase its photodynamic efficiency. Based on this approach, the dicholesteryl-substituted Ge(IV) photosensitizer (GePc) (**1.33**) was prepared by Segalla at al.[69] GePc incorporated in small unilamellar liposomes (CGP 55398) was injected systemically into mice bearing an intramuscularly implanted MS-2 fibrosarcoma. The photosensitizer was quantitatively transferred to serum lipoproteins and localized in the tumor tissue with a good efficiency. Irradiation of the GePc-loaded fibrosarcoma caused a fast and massive tumor necrosis involving both the malignant cells and blood vessels.

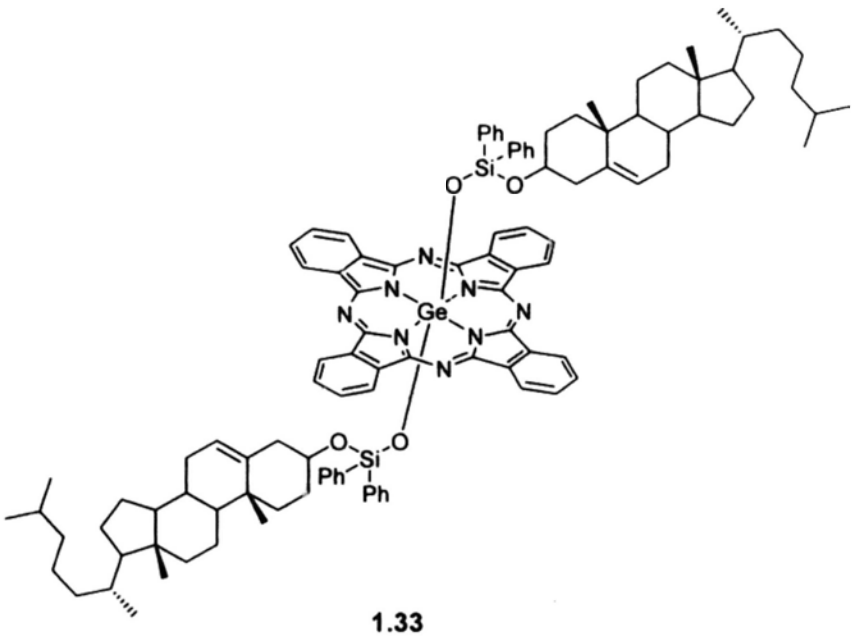

1.33

To improve the uptake of photosensitizers by receptor-rich endocrine tumors, van Lier et al. prepared several phthalocyanine-estradiol conjugates using the palladium-catalyzed Sonogashira coupling reaction.[70] They prepared a series of lipophilic tri(*tert*-butyl) phthalocyanine-estradiol conjugates (Scheme 1.1) and compared their biological activities with those of the hydrophilic water-soluble

trisulfonated conjugates (Scheme 1.2).[70a] The photocytotoxic activity of these compounds and their relative binding affinity for estrogen receptors were measured on murine EMT-6. Lipophilic conjugates **1.34-1.38** were photo-inactive up to 1 μM, but they exhibited dark toxicity at 5 μM. The highest receptor binding affinities were observed with lipophilic conjugates coupled *via* a relatively long spacer while the sulfonated analogues showed little binding affinities. Surprisingly, the most hydrophilic trisulfonated phthalocyanines **1.37a** and **1.37b** showed the highest photocytotoxicity (LD_{90} = 2.9 and 3.0 J cm^{-2}, respectively, where LD_{90} is the light dose (J cm^{-2}) required to kill 90% of the EMT-6 cells after incubations with 1 μM of the conjugate) for 24 h, which are comparable to those of the non-conjugated $ZnPcS_3$. The nature of the spacer did not seem to influence the biological activity.

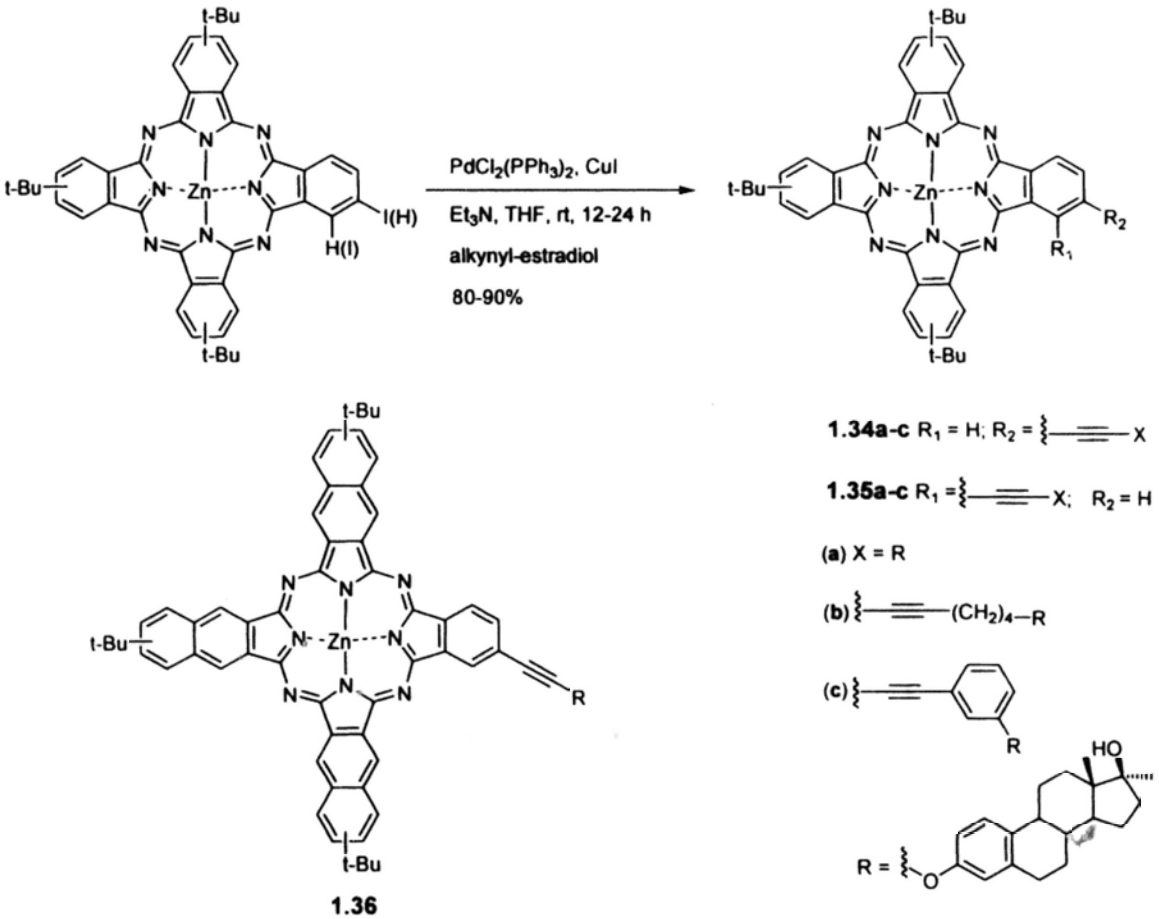

Scheme 1.1 Preparation of estradiol-containing zinc(II) tri(*tert*-butyl)-phthalocyanines.

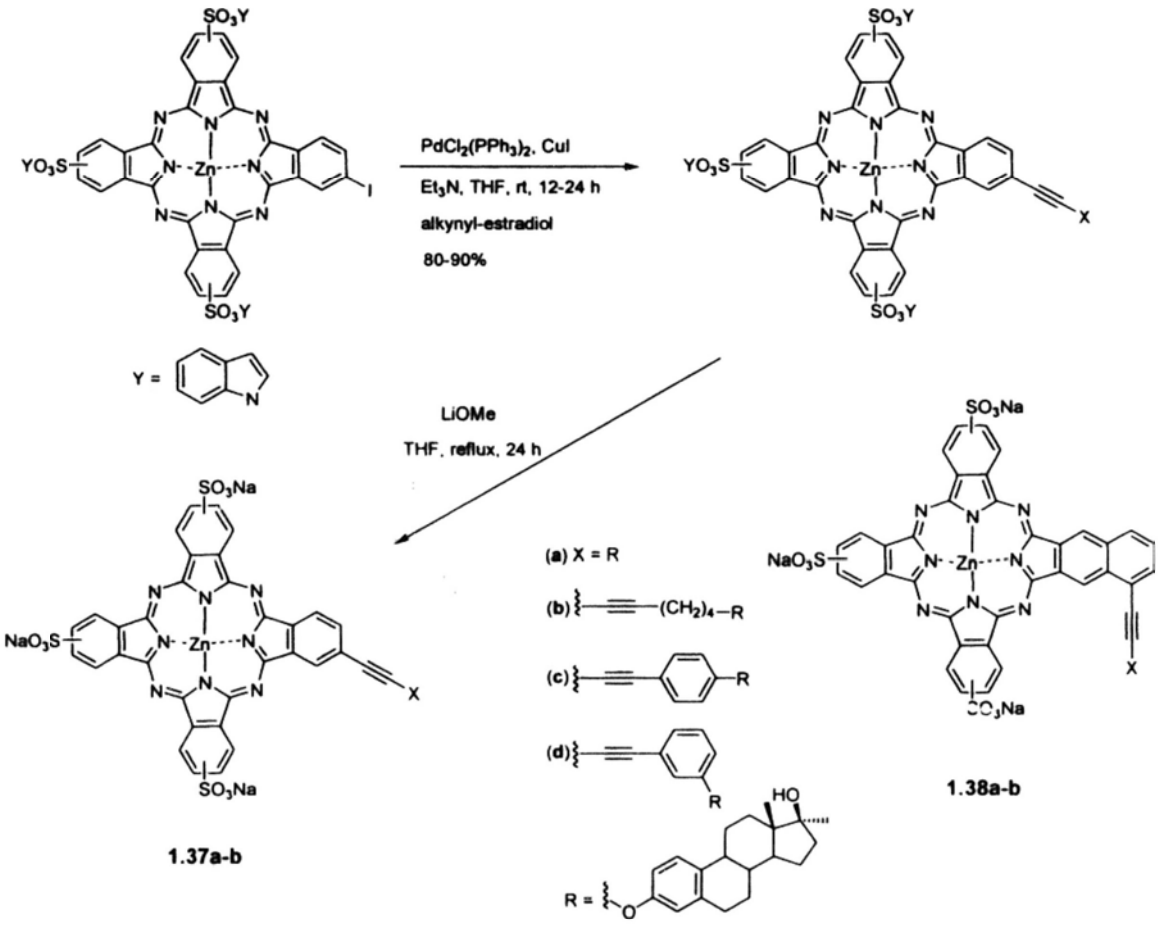

Scheme 1.2. Preparation of estradiol-containing zinc(II) trisulfonated phthalocyanines.

1.4.3.3 Photosensitizers Conjugated with Folic Acid

Folic acid is a vitamin that binds selectively the folate receptor (FR), a glycosylphosphatidylinositol-anchored cell surface receptor that is overexpressed in many human tumors.[71] Upon receptor interaction, the folic acid-FR complex is taken up by cells and moves through many organelles.[72] The folate receptor mediated endocytosis was largely investigated to expand the therapeutic value of drugs by facilitation their delivery to the target tissue. Examples of targetable drug delivery carriers conjugated with folic acid conjugation include radionuclide deferoxamine-folate complexes for radiopharmaceutical imaging,[73] protein toxin-folate complexes,[74]

chemotherapeutant-folate conjugates,[75] folate-immunotherapeutic agent complexes,[76] liposome-folate encapsulated drugs,[77] and folic acid decorated nanoparticles.[78]

Recently, Schneider et al. have reported for the first time the conjugation of tetraphenylporphyrin to folic acid (**1.39-1.40**).[79] The photodynamic activities of conjugates **1.39** and **1.40** toward KB cells, which overexpress the folate receptor (297 × 10^3 folate receptors/cell), have been evaluated. It has been found that after 24 h incubation, cellular uptake of conjugates **1.39** and **1.40** is on average 7-fold higher than that of tetraphenylporphyrin (TPP) (**1.15**). This suggests an active transport via receptor-mediated endocytosis. The cellular uptake of **1.39** and **1.40** shows a reduction of 70% in the presence of a competitive concentration of folic acid. The in vitro photocytotoxicity of the porphyrin-folate conjugates **1.39** and **1.40** is also higher than that of TPP. Under the same experimental conditions, TPP displays no photocytotoxicity while conjugats **1.39** and **1.40** are potent with ID_{50} values of 22.6 and 6.7 J cm^{-2}, respectively.

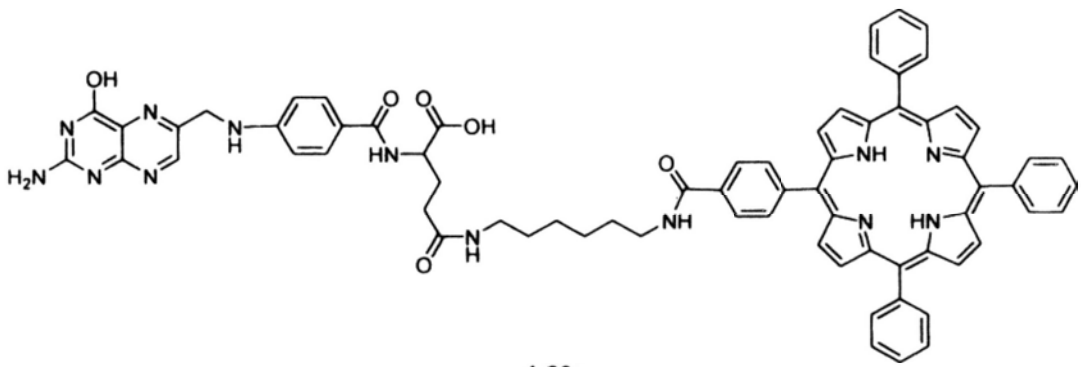

1.39

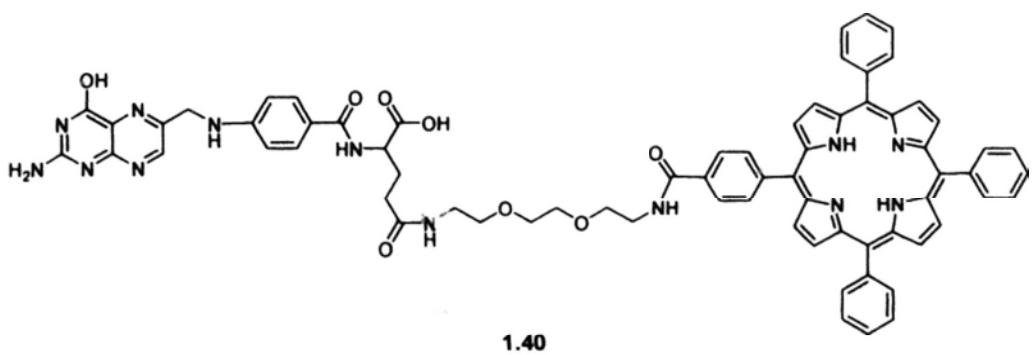

1.40

1.4.3.4 Photosensitizers Conjugated with Polyamines

The native polymines such as putrescine, spemidine, and spermine play multifunctional roles in a number of cell processes including cell proliferation and differentiation.[80] These compounds, in a polycationic form at physiological pH, can be biosynthesized internally and imported from exogenous sources through specific active transport systems. In the rapidly proliferating cells such as cancer cells, the polyamine requirement exceeds biosynthetic capabilities. The activity of these polyamine transporters (PAT) is therefore higher in these cells to increase the uptake of these materials to sustain the rapid cell division.[81] These characteristics have led to the use of polyamines as potential vectors for the selective delivery of chemotherapeutic and DNA targeted agents into cancer cells.[82] Consequently, a substantial number of polyamine conjugates with cytotoxic drugs such as chlorambcil,[83] nitroimidazole,[84] aziridine,[85] acridine,[86] enediyne,[87] taxol,[88] camptothecin,[89] and anthrancen[90] have been reported. In most of the cases, the cytotoxicity and drug selectivity for tumor cells is enhanced.

Recently, Sol et al. have recently reported a series of tritolylporphyrin and protoporphyrin IX polyamine conjugates (**1.41-1.44**).[91] These compounds contain one or two polyamine unit(s) (spermidine or spermine) covalently tethered to macrocycles via the N^4 polyamine position. The photocytotoxicity of these compounds has been evaluated against K562 human chronic myelogenous leukemia cells and compared with that of Photofrin II@. These polyamine conjugates **1.41-1.44** exhibit a much higher photocytoxicity compared with photofrin II@ and induce necrosis in the treated cells.

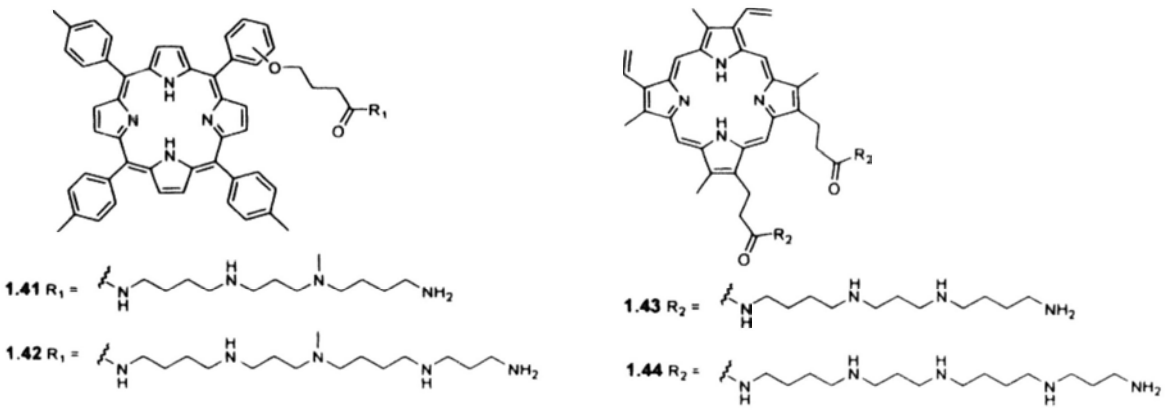

1.4.3.5. Activatable Photosensitizers

Vious activable photosensitizers have been reviewed very recently.[92] The function of same photosensitizers can be switched on by changing the environment. For examply, the singlet oxygen production efficiency of photosensitizers is dependent on solvent properties including pH and hydrophobicity. The common photosensitizers methylene blue (**1.45**) and toluidine blue (**1.46**) display a ca. 5-fold enhancement in singlet oxygen quantum yield as the pH increases from 5 to 9 and the photosenistizers become deprotonated. Solvent hydrophobicity also plays a high role in determining the photosensitizer efficiency. For example, Pb-bacteriopheohorbide (**1.14**) undergoes an approximately 2-fold change in singlet oxygen quantum yield as the solvent chagnes from acetone to deuterated water.

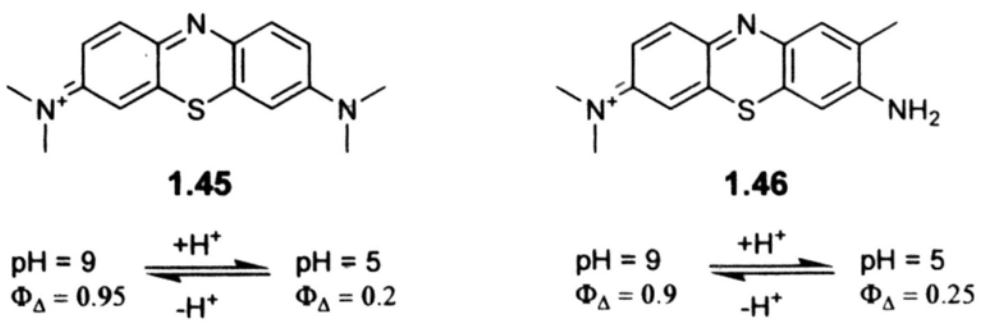

Although the effects of solvents and pH have long been known to affect singlet oxygen production, these factors have recently been applied for the design of activated photosensitizers. Recently, McDonnell et al. have developed a novel series of amine-containing BF_2-chelated azadipyrromethenes **1.47-1.50** for application in PDT.[93] These compounds can be switched on and off in the fluorescence and singlet oxygen production in DMF by changing the pH environment. Upon addition of HCl, the amino groups are protonated, which inhibits the photoinduced electrion transfer, thereby promoting singlet oxygen generation. The rate for **1.48**, for example, increases by up to 8.5-fold.

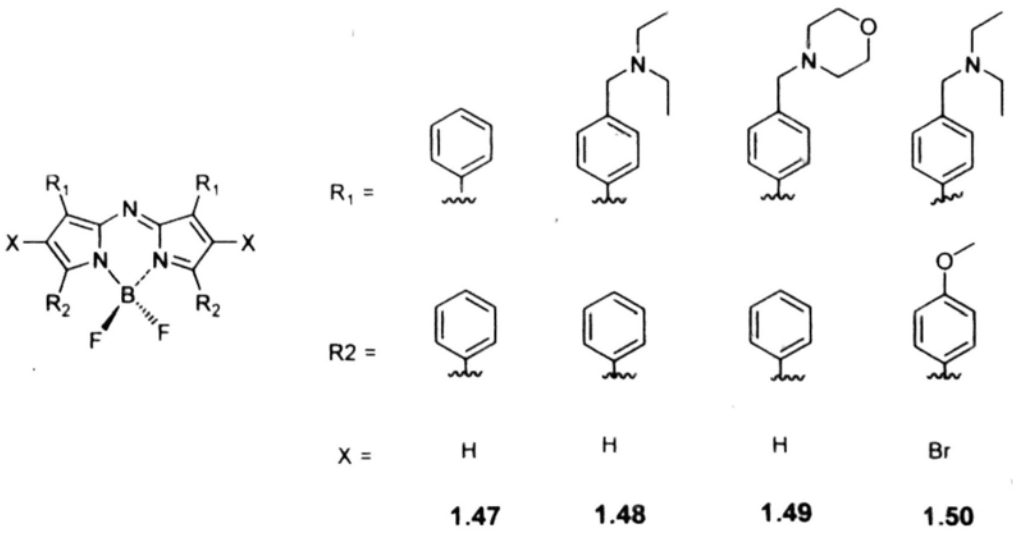

1.47 **1.48** **1.49** **1.50**

A major difference between various solid tumors and the surrounding normal tissues is the nutritional and metabolic environment. The vasculature of tumors is often insufficient to supply enough oxygen and nutritional needs for the growth of tumor cells. The production of lactic acid under hypoxic conditions and the hydrolysis of ATP in an energy-deficient environment contribute to an acidic micro-environment, which has been found in many types of tumors.[94] Most solid tumors have lower extracelluar pH (pHe) (< 7.2) than the surrounding tissues and blood (pH 7.5).[94a] The extracellular pH values of some tumors and normal tissues are shown in Table 1.3.[95]

The extracellular pH difference between tumors and normal tissues has been proposed to be a factor contributing to the tumor selective activation of the pH-sensitive photosensitizers.[96]

Table 1.3. Extracellular pH values of some tumors and normal tissues.[95]

Tissue	**Average extracellular pH**
Breast cancer	7.27 ± 0.23
Sucutis	7.58 ± 0.15
Glioblastoma	6.87 ± 0.24
Adjacent normal brain	7.12 ± 0.22
Astrocytoma	6.75 ± 0.40
Adjacent normal brain	7.12 ± 0.04
Ca Uterus/vulva	6.92 ± 0.37
Subcutis/muscle	7.65 ± 0.28
Melanoma	6.76 ± 0.09
Subcutis	7.43 ± 0.08

1.5 References

1. (a) Sternberg, E. D.; Dolphin, D. *Tetrahedron* **1998**, *54*, 4151. (b) Ackroyd, R.; Kelty, C.; Brown, N.; Reed, M. *Photochem. Photobiol.* **2001**, *74*, 656.
2. Raab, O. *Z. Biol.* **1990**, *39*, 524.
3. von Tappeiner, H.; Jesionek, A. *Muench Med. Wochenschr.* **1903**, *47*, 2042.
4. von Tappeiner, H.; Jesionek, A. *Dtsch. Arch. Klin. Med.* **1904**, *80*, 427.
5. Giuliano, E. A.; Ota, J.; Tucker, S. A. *Vet. Ophthalmol.* **2007**, *10*, 337.
6. (a) MacDonald, I. J.; Dougherty, T. J. *J. Porphyrins Phthalocyanines* **2001**, *5*, 105. (b) Huang, Z. *Technol. Cancer Res. Treat.* **2005**, *4*, 283.
7. Lipson, R. L.; Blades, E. J.; Olsen, A. M. *J. Natl. Cancer Inst.* **1961**, *26*, 1.
8. Dougherty, T. J.; Potter, W. R.; Weishaupt, K. R. *Prog. Clin. Biol. Res.* **1984**, *170*, 301.
9. Serra, A.; Pineiro, M.; Pereira, N.; Gonsalves, A. R.; Laranjo, M.; Abrantes, M.; Botelho, F. *Oncol. Rev.* **2008**, *2*, 235.
10. Brown, S. B.; Brown, E. A.; Walker, I. *Lancet Oncol.* **2004**, *5*, 497.
11. Capella, M. A. M.; Capella, L. S. *J. Biomed. Sci.* **2003**, *10*, 361.
12. Grant, W. E.; Speight, P. M.; Hopper, C.; Bown, S. G.; *Int. J. Cancer* **1997**, *71*, 937.
13. Miller, J. D.; Baron, E. D.; Scull, H.; Hsia, A.; Berlin, J. C.; McCormick, T.; Colussi, V.; Kenney, M. E.; Cooper, K. D.; Oleinick, N. L. *Toxicology Appl. Pharmacol.* **2007**, *224*, 290.
14. Sharman, W. M.; Allen, C. M.; van Lier, J. E. *Drug Discov. Today* **1999**, *4*, 507.
15. Weishaupt, K. R.; Gomer, C. J.; Dougherty, T. J. *Cancer Res.* **1976**, *36*, 2326.
16. Castano, A. P.; Demidova, T. N.; Hamblin, M. R. *Photodiag. Photodyn. Ther.* **2004**, *1*, 279.

17. (a) Oleinick, N. L.; Morris, R. L.; Belichenko, I. *Photochem. Photobiol. Sci.* **2002**, *1*, 1. (b) Almeida, R. D.; Manadas, B. J.; Carvalho, A. P.; Duarte, C. B. *Biochimi. Biophys. Acta* **2004**, *1704*, 59. (c) Macdonald, I. J.; Dougherty, T. J. *J. Porphyrins phthalocyanines* **2001**, *5*, 105.

18. (a) Luo, Y.; Kessel, D. *Photochem. Photobiol.* **1997**, *66*, 479. (b) Ben-Hur, E.; Oetjen, J.; Horowitz, B. *Photochem. Photobiol.* **1997**, *65*, 456. (c) He, X. Y.; Sikes, R. A.; Thomsen, S.; Chung, L. W. K.; Jacques, S. L. *Photochem. Photobiol.* **1994**, *59*, 468. (d) Noodt, B. B.; Berg, K.; Stokke, T.; Peng, Q.; Nesland, J. M. *Br. J. Cancer* **1996**, *74*, 22. (e) Castano, A. P.; Demidova, T. N.; Hamblin, M. R. *Photodiag. Photodyn. Ther.* **2005**, *2*, 1.

19. Dougherty, T. J.; Gomer, C. J.; Henderson, B. W.; Jori, G.; Kessel, D.; Korbelik, M.; Moan, J.; Peng, Q. *J. Natl. Cancer Inst.* **1998**, *90*, 889.

20. (a) Christensen, T.; Feren, K.; Moan, J.; Pettersen, E. *Br. J. Cancer* **1981**, *44*, 717. (b) Fingar, V. H.; Wieman, T. J.; Wiehle, S. A; Cerrito, P. B. *Cancer Res.* **1992**, *52*, 4914.

21. Korbelik, M.; *J. Clin. Laser Med. Surg.* **1996**, *14*, 329. (b) Musser, D. A; Fiel, R. J. *Photochem. Photobiol.* **1991**, *53*, 119. (c) Korbelik, M.; Dougherty, G. J. *Cancer Res.* **1999**, *59*, 1941.

22. Vrouenraets, M. B.; Visser, G. W. M.; Snow, G. B.; van Dongen, G. A. M. S. *Anticancer Res.* **2003**, *23*, 505.

23. (a) Lunardi, C. N. Tedesco, A. C. *Curr. Org. chem.* **2005**, *9*, 813. (b) Tedesco, A. C.; Rotta, J. C.; Lunardi, C. N. *Curr. Org. chem.* **2003**, *7*, 187. (c) Lang, K.; Mosinger, J.; Wagnerová, D. M. *Coord. Chem. Rev.* **2004**, *248*, 321.

24. Wöhrle, D.; Hirth, A.; Bogdahn-Rai, T.; Schnurpfeil, G.; Shopova, M. *Russ. Chem. Bull.* **1998**, *47*, 807.

57. Schmidt-Erfurth, U.; Diddens, H.; Birngruber, R.; Hasan, T. *Br. J. Cancer* **1997**, *75*, 54.

58. van Dongen, G. A. M. S.; Visser, G. W. M.; Vrouenraets, M. B. *Adv. Drug Deliv. Rev.* **2004**, *56*, 31.

59. (a) Carter, P. *Nat. Rev. Cancer* **2001**, *1*, 118. (b) Trikha, M.; Yan, L. Nakada, M. T. *Curr. Opin. Biotechnol.* **2002**, *13*, 609.

60. Oseroff, A. R.; Ara, G.; Ohuoha, D.; Aprille, J.; Bommer, J. C.; Yarmush, M. L.; Foley, J.; Cincotta, L. *Photochem. Photobiol.* **1987**, *46*, 83.

61. Vrouenraets, M. B.; Visser, G. W. M.; Stigter, M.; Oppelaar, H.; Snow, G. B.; van Dongen, G. A. M. S. *Int. J. Cancer* **2002**, *98*,793.

62. Malatesti, N.; Smith, K.; Savoie, H.; Greenman, J.; Boyle, R. W. *Int. J. Oncol.* **2006**, *28*, 1561.

63. Tian, Y. Y.; Wang, L. L.; Wang, W. *Laser Phys.* **2008**, *18*, 1119.

64. (a) Zheng, X.; Pandey, R. K. *Anticancer Agents Med. Chem.* **2008**, *8*, 241. (b) Wallberg-Henriksson, H.; Zierath, J. R. *Mol. Membr. Biol.* **2001**, *18*, 205. (c) Macheda, M.; Rogers, S.; Best, J. D. *J. Cell. Physio.* **2005**, *202*, 654.

65. Zhang, M.; Zhang, Z.; Blessington, D.; Li, H.; Busch, T. M.; Madrak, V.; Miles, J.; Chance, B.; Glickson, J. D.; Zheng, G. *Bioconjugate Chem.* **2003**, *14*, 709.

66. Lo, P. C.; Chan, C. M. H.; Liu, J. Y.; Fong, W. P.; Ng, D. K. P. *J. Med. Chem.* **2007**, *50*, 2100.

67. Liu, J. Y.; Lo, P. C.; Fong, W. P.; Ng, D. K. P. *Org. Biomol. Chem.* **2009**, *7*, 1583.

68. Candide, C.; Molière, P.; Goldstein, S.; Santus, R.; Dubertret, I.; Reyftmann, J. P.; Polonovski, J. *FEBS Lett.* **1986**, *207*, 133.

69. Segalla, A.; Milanesi, C.; Jori, G.; Capraro, H. G.; Isele, U.; Schieweck, K. *Br. J. Cancer* **1994**, *69*, 817.

70. (a) Khan, E. H.; Ali, H.; Tian, H.; Rousseau, J.; Tessier, G.; van Lier, J. E. *Bioorg. Med. Chem.* **2003**, *13*, 1287. (b) Ali, H.; van Lier, J. E. *Tetrahedron Lett.* **1997**, *38*, 1157.

71. Campbell, I. G.; Jones, T. A.; Foulkes, W. D.; Trowsdale, J. *Cancer Res.* **1991**, *51*, 5329.

72. Jackman, A. L.; Theti, D. S.; Gibbs, D. D. *Adv. Drug Deliv. Rev.* **2004**, *56*, 1111.

73. Ke, C. Y.; Mathias, C. J.; Green, M. A. *Adv. Drug Deliv. Rev.* **2004**, *56*, 1143.

74. (a) Ward, C. M.; Acheson, N.; Seymour, L. W. *J. Drug Target* **2000**, *8*, 119. (b) Lu, J. Y.; Lowe, D. A.; Kenndy, M. D.; Low, P. S. *J. Drug Target* **1999**, *7*, 43.

75. (a) Ladino, C. A.; Chari, R. V.; Bourret, L. A.; Kedersha, N. L.; Goldmacher, V. S. *Int. J. Cancer* **1997**, *73*, 859. (b) Steinberg, G.; Broch, R. F. *J. Med. Chem.* **2001**, *44*, 69. (c) Leamon, C. P.; Reddy, J. A. *Adv. Drug Deliv. Rev.* **2004**, *56*, 1127.

76. (a) Roy, E. J.; Gawlick, U.; Orr, B. A.; Kranz, D. M. *Adv. Drug Deliv. Rev.* **2004**, *56*, 1219. (b) Lu, Y.; Sega, E.; Leamon, C. P.; Low, P. S. *Adv. Drug Deliv. Rev.* **2004**, *56*, 1161. (c) Lu, Y.; Low, P. S. *J. Control Release* **2003**, *91*, 17.

77. (a) Anderson, K. E.; Eliot, L. A.; Stevenson, B. R.; Rogers, J. A. *Pharm. Res.* **2001**, *18*, 316. (b) Gabizon, A.; Shmeeda, H; Horowitz, A. T.; Zalipsky, S. *Adv. Drug Deliv Rev.* **2004**, *56*, 1177.

78. (a) Nayak, S.; Lee, H.; Chmielewski, J.; Lyon, L. A. *J. Am. Chem. Soc.* **2004**, *126*, 10258. (b) Salmaso, S.; Semenzato, A.; Caliceti P.; Hoebeke, J.; Sonvico, F.; Dubernet, C.; Couvreur, P. *Bioconjug. Chem.* **2004**, *15*, 997.

79. Schneider, R.; Schmitt, F.; Frochot, C.; For, Y.; Lourette, N.; Guillemin, F.; Müller, J.; Barberi-Heyob, M. *Bioorg. Med. Chem.* **2005**, *13*, 2799.

80. Barret, J. M.; Kruczynski, A.; Vispé, S.; Annereau, J. P.; Brel, V.; Guminski, Y.; Delcros, J. G.; Lansiaux, A.; Guilaud, N.; Imbert, T.; Bailly, C. *Caner Res.* **2008**, *68*, 9845.

81. (a) Bachrach, U.; Seiler N. *Cancer Res.* **1981**, *41*, 1205. (b) Chem, K. Y.; Rinehart, C. A.; Jr. *Biochem. Biophys. Res. Commun.* **1981**, *101*, 242.

82. (a) Karigiannism G.; Papaioannou, D. *Eur. J. Org. Chem.* **2000**, 1841. (b) Seiler, N. *Pharmaco. Ther.* **2005**, *107*, 99.

83. (a) Holley, J. L.; Mather, A.; Wheelhouse, R. T.; Cullis, P. M.; Hartley, J. A.; Bingham, J. P.; Cohen, G. M. *Cancer Res.* **1992**, *52*, 4190. (b) Cullis, P. M.; Merson-Davies, L.; Weaver, R. *J. Am. Chem. Soc.* **1995**, *117*, 8033.

84. Holley, J.; Mather, A.; Cullis, P.; Symons, M. R.; Wardman, P.; Watt, R. A.; Cohen, G. M. *Biochem. Pharmacol.* **1992**, *43*, 763.

85. Eiseman, J. L.; Rogers, F. A.; Guo, Y.; Kauffman, J.; Sentz, D. L.; Klinger, M. F.; Callery, P. S.; Kyprianou, N. *Cancer Res.* **1998**, *58*, 4864.

86. Delcros, J. D.; Tomasi, S.; Carrington, S.; Martin, B.; Renault, J.; Blagbrough, I. S.; Uriac, P. *J. Med. Chem.* **2002**, *45*, 5098.

87. Suzuki, I.; Shigenaga, A.; Nemoto, H.; Shibuya, M. *Tetrahedron Lett.* **2004**, *45*, 1955.

88. Battaglia, A.; Guerrini, A.; Baldelli, E.; Fontanna, G.; Varchi, G.; Samori, C.; Bambrdelli, E. *Tetrahedron Lett.* **2006**, *47*, 2667.

89. Dallavalle, S.; Giannini, G.; Alloatti, D.; Casati, A.; Marastoni, E.; Musso, L.; Merlini, L.; Morini, G.; Penco, S.; Pisano, C.; Tinelli, S.; De Cesare, M.; Beretta, G. L.; Zunino, F. *J. Med. Chem.* **2006**, *49*, 5177.

90. (a) Wang, J.; Xie, S.; Li, Y.; Guo, Y.; Ma, Y.; Zhao, J.; Phanstiel IV, O.; Wang, C. *Bioorg. Med. Chem.* **2008**, *16*, 7005. (b) Wang, C.; Delcros, J.-G.; Biggerstaff,

25. Moore, C. M.; Pendse, D.; Emberton, M. *Nat. Clin. Pract. Urol.* **2009**, *6*, 18.

26. Wiedmann, M. W.; Caca, K. *Curr. Pharm. Biotechnol.* **2004**, *5*, 397.

27. (a) Kessel, D.; Thompson, P.; Saatio, K.; Nantwi, K. D. *Photochem. Photobiol.* **1987**, *45*, 787. (b) Wilkinson, F.; Helman, W. P.; Ross, A. B.; *J. Phys. Chem. Ref. Data* **1993**, *22*, 113.

28. Stilts, C. E.; Nelen, M. I.; Hilmey, D. G.; Davies, S. R.; Gollnick, S. O.; Oseroff, A. R.; Gibson, S. L.; Hilf, R.; Detty, M. R. *J. Med. Chem.* **2000**, *43*, 2403.

29. Nelson, J. S.; Roberts, W. G.; Berns, M. W. *Cancer Res.* **1987**, *47*, 4681. (b) Roberts, W. G.; Shiau, F. Y.; Nelson, J. S.; Smith, K. M.; Berns, M. W. *J. Natl. Cancer. Inst.* **1988**, *80*, 330. (c) Leach, M. W.; Higgins, R. J.; Autry, S. A.; Boggan, J. E.; Lee, S. J.; Smith, K. M. *Photochem. Photobiol.* **1993,** *58*, 653.

30. Pandey, R. K.; Potter, W. R.; Meunier, I.; Sumlin, A. B.; Smith, K. M. *Photochem. Photobiol.* **1995**, *62*, 764.

31. Morgan, A. R.; Rampersaud, A.; Keck, R. W.; Selman, S. H. *Photochem. Photobiol.* **1987**, *46*, 441.

32. Ma, L.; Moan, J.; Berg, K. *Int. J. Cancer* **1994**, *57*, 883.

33. Nyman, E. S.; Hynninen, P. H. *J. Photochem. Photobiol. B: Biol.* **2004**, *73*, 1.

34. Farooq, F. T.; Berlin, J.; Baron, E.; Faulx, A. L.; Marks, J. M.; Chak, A. *Castrointest. Endosc.* **2007**, *65*, AB155.

35. Photodynamic therapy: basic principles and clinical applications, Henderson, B. W., Jougherty, T. J., Marcel Dekker : USA, 1992.

36. (a) Wagner, J. R.; Ali, H.; Langlois, R.; Brasseur, N.; van Lier, J. E. *Photochem. Photobiol.* **1987**, *45*, 587. (b) Darwent, J. R.; Douglas, P.; Harriman, A.; Porter, G.; Richoux, M. C. *Coord. Chem. Rev.* **1982**, *44*, 83. (c) Ali, H.; van Lier, J. E. *Chem. Rev.* **1999**, *99*, 2379.

37. Lo, P. C.; Huang, J. D.; Cheng, D. Y. Y.; Chan, E. Y. M.; Fong, W. P.; Ko, W. H.; Ng, D. K. P. *Chem. Eur. J.* **2004**, *10*, 4831.

38. Moreira, J. N.; Gaspar, R.; Allen, T. M. *Biochim. Biophys. Acta* **2001**, *1515*, 167.

39. Derycke, A. S. L.; de Witte, P. A. M. *Adv. Drug Deliv. Rev.* **2004**, *56*, 17.

40. (a) Garrec, D. L.; Taillefer, J.; Vanlier, J. E.; Lenaerts, V.; Leroux, J. C. *J. Drug Target.* **2002**, *10*, 429. (b) van Nostrum, C. F. *Adv. Drug Deliv. Rev.* **2004**, *56*, 9.

41. (a) Rodal, G. H.; Rodal, S. K.; Moan, J.; berg, K. *J. Photochem. Photobiol. B: Biol.* **1998**, *45*, 150. (b) Renno, R. Z.; Miller, J. W. *Adv. Drug Deliv. Rev.* **2001**, *52*, 63. (c) Shum, P.; Kim, J. M.; Thompson, D. H. *Adv. Drug Deliv. Rev.* **2001**, *53*, 273.

42. (a) Wang, Z. J.; He, Y. Y.; Huang, C. G.; Huang, J. S.; Huang, Y. C.; An, J. Y.; Gu, Y.; Jiang, L. *Photochem. Photobiol.* **1999**, *70*, 773. (b) Decreau, R.; Richard, M. J.; Verrando, P.; Chanon, M.; Juliard, M. *J. Photochem. Photobiol. B Biol.* **1999**, *48*, 48. (c) Damoiseau, X.; Schuitmaker, H. J.; Lagerberg, J. W. M.; Hoebeke, M. *J. Photochem. Photobiol. B Biol.* **2001**, *60*, 50.

43. Richter, A. M.; Waterfield, E.; Jain, A. K.; Canaan, J. A.; Allison, B. A.; Levy, J. G. *Photochem. Photobiol.* **1993**, *57*, 1000.

44. (a) Li, Y.; Jang, W. D.; Nishiyama, N.; Kishimura, A.; Kawauchi, S.; Morimoto, Y.; Miake, S.; Yamashita, T.; Kikuchi, M.; Aida, T.; Kataoka, K. *Chem. Mater.* **2007**, *19*, 5557. (b) Smith, G. J. *Photochem. Photobiol.* **1985**, *41*, 23. (c) Bennet, L. E.; Chiggino, K. P.; Henderson, R. W. *J. Photochem. Photobiol. B: Biol.* **1988**, *3*, 81. (d) Cauchon, N.; Tian, H.; Langlois, R.; La Madeleine, C.; Martin, S.; Ali, H.; Hunting, D.; van Lier, J. E. *Bioconjugate Chem.* **2005**, *16*, 80. (e) Nishiyama, N.; Morimoto, Y. J.; Jang, W. D.; Kataoka, K. *Adv. Drug Deliv. Rev.* **2009**, *61*, 327.

45. (a) Jang, W. D.; Nakagishi, Y.; Nishiyama, N.; Kawauchi, S.; Morimoto, Y.; Kikuchi, M.; Kataoka, K. *J. Control. Release* **2006**, *113*, 73. (b) Nishiyama, N.; Stapert, H. R.; Zhang, G. D.; Takasu, D.; Jiang, D. L.; Nagano, T.; Aida, T.; Kataoka, K. *Bioconjugate Chem.* **2003**, *14*, 58.

46. Li, Y.; Jang, W. D.; Nishiyama, N.; Kishimura, A.; Kawauchi, S.; Morimoto, Y.; Miake, S.; Yamashita, T.; Kikuchi, M.; Aida, T.; Kataoka, K. *Chem. Mater.* **2007**, *19*, 5557.

47. Jang, W. D.; Nakagishi, Y.; Nishiyama, N.; Kawauchi, S.; Morimoto, Y.; Kikuchi, M.; Kataoka, K. *J. Control. Release* **2006**, *113*, 73.

48. Chatterjee, D. K.; Fong, L. S.; Zhang, Y. *Adv. Drug Deliv. Rev.* **2008**, *60*, 1627.

49. Konan, Y. N.; Gurny, R.; Allemann, E. *J. Photochem. Photobiol. B: Biol.* **2002**, *66*, 89.

50. McCarthy, J. R.; Perez, J. M.; Bruckner, C.; Weissleder, R. *Nano Lett.* **2005**, *5*, 2552.

51. Ricci-Junior, E.; Marchetti, J. M. *Int. J. Pharm.* **2006**, *310*, 187.

52. Chung, N. S.; Wasan, K. M. *Adv. Drug Deliv. Rev.* **2004**, *56*, 1315.

53. (a) Firestone, R. A. *Bioconjugate Chem.* **1994**, *5*, 106. (b) Thirumamgal, B. T. S.; Zhao, X. B.; Bandyopadhyaya, A. K.; Narayanasamy, S.; Johnsamuel, J.; Tiwri, R.; Golightly, D. W.; Patel, V.; Jehning, B. T.; Backer, M. V.; Barth, R. F.; Lee, R. J.; Backer, J. M.; Tjarks, W. *Bioconjugate Chem.* **2006**, *17*, 1141.

54. Konan, Y. N.; Gurny, R.; Allémann, E. *J. Photochem. Photobiol. B: Biol.* **2002**, *66*, 89.

55. Polo, L.; Valduga, G.; Jori, G.; Reddi, E. *Int. J. Biochem. Cell. Biol.* **2002**, *34*, 10.

56. Allison, B. A.; Waterfield, E.; Richter, A. M.; Levy, J. G. *Photochem. Photobiol.*, **1991**, *54*, 709.

J.; Phanstiel IV, O. *J. Med. Chem.* **2003**, *46*, 2663. (c) Breitbeil III, F.; Kaur, N.; Delcros, J.-G.; Martin, B.; Abboud, K. A.; Phanstiel IV, O. *J. Med. Chem.* **2006**, *49*, 2407. (c) Tsen, C.; Lltis, M.; Kaur, N.; Bayer, C.; Delcros, J.-G.; von Kalm, L.; Phanstiel IV, O. *J. Med. Chem.* **2008**, *51*, 324.

91. Sol, V.; Lamarche, F.; Enache, M.; Garcia, G.; Granet, R.; Guilloton, M.; Blais, J. C.; Krausz, P. *Bioorg. Med. Chem.* **2006**, *14*, 1364.

92. Lovell, J. F.; Liu, T. W. B.; Chen, J.; Zheng, G. *Chem. Rev.***2010**, ASAP article, DIO: 10.1021/cr900396q.

93. McDonnell, S. O.; Hall, M. J.; Allen, L. T.; Byrne, A.; Gallagher, W. M.; O'Shea, D. F. *J. Am. Chem. Soc.* **2005**, *127*, 16360.

94. (a) Na, K.; Bae, Y. H. *Pharm. Res.* **2002**, *19*, 681. (b) Tannock, I. F.; Rotin, D. *Cancer Res.* **1989**, *49*, 4373; (c) Stubbs, M.; McSheehy, P. M. J.; Griffiths, J. R.; Bashford, C. L. *Mol. Med. Today* **2000**, *6*, 15.

95. Gerweck, L. E. *Drug Resist. Updates* **2000**, *3*, 49.

96. (a) Friberg, E. G.; Cunderlíková, B.; Pettersen, E. O.; Moan, J. *Cancer Lett.* **2003**, *195*, 73. (b) Cunderlíková, B.; Moan, J.; Sjaastad, I. *Cancer Lett.* **2005**, *222*, 39. (c) Sharma, M.; Dube, A.; Bansal, H.; Gupta, P. K. *Photochem. Photobiol. Sci.* **2004**, *3*, 231. (d) Sharma, M.; Sahu, K.; Dube, A.; Gupta, P. K. *J. Photochem. Photobiol. B: Biol.* **2005**, *81*, 107. (e) Mojzisova, H.; Bonneau, S.; Vever-Bizet, C.; Brault, D. *Biochim. Biophys. Acta* **2007**, *1768*, 2748. (f) Bellnier, D. A.; Young, D. N.; Detty, M. R.; Camacho, S. H.; Oseroff, A. R. *Photochem. Photobiol.* **1999**, *70*, 630. (g) Arnbjerg, J.; Johnsen, M.; Nielsen, C. B.; Jørgensen, M.; Ogilby, P. R. *J. Phys. Chem. A* **2007**, *111*, 4573.

CHAPTER 2

A Tetraamino Silicon(IV) Phthalocyanine and Its N-methylated Derivatives. Synthesis, Photodynamic Activity, and pH-Dependent Behavior

2.1 Introduction

Photodynamic therapy (PDT) is an attractive modality for the treatment of malignant tumors and other diseases such as age-related macular degeneration.[1] It utilizes the combined action of photosensitizer, light, and oxygen to generate reactive oxygen species (ROS), particularly singlet oxygen, to destroy cancer cells. The therapeutic outcome greatly depends on the photosensitizer's photophysical properties and its selectivity toward cancer cells. Phthalocyanines have emerged to be a promising class of second-generation photosensitizers because of their desirable features, including strong absorption in the red visible region and high efficiency at generating singlet oxygen.[2] However, they have a strong tendency to aggregate in aqueous media, which results in some inevitable problems such as poor delivery in blood circulation, short triplet state lifetime, low fluorescence quantum yields, and low singlet oxygen quantum yields.[3] Development of hydrophilic and nonaggregated phthalocyanines is therefore important and potentially useful. To date, only few examples of water-soluble and nonaggregated phthalocyanines have been reported. Most of them they contain anionic[3b] or cationic[4] substituents. However, these ionic photosensitizers are difficult to penetrate the lipid bilayer membrane of the tumor cells resulting in poor cellular uptake.[4a,5] To our knowledge, there are very few non-ionic phthalocyanines which exist in monomeric form in physiological pH in the absence of surfactants or other disaggregating agents. We report herein a tetraamino silicon(IV) phthalocyanine (**2.1**) together with its di- and tetra-N-methylated derivatives (**2.2** and **2.3**). All these compounds are non-aggregated in aqueous solutions. Their photophysical properties, cellular uptake, and in vitro photocytotoxicity have also been investigated. Interestingly, the non-ionic compound **2.1** exhibits a pH-sensitive property. In the free amino form, the amine moieties

effectively quench the singlet excited state of phthalocyanine by photoinduced electron transfer (PET), reducing the chance of intersystem crossing and hence hindering the singlet oxygen generation. In the acidic environment, the amine moieties are protonated, which are no longer electron donors, thus restoring the singlet oxygen production.

2.2 Results and Discussion

2.2.1 Synthesis and Characterization

Scheme 2.1 shows the synthetic route to prepare phthalocyanines **2.1**-**2.3**. Treatment of the readily available silicon(IV) phthalocyanine dichloride with 2-{[2-(dimethylamino)ethyl]methylamino}ethanol in the presence of pyridine in toluene led to the formation of the disubstituted product **2.1** in satisfactory yield. Reaction of **2.1** with excess iodomethane in $CHCl_3$ gave the di-N-methylated derivative **2.2**. Further methylation of **2.2** with iodomethane in DMF gave the tetra-N-methylated derivative **2.3.** Phthalocyanine **2.1** has a good solubility in $CHCl_3$, while the cationic derivatives **2.2** and **2.3** are not soluble in $CHCl_3$. Due to the difference in solubility, all these compounds could be purified readily by washing with different solvents.

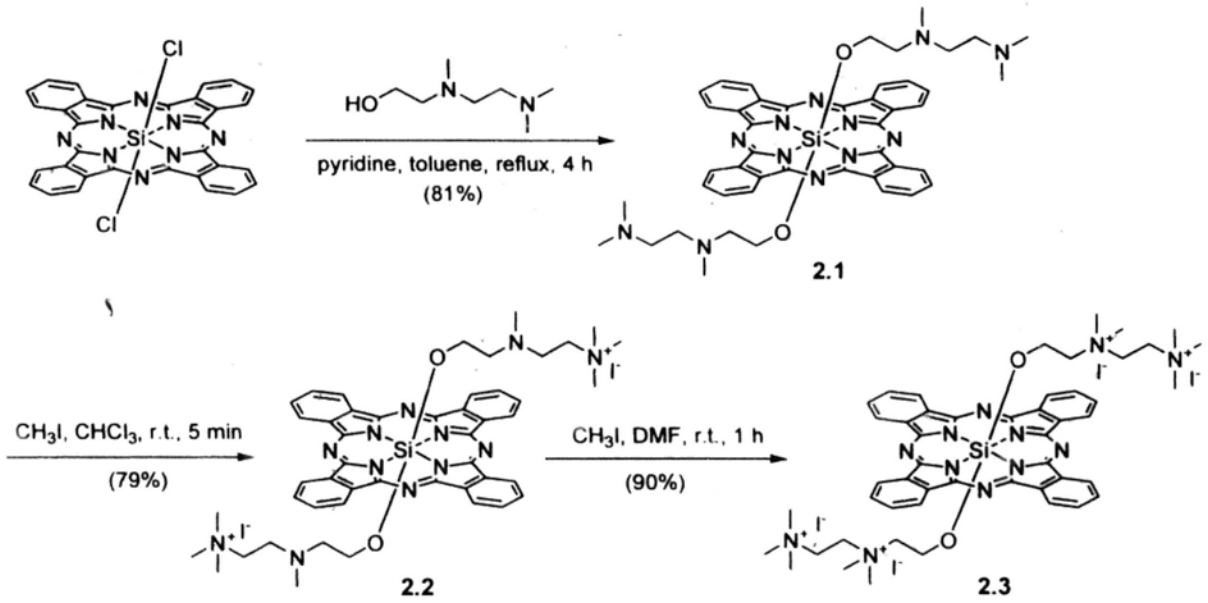

Scheme 2.1. Synthetic route of phthalocyanines **2.1-2.3**.

Compounds **2.1-2.3** were fully characterized with various spectroscopic methods and elemental analysis. The ^{1}H NMR spectra of these compounds showed two typical downfield (δ = 8-10 ppm) AA'BB' multiplets for the α and β protons of the phthalocyanine ring and upfield-shifted signals for the axial substituents due to the ring current effect. Figure 2.1 shows the ^{1}H NMR spectrum of compound **2.1** in CD_3OD. The two downfield multiplets at δ 9.57-9.61 and 8.30-8.34 are due to the phthalocyanine α and β ring protons, respectively. In addition, four well-separated triplets and two singlets are also observed for the methylene and methyl protons of the axial chains, respectively. Due to the shielding effect by the ring current, these signals are significantly shifted upfield (up to δ -1.9). For the methylated derivatives **2.2** and **2.3**, the signals of the methylene and methyl protons are shifted downfield.

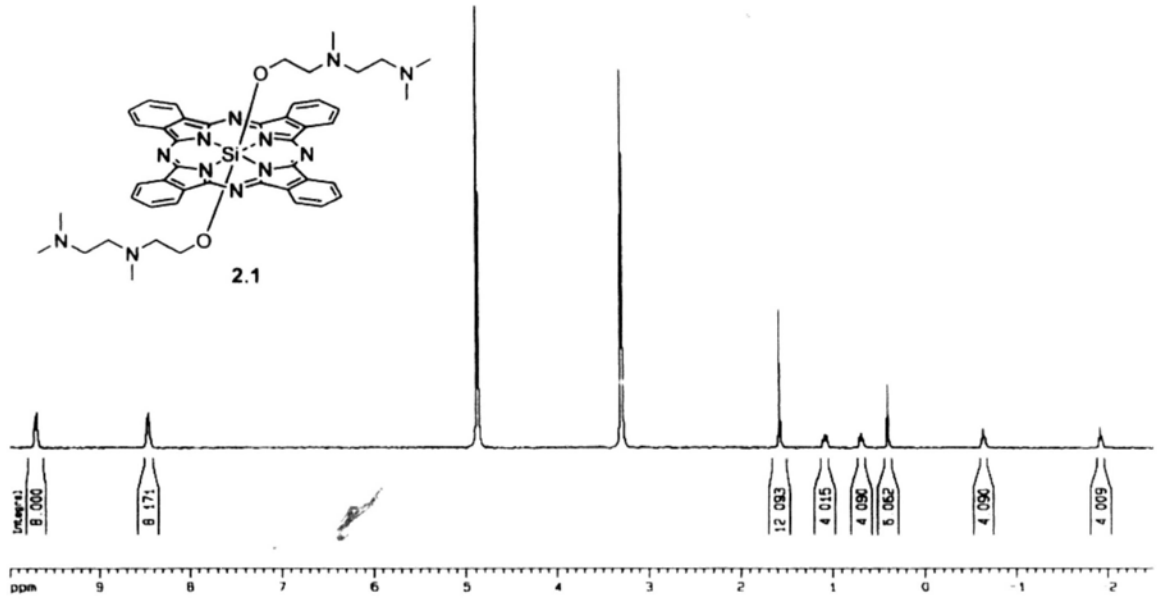

Figure 2.1. ^{1}H NMR spectrum of **2.1** in CD_3OD.

2.2.2 Electronic Absorption and Photophysical Properties

Figure 2.2 (a) and (b) show the UV-Vis spectra of compounds **2.1**-**2.3** in DMF and H_2O. The spectra are typical for non-aggregated phthalocyanines, all showing a B-band at 350-357 nm, as well as an intense and sharp Q-band at 674-684 nm. Upon excitation at 610 nm, compounds **2.1** and **2.2** showed a weak fluorescence emission with a fluorescence quantum yield (Φ_F) of 0.01-0.05 in both DMF and H_2O. By contrast, the tetracationic derivative **2.3** gave a strong fluorescence emission in both solvents (Φ_F = 0.35 in DMF; Φ_F = 0.21 in water) (Figure 2.2). The data are summarized in Table 2.1 and Table 2.2.

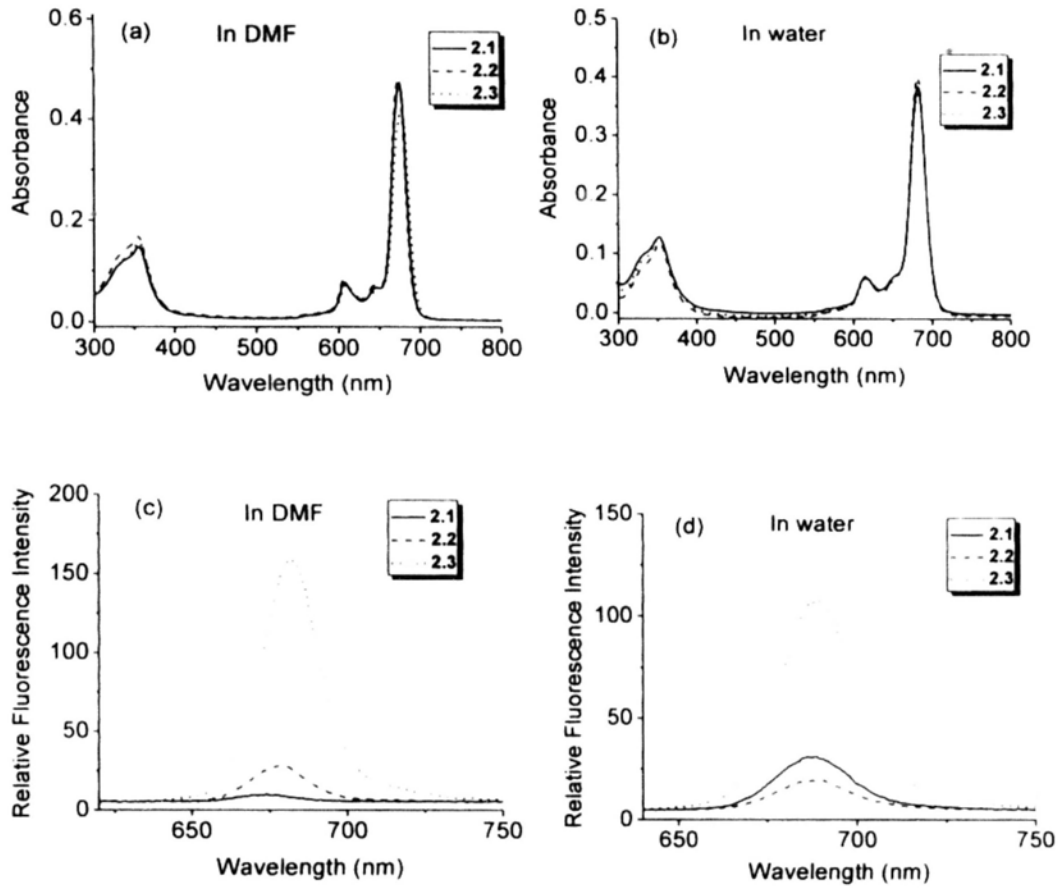

Figure 2.2. UV-Vis and fluorescence spectra of **2.1**-**2.3** (2 μM) in DMF and water (in the presence of 0.1% DMF).

To evaluate the photosensitizing efficiency of these compounds, their singlet oxygen quantum yields (Φ_Δ) were determined by a steady-state method with 1,3-diphenylisobenzofuran (DPBF) as the scavenger.[6] It was found that the tetra-cationic derivative **2.3** is an excellent singlet oxygen generator with a Φ_Δ value of 0.37 in DMF. However, compounds **2.1** and **2.2** exhibit very low Φ_Δ values (Figure 2.3). It is likely that the amino moieties in **2.1** and **2.2** quench the singlet exited state of the phthalocyanine by PET process, resulting in a weaker fluorescence emission and lower singlet oxygen generation efficiency.

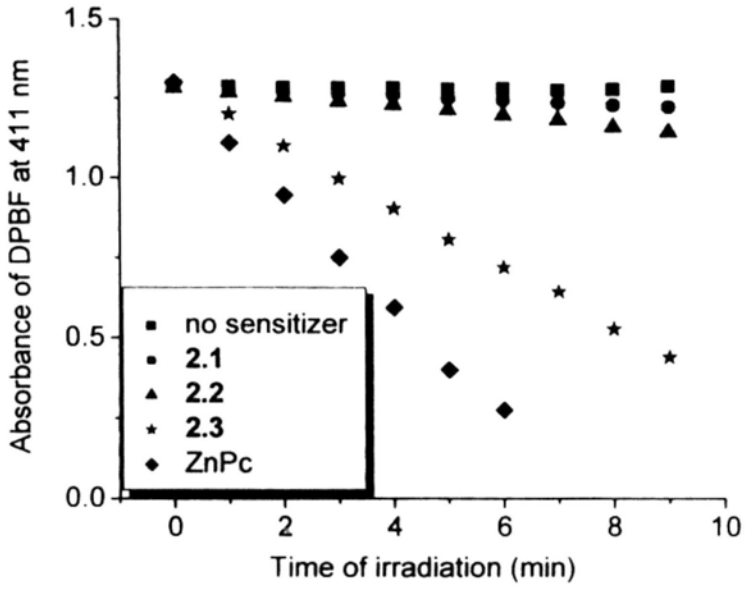

Figure 2.3. Comparison of the rate of degradation of DPBF in DMF using **2.1**-**2.3** and the unsubstituted zinc(II) phthalocyanine (ZnPc) as the photosensitizers.

Table 2.1. Electronic absorption and photophysical data for **2.1**-**2.3** in DMF.

compound	λ_{max} (nm) (log ε)	λ_{em} (nm)[a]	Φ_F[b]	Φ_Δ[c]
2.1	354 (4.87), 606 (4.57), 644 (4.51), 674 (5.36)	676	0.01	0.02
2.2	357 (4.90), 607 (4.58), 647 (4.50), 676 (5.36)	679	0.05	0.05
2.3	346 (4.85), 610 (4.53), 678 (5.28)	681	0.35	0.37

[a] Excited at 610 nm. [b] Using ZnPc in DMF as the reference [fluorescence quantum yield (Φ_F) = 0.28]. [c] Using ZnPc as the reference [singlet oxygen quantum yield (Φ_Δ) = 0.56 in DMF].

Table 2.2. Electronic absorption and photophysical data for **2.1**-**2.3** in water[a].

compound	λ_{max} (nm) (log ε)	λ_{em} (nm)[b]	Φ_F[c]
2.1	352 (4.84), 614 (4.50), 684 (5.29)	689	0.05
2.2	351 (4.89), 615 (4.53), 683 (5.31)	689	0.03
2.3	350 (4.84), 616 (4.48), 683 (5.25)	689	0.21

[a] In the presence of 0.1% DMF. [b] Excited at 610 nm. [c] Using ZnPc in DMF as the reference [fluorescence quantum yield (Φ_F) = 0.28].

The electronic absorption and fluorescence spectra of compound **2.1** were also measured in citrate buffer solutions with different pH values. There is no obvious change in the absorption spectrum of compound **2.1** at different pH (from 3.0 to 9.0) (Figure 2.4). However, the fluorescence emission spectrum changes remarkably with pH (Figure 2.5). The fluorescence intensity of **2.1** increases significantly as the pH decreases, due to protonation of the amine moieties which prevents the PET process. The fluorescence intensity increases by 6 folds when the pH decreases from 7.0 to 4.0. As the intracellular pH is in the range of 4.5-7.4,[7] it is believed that compound **2.1** is potentially useful for intracellular pH imaging. Intracellular pH plays a pivotal role in many cellular events.[7] Changes in the pH of cytoplasm or acidic organelles may be an indication of some diseases.[8]

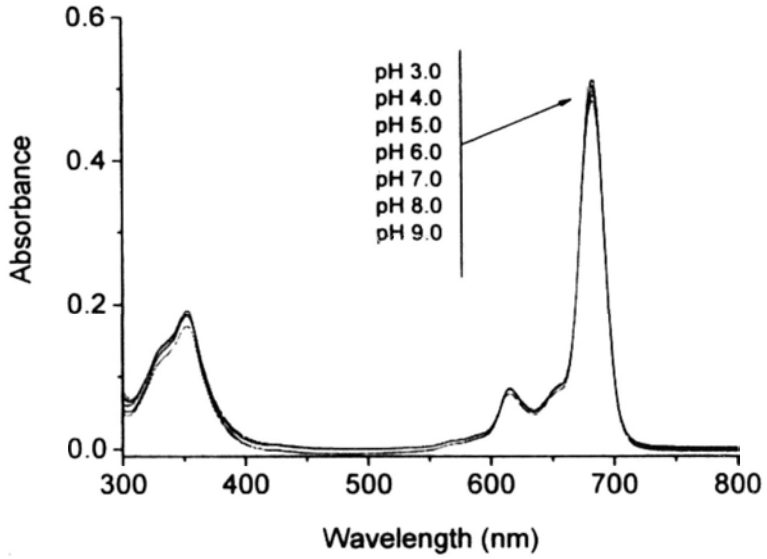

Figure 2.4. Electronic absorption spectra of **2.1** (2 μM) in citrate buffer solutions with different pH values.

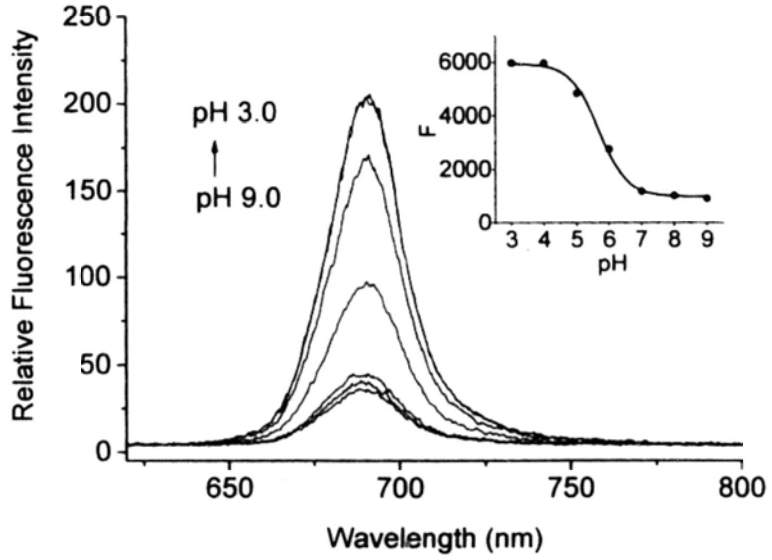

Figure 2.5. Fluorescence spectra of **2.1** (2 μM) in citrate buffer solutions with different pH values. The inset plots the relative fluorescence intensity (F) vs. the pH value. Excitation was made at 610 nm.

An additional examination was carried out to determine whether metal ions will affect the pH-sensitive property of compound **2.1**. It is well known that many metal ions such as Hg^{2+} and Zn^{2+} can coordinate with free amines.[9] As shown in Figure 2.6, the relative fluorescence intensity of compound **2.1** remains essentially unchanged in the presence of various metal ions. These results suggest that the pH-dependent property of compound **2.1** will not be affected by metal ions.

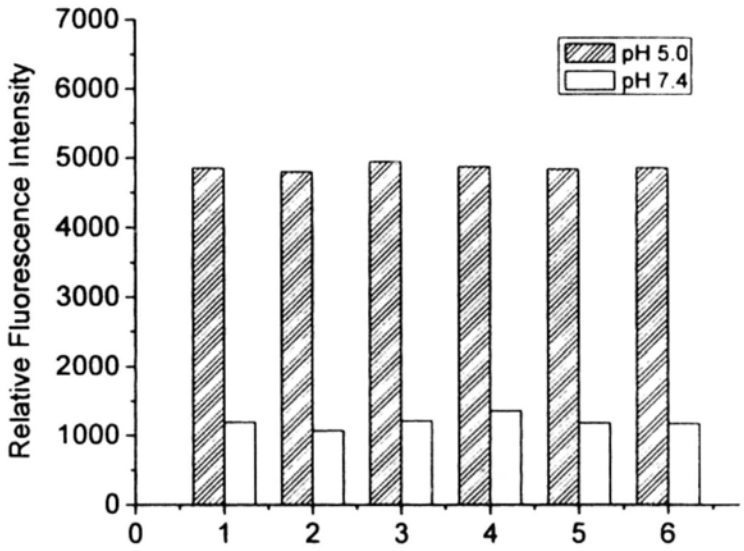

Figure 2.6. Relative fluorescence intensity of **2.1** (2 μM) in the absence or presence of 100 μM of Cu^{2+}, Zn^{2+}, Hg^{2+}, Ca^{2+}, or Mg^{2+} ions in citrate buffer solutions at pH 5.0 and 7.4. Excitation was made at 610 nm. 1: **2.1** only; 2: **2.1** + Cu^{2+}; 3: **2.1** + Zn^{2+} ; 4: **2.1** + Hg^{2+} ; 5: **2.1** + Ca^{2+} ; 6: **2.1** + Mg^{2+}.

Compound **2.1** exhibits an acid-triggered photooxidation property in DMF. In the absence of acid, this compound is not an efficient singlet oxygen generator. Its singlet oxygen quantum yield (Φ_Δ) is only 0.02 in DMF (Table 2.1). However, the singlet oxygen quantum yield increases significantly upon addition of HCl (Figure 2.7). The value of Φ_Δ increases by about 26 folds after the addition of 100 equiv. of HCl. In addition, its ability to generate superoxide radical ($O_2^{\cdot-}$) was also determined using dihydroethidium (DHE) as a probe in different buffer solutions. DHE is oxidized by superoxide radical to form ethidium, which fluoresces strongly at around 550 to 650 nm upon excitation.[10] Figure 2.8 compares the rate of oxidation of DHE by **2.1** in buffers with different pH values. It can be seen that the fluorescence intensity increases steadily upon irradiation and the rate of enhancement is about 3 folds faster at pH 6.0 compared with that at pH 7.4. It further demonstrates that compound **2.1** exhibits an acid-triggered photooxidation property in aqueous solution. On the basis that solid tumor has a lower extracellular pH profile than normal tissue,[11] the pH-controlled photocytotoxicity can provide an alternative way to enhance the selectivity of PDT. This strategy has been demonstrated briefly by O'Shea et al. using a series of amine-containing BF_2-chelated azadipyrromethenes.[12]

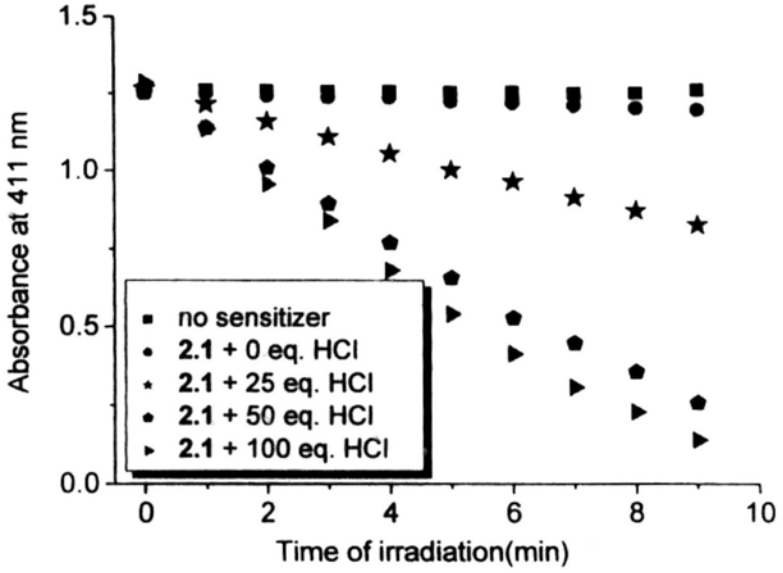

Figure 2.7. Comparison of the rate of degradation of DPBF in DMF using **2.1** (2 μM) as the photosensitizer with different amount of HCl (from 0 eq. to 100 eq.).

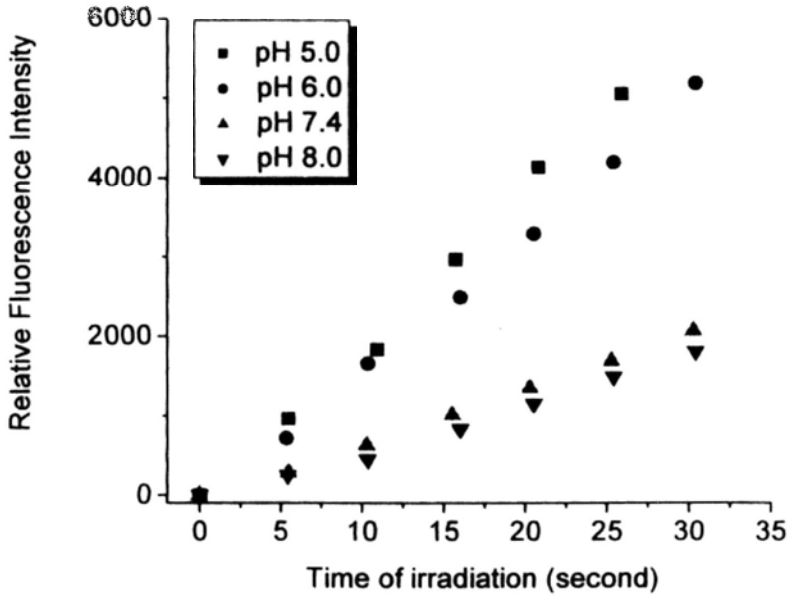

Figure 2.8. Changes in fluorescence intensity of ethidium with the irradiation time. The mixtures contained dihydroethidium (20 μM) and phthalocyanine **2.1** (4 μM) in citrate buffers with different pH.

2.2.3 In Vitro Studies

The cellular uptake of compounds **2.1**-**2.3** by human colon adenocarcinoma HT29 cells was studied by confocal laser scanning microscopy. Compound **2.1** gave a strong intracellular fluorescence emission. By contrast, the cationic derivatives **2.2** and **2.3** showed very weak intracellular fluorescence emission (Figure 2.9). Since the fluorescence quantum yields of these compounds in H_2O follow the order **2.1** $\approx$ **2.2** < **2.3**, the apparent cellular uptake of the dyes is in the order: **2.1** > **2.2** > **2.3**. These results indicate that cationic substituents hinder the cellular uptake process.

The intracellular fluorescence of **2.1** in living cells under different pH conditions was also investigated to evaluate the suitability of **2.1** as intracellular pH sensor. The HT29 cells were incubated with **2.1** (0.5 μM) at 37 °C for 30 min, then with the ionophore nigericin at different pH (5.0, 6.0, and 7.4) for 20 min. Nigericin is an H^+/K^+ antiporter, which enables the electroneutral transport of extracellular H^+ ions in exchange for intracellular K^+ ions, and can equilibrate intracellular and extracellular pH.[13] The intracellular fluorescence images of **2.1** were obtained by confocal microscopy. As shown in Figure 2.10, almost no intracellular fluorescence of compound **2.1** can be observed when the intracellular pH is 7.4. However, at pH 6.0 or 5.0, compound **2.1** gives a very strong fluorescence emission. The intensity increases by around 16 folds when the intracellular pH decreases from 7.4 to 6.0.

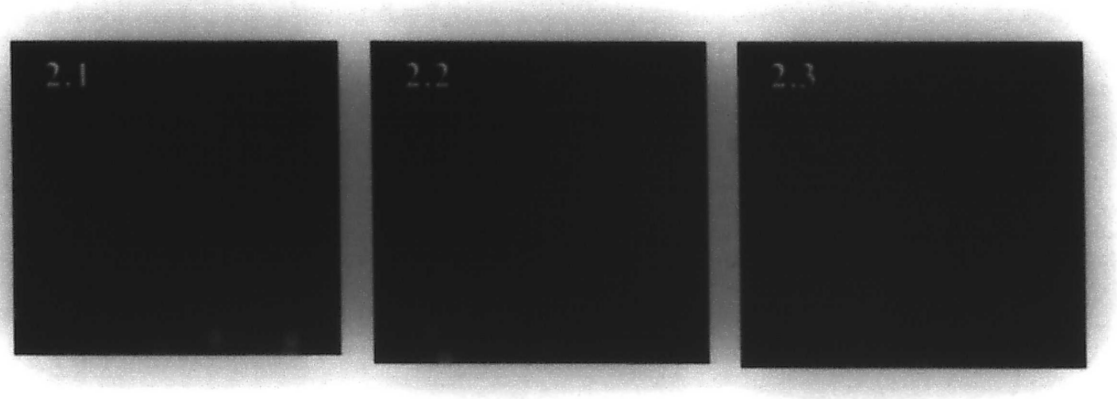

Figure 2.9. Visualization of intracellular fluorescence of HT29 cells after incubation with **2.1** (2 μM), **2.2** (8 μM), and **2.3** (8 μM) for 2 h, respectively.

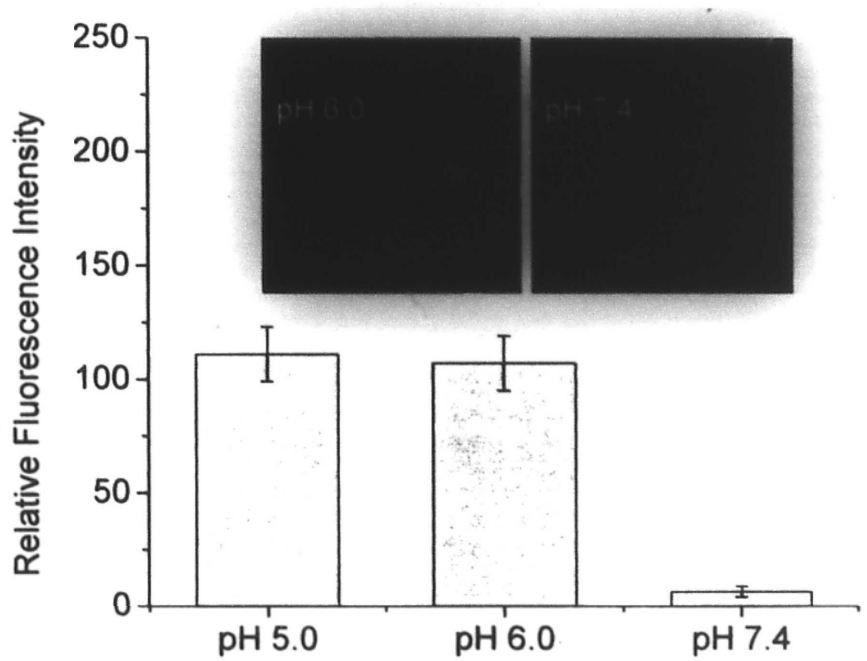

Figure 2.10. Comparison of the relative intracellular fluorescence intensity of **2.1** in different intracellular pH. Data are expressed as mean ±SD (number of cells = 25). The insert shows the intracellular fluorescence images of HT29 cells after incubation with **2.1** (0.5 μM) for 30 min, followed by 20 min incubation with nigericin solutions (25 μM) at pH 6.0 and pH 7.4.

The photodynamic activities of phthalocyanines **2.1-2.3** were investigated against HepG2 (human heptocarcinoma) and HT29 cells. The IC_{50} values defined as the dye concentration required to kill 50 % of the cells are summarized in Table 2.3. All these compounds are essentially non-cytotoxic in the dark, but upon illumination, they exhibit substantial cytotoxicity (Figures 2.11 and 2.12). Compound **2.1** exhibits a very high photocytotoxicity with IC_{50} values down to 0.01 μM against HepG2 cells which are about 20 times lower than those of **2.2** and about 180 times lower than those of **2.3**. The results suggest that the higher positive charged compounds show a lower photodynamic potency, which may be due to their lower cellular uptake as described above.

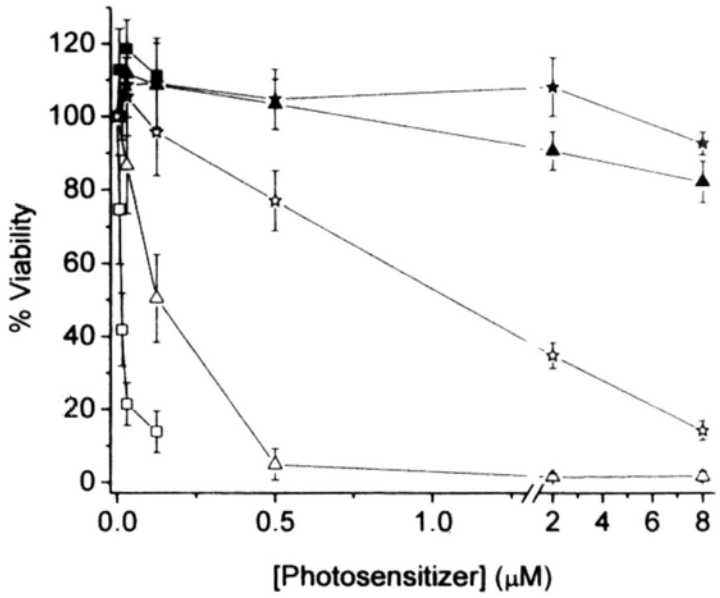

Figure 2.11. Effects of **2.1** (squares), **2.2** (triangles), and **2.3** (stars) on HepG2 in the absence (closed symbols) and presence (open symbols) of light ($\lambda > 610$ nm, 40 mW cm^{-2}, 48 J cm^{-2}). Data are expressed as mean values ± S.E.M. of three independent experiments, each performed in quadruplicate.

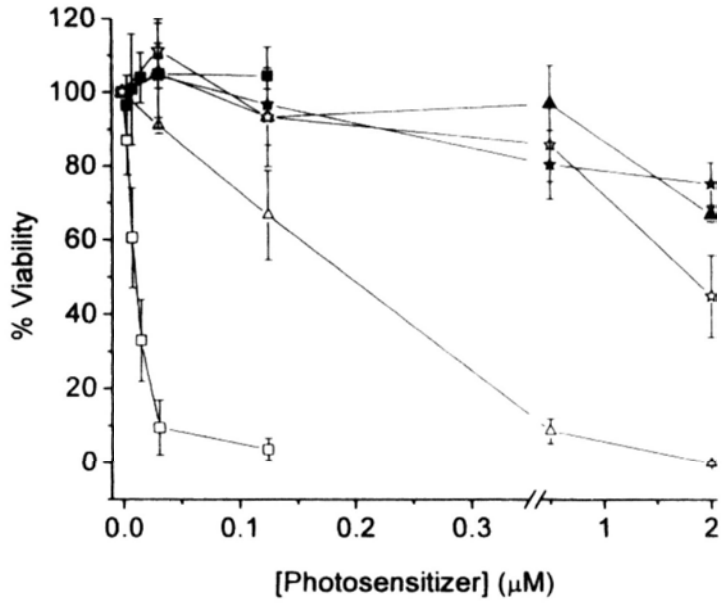

Figure 2.12. Effects of **2.1** (squares), **2.2** (triangles), and **2.3** (stars) on HT29 in the absence (closed symbols) and presence (open symbols) of light ($\lambda > 610$ nm, 40 mW cm^{-2}, 48 J cm^{-2}). Data are expressed as mean values ± S.E.M. of three independent experiments, each performed in quadruplicate.

Table 2.3. Comparison of the IC_{50} values of phthalocyanines **2.1**-**2.3** against HepG2 and HT29 cells.

Compound	IC_{50} (μM)	
	HepG2	HT29
2.1	0.01	0.01
2.2	0.23	0.13
2.3	1.82	1.47

The pH-dependent photocytotoxicity study of the pH-sensitive derivative **2.1** against HT29 and HepG2 cells was also performed. However, when the cells were maintained in an acidic medium (e.g. pH = 6.5) for several hours, most of the cells were killed even in the absence of the drug. Therefore, the study could not give meaningful results.

2.3 Conclusions

In summary, a novel silicon(IV) phthalocyanine substituted with two diamino axial groups together with its di- and tetramethylated derivatives have been synthesized and characterized. The non-ionic analogue **2.1** exists mainly as monomeric species in physiological condition and shows a high photocytotoxicity toward HT29 and HepG2 cancer cells with IC_{50} values down to 0.01 μM. Interestingly, this compound exhibits a pH-dependent behavior. The intracellular fluorescence intensity increases by 16-fold and the superoxide radical generation efficiency increases by 3-fold when the pH changes from 7.4 to 6.0. The preliminary results suggest that this compound is a promising photosensitizer of which the photodynamic activity can be modulated by changing the pH of the environment.

2.4 Experimental Section

2.4.1 General

All the reactions were performed under an atmosphere of nitrogen. DMF, pyridine, and toluene were distilled from barium oxide, calcium hydride, and sodium, respectively. All the other solvents and reagents were of reagent grade and used as received.

^1H and $^{13}C\{^1H\}$ NMR spectra were recorded on a Bruker DPX 300 spectrometer (^1H, 300; ^{13}C, 75.4 MHZ) in $CDCl_3$, CD_3OD, or DMSO-d_6. Spectra were referenced internally using the residual solvent (^1H: δ 3.31 for CD_3OD, δ 2.49 for DMSO-d_6; ^{13}C: δ 77.0 for $CDCl_3$, δ 39.5 for DMSO-d_6) resonances relative to $SiMe_4$. Electrospray ionization (ESI) mass spectra were recorded on a Thermo Finnigan MAT 95 XL mass spectrometer. Elemental analyses were performed by Shanghai Institute of Organic Chemistry, Chinese Academic of Sciences, China.

UV-Vis and steady-state fluorescence spectra were taken on a Cary 5G UV-vis-NIR spectrophotometer and a Hitachi F-4500 spectrofluorometer, respectively. The Φ_F values were determined by the equation: $\Phi_{F(sample)} = (F_{sample}/F_{ref})(A_{ref}/A_{sample})(n_{sample}^2/n_{ref}^2)\,\Phi_{F(ref)}$, where F, A, and n are the measured fluorescence (area under the emission peak), the absorbance at the excitation position (610 nm), and the refractive index of the solvent, respectively. The unsubstituted zinc(II) phthalocyanine (ZnPc) in DMF was used as the reference [$\Phi_{F(ref)} = 0.28$].[14] To minimize reabsorption of radiation by the ground-state species, the emission spectra were obtained in very dilute solutions where the absorbance at 610 nm was about 0.03. The Φ_Δ values were measured in DMF by the method of chemical quenching of DPBF using ZnPc as reference ($\Phi_\Delta = 0.56$).[15]

ROS measurements of **2.1** were performed at different pH in the citrate buffer solutions. Firstly, a mixture of phthalocyanine (4 μM) and dihydroethidium (20 μM) in buffer solution (3 mL) was prepared in a quartz cell. It was illuminated with red light from a 100 W halogen lamp with a color glass filter (Newport) cut-on 610 nm every 5 seconds and then immediately monitored by fluorescence spectroscopy (excitation at 465 nm and emission at 500-700 nm). The rate of oxidation of

dihydroethidium, which indicates the ROS generating efficiency of photosensitizers, was monitored for totally 30 seconds.

2.4.2 Synthesis

Preparation of $SiPc(OCH_2CH_2N(CH_3)CH_2CH_2N(CH_3)_2)_2$ (2.1). A mixture of 2-{[2-(dimethylamino)ethyl]methylamino}ethanol (0.42 g, 2.87 mmol), silicon(IV) phthalocyanine dichloride (0.22 g, 0.36 mmol), pyridine (0.5 mL), and toluene (15 mL) was refluxed under nitrogen for 4 h. After cooling, the solvent was evaporated in vacuo. The residue was washed with water (500 mL) and hexane (250 mL), then dissolved in CH_2Cl_2 (100 mL) and dried over anhydrous Na_2SO_4. The product (0.24 g, 81%) was obtained as a blue solid after evaporation of the solvent. ^{1}H NMR (CD_3OD): δ = 9.69-9.72 (m, 8 H, Pc-H_α), 8.45-8.48 (m, 8 H, Pc-H_β), 1.59 (s, 12 H, CH_3), 1.09 (vt, J = 7.5 Hz, 4 H, CH_2), 0.69 (vt, J = 6.9 Hz, 4 H, CH_2), 0.41 (s, 6 H, CH_3), -0.63 (t, J = 6.0 Hz, 4 H, CH_2), -1.91 (t, 4 H, J = 6.0 Hz, OCH_2); ^{13}C{^{1}H}NMR ($CDCl_3$): δ = 149.2, 136.0, 130.8, 123.6, 56.6, 56.3, 54.2, 53.1, 45.1, 41.3; HRMS (ESI): m/z calcd for $C_{46}H_{50}N_{12}O_2SiNa$ $[M+Na]^+$: 853.3841; found: 853.3842; elemental analysis (%) calcd for $C_{46}H_{50}N_{12}O_2Si$: C 66.48, H 6.06, N 20.22; found: C 66.23, H 6.02, N 20.16.

Preparation of $SiPc(OCH_2CH_2N(CH_3)CH_2CH_2N^+(CH_3)_3I^-)_2$ (2.2). A mixture of **2.1** (0.16 g, 0.19 mmol) and iodomethane (0.29 g, 2.04 mmol) in $CHCl_3$ was stirred at room temperature for 5 min. The resulting green precipitate was collected by filtration, washed thoroughly with $CHCl_3$, CH_2Cl_2, and THF, and then dried in vacuo (0.17 g, 79%). ^{1}H NMR (DMSO-d_6): δ = 9.67-9.70 (m, 8 H, Pc-H_α), 8.52-8.55 (m, 8 H, Pc-H_β), 2.18 (s, 18 H, CH_3), 2.14 (t, J = 6.6 Hz, 4 H, CH_2), 0.95 (vt, J = 7.2 Hz, 4 H, CH_2), 0.11 (s, 6 H, CH_3), -0.74 (t, J = 5.7 Hz, 4 H, CH_2), -2.06 (t, J = 5.7 Hz, 4 H,

OCH_2); $^{13}C\{^1H\}$NMR (DMSO-d_6): δ = 148.8, 134.9, 132.2, 123.7, 60.4, 55.0, 52.5, 51.8, 49.7; HRMS (ESI): m/z calcd for $C_{48}H_{56}N_{12}O_2Si$ $[M-2I]^{2+}$: 430.2204; found: 430.2208; elemental analysis (%) calcd for $C_{48}H_{58}N_{12}O_3SiI_2$ (**2.2**·H_2O): C 50.89, H 5.16, N 14.84; found: C 50.51, H 5.48, N 14.50.

Preparation of SiPc($OCH_2CH_2N^+(CH_3)_2I^-CH_2CH_2N^+(CH_3)_3I^-)_2$ (2.3) A mixture of **2.2** (0.11 g, 0.10 mmol) and iodomethane (2.84 g, 20.01 mmol) in DMF (10 mL) was stirred at room temperature for 1 h. The mixture was then poured into diethyl ether (100 mL) to give green precipitate, which was filtered and washed thoroughly with $CHCl_3$, CH_2Cl_2, THF, and diethyl ether. The residue was then dried in vacuo (0.13 g, 90%). ^1H NMR (DMSO-d_6): δ = 9.73-9.76 (m, 8 H, Pc-H_α), 8.58-8.60 (m, 8 H, Pc-H_β), 2.60 (vt, 4 H, J = 7.5 Hz, CH_2), 2.45 (s, 18 H, CH_3), 2.06 (vt, J = 6.9 Hz, 4 H,CH_2), 0.76 (s, 12 H, CH_3), 0.56 (s, 4 H, CH_2), -1.73 (s, 4 H, OCH_2); $^{13}C\{^1H\}$NMR (DMSO-d_6): δ = 148.9, 134.7, 132.5, 124.0, 62.6, 55.7, 55.5, 52.2, 49.2, 48.2; HRMS (ESI): m/z calcd for $C_{50}H_{62}N_{12}O_2Si$ $[M-4I]^{4+}$: 222.6217; found: 222.6218; elemental analysis (%) calcd for $C_{50}H_{70}N_{12}O_6SiI_4$ (**2.3**·$4H_2O$): C 40.83, H 4.80, N 11.43; found: C 41.14, H 4.93, N 11.37.

2.4.3 In Vitro Studies

Cell Lines and Culture Conditions. The HT29 human colorectal carcinoma cells (from ATCC, no. HTB-38) were maintained in Dulbecco's modified Eagle's medium (DMEM; Invitrogen, no.10313-021) supplemented with fetal calf serum (10%), penicillin-streptomycin (100 units mL^{-1} and 100 μg mL^{-1}, respectively), L-glutamine (2 mM), and transferrin (10 μg mL^{-1}). The HepG2 human hepatocarcinoma cells (from ATCC, no. HB-8065) were maintained in RPMI medium 1640 (Invitrogen, no.

23400-021) supplemented with fetal calf serum (10%) and penicillin-streptomycin (100 units mL^{-1} and 100 μg mL^{-1}, respectively). Approximately 3×10^4 (for HT29) or 4×10^4 (for HepG2) cells per well in these media were inoculated in 96-multiwell plates and incubated overnight at 37 °C in a humidified 5% CO_2 atmosphere.

Photocytotoxicity Assay. Phthalocyanines **2.1-2.3** were first dissolved in DMF to give 1.6 mM solutions, which were diluted to appropriate concentrations with the culture medium. The cells, after being rinsed with PBS, were incubated with 100 μL of these phthalocyanine solutions for 2 h at 37 °C under 5% CO_2. The cells were then rinsed again with PBS and refed with 100 μL of the culture medium before being illuminated at ambient temperature. The light source consisted of a 300 W halogen lamp, a water tank for cooling, and a color glass filter (Newport) cut-on 610 nm. The fluence rate ($\lambda > 610$ nm) was 40 mW cm^{-2}. An illumination of 20 min led to a total fluence of 48 J cm^{-2}.

Cell viability was determined by means of the colorimetric MTT assay.[16] After illumination, the cells were incubated at 37 °C under 5% CO_2 overnight. An MTT (Sigma) solution in PBS (3 mg mL^{-1}, 50 μL) was added to each well followed by incubation for 2 h under the same environment. A solution of sodium dodecyl sulfate (SDS, Sigma; 10% by weight, 50 μL) was then added to each well. The plate was incubated in an oven at 60 °C for 30 min, then 80 μL of *iso*-propanol was added to each well. The plate was agitated on a Bio-Rad microplate reader at ambient temperature for 10 s before the absorbance at 540 nm at each well was taken. The average absorbance of the blank wells, which did not contain the cells, was subtracted from the readings of the other wells. The cell viability was then determined by the

following equation: % viability = $[\sum(A_i/A_{control} \times 100)]/n$, where A_i is the absorbance of the ith data (i = 1, 2, ..., n), $A_{control}$ is the average absorbance of the control wells in which the phthalocyanine was absent, and n (= 4) is the number of the data points.

Cellular Uptake Studies. About 6.0×10^4 HT29 cells in the culture medium (2 mL) were seeded on a coverslip and incubated overnight at 37 °C under 5% CO_2. The medium was then removed. The cells were incubated with a solutions of **2.1**-**2.3** in the medium (2 μM for **2.1**, 8 μM for **2.2** and **2.3**, 2 mL) for 2 h under the same conditions. Then the cells were rinsed with PBS and viewed with a Leica SP5 confocal microscope equipped with a 633 helium neon laser. Phthalocyanies **2.1**-**2.3** were excited at 633 nm and monitored at 640-700 nm. Images were digitized and analyzed using Leica Application Suite Advanced Fluorescence.

Effect of pH on the Intracellular Fluorescence of Photosensitizer. About 1.2×10^4 HT29 cells in the growth medium (2 mL) were seeded on a coverslip and incubated overnight at 37 ℃ under 5 % CO_2. The medium was removed, then the cells were incubated with a solution of phthalocyanine **2.1** in the medium (0.5 μM, 2 mL) for 30 min under the same conditions. The cells were then rinsed with PBS and incubated with nigericin (Sigma) in PBS (25 μM, 2 mL) at different pH (pH 7.4, pH 6.0, and pH 5.0) for further 20 min under the same conditions. The cells were viewed with a Leica SP5 confocal microscope equipped with a 633 nm helium neon laser (Laser power = 15 %, Gain = 750 V). Emission signals from 640-700 nm were collected and the images were digitized and analyzed by Leica Application Suite,

Advanced Fluorescence. The intracellular fluorescence intensities of cells (totally 25 cells for each pH solution) were also determined.

2.5 References

1 (a) Dolmans, D. E. J. G. J.; Fukumura, D.; Jain, R. K. *Nat. Rev. Cancer* **2003**, *3*, 380. (b) Tian, Y. Y.; Wang, L. L.; Wang, W. *Laser Phys.* **2008**, *18*, 1119. (c) Serra, A.; Pineiro, M.; Pereira, N.; Gonsalves, A. R.; Laranjo, M.; Abrantes, M.; Botelho, F. *Oncol. Rev.* **2008**, *2* , 235.

2 (a) Lunardi, C. N.; Tedesco, A. C. *Curr. Org. Chem.* **2005**, *9*, 813. (b) Taquet, J.-P.; Frochot, C.; Manneville, V.; Barberi-Heyob, M. *Curr. Org. Chem.* **2007**, *14*, 1673.

3 (a) Choi, C.-F.; Tsang, P.-T.; Huang, J.-D.; Chan, E. Y. M.; Ko, W.-H.; Fong, W.-P.; Ng, D. K. P. *Chem. Commun.* **2004**, 2236. (b) Liu, W.; Jensen, T. J.; Fronczek, F. R.; Hammer, R. P.; Smith, K. M.; Vicente, M. G. H. *J. Med. Chem.* **2005**, *48*, 1033. (c) Lo, P.-C.; Chan, C. M. H.; Liu, J.-Y.; Fong, W.-P.; Ng, D. K. P. *J. Med. Chem.* **2007**, *50*, 2100.

4 (a) Lo, P.-C.; Huang, J.-D.; Cheng, D. Y. Y.; Chan, E. Y. M.; Fong, W.-P.; Ko, W.-H.; Ng, D. K. P. *Chem. E. J.* **2004**, *10*, 4831. (b) Jiang, X.-J.; Huang, J.-D.; Zhu, Y.-J.; Tang, F.-X.; Ng, D. K. P.; Sun, J.-C. *Bioorg, Med. Chem. Lett.* **2006**, *16*, 2450. (c) Li, H.; Jensen, T. J.; Fronczek, F. R.; Vicente, M. G. H. *J. Med. Chem.* **2008**, *51*, 502.

5 (a) Bose, B.; Dube, A. *J. Photochem. Photobiol. B: Biol.* **2008**, *93*, 32. (b) Bronshtein, I.; Smith, K. M.; Ehrenberg, B. *Photochem. Photobiol.* **2005**, *81*, 446.

6 Maree, M. D.; Kuznetsova, N.; Nyokong, T. *J. Photochem. Photobiol. A: Chem.* **2001**, *140*, 117.

7 Tang, B.; YU, F.; Li, P.; Tong, L.; Duan, X.; Xie, T.; Wang, X. *J. Am. Chem. Soc.* **2009**, *131*, 3016.

8 Schindler, M.; Grabski, S.; Hoff, E.; Simon, S. M. *Biochemistry* **1996**, *35*, 2811.

9 (a) Tang, B.; Liu, X.; Xu, K.; Huang, H.; Yang, G.; An, L. *Chem. Commun.* **2007**, 3726. (b) Callan, J. F.; de Silva, A. P.; Magri, D. C. *Tetrahedron* **2005**, *61*, 8551.

10 Halliwell, B.; Whiteman, M. *Br. J. Pharmacol.* **2004**, *142*, 231.

11 (a) Gerweck, L. E. *Drug Resist. Updates* **2000**, *3*, 49. (b) Lee, E. S.; Gao, Z.; Bae, Y. H. *J. controlled Release* **2008**, *132*, 164.

12 McDonnell, S. O.; Hall, M. J.; Allen, L. T.; Byrne, A.; Gallager, W. M.; O'Shea, D. F. *J. Am. Chem. Soc.* **2005**, *127*, 16360.

13 (a) Jähde, E.; Glüsenkamp, K.-H.; Rajewsky, M. F. *Cancer Chemother. Pharmacol.* **1991**, *27*, 440. (b) Varnes, M. E.; Bayne, M. T.; Bright, G. R. *Photochem. Photobiol.* **1996**, *64*, 853.

14 Scalise, I.; Durantini, E. N. *Bioorg. Med. Chem.* **2005**, *13*, 3037.

15 Maree, M. D.; Kuznetsova, N.; Nyokong, T. *J. Photochem. Photobiol. A: Chem.* **2001**, *140*, 117.

16 MTT = 3-(4,5-dimethyl-2-thiazolyl)-2,5-diphenyl-2*H*-tetrazolium bromide. Tada, H.; Shiho, O.; Kuroshima, K.; Koyama, M.; Tsukamoto, K. *J. Immunol. Methods* **1986**, *93*, 157.

CHAPTER 3

Phthalocyanine-Aryl Polyamine Conjugates as pH-Controlled Photosensitizers for Photodynamic Therapy

3.1 Introduction

Photodynamic therapy (PDT) is a noninvasive therapeutic modality for a variety of premalignant and malignant diseases. A introduction has been mentioned in Chapters 1. Recently, considerable effort has been devoted to improving the selectivity of phtotosensitizers toward malignant tissues. For targeted delivery of photosensitizers to cancer cells, various approaches have been explored. These include conjugation of photosensitizers to tumor-specific vectors such as antibodies, synthetic peptides, epidermal growth factor, and adenoviruses,[1] and encapsulation of photosensitizers in colloidal carriers such as liposomes, polymeric micelles, and silica nanoparticles.[2] An alternative strategy takes advantage of the lower extracellular pH in tumors (ca. 6.8) as compared to normal tissues (ca. 7.3).[3] The different pH environment may change the stability, aggregation tendency, lipophilicity, and cellular uptake of the photosensitizers, thereby offering a new level of selectivity.

The pH-dependent behavior of several classes of photosensitizers such as porphyrins,[4] chlorins,[4,5] chalcogenopyrylium dyes,[6] and phenylene vinylenes[7] has been briefly examined. Recently, O'Shea et al. have reported a novel series of amine-containing BF_2-chelated azadipyrromethenes which can switch on and off the singlet oxygen production in DMF through changing the pH environment.[8] Upon addition of HCl, the singlet oxygen generation rates increase by up to 10 folds. In addition to pH-sensitive photosensitizers, pH-responsive fluorescence probes[9] and polymeric micelles[10] have also received much current attention because of their potential application in in vitro and in vivo cancer imaging, and targeted delivery of chemotherapeutic agents, respectively. All of them work on the basis of the slightly acidic extracellular pH environment of solid tumors.

In Chapter 2, we report a silicon(IV) phthalocyanine substituted with two diamino axial groups. This compound exhibits a pH-dependent behavior and is a promising photosensitizer of which the photodynamic activity can be modulated by changing the pH of the environment. As a continuing effort, we report herein another series of pH-controlled photosensitizers in which a silicon(IV) phthalocyanine core is axially substituted with aryl polyamine moieties (compounds **3.1**-**3.5**). These substituents can modulate the photophysical and photosensitizing properties of the macrocycles in both organic and aqueous media at different pH values. An acid-enhanced fluorescence emission effect has also been observed at the cellular level. These compounds therefore serve as potential tumor-selective photosensitizers for PDT. The pH-dependent behavior as well as the in vitro photodynamic activity of these compounds is reported.

3.2 Results and Discussion

3.2.1 Synthesis and Characterization

Scheme 3.1 shows the synthetic route used to prepare phthalocyanines **3.1**-**3.5**. Treatment of hydroxyamines **3.6**-**3.7** with benzaldehydes **3.8**-**3.11** and $NaBH_4$ led to reductive amination giving compounds **3.12**-**3.16** in good yields. The procedure was similar to that reported earlier for the preparation of bis(2-pyridylmethyl)amine.[14] These compounds were then treated with silicon(IV) phthalocyanine dichloride (**3.17**) in the presence of pyridine in toluene to give the disubstituted products **3.1**-**3.5**, which were purified by extraction with CH_2Cl_2 followed by recrystallization from a mixture of $CHCl_3$ and 1-hexane (1:4 v/v). All the new compounds were characterized with various spectroscopic methods and elemental analysis (or accurate mass measurement for hydroxyamines **3.13**-**3.16**).

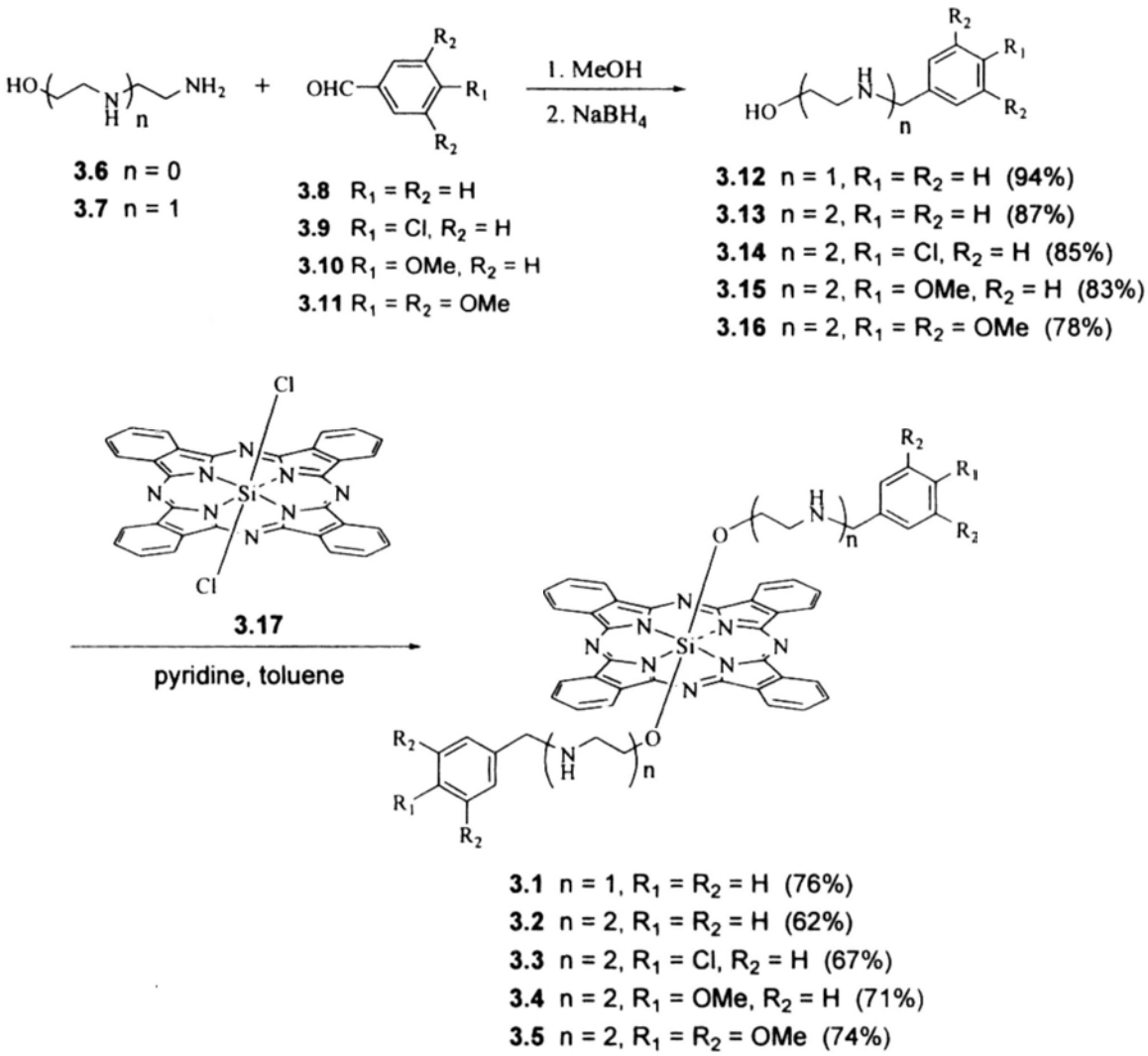

3.6 n = 0
3.7 n = 1

3.8 $R_1 = R_2 = H$
3.9 R_1 = Cl, R_2 = H
3.10 R_1 = OMe, R_2 = H
3.11 $R_1 = R_2$ = OMe

3.12 n = 1, $R_1 = R_2 = H$ (94%)
3.13 n = 2, $R_1 = R_2 = H$ (87%)
3.14 n = 2, R_1 = Cl, R_2 = H (85%)
3.15 n = 2, R_1 = OMe, R_2 = H (83%)
3.16 n = 2, $R_1 = R_2$ = OMe (78%)

3.1 n = 1, $R_1 = R_2 = H$ (76%)
3.2 n = 2, $R_1 = R_2 = H$ (62%)
3.3 n = 2, R_1 = Cl, R_2 = H (67%)
3.4 n = 2, R_1 = OMe, R_2 = H (71%)
3.5 n = 2, $R_1 = R_2$ = OMe (74%)

Scheme 3.1. Preparation of phthalocyanines **3.1-3.5**.

The ^{1}H NMR spectra of all phthalocyanines **3.1-3.5** showed two typical downfield-shifted AA'BB' multiplets at δ 8-10 for the α and β protons of the phthalocyanine ring. The axial ethylamino linker resonated as two triplets at very upfield positions (down to δ = -2 ppm) due to the shielding effect of the phthalocyanine ring. Figure 3.1 shows the ^{1}H NMR spectrum of compound **3.3** in $CDCl_3$ as an example. The two downfield multiplets at δ 9.57-9.61 and 8.30-8.34 are due to the phthalocyanine α and β ring protons, respectively. The four triplets at δ 1.55, 0.89. -0.34, and -1.97 are due to the ethylene protons, which are shielded by the

phthalocyanine ring current. A singlet at δ 3.21 (for the benzyl CH_2 protons) and two doublets at δ 7.19 and 6.89 (for *p*-phenylene protons) are also observed.

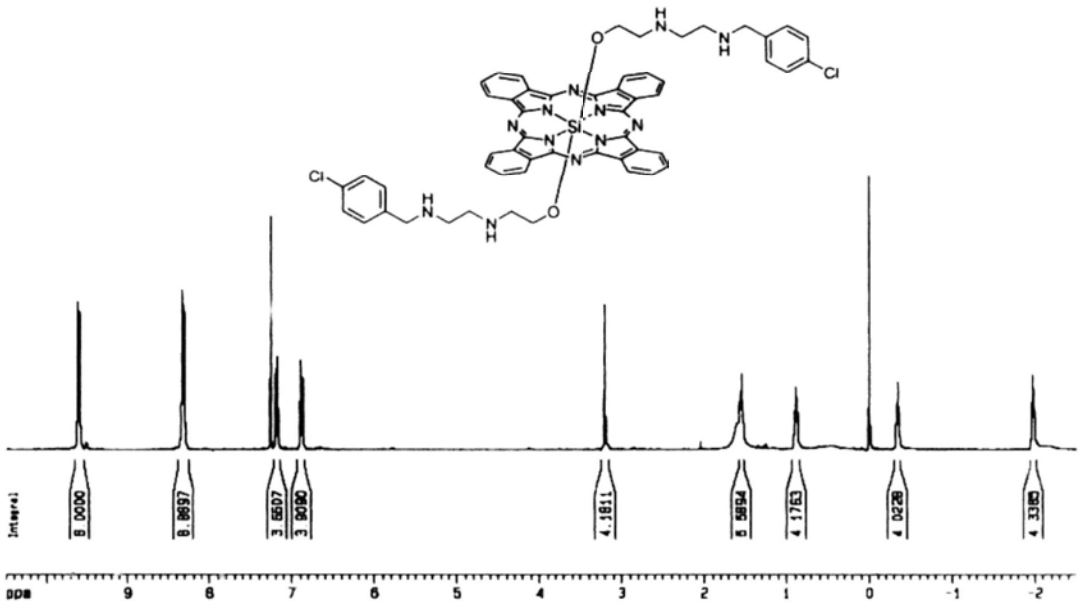

Figure 3.1. ^{1}H NMR spectrum of **3.3** in $CDCl_3$.

3.2.2 Electronic Absorption and Photophysical Properties

UV-Vis spectra of phthalocyanines **3.1-3.5** were measured in DMF and the data are summarized in Table 3.1. The spectra are typical for nonaggregated phthalocyanines, all showing a Soret band at 354 nm, two vibronic bands at 607 nm and 644 nm, together with a sharp Q band at 674 nm [see the spectra of **3.1** (Figure 3.2) given as an example]. The absorption positions of all these compounds are identical, suggesting that the axial substituents do not perturb the phthalocyanine π system. Upon excitation at 610 nm, these compounds showed a weak fluorescence emission at 675-677 nm with a fluorescence quantum yield (Φ_F) of 0.01-0.04 relative to ZnPc. The weak fluorescence is due to the presence of amino moieties, which

quench the singlet excited state of the phthalocyanine core by intramolecular photoinduced electron transfer (PET). Upon addition of HCl (0.6 mM), the emission band of all the compounds shifted slightly to the red (by 3-5 nm) and increased greatly in intensity (Figure 3.3). The fluorescence quantum yield increased significantly to 0.26-0.30 (Table 3.1). The great changes can be attributed to protonation of the amino moieties under an acidic environment, which inhibits the PET process.[8,9c]

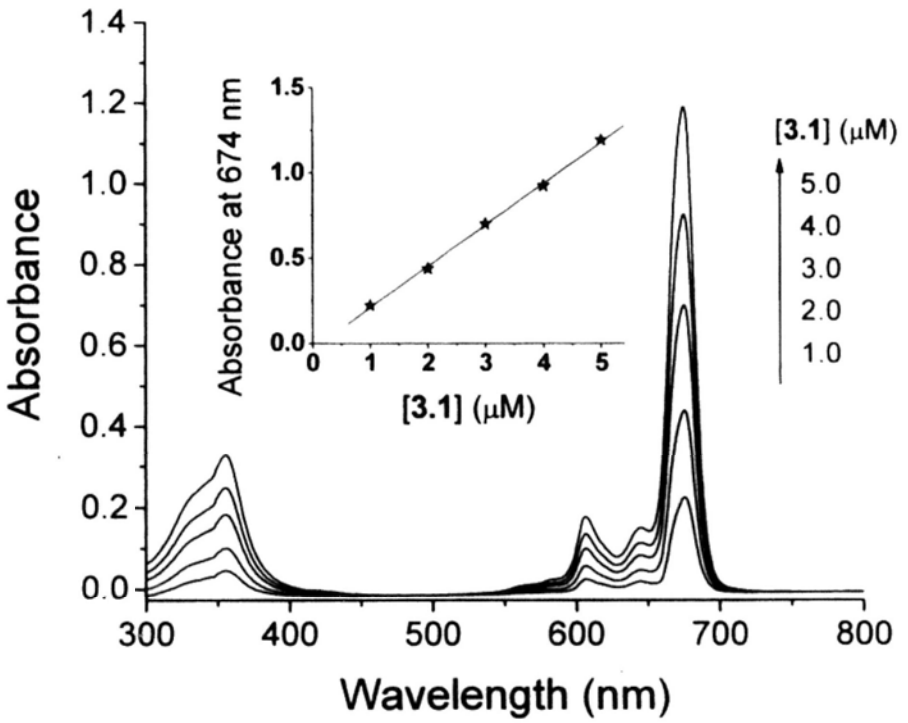

Figure 3.2. UV-Vis spectra of **3.1** in DMF. The inset plots the Q-band absorbance versus the concentration of **3.1**.

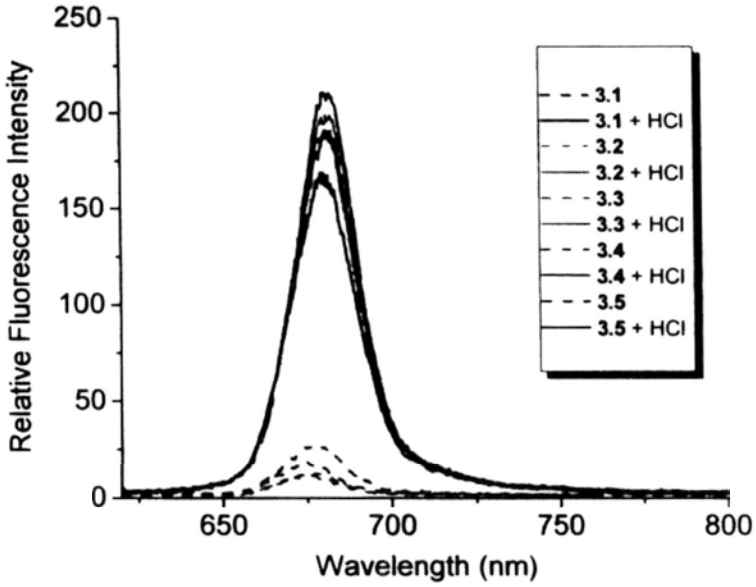

Figure 3.3. Fluorescence spectra of **3.1-3.5** (1 μM) in the absence (dash lines) and presence (solid lines) of HCl (0.6 mM) in DMF.

The absorption and fluorescence spectra of **3.1-3.5** were also measured in citrate buffer solutions with different pH. Figure 3.4 shows the UV-Vis spectra of **3.3** in the buffers given as an example. It can be seen that the Q band remains sharp and intense at pH 4-6. However, it becomes weaker and broadened when the pH increases to 7-8. It is likely that under acidic conditions, the amino moieties are protonated. The charged substituents induce mutual repulsion reducing the aggregation of the phthalocyanine. This results in the occurrence of a sharp and intense monomeric Q band. By contrast, the compound remains aggregated under neutral and slightly alkaline conditions in the buffers leading to a broad and weak Q band. Figure 3.5 shows the fluorescence spectra of **3.3** in citrate buffer solutions. It can be seen that almost no fluorescence emission is observed at pH 8.0. When pH value decreases, this compound gives strong fluorescence emission.

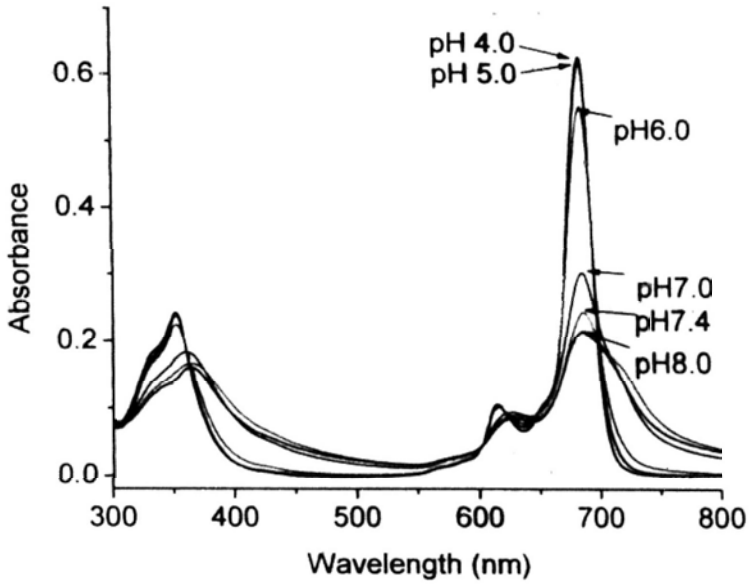

Figure 3.4. UV-Vis spectra of **3.3** (3 μM) in citrate buffer solutions with different pH.

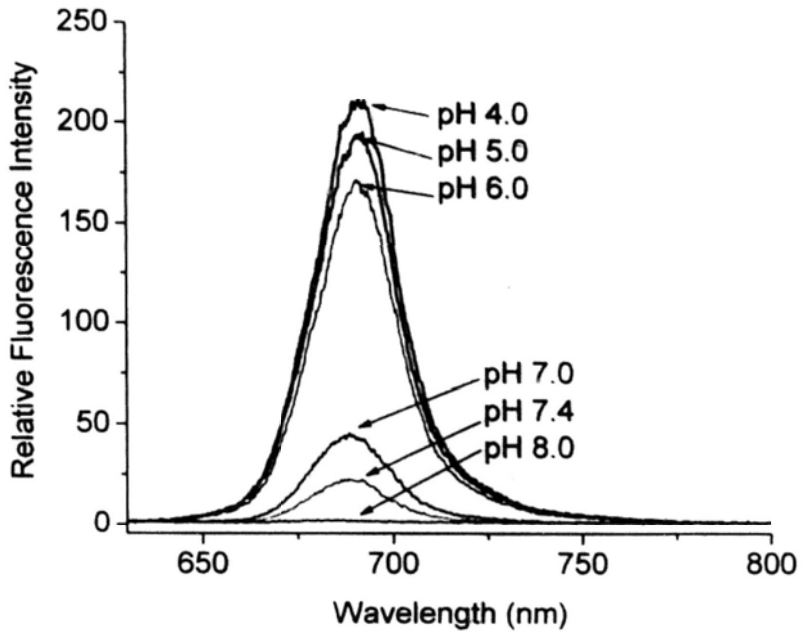

Figure 3.5. Fluorescence spectra of **3.3** (3 μM) in citrate buffer solutions with different pH. Excitation was made at 610 nm.

All of the phthalocyanines **3.1-3.5** showed a similar pH-dependent behavior, but the extent was different for different compounds. Figure 3.6 plots the variation of the Q-band absorbance at 684 nm with the pH value for all these compounds. Generally, the absorbance decreases as the pH increases. Compound **3.3** shows the most distinct decrease in absorbance when the pH increases from 6.0 to 7.4, which can roughly mimic the environment around tumors and normal tissues, respectively. The change in fluorescence intensity with pH for all these compounds also follows a similar trend as depicted in Figure 3.7. Again, compound **3.3** shows the most remarkable change in the region between pH 6.0 to 7.4. The results show that the axial substituents of **3.1-3.5** can modulate the pH-dependent absorption and emission properties of the phthalocyanines in aqueous media, probably through adjustment of the aggregation tendency, and that compound **3.3** exhibits the most desirable pH-dependent spectral changes.

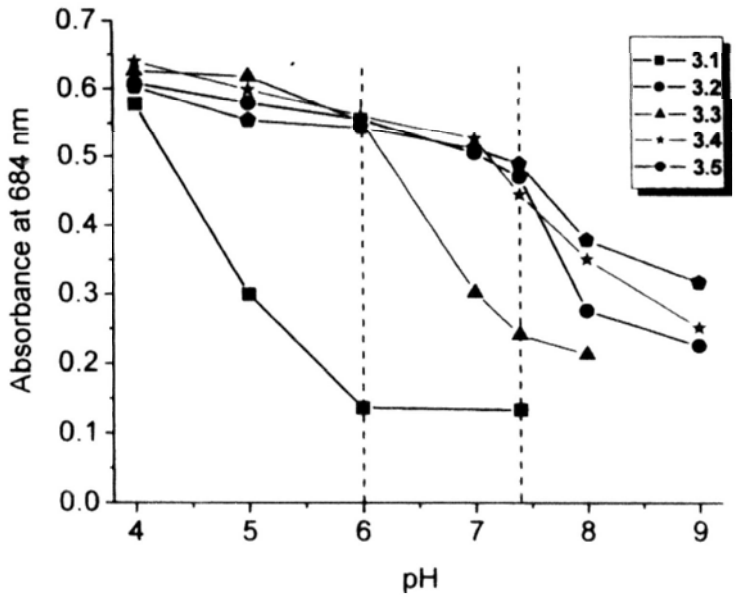

Figure 3.6. Change in the Q-band absorbance at 684 nm with pH for **3.1-3.5** (3 μM) in citrate buffer solutions.

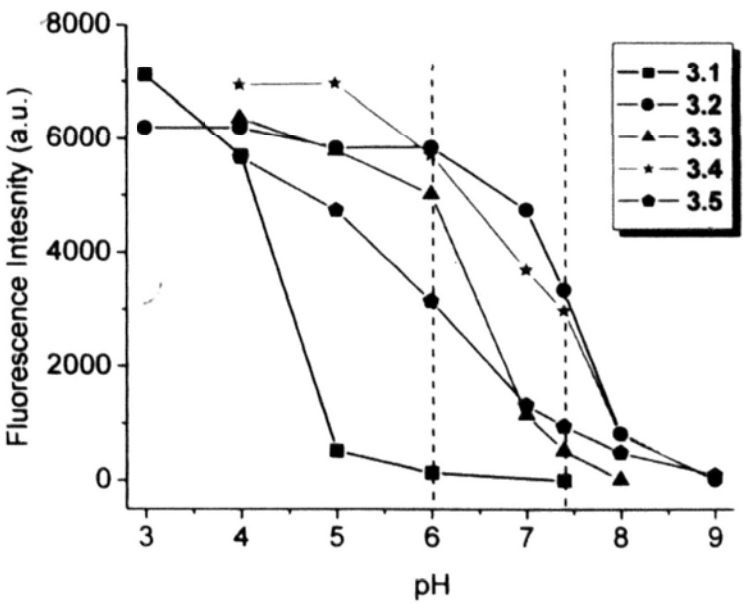

Figure 3.7. Change in the fluorescence intensity with pH for **3.1-3.5** (3 μM) in citrate buffer solutions upon excitation at 610 nm.

To evaluate the photosensitizing efficiency of these compounds, their singlet oxygen quantum yields (Φ_Δ) were determined by a steady-state method using 1,3-diphenylisobenzofuran (DPBF) as the scavenger.[12] The concentration of the quencher was monitored spectroscopically at 414 nm with time (Figure 3.8), from which the values of Φ_Δ could be determined. As shown in Table 3.1, all of the phthalocyanines **3.1**-**3.5** can generate singlet oxygen in DMF but with a low efficiency. The values of Φ_Δ are only 0.03 to 0.07 relative to ZnPc. However, in the presence of HCl (600 equiv.), their Φ_Δ values are greatly enhanced to 0.34-0.65 and follow the order **3.1** ≈ **3.2** ≈ **3.4** < **3.5** < **3.3** (Table 3.1). The significant enhancement can again be attributed to the protonation of the amino moieties, which inhibits the PET process and promotes the intersystem crossing and eventually the singlet oxygen formation.

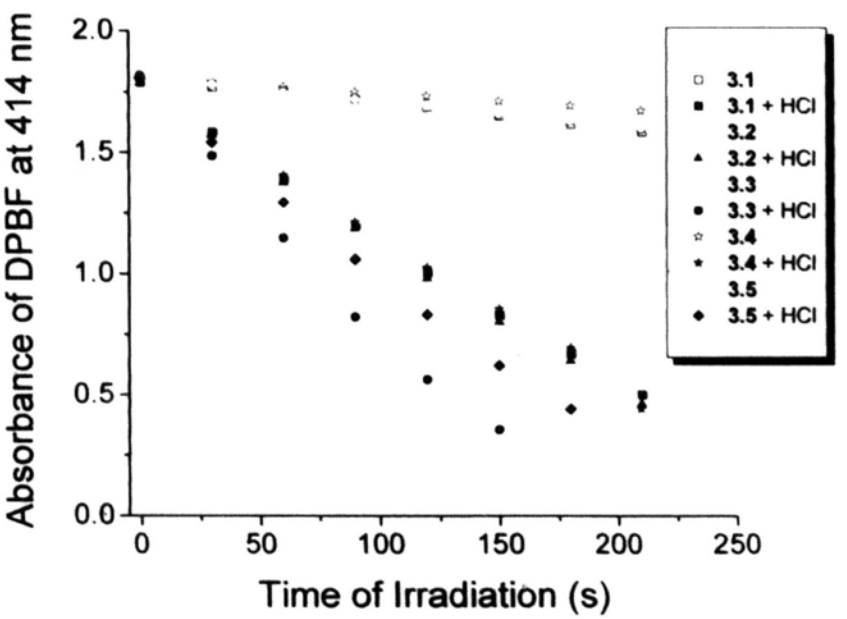

Figure 3.8. Comparison of the rate of photodegradation of DPBF in DMF (open symbols) and in acidic DMF (in the presence of 1.2 mM HCl, closed symbols) using **3.1**-**3.5** (2 μM) as the photosensitizers.

Table 3.1. Electronic absorption and photophysical data for **3.1-3.5** in DMF.

Dye	λ_{max} (nm) (log ε)	In the Absence of HCl			In the Presence of HCl[a]		
		λ_{em}[b]	Φ_F[c]	Φ_Δ[d]	λ_{em}[b]	Φ_F[c]	Φ_Δ[d]
3.1	354 (4.85), 607 (4.59), 644 (4.52), 674 (5.38)	676	0.04	0.06	681	0.30	0.34
3.2	354 (4.80), 607 (4.54), 644 (4.47), 674 (5.34)	677	0.01	0.03	680	0.28	0.38
3.3	354 (4.74), 607 (4.49), 644 (4.43), 674 (5.30)	676	0.01	0.07	681	0.30	0.65
3.4	354 (4.84), 607 (4.56), 644 (4.49), 674 (5.36)	676	0.01	0.04	681	0.29	0.36
3.5	354 (4.83), 607 (4.54), 644 (4.49), 674 (5.32)	675	0.02	0.06	680	0.26	0.47

[a] 600 Equiv. relative to phthalocyanine. [b] Excited at 610 nm. [c] Using ZnPc in DMF as the reference (Φ_F = 0.28). [d] Using ZnPc as the reference (Φ_Δ = 0.56 in DMF).

To better mimic the biological environment, the superoxide radical ($O_2^{\bullet-}$) generation efficiency of phthalocyanines **3.1-3.5** was also examined in the buffer solutions using dihydroethidium (DHE) as a probe for superoxide radical.[11] It is generally believed that ethidium is the oxidized product, which fluoresces strongly at around 600 nm upon excitation. Figure 3.9 shows the change in fluorescence intensity of ethidium with time using compound **3.3** as the sensitizer at two different pH environments (6.0 and 7.4). In the absence of light, no fluorescence could be detected at both pH values, showing that compound **3.3** could not generate superoxide radical under these conditions. By contrast, the fluorescence intensity increased steadily upon irradiation and the rate of enhancement was much faster at pH 6.0 compared with that at pH 7.4. The results show that compound **3.3** works as an

efficient superoxide radical generator, particularly at a low-pH environment. All of the compounds **3.1-3.5** exhibit a similar behavior and the results are summarized in Table 3.2. It can be seen that all of them can generate superoxide radical and are more efficient at pH 6.0 than at pH 7.4. The difference is most remarkable for compound **3.3**, for which there is a 9.5-fold increase.

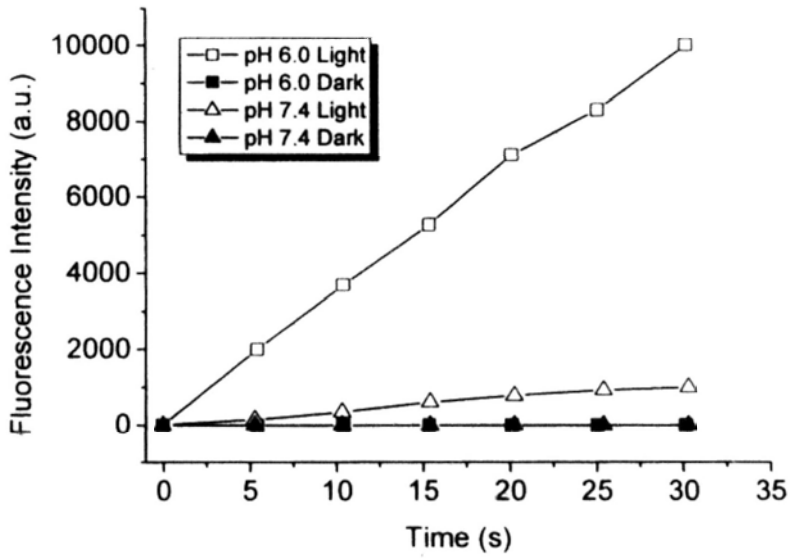

Figure 3.9. Change in fluorescence intensity of ethidium with irradiation time (open symbols). The mixture contained phthalocyanine **3.3** (4 μM) and dihydroethidium (20 μM) in citrate buffer solution at pH 6.0 (squares) or 7.4 (triangles), and was irradiated with red light ($\lambda > 610$ nm). The corresponding data obtained without irradiation are given as closed symbols as a control.

Table 3.2. Comparison of the rates of superoxide radical generation using **3.1**-**3.5** as the photosensitizers at pH 6.0 and 7.4.

Dye	Rate of $O_2^{\bullet-}$ Generation (pH 6.0)[a]	Rate of $O_2^{\bullet-}$ Generation (pH 7.4)[a]	Relative Rate of $O_2^{\bullet-}$ Generation[b]
3.1	39	13	3.0
3.2	345	236	1.5
3.3	331	35	9.5
3.4	341	220	1.6
3.5	238	76	3.1

[a] Determined as the slope of the best-fitted line plotting the fluorescence intensity of ethidium versus irradiation time (as shown in Figure 3.9). [b] Ratio of the rate of superoxide radical generation at pH 6.0 to that at pH 7.4.

3.2.3 In Vitro Photodynamic Activities

The pH-dependent fluorescence emission of **3.3** at the cellular level was also examined. In this study, human colon adenocarcinoma HT29 cells were incubated with **3.3** followed with the ionophore nigericin at different pH (6.0, 6.5, 7.4, and 8.0). The bright field and fluorescence images of the cells were then captured with a confocal microscope (Figure 3.10a), and the intracellular fluorescence intensities were determined (Figure 3.10b). As shown in Figure 3.10, the intracellular intensities are much stronger at pH 6.0 and 6.5 compared with those at pH 7.4 and 8.0. The results further demonstrate that compound **3.3** is a promising fluorescence probe and photosensitizer that can target tumor on the basis of its remarkable pH-responsive

properties in the region between pH 6.5 and 7.4, which are the general pH environments for tumors and normal tissues, respectively.[5]

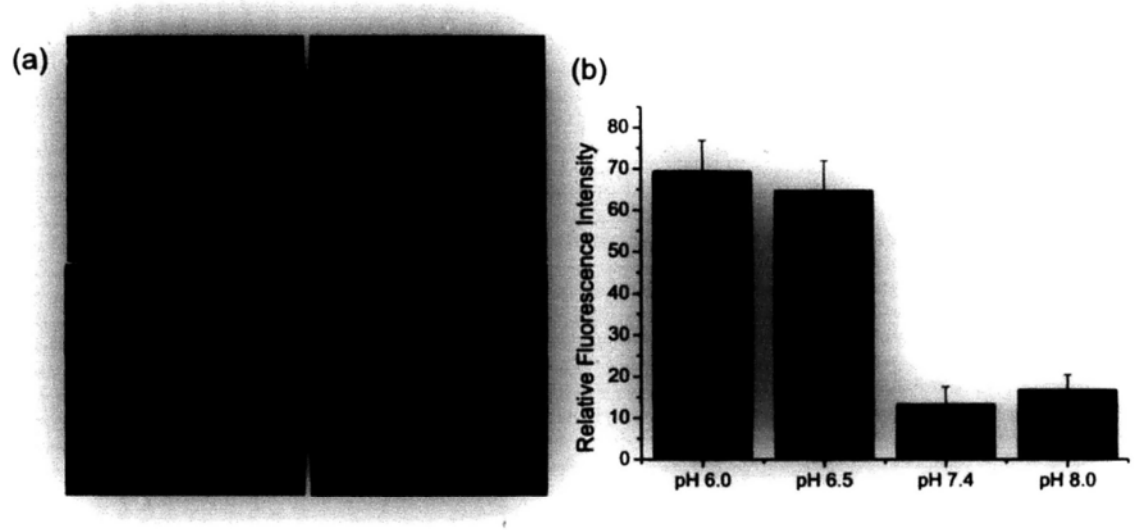

Figure 3.10 (a) Visualization of bright field (upper row) and intracellular fluorescence (lower row) images of HT29 cells after incubation with **3.3** (0.5 μM) for 30 min, followed with nigericin solutions (25 μM) at (i) pH 6.5 and (ii) pH 7.4 for 20 min. (b) Comparison of the intracellular fluorescence intensity of **3.3** in the presence of nigericin at different pH. Data are expressed as mean ± SD (number of cells = 25).

The photodynamic activities of phthalocyanines **3.1-3.5** were also evaluated against two different cell lines, namely HT29 and human heptocarcinoma HepG2 cells. Figure 3.11 shows the effects of **3.3** on HT29 cells, which are typical for all these phthalocyanines. All of them are essentially noncytotoxic in the absence of light, but exhibit high photocytotoxicity. The IC_{50} values, defined as the dye concentration required to kill 50% of the cells, are summarized in Table 3.3. Compounds **3.2-3.5** are highly potent with IC_{50} values in the range of 0.03 to 0.06 μM, which are comparable with those of some other silicon(IV) phthalocyanine-based photosensitizers reported by us earlier.[12] Compound **3.1**, which only has one

amino group in the axial substituent is significantly less photocytotoxic. This can easily be seen in Figure 3.12, which compares the effects of **3.1** and **3.2** on HepG2 cells. The IC_{50} values of **3.1** (0.45-0.49) are roughly 10-folds higher compared with those of the other analogues (Table 3.3). It is believed that the extra ethylamino unit in **3.2-3.5** can increase the water-solubility and enhance the cellular uptake of the phthalocyanines, resulting in higher photocytotoxicity.

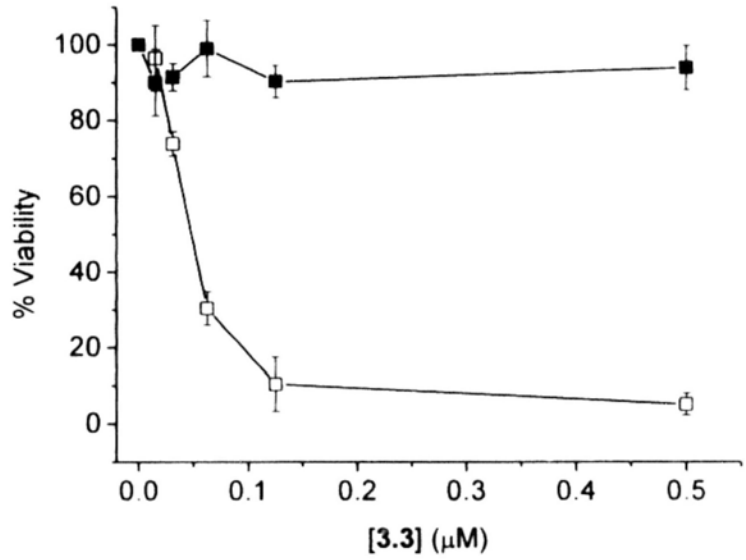

Figure 3.11. Effects of **3.3** on HT29 in the absence (closed symbol) and presence (open symbol) of light. For the latter, the cells were illuminated with a red light ($\lambda >$ 610 nm, 40 mW cm^{-2}, 48 J cm^{-2}). Data are expressed as mean values ± S.E.M. of three independent experiments, each performed in quadruplicate.

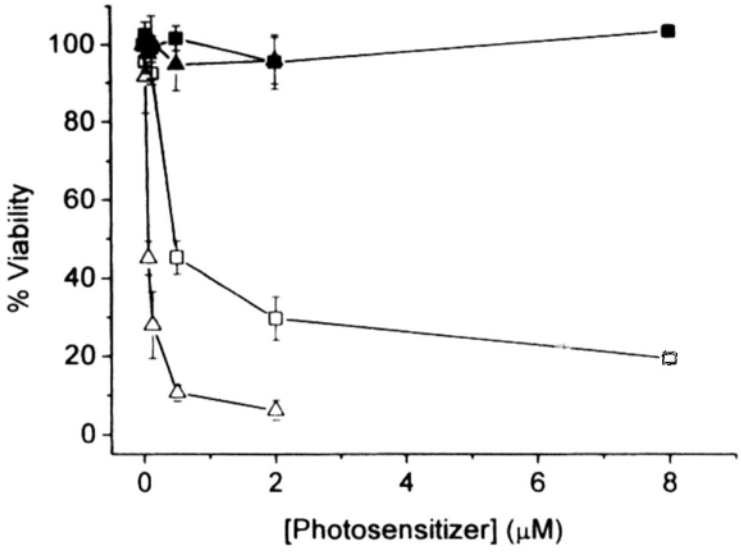

Figure 3.12. Effects of **3.1** (square) and **3.2** (triangle) on HepG2 in the absence (closed symbols) and presence (open symbols) of light. For the latter, the cells were illuminated with a red light ($\lambda > 610$ nm, 40 mW cm^{-2}, 48 J cm^{-2}). Data are expressed as mean values ± S.E.M. of three independent experiments, each performed in quadruplicate.

Table 3.3. Comparison of the IC_{50} values of phthalocyanines **3.1**-**3.5** against HT29 and HepG2 cells.

Compound	IC_{50} (μM)	
	HT29	HepG2
3.1	0.45	0.49
3.2	0.03	0.06
3.3	0.05	0.06
3.4	0.03	0.03
5.5	0.03	0.06

The subcellular localization of **3.3** in HT29 cells was also investigated. The cells were stained with **3.3** together with LysoTracker Green DND 26 or MitoTracker Green FM, which are specific fluorescence dyes for lysosomes and mitochondria, respectively. As shown in Figures 3.13a-c, the fluorescence caused by the LysoTracker (excited at 488 nm, monitored at 500-570 nm) is well superimposed with the fluorescence caused by **3.3** (excited at 633 nm, monitored at 640-700 nm). The very similar fluorescence intensity profiles of **3.3** and LysoTracker traced along the green line in Figure 3.13c (Figure 3.13d) also confirms that compound **3.3** can target lysosomes of the cells. By contrast, the fluorescence images of **3.3** and the Mitotracker (excited at 488 nm, monitored at 500-570 nm) cannot be superimposed (Figure 3.14), indicating that **3.3** is not localized in the mitochondria.

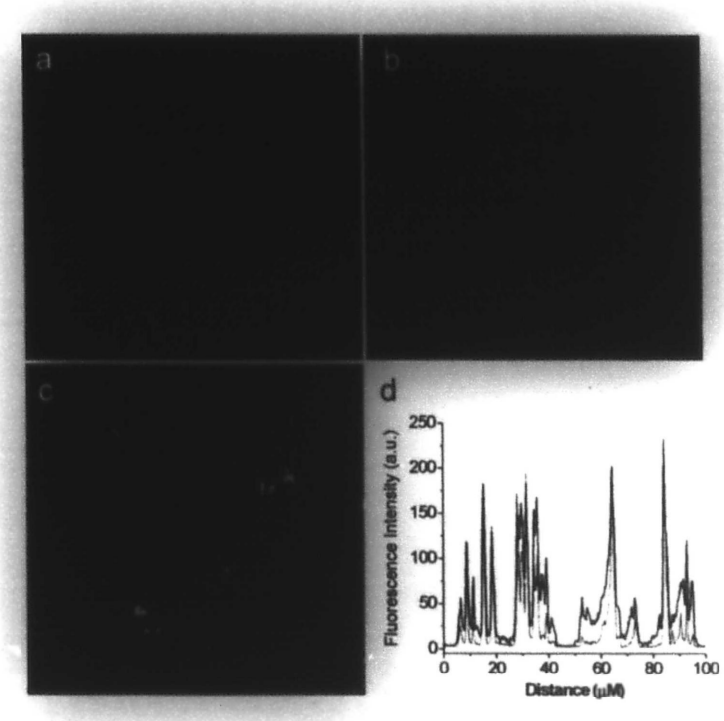

Figure 3.13. Visualization of intracellular fluorescence of HT29 using filter sets specific for (a) phthalocyanine **3.3** (in green) and (b) LysoTracker (in red), and (c) the corresponding superimposed image. Figure (d) shows the fluorescence intensity profiles of **3.3** (green) and LysoTracker (red) traced along the green line in Figure (c).

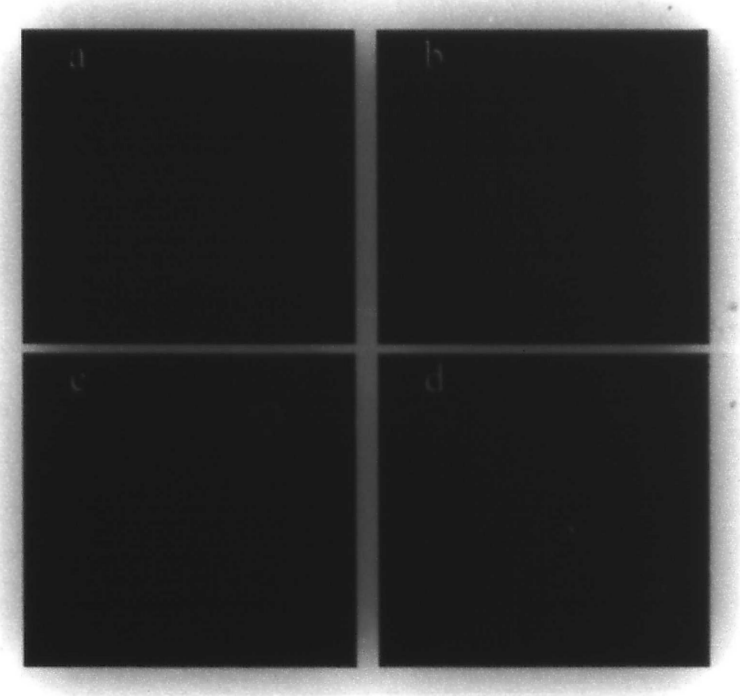

Figure 3.14. Visualization of intracellular fluorescence of HT29 using filter sets specific for (a) phthalocyanine **3.3** (in green) and (b) MitoTracker (in red), and (c) the corresponding superimposed image. Figure (d) shows the bright field image.

3.3 Conclusions

We have prepared and characterized a series of novel silicon(IV) phthalocyanines axially substituted with aryl polyamine moieties. These compounds show pH-dependent UV-Vis and fluorescence spectroscopic properties in DMF and citrate buffer solutions. In acidic media, all of them can generate ROS including singlet oxygen and superoxide radical effectively. Compound **3.3** is of particular interest because of its remarkably different behavior in the pH range (ca. 6.5 to 7.4) differentiating the tumor and normal tissue environments. Phthalocyanines **3.1-3.5** also exhibit high photocytotoxicity against HT29 and HepG2 cells with IC_{50} values as low as 0.03 μM. As revealed by confocal microscopy, compound **3.3** also shows a high selectivity toward lysosomes of the cells. The results presented herein show that these phthalocyanines, particularly compound **3.3**, are promising pH-controlled and tumor-selective photosensitizers for PDT.

3.4 Experimental Section

3.4.1 General

Details regarding the purification of solvents , instrumentation, photophysical measurements, and in vitro studies have been described in Chapter 2.

Subcellular Localization Studies. About 6.0×10^4 HT29 cells in the culture medium (2 mL) were seeded on a coverslip and incubated overnight at 37 °C under 5% CO_2. The medium was then removed. For the study using LysoTracker, the cells were incubated with a solution of **3.3** in the medium (0.5 μM, 2 mL) for 115 min under the same conditions. LysoTracker Green DND 26 (Molecular Probes; 4 μM in

the culture medium) was then added, and the cells were incubated under these conditions for a further 5 min. For the study using MitoTracker, the cells were incubated with MitoTracker Green FM (Molecular Probes; 0.2 μM) in the medium (2 mL) for 30 min. Then the cells were rinsed with PBS and incubated again with a solution of **3.3** in the medium (2 μM, 2 mL) for 2 h under the same conditions. For both cases, the cells were then rinsed with PBS and viewed with a Leica SP5 confocal microscope equipped with a 488 nm Argon laser and a 633 helium neon laser. Both LysoTracker and MitroTracker were excited at 488 nm and monitored at 500-570 nm, while compound **3.3** was excited at 633 nm and monitored at 640-700 nm. Images were digitized and analyzed using Leica Application Suite Advanced Fluorescence. The subcellular localization of **3.3** was revealed by comparing the intracellular fluorescence images caused by the LysoTracker or MitoTracker and this dye.

3.4.2 Synthesis

Preparation of Hydroxyamine 3.12. A solution of benzaldehyde (**3.8**) (2.80 g, 26.4 mmol) in methanol (150 mL) was cooled in an ice-bath. 2-Aminoethanol (**3.6**) (1.40 g, 22.9 mmol) was then added, and the mixture was stirred at room temperature for 8 h. Sodium borohydride (2.00 g, 52.9 mmol) was added slowly to the reaction mixture, which was maintained at 0 °C using an ice-bath. After the addition, the mixture was stirred at room temperature for 12 h. The reaction was quenched by the addition of HCl (6 M) with cooling until the pH was adjusted to 4. The solvent was removed under reduced pressure. The residue was dissolved in water (100 mL) and washed with CH_2Cl_2 (100 mL × 3) to remove the organic impurities. The aqueous phase was separated and its pH was adjusted to 10 using solid Na_2CO_3. It was then extracted with CH_2Cl_2 (150 mL). The organic portion was dried over anhydrous $MgSO_4$ and

evaporated in vacuo to give the product as a colorless oil (3.25 g, 94%). ^{1}H NMR: δ 7.27-7.33 (m, 5 H, ArH), 3.80 (s, 2 H, CH_2), 3.65 (t, J = 5.1 Hz, 2 H, CH_2), 2.80 (t, J = 5.1 Hz, 2 H, CH_2). ^{13}C{^{1}H} NMR: δ 138.9, 128.1, 128.0, 126.8, 60.0, 53.0, 50.3. The NMR data are essentially the same as those given elsewhere.[13]

Preparation of Hydroxyamine 3.13. According to the procedure described for **3.12**, compound **3.13** was prepared as a colorless oil by treating benzaldehyde (**3.8**) (2.12 g, 20.0 mmol) with 2-(2-aminoethylamino)ethanol (**3.7**) (2.08 g, 20.0 mmol), followed by reduction using sodium borohydride (1.52 g, 40.2 mmol) (3.38 g, 87%). ^{1}H NMR: δ 7.27-7.33 (m, 5 H, ArH), 3.78 (s, 2 H, CH_2), 3.62 (t, J = 5.1 Hz, 2 H, CH_2), 2.71-2.74 (m, 6 H, CH_2). ^{13}C{^{1}H} NMR: δ 139.9, 128.2, 128.0, 126.8, 60.4, 53.7, 51.2, 48.7, 48.4. MS (FAB): *m/z* 195 (100%, $[M+H]^+$). HRMS (FAB): *m/z* calcd for $C_{11}H_{19}N_2O$ $[M+H]^+$ 195.1492, found 195.1490.

Preparation of Hydroxyamine 3.14. According to the procedure described for **3.12**, compound **3.14** was synthesized by treating 4-chlorobenzaldehyde (**3.9**) (1.97 g, 14.0 mmol) with 2-(2-aminoethylamino)ethanol (**3.7**) (1.46 g, 14.0 mmol), followed by reduction using sodium borohydride (1.06 g, 28.0 mmol). The product was isolated as a brown oil (2.72 g, 85%). ^{1}H NMR: δ 7.22-7.29 (m, 4 H, ArH), 3.73 (s, 2 H, CH_2), 3.61 (t, J = 5.4 Hz, 2 H, CH_2), 2.69-2.72 (m, 6 H, CH_2). ^{13}C{^{1}H} NMR: δ 138.5, 132.5, 129.4, 128.4, 60.6, 53.0, 51.2, 48.7, 48.5. MS (FAB): *m/z* 229 (100%, $[M]^+$). HRMS (FAB): *m/z* calcd for $C_{11}H_{17}ClN_2O$ $[M]^+$ 229.1102, found 229.1094.

Preparation of Hydroxyamine 3.15. According to the procedure described for **3.12**, 4-methoxybenzaldehyde (**3.10**) (1.91 g, 14.0 mmol) was treated with 2-(2-

aminoethylamino)ethanol (**3.7**) (1.46 g, 14.0 mmol) and sodium borohydride (1.06 g, 28.0 mmol) to give **3.15** as a brown oil (2.61 g, 83%). ^{1}H NMR: δ 7.24 (d, J = 8.7 Hz, 2 H, ArH), 6.87 (d, J = 8.7 Hz, 2 H, ArH), 3.80 (s, 3 H, CH_3), 3.74 (s, 2 H, CH_2), 3.64 (t, J = 5.4 Hz, 2 H, CH_2), 2.75-2.79 (m, 6 H, CH_2). ^{13}C{^{1}H} NMR: δ 158.7, 131.7, 129.5, 113.8, 60.5, 55.2, 53.1, 51.0, 48.4, 48.1. MS (FAB): *m/z* 121 (100%, $[C_6H_4(OCH_3)CH_2]^+$), 225 (54%, $[M+H]^+$). HRMS (FAB): *m/z* calcd for $C_{12}H_{21}N_2O_2$ $[M+H]^+$ 225.1598, found 225.1605.

Preparation of Hydroxyamine 3.16. According to the procedure described for **3.12**, 3,4,5-trimethoxybenzaldehyde (**3.11**) (2.75 g, 14.0 mmol) was reacted with 2-(2-aminoethylamino)ethanol (**3.7**) (1.46 g, 14.0 mmol) and sodium borohydride (1.06 g, 28.0 mmol) to give **3.16** as a brown oil (3.11 g, 78%). ^{1}H NMR: δ 6.56 (s, 2 H, ArH), 3.87 (s, 6 H, CH_3), 3.83 (s, 3 H, CH_3), 3.74 (s, 2 H, CH_2), 3.64 (t, J = 5.1 Hz, 2 H, CH_2), 2.75-2.78 (m, 6 H, CH_2). ^{13}C{^{1}H} NMR: δ 153.2, 136.8, 135.6, 104.9, 60.8, 60.7, 56.1, 54.1, 51.0, 48.5, 48.4. MS (FAB): *m/z* 181 (100%, $[C_6H_2(OCH_3)_3CH_2]^+$), 285 (13%, $[M+H]^+$). HRMS (FAB): calcd for $C_{14}H_{25}N_2O_4$ $[M+H]^+$ 285.1809, found 285.1806.

Preparation of Phthalocyanine 3.1. A mixture of silicon(IV) phthalocyanine dichloride (**3.17**) (0.20 g, 0.33 mmol), 2-benzylaminoethanol (**3.12**) (0.15 g, 1.0 mmol), and pyridine (0.5 mL) in toluene (30 mL) was refluxed for 4 h. After evaporating the solvent in vacuo, the residue was dissolved in CH_2Cl_2 (100 mL) and then washed with water (100 mL × 3). The organic layer was collected and evaporated under reduced pressure. The crude product was recrystallized from $CHCl_3$/1-hexane (1:4 v/v) to give the product as a blue solid (0.21 g, 76%). ^{1}H NMR:

δ 9.60-9.64 (m, 8 H, Pc-H_α), 8.32-8.36 (m, 8 H, Pc-H_β), 6.94 (t, J = 7.2 Hz, 2 H, ArH), 6.84 (t, J = 7.2 Hz, 4 H, ArH), 6.09 (d, J = 7.2 Hz, 4 H, ArH), 2.01 (s, 4 H, CH_2), -0.27 (t, J = 5.4 Hz, 4 H, CH_2), -1.93 (t, J = 5.4 Hz, 4 H, CH_2). $^{13}C\{^1H\}$ NMR: δ 149.2, 139.5, 135.9, 130.9, 127.7, 126.9, 126.0, 123.7, 53.7, 51.3, 47.6. HRMS (ESI): *m/z* calcd for $C_{50}H_{40}N_{10}NaO_2Si$ $[M+Na]^+$ 863.2997, found 863.2999. Anal. Calcd for $C_{50}H_{40}N_{10}O_2Si$: C, 71.41; H, 4.79; N, 16.65. Found: C, 71.56; H, 5.06; N, 16.36.

Preparation of Phthalocyanine 3.2. According to the procedure described for **3.1**, silicon(IV) phthalocyanine dichloride (**3.17**) (0.20 g, 0.33 mmol) was treated with hydroxyamine **3.13** (0.19 g, 1.0 mmol) and pyridine (0.5 mL) in toluene (30 mL) to give **3.2** as a blue solid (0.19 g, 62%). ^1H NMR: δ 9.58-9.62 (m, 8 H, Pc-H_α), 8.29-8.33 (m, 8 H, Pc-H_β), 7.20-7.25 (m, 6 H, ArH), 7.00 (d, J = 7.5 Hz, 4 H, ArH), 3.26 (s, 4 H, CH_2), 1.58 (t, J = 6.0 Hz, 4 H, CH_2), 0.88 (t, J = 6.0 Hz, 4 H, CH_2), -0.35 (t, J = 5.4 Hz, 4 H, CH_2), -1.97 (t, J = 5.4 Hz, 4 H, CH_2). $^{13}C\{^1H\}$ NMR: δ 149.2, 140.3, 135.9, 131.0, 128.1, 127.9, 126.6, 123.6, 53.7, 53.3, 47.8 (two overlapping signals), 46.9. HRMS (ESI): *m/z* calcd for $C_{54}H_{51}N_{12}O_2Si$ $[M+H]^+$ 927.4022, found 927.4029. Anal. Calcd for $C_{54}H_{52}N_{12}O_3Si$ (**3.2**·H_2O): C, 68.62; H, 5.55; N, 17.78. Found: C, 68.45; H, 5.79; N, 17.33.

Preparation of Phthalocyanine 3.3. According to the procedure described for **3.1**, silicon(IV) phthalocyanine dichloride (**3.17**) (0.20 g, 0.33 mmol) was treated with hydroxyamine **3.14** (0.23 g, 1.0 mmol) and pyridine (0.5 mL) in toluene (30 mL) to give **3.3** as a blue solid (0.22 g, 67%). ^1H NMR: δ 9.57-9.61 (m, 8 H, Pc-H_α), 8.30-8.34 (m, 8 H, Pc-H_β), 7.19 (d, J = 8.4 Hz, 4 H, ArH), 6.89 (d, J = 8.4 Hz, 4 H, ArH), 3.21 (s, 4 H, CH_2), 1.55 (t, J = 5.7 Hz, 4 H, CH_2), 0.89 (t, J = 5.7 Hz, 4 H, CH_2), -0.34

(t, J = 5.1 Hz, 4 H, CH_2), -1.97 (t, J = 5.1 Hz, 4 H, CH_2). $^{13}C\{^1H\}$ NMR: δ 149.2, 138.9, 135.9, 132.2, 131.0, 129.1, 128.2, 123.6, 53.8, 52.5, 47.9, 47.7, 46.9. HRMS (FAB): *m/z* calcd for $C_{54}H_{49}Cl_2N_{12}O_2Si$ $[M+H]^+$ 995.3242, found 995.3214. Anal. Calcd for $C_{54}H_{48}Cl_2N_{12}O_2Si$: C, 65.12; H, 4.86; N, 16.87. Found: C, 64.75; H, 4.62; N, 16.56.

Preparation of Phthalocyanine 3.4. According to the procedure described for **3.1**, silicon(IV) phthalocyanine dichloride (**3.17**) (0.20 g, 0.33 mmol) was treated with hydroxyamine **3.15** (0.22 g, 1.0 mmol) and pyridine (0.5 mL) in toluene (30 mL) to give **3.4** as a blue solid (0.23 g, 71%). ^1H NMR: δ 9.59-9.62 (m, 8 H, Pc-H_α), 8.30-8.33 (m, 8 H, Pc-H_β), 6.91 (d, J = 8.4 Hz, 4 H, ArH), 6.76 (d, J = 8.4 Hz, 4 H, ArH), 3.78 (s, 6 H, CH_3), 3.19 (s, 4 H, CH_2), 1.56 (t, J = 6.0 Hz, 4 H, CH_2), 0.88 (t, J = 6.0 Hz, 4 H, CH_2), -0.36 (t, J = 5.4 Hz, 4 H, CH_2), -1.98 (t, J = 5.4 Hz, 4 H, CH_2). $^{13}C\{^1H\}$ NMR: δ 158.3, 149.2, 135.9, 132.5, 130.9, 129.0, 123.7, 113.5, 55.2, 53.8, 52.7, 47.9, 47.7, 46.9. HRMS (FAB): *m/z* calcd for $C_{56}H_{55}N_{12}O_4Si$ $[M+H]^+$ 987.4233, found 987.4196. Anal. Calcd for $C_{56}H_{56}N_{12}O_5Si$ (**3.4**·H_2O): C, 66.91; H, 5.62; N, 16.72. Found: C, 67.36; H, 5.53; N, 16.45.

Preparation of Phthalocyanine 3.5. According to the procedure described for **3.1**, silicon(IV) phthalocyanine dichloride (**3.17**) (0.20 g, 0.33 mmol) was treated with hydroxyamine **3.16** (0.28 g, 1.0 mmol) and pyridine (0.5 mL) in toluene (30 mL) to give **3.5** as a blue solid (0.27 g, 74%). ^1H NMR: δ 9.59-9.62 (m, 8 H, Pc-H_α), 8.31-8.34 (m, 8 H, Pc-H_β), 6.20 (s, 4 H, ArH), 3.78 (s, 6 H, CH_3), 3.72 (s, 12 H, CH_3), 3.19 (s, 4 H, CH_2), 1.59 (t, J = 6.0 Hz, 4 H, CH_2), 0.91 (t, J = 6.0 Hz, 4 H, CH_2), -0.34 (t, J = 5.1 Hz, 4 H, CH_2), -1.96 (t, J = 5.1 Hz, 4 H, CH_2). $^{13}C\{^1H\}$ NMR: δ 152.9, 149.2,

136.5, 136.1, 135.9, 131.0, 123.6, 104.5, 60.8, 55.9, 53.7, 53.5, 47.9, 47.7, 46.9. HRMS (FAB): *m/z* calcd for $C_{60}H_{63}N_{12}O_8Si$ $[M+H]^+$ 1107.4656, found 1107.4604. Anal. Calcd for $C_{60}H_{64}N_{12}O_9Si$ (**3.5**·H_2O): C, 64.04; H, 5.73; N, 14.94. Found: C, 64.21; H, 5.91; N, 14.79.

3.5 References

1 (a) Sharman, W. M.; van Lier, J. E.; Allen, C. M. *Adv. Drug Deliv. Rev.* **2004**, *56*, 53. (b) Solban, N.; Rizvi, I.; Hasan, T. *Lasers Surg. Med.* **2006**, *38*, 522. (c) Verma, S.; Watt, G. M.; Mai, Z.; Hasan, T. *Photochem. Photobiol.* **2007**, *83*, 996.

2 (a) Roy, I.; Ohulchanskyy, T. Y.; Pudavar, H. E.; Bergey, E. J.; Oseroff, A. R.; Morgan, J.; Dougherty, T. J.; Prasad, P. N. *J. Am. Chem. Soc.* **2003**, *125*, 7860. (b) Nishiyama, N.; Jang, W.-D.; Kataoka, K. *New J. Chem.* **2007**, *31*, 1074. (c) Zhang, L.; Gu, F. X.; Chan, J. M.; Wang, A. Z.; Langer, R. S.; Farokhzad, O. C. *Clin. Pharm. Ther.* **2008**, *83*, 761.

3 (a) Stubbs, M.; McSheehy, P. M. J.; Griffiths, J. R.; Bashford, C. L. *Mol. Med. Today* **2000**, *6*, 15. (b) Gerweck L. E. *Drug Resist. Updates* **2000**, *3*, 49.

4 (a) Friberg, E. G.; Cunderlíková, B.; Pettersen, E. O.; Moan, J. *Cancer Lett.* **2003**, *195*, 73. (b) Cunderlíková, B.; Moan, J.; Sjaastad, I. *Cancer Lett.* **2005**, *222*, 39.

5 (a) Sharma, M.; Dube, A.; Bansal, H.; Gupta, P. K. *Photochem. Photobiol. Sci.* **2004**, *3*, 231. (b) Sharma, M.; Sahu, K.; Dube, A.; Gupta, P. K. *J. Photochem. Photobiol. B: Biol.* **2005**, *81*, 107. (c) Mojzisova, H.; Bonneau, S.; Vever-Bizet, C.; Brault, D. *Biochim. Biophys. Acta* **2007**, *1768*, 2748.

6 Bellnier, D. A.; Young, D. N.; Detty, M. R.; Camacho, S. H.; Oseroff, A. R. *Photochem. Photobiol.* **1999**, *70*, 630.

7 Arnbjerg, J.; Johnsen, M.; Nielsen, C. B.; Jørgensen, M.; Ogilby, P. R. *J. Phys. Chem. A* **2007**, *111*, 4573.

8 McDonnell, S. O.; Hall, M. J.; Allen, L. T.; Byrne, A.; Gallagher, W. M.; O'Shea, D. F. *J. Am. Chem. Soc.* **2005**, *127*, 16360.

9 For some recent examples, see (a) Hilderbrand, S. A.; Kelly, K. A.; Niedre, M.; Weissleder, R. *Bioconjugate Chem.* **2008**, *19*, 1635. (b) Tang, B.; Yu, F.; Li, P.; Tong, L.; Duan, X.; Xie, T.; Wang, X. *J. Am. Chem. Soc.* **2009**, *131*, 3016. (c) Urano, Y.; Asanuma, D.; Hama, Y.; Koyama, Y.; Barrett, T.; Kamiya, M.; Nagano, T.; Watanabe, T.; Hasegawa, A.; Choyke, P. L.; Kobayashi, H. *Nat. Med.* **2009**, *15*, 104.

10 Lee, E. S.; Gao, Z.; Bae, Y. H. *J. Control. Release* **2008**, *132*, 164.

11 (a) Zhao, H.; Kalivendi, S.; Zhang, H.; Joseph, J.; Nithipatikom, K.; Vásquez-Vivar, J.; Kalyanaraman, B. *Free Rad. Biol. Med.* **2003**, *34*, 1359. (b) Halliwell, B.; Whiteman, M. *Br. J. Pharm.* **2004**, *142*, 231.

12 For some recent examples, see (a) Lo, P.-C.; Huang, J.-D.; Cheng, D. Y. Y.; Chan, E. Y. M.; Fong, W.-P.; Ko, W.-H.; Ng, D. K. P. *Chem. Eur. J.* **2004**, *10*, 4831. (b) Lo, P.-C.; Fong, W.-P.; Ng, D. K. P. *ChemMedChem* **2008**, *3*, 1110-1117. (c) Lee, P. P. S.; Lo, P.-C.; Chan, E. Y. M.; Fong, W.-P.; Ko, W.-H.; Ng, D. K. P. *Tetrahedron Lett.* **2005**, *46*, 1551-1554.

13 *The Aldrich Library of* ^{13}C *and* ^{1}H *FT NMR Spectra*; Pouchert, C. J., Behnke, J., Eds.; Aldrich Chemical Company: USA, 1993; Vol. 2.

CHAPTER 4

Synthesis and Photodynamic Activities of Phthalocyanine-Polyamine Conjugates

4.1 Introduction

The native polyamines such as putrescine, spemidine, and spermine play multifunctional roles in a number of cell processes including cell proliferation and differentiation.[1] All cells have methods of manufacturing polyamines from amino acid sources. In addition, cells can import polyamines from outside the cells via polyamine transporters (PATs). Many cancer cells are unable to produce enough polyamines to sustain their growth and therefore rely upon polyamine import to grow.[2] These characteristics lead to the use of polyamines as potent vectors for the selective delivery of chemotherapeutic and DNA targeted agents into cancer cells. Consequently, a substantial number of polyamine conjugates with cytotoxic drugs such as chlorambcil,[3] nitroimidazole,[4] aziridine,[5] acridine,[6] enediyne,[7] taxol,[8] camptothecin,[9] anthrancen,[10] and porphyrin[11] have been reported. In most of the cases, the cytotoxicity and drug selectivity for tumor cells is enhanced. In this Chapter, we report a new series of polyamine-containing silicon(IV) phthalocyanines, including their synthesis, photophysical properties, and photodynamic activities, both in vitro and in vivo.

4.2 Results and Discussion

4.2.1 Preparation and Characterization

Scheme 4.1 and Scheme 4.2 show the synthetic routes of the precursors **4.9a-4.9e** and **4.13**, respectively. According to the amino-alcohol strategy developed earlier,[12] reaction of 3-aminopropanol (**4.2a**) or 4-aminobutanol (**4.2b**) with excess methyl formate followed by reduction with $LiAlH_4$ led to the *N*-methyl product **4.4a** or **4.4b**. Sequential protection of **4.4a** (or **4.4b**) with di-*tert*-butyl dicarbonate

[$(Boc)_2O$] and reaction of methanesulfonyl chloride (MsCl) in the presence of triethylamine gave compound **4.6a** (or **4.6b**). Further mesylate displacement reaction with amino alcohol **4.2a**, **4.4a** or **4.7** afforded **4.8a-4.8e**, which then underwent *N*-Boc deprotection with hydrochloric acid to give the hydroxyl diamines **4.9a-4.9e**. By repeating the *N*-Boc protection followed by *O*-sulfonylation procedure, compound **4.8a** was converted to **4.11**. Substitution reaction of compound **4.11** with (3-hydroxylpropyl)methylamine (**4.4a**) followed by *N*-Boc deportection gave the hydroxyl triamine **4.13**.

The precursors **4.4a-4.4b**, **4.9a-4.9e**, and **4.13** were then treated with silicon(IV) phthalocyanine dichloride in the presence of pyridine in toluene to give the disubstituted products **4.1a-4.1i** (Scheme 4.3). The products could be purified readily by extraction with CH_2Cl_2/water, followed by recrystallization using a mixture of $CHCl_3$ and 1-hexane (1:4 v/v).

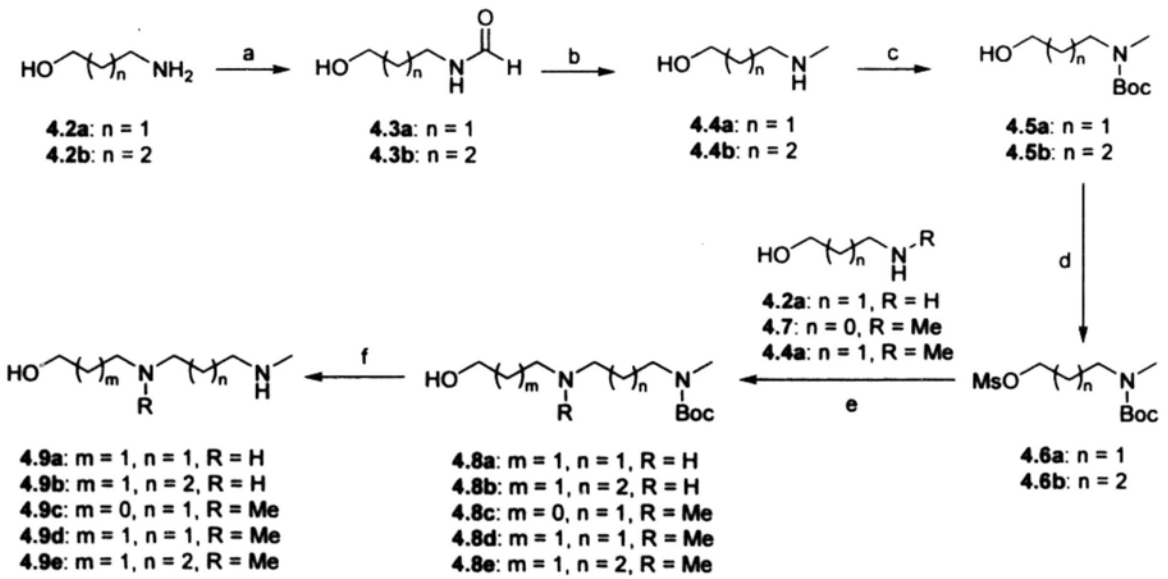

Scheme 4.1. Reagents and conditions: (a) HCOOMe, 16 h; (b) $LiAlH_4$, THF, 16 h; (c) $(Boc)_2O$, Et_3N, MeOH, 16 h; (d) MsCl, Et_3N, CH_2Cl_2, 16 h; (e) CH_3CN, 16 h; (f) i: 4 N HCl, MeOH, 16 h, ii: Na_2CO_3.

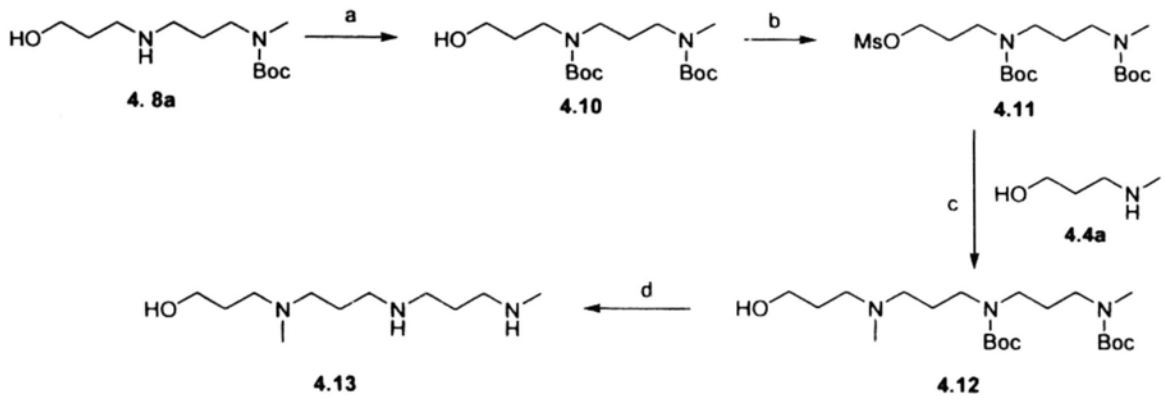

Scheme 4.2. Reagents and conditions: (a) $(Boc)_2O$, Et_3N, MeOH, 16 h; (b) MsCl, Et_3N, CH_2Cl_2, 16 h; (c) CH_3CN, 16 h; (d) i: 4 N HCl, MeOH, 16 h, ii: Na_2CO_3.

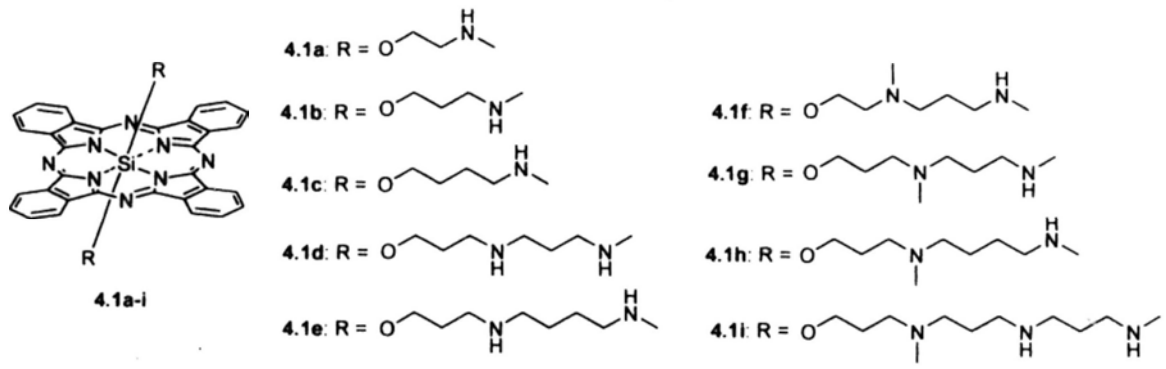

Scheme 4.3. Structure of phthalocyanines **4.1a-4.1i**.

Phthalocyanines **4.1a-4.1i** were fully characterized with various spectroscopic methods and elemental analysis. Figure 4.1 shows the ^1H NMR spectrum of **4.1d** in $CDCl_3$. The two downfield multiplets at δ 9.63-9.66 and 8.34-8.37 are due to the phthalocyanines α and β ring protons, respectively. The axial groups resonate as a singlet at δ 2.25 (for the methyl protons), four triplets at δ 2.05, 1.29, -0.06, and -2.06 (for NCH_2 and OCH_2 protons), and two multiplets at δ 0.68-0.78 and -1.35 to -1.31 (for CCH_2C protons). These signals appear at very upfield positions due to the shielding effect of the phthalocyanine ring.

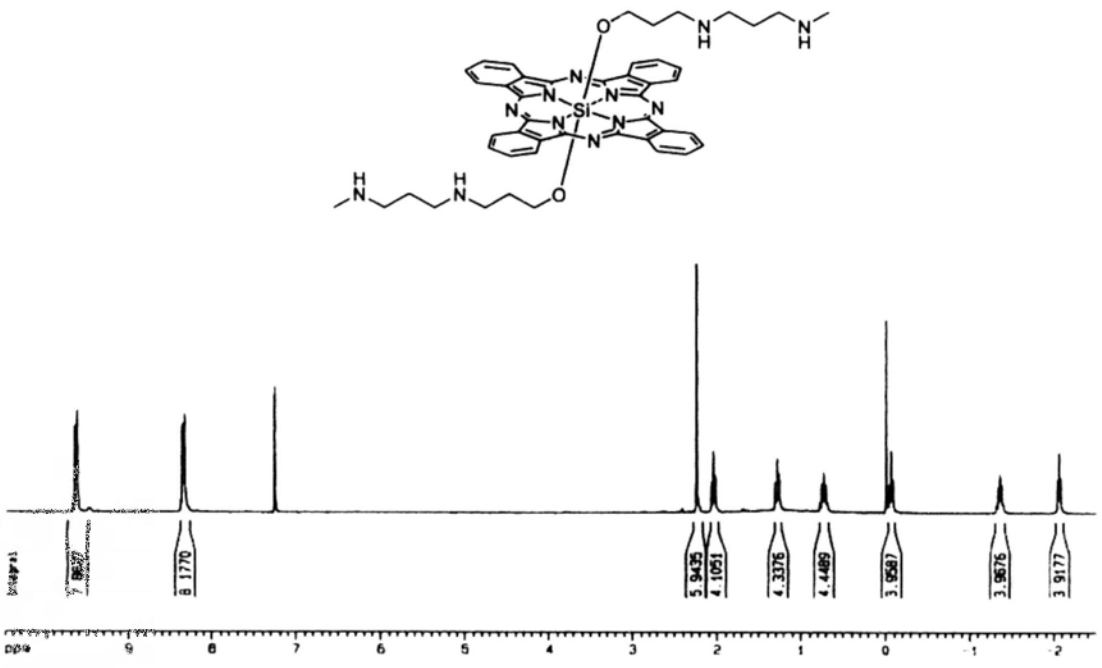

Figure 4.1. ^{1}H NMR spectrum of **4.1d** in $CDCl_3$.

4.2.2 Electronic Absorption and Photophysical Properties

The electronic absorption and photophysical data for **4.1a**-**4.1i** measured in DMF are summarized in Table 4.1. All the compounds give typical absorption spectra of non-aggregated phthalocyanines, showing the B-band at 354-356 nm, Q band at 672-674 nm, together with two vibronic bands at 604-607 nm and 643-647 nm. The very similar Q-band absorptions indicate that the macrocyclic π system is not perturbed by the axial ligands. Figure 4.2 shows the UV-Vis spectra of **4.1a** in DMF at various concentrations given as an example. The Q band absorption strictly follows the Lambert Beer's Law, suggestion that aggregation is not significant for this compound. Upon excitation at 610 nm, all these compounds show a weak fluorescence emission at 676-678 nm with a fluorescence quantum yield (Φ_F) of 0.03-0.08 relative to ZnPc (Φ_F = 0.28). The weak fluorescence is attributed to the axial

amino moieties, which can quench the singlet excited state of the phthalocyanine core by intramolecular photoinduced electron transfer (PET).

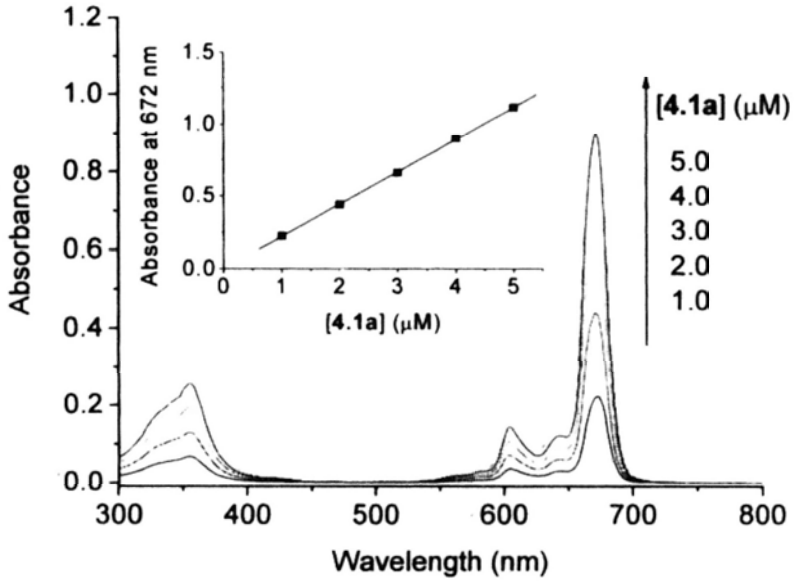

Figure 4.2. UV-Vis spectra of **4.1a** in DMF. The inset plots the Q-band absorbance versus the concentration of **4.1a**.

To evaluate the photosensitizing efficiency of these compounds, their singlet oxygen quantum yields (Φ_Δ) were determined by a steady-state method using 1,3-diphenylisobenzofuran (DPBF) as the scavenger. The concentration of the quencher was monitored spectroscopically at 414 nm with time of irradiation (Figure 4.3), from which the values of Φ_Δ could be determined. As shown in Table 4.1, all of the phthalocyanines **4.1a-4.1i** can generate singlet oxygen in DMF, but not in an effective manner. The values of Φ_Δ are only 0.03 to 0.15 relative to ZnPc (Φ_Δ = 0.56). The low singlet oxygen generation efficiency can also be attributed to the PET process.

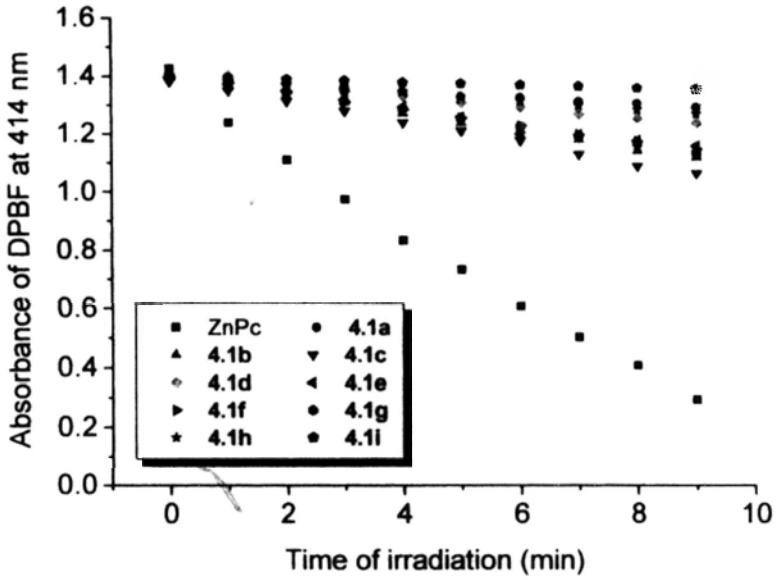

Figure 4.3. Comparison of the rates of photooxidation of DPBF in DMF using **4.1a-4.1i** and ZnPc as the photosensitizers

Table 4.1. Electronic absorption and photophysical data for **4.1a-4.1i** in DMF.

Compound	λ_{max} (nm) (log ε)	λ_{em} (nm)[a]	Φ_F[b]	Φ_Δ[c]
4.1a	354 (4.81), 604 (4.55), 643 (4.48), 672 (5.35)	676	0.03	0.06
4.1b	354 (4.85), 606 (4.58), 644 (4.50), 673 (5.38)	678	0.05	0.13
4.1c	356 (4.77), 606 (4.51), 644 (4.45), 673 (5.31)	677	0.07	0.15
4.1d	354 (4.78), 606 (4.52), 644 (4.45), 673 (5.32)	677	0.06	0.09
4.1e	356 (4.85), 606 (4.57), 644 (4.50), 673 (5.37)	677	0.04	0.13
4.1f	356 (4.86), 607 (4.57), 647 (4.51), 674 (5.37)	677	0.07	0.14
4.1g	354 (4.85), 606 (4.59), 644 (4.52), 674 (5.39)	678	0.08	0.13
4.1h	356 (4.83), 606 (4.55), 644 (4.48), 673 (5.34)	677	0.04	0.06
4.1i	354 (4.82), 606 (4.56), 644 (4.49), 673 (5.35)	677	0.03	0.03

[a] Excited at 610 nm. [b] Using ZnPc in DMF as the reference [Φ_F = 0.28]. [c] Using ZnPc as the reference [Φ_Δ = 0.56 in DMF].

All the compounds **4.1a-4.1i** are also soluble in water because of the hydrophilicity of the axial amino substituents. In the presence of 0.1% THF (for **4.1a-4.1c**) or 0.1% MeOH (for **4.1d-4.1i**), all the compounds exist mainly in monomeric form in water as shown by their absorption spectra. Figure 4.4 shows the absorption spectra of phthalocyanines **4.1a** and **4.1b** in water (with 0.1% THF). Both spectra

show the B-band at 352 nm, a vibronic band at 614 nm, and a Q-band at 683 nm. The Q-band of **4.1b** is particularly intense indicating that this compound is essentially non-aggregated in water. Compounds **4.1c-4.1i** show similar spectra features and it can be concluded that they are also essentially non-aggregated in water. Upon excitation at 610 nm, these compounds show a fluorescence emission at 687-688 nm with a fluorescence quantum yield (Φ_F) of 0.12-0.21. The fluorescence quantum yields of these compounds are relatively higher in water than those in DMF because the amino moieties are protonated in the aqueous environment, resulting in the inhibition of PET process. The absorption as well as the fluorescence emission data of these compounds are compiled in Table 4.2. Compared with the data recorded in DMF, both the Q-band absorptions and fluorescence emissions are slightly red-shifted.

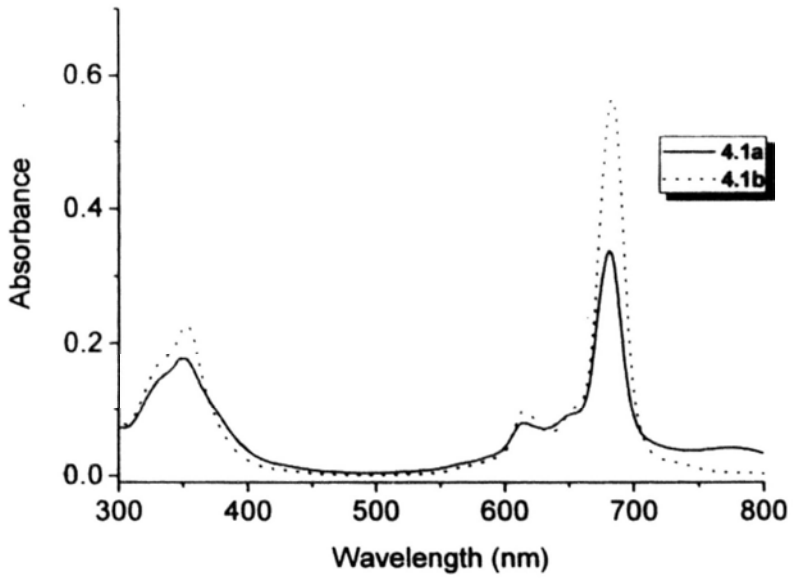

Figure 4.4. UV-Vis spectra of **4.1a** and **4.1b** (3.0 μM) in water (with 0.1% THF).

Table 4.2. Electronic absorption and photophysical data for **4.1a-4.1i** in water.

Compound	λ_{max} (nm) (log ε)	λ_{em} (nm)[a]	Φ_F[b]
4.1a	352 (4.71), 614 (4.39), 683 (4.99), 774 (4.23)	687	0.14
4.1b	352 (4.85), 614 (4.52), 683 (5.26)	688	0.19
4.1c	352 (4.76), 614 (4.44), 683 (5.16)	687	0.16
4.1d	352 (4.77), 614 (4.44), 683 (5.21)	687	0.21
4.1e	352 (4.79), 614 (4.46), 683 (5.23)	687	0.19
4.1f	352 (4.85), 614 (4.51), 683 (5.27)	687	0.16
4.1g	352 (4.85), 614 (4.49), 683 (5.29)	687	0.18
4.1h	352 (4.81), 614 (4.46), 683 (5.24)	688	0.13
4.1i	352 (4.79), 614 (4.46), 683 (5.23)	677	0.12

[a] Excited at 610 nm. [b] Using ZnPc in DMF as the reference [Φ_F = 0.28].

The electronic absorption and fluorescence spectra of these polyamine-phthalocyanine conjugates were also measured in citrate buffer solutions with different pH values. Figure 4.5 plots the variation of the Q-band absorbance at 684 nm with the pH value for all these compounds. Compound **4.1a** is relatively aggregated in the pH region between 5.0 to 9.0. The other compounds are non-aggregated essentially under a neutral or acidic condition (pH < 8). The changes in fluorescence

intensity with pH for these compounds are summarized in Figure 4.6. All these compounds exhibit a pH-dependent property in fluorescence emission. Interestingly, while the absorption spectra of all these phthalocyanines with axial amino substituents are almost identical, the amino groups exhibit a great effect on the aggregation tendencies and photophysical properties of the macrocycles in aqueous solutions. For example, the aryl polyamino derivatives **3.2-3.5** show remarkable pH-dependent aggregation and fluorescence emission properties in the buffer solution in the pH regon between 6.0 to 8.0, the polyamino derivatives **4.1b-4.1i** show a pH-dependent fluorescence emission in the region between pH 7.0 to 9.0, and the tetraamino derivative **2.1** shows the most distinct change in fluorescence intensity when pH increases from 4.0 to 7.0.

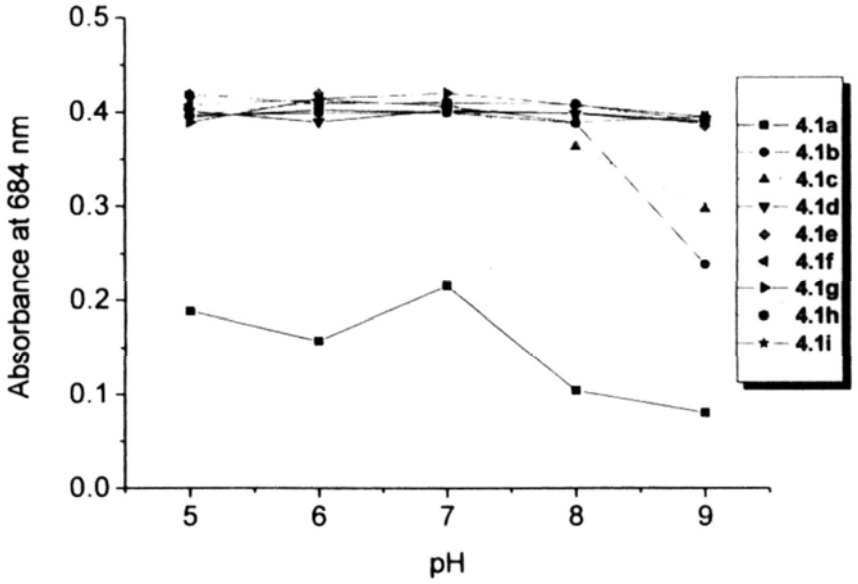

Figure 4.5. Change in the Q-band absorbance at 684 nm with pH for **4.1a-4.1i** (2 μM) in citrate buffer solutions.

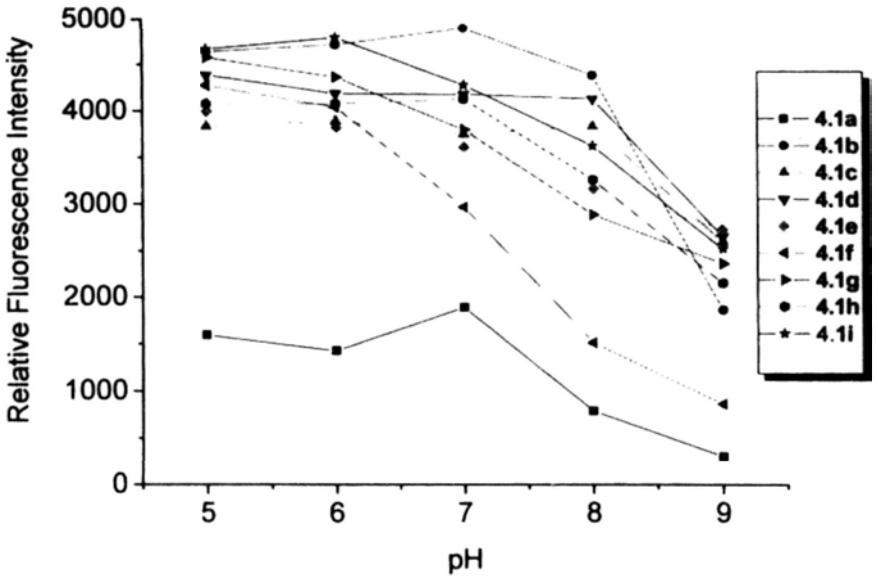

Figure 4.6. Change in the fluorescence intensity with pH for **4.1a-4.1i** (2 μM) in citrate buffer solutions upon excitation at 610 nm.

4.2.3 In Vitro Studies

The photodynamic activities of phthalocyanines **4.1a-4.1i** were evaluated against two different cell lines, namely human colon adenocarcinoma (HT29) and Chinese hamster ovary (CHO) cells. The latter cell line has chosen because of its higher PAT activity. This part of study was in collaboration with Prof. Wing-Ping Fong of the Biochemistry Department. Figure 4.7 shows the effects of **4.1b** on both cells give as an example. It is essentially noncytotoxic in the absence of light, but exhibits high photocytotoxicity. All the compounds show similar survival curves and their IC_{50} values are summarized in Table 4.3. Interestingly, most of the phthalocyanines show stronger photodynamic action against HT29 cells. It can be seen that the IC_{50} values of **4.1b** and **4.1c** against CHO cells are about 30-fold higher than those for HT29 cells. These results show that these phthalocyanines are selective toward HT29 tumor cells rather than CHO normal cells.

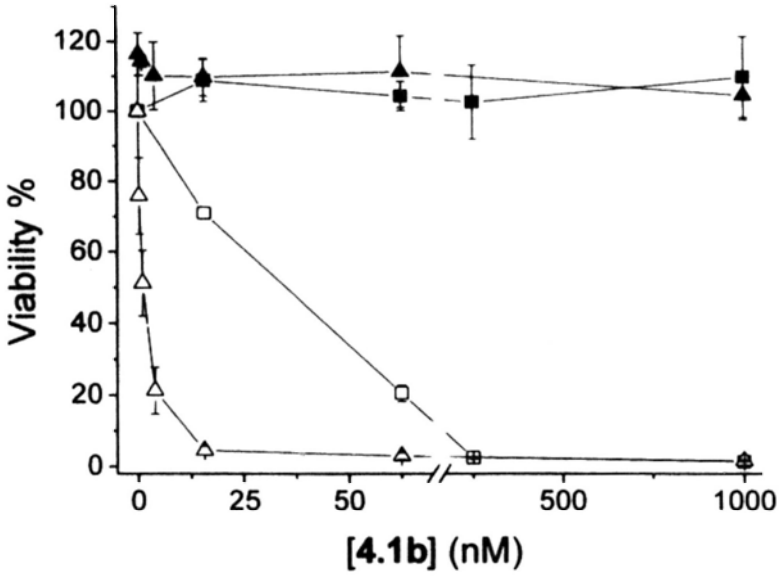

Figure 4.7. Comparison of the cytotoxic effects of **4.1b** on CHO cells (squares) and HT29 cells (triangles) in the absence (closed symbols) and presence (open symbols) of light ($\lambda > 610$ nm, 40 mW cm^{-2}, 48 J cm^{-2}). Data are expressed as mean values ± S.E.M. of three independent experiments, each performed in quadruplicate.

Table 4.3. Comparison of the IC_{50} values of phthalocyanines **4.1a-4.1i** against HT29 and CHO cells.

Compound	IC_{50} (nM)	
	HT29	CHO
4.1a	11.4	61.9
4.1b	1.1	35.0
4.1c	1.4	33.1
4.1d	5.5	29.0
4.1e	31.3	25.8
4.1f	21.7	36.5
4.1g	8.8	15.6
4.1h	23.4	21.3
4.1i	22.8	46.2

For the light source that we used (halogen lamp, $\lambda > 610$ nm), only a narrow region of the light (at ca. 610-700 nm) is absorbed by the compounds to initiate the photodynamic action. Hence, the actual total fluence required should be much lower than 48 J cm^{-2}. To study the effects of light dose, the cytotoxicity of **4.1b** on HT29 cells, upon illumination with a diode laser at 675 nm, was also evaluated. It was found that a total fluence of 16 J cm^{-2} (power = 0.2 W) is sufficient to attain a similar effect (IC_{50} = 1 nM) (Figure 4.8). By reducing the total fluence to 4 J cm^{-2}, the photoactivity was lower giving an IC_{50} value of 14.5 nM.

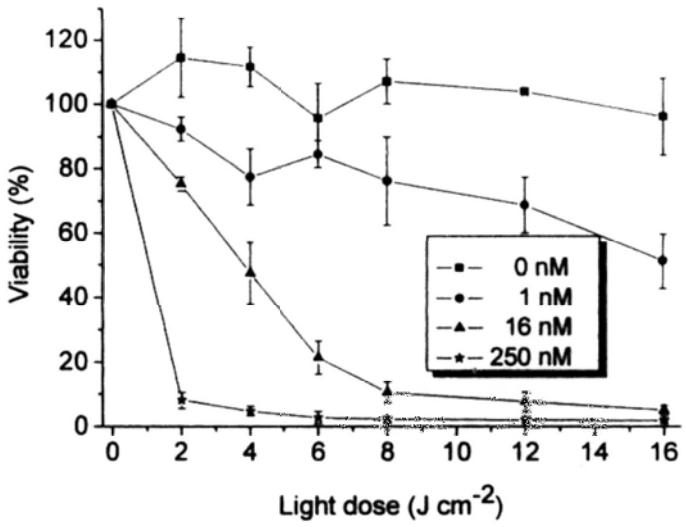

Figure 4.8. Light dose dependent photocytotoxicity of **4.1b** against HT29 cells. The cells were illuminated with a diode laser at 675 nm. Data are expressed as mean values ± S.E.M. of three independent experiments, each performed in quadruplicate.

It has been reported that PDT can initiate apoptosis causing cell death.[13] A hallmark of apoptosis is the change in membrane permeability that is demonstrated by phosphatidylserine externalization on the outer leaflet of the plasma membrane.[14] Annexin V-GFP is a sensitive probe for identifying apoptotic cells with a high affinity for phosphatidylserine. Propidium iodide (PI) is a standard flow cytometric viability

probe which is used to distinguish viable from nonviable cells. In this experiment, the apoptosis determination is conducted by the dual fluorescence of Annexin V-GFP/PI and is measured by flow cytometry to distinguish necrotic cells (GFP^+/PI^+), apoptotic cells (GFP^+/PI^-), and intact cells (GFP^-/PI^-). To investigate cell death mechanism triggered by these phthalocyanines, the most potent compound **4.1b** was selected to kill HT29 cells. HT29 cells were treated with phthalocyanine **4.1b** (16 nM) for 2 h. After illumination, they were stained with Annexin V-GFP and PI. As shown in Figure 4.9, most of the cells were negative with either Annexin V-GFP or PI in the absence of light, indicating that **4.1b** is noncytotoxic toward HT29 cells in darkness. After illumination, 94% of the cells were Annexin-postive and PI-negative. From these results, it can be concluded that these amino phthalocyanines induce apoptosis extensively.

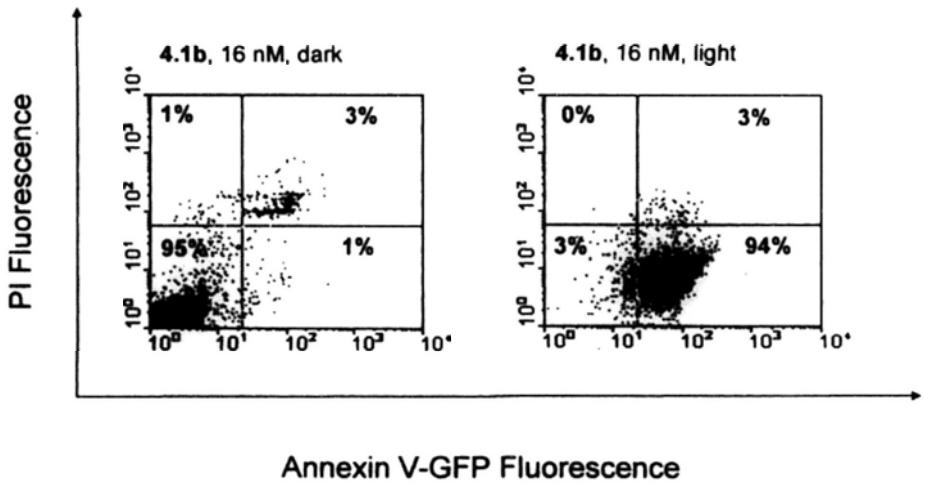

Figure 4.9. Contour diagram of Annexin V-GFP/PI flow cytometry of HT29 cells after incubation with **4.1b** (16 nM) in the absence and presence of light ($\lambda > 610$ nm, 40 mW cm^{-2}, 48 J cm^{-2}). The lower left quadrants of each panels show the viable cells, negative for Annexin V-GFP and PI. The upper right quadrants contain necrotic cells, positive for Annexin V-GFP and PI. The lower right quadrants represent the apoptotic cells, Annexin V-GFP positive and PI negative, demonstrating cytoplasmic membrane

integrity. The distribution of cell populations was determined by three independent trials with standard deviations obtained.

The subcellular localizations of **4.1b** and **4.1e** in HT29 cells were also investigated. The cells were incubated with these phthalocyanines together with LysoTracker Green DND 26 or MitoTracker Green FM, which are specific fluorescence dyes for lysosomes and mitochondria, respectively. As shown in Figure 4.10, the fluorescence caused by the LysoTracker (excited at 488 nm, monitored at 500-570 nm) is well superimposed with the fluorescence caused by both **4.1b** and **4.1e** (excited at 633 nm, monitored at 640-700 nm). The very similar fluorescence intensity profiles of phthalocyanine and LysoTracker traced along the green line also confirms that these compounds can target lysosomes of the cells. By contrast, the fluorescence images of these compounds and the Mitotracker (excited at 488 nm, monitored at 500-570 nm) cannot be superimposed, indicating that these compounds are not localized in the mitochondria.

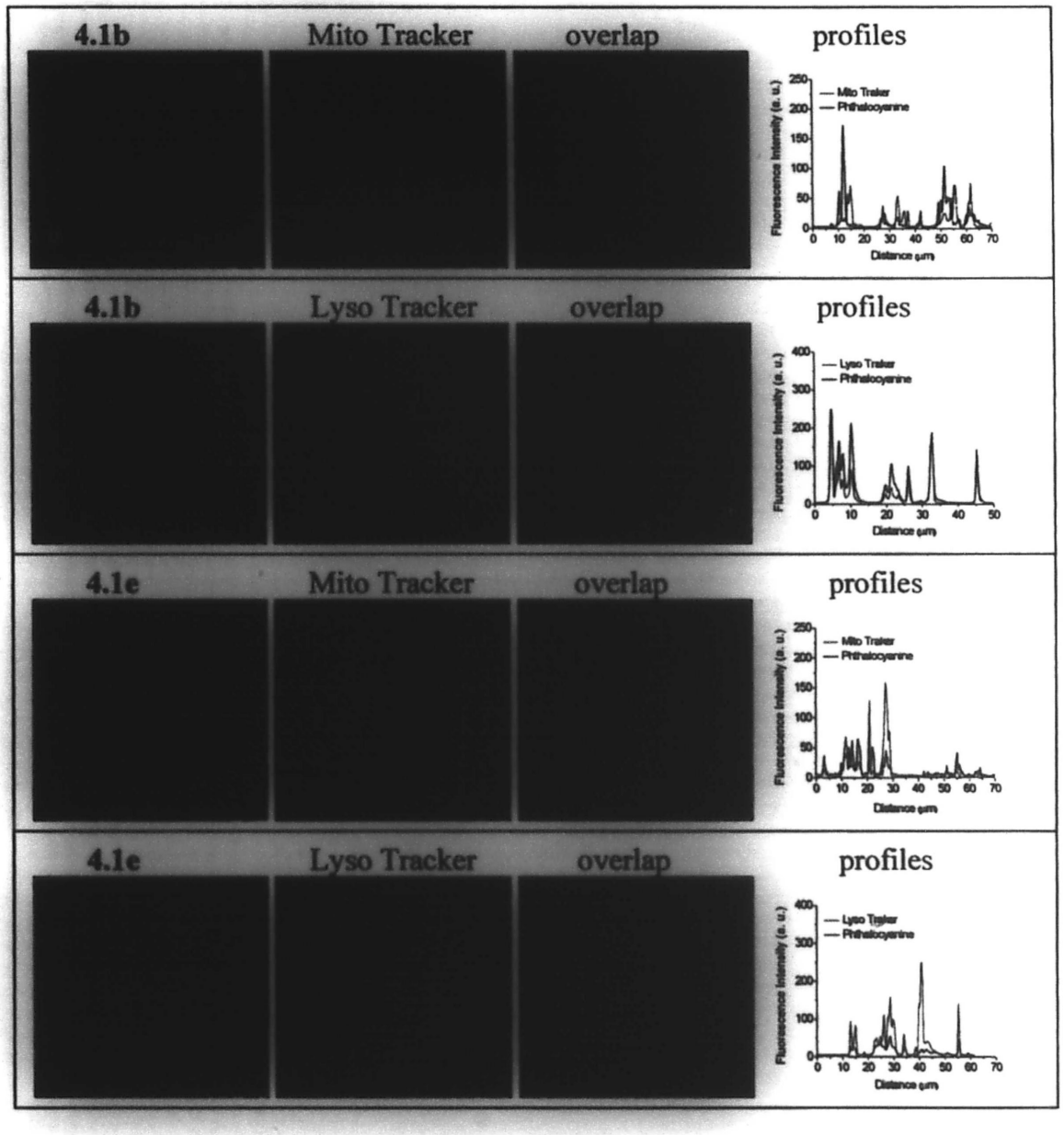

Figure 4.8. Visualization of intracellular fluorescence of HT29 using filter sets specific for phthalocyanines **4.1b**, and **4.1e**, Mito Tracker, and Lyso Tracker. The corresponding superimposed images and the fluorescence intensity profiles of these phthalocyanines and Mito Tracker or Lyso Tracker traced along the green line in the overlap images are also shown.

4.2.4 In Vivo Studies.

Phthalocyanines **4.1b** and **4.1e** were selected for in vivo evaluation of their PDT effectiveness. The study was performed by Prof. Wing-Ping Fong of the Biochemistry Department. Nude mice bearing HT29 cells were treated with an intravenous dose of phthalocyanine (1 μmol Kg^{-1}), and tumors were illuminated (30 J cm^{-2}) 24 h post-injection. The tumor size was monitored continuously for 2 weeks after PDT. As shown in Figure 4.11, phthalocyanines **4.1b** and **4.1e** are able to suppress and even reduce the tumor growth in mice. No significant difference in tumor regression could be seen for **4.1b** and **4.1e**, despite their in vitro IC_{50} values are remarkably different (Table 4.3).

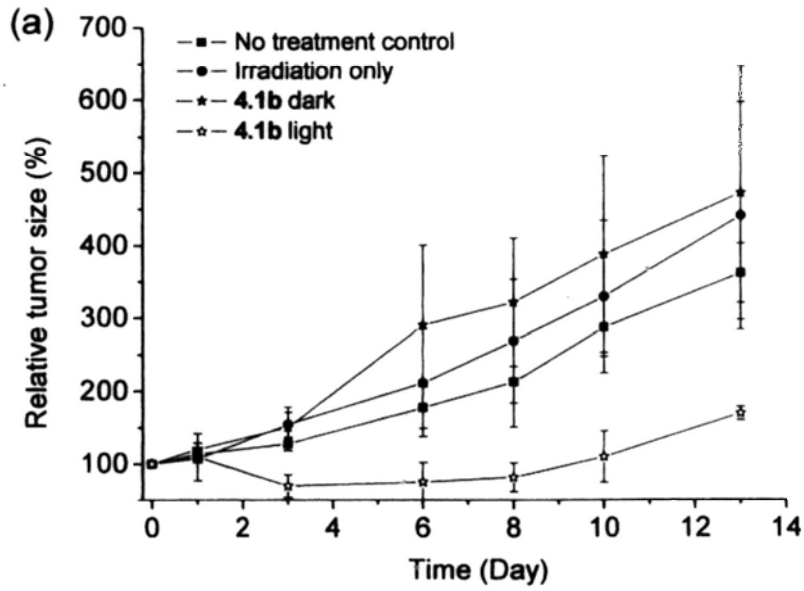

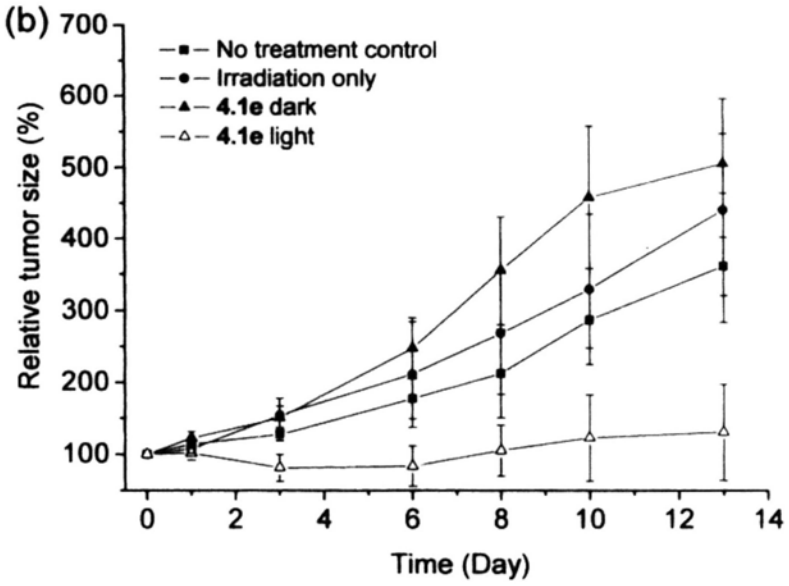

Figure 4.11. Tumor growth delay after PDT by phthalocyanines **4.1b** (a) and **4.1e** (b). Nude mice bearing HT29 cells subcutaneously were treated with an intravenous dose the of drug (1 μmol kg^{-1}). Illumination with laser light (30 J cm^{-2}) was applied for the PDT (n = 5 for each group) and the light-only group control (n = 3). The mice for dark control (n = 3 for each group) and no treatment control (n = 6) were kept in darkness. The tumor size was monitored continuously for 2 weeks after PDT.

The in vivo dark toxicity of phthalocyanines was determined by using plasma enzyme assay. The blood was collected from mice at the end of tumor regression study by cardiac puncture. Hepatic enzymes aspartate aminotransferase (AST) and alanine aminotransferase (ALT) marker enzymes activity levels in serum were detected. As shown in Figure 4.12, no significant injuries in liver of the mice were detected.

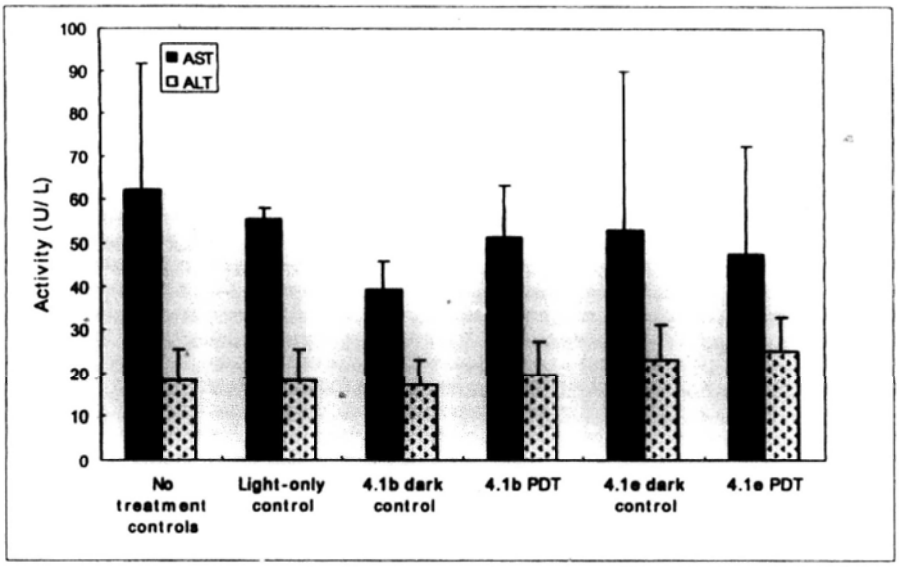

Figure 4.12. In vivo toxicity of **4.1b** and **4.1e**. The blood was collected from mice (n = 3 for each group) at the end of tumor regression study by cardiac puncture. Hepatic (AST and ALT) marker enzymes activity levels in serum were detected. The error bars represent the standard deviation. No significant injuries in liver of the mice were detected.

4.3 Conclusions

We have prepared and characterized a series of novel silicon(IV) phthalocyanines axially substituted with polyamine moieties. These hydrophilic compounds are nonaggregated in aqueous media. The in vitro photocytotoxic experiments show that most compounds are highly potent and the effects on HT29 cells are greater than those on CHO cells. For example, the IC_{50} value of compound **4.1b** against HT29 cells is 1.1 nM, while the value agaist CHO cells is 35.0 nM. These results indicate that these compounds may exhibit a higher potency for certain tumor cells such as HT29 cells, although the precise mechanism of selectivity remains elusive. Phthalocyanine **4.1b** predominately induces apoptosis in HT29 cells. As

revealed by confocal microscopy, **4.1b** and **4.1e** show a high selectivity toward lysosomes of the HT29 cells. The two compounds also inhibit the growth of tumor in vivo. All of these results indicate that this series of novel phthalocyanine-aryl polyamine conjugates are promising photosensitizers for PDT.

4.4 Experimental Section

Details regarding the purification of solvents, instrumentation, photophysical measurements, and in vitro studies have been described in Chapter 2.

4.4.1 Synthesis

***N*-(3-Hydroxypropyl)formamide (4.3a)**. This compound was prepared by a modified literature procedure.[15] Treatment of 3-hydroxyproprylamine (**4.2a**) (35.1 g, 0.47 mol) with methyl formate (90.1 g, 1.5 mol) gave the formamide **4.3a** (47.6 g, 98%). ^{1}H NMR (300 MHz, $CDCl_3$): δ 8.17 (s, 1 H, HCO), 6.58 (s, 1 H, NH), 3.66-3.76 (m, 2 H, OCH_2), 3.36-3.48 (m, 2 H, NCH_2), 1.69-1.80 (m, 2 H, CH_2).

***N*-(4-Hydroxybutyl)formamide (4.3b)**.[16] According to the procedure described for **4.3a**, treatment of 4-hydroxybutylamine (**4.2b**) (5.0 g, 56.1 mmol) with methyl formate (10.2 g, 0.17 mol) gave the formamide **4.3b** (6.5 g, 99%). ^{1}H NMR (300 MHz, $CDCl_3$): δ 8.17 (s, 1 H, HCO), 5.82 (s, 1 H, NH), 3.68-3.72 (m, 2 H, OCH_2), 3.27-3.37 (m, 2 H, NCH_2), 1.63-1.67 (m, 4 H, CH_2).

***N*-Methyl-3-hydroxypropylamine (4.4a)**. This compound was prepared by a modified literature procedure.[16] It was synthesized by adding a solution of **4.3a** (44.0 g, 0.43 mol) in THF (50 mL) to a vigorously stirred suspension of $LiAlH_4$ (22.1 g,

0.58 mol) in THF (200 mL) at 0 °C. After addition, the mixture was heated at reflux for 16 h. The suspension was then cooled to 0 °C. Water (30 mL) and then NaOH (10% w/w, 100 mL) were added to hydrolyze the mixture. The mixture was stirred at room temperature for 30 min. The insoluble precipitate was filtered off, and the filtrate was evaporated in vacuo. The residue was purified by distillation under reduced pressure (29.7 g, 77%). ^{1}H NMR (300 MHz, $CDCl_3$): δ 3.78 (t, J = 5.7 Hz, 2 H, OCH_2), 2.82 (t, J = 6.0 Hz, 2 H, NCH_2), 2.42 (s, 3 H, CH_3), 1.66-1.74 (m, 2 H, CH_2).

***N*-Methyl-3-hydroxybutylamine (4.4b).**[16] According to the procedure described for **4.4a**, treatment of **4.3b** (5.1 g, 43.1 mmol) with $LiAlH_4$ (5.1 g, 0.13 mol) in THF (200 mL) gave **4.4b** (4.4 g, 98%). ^{1}H NMR (300 MHz, $CDCl_3$): δ 3.57 (t, J = 4.8 Hz, 2 H, OCH_2), 2.62 (t, J = 5.7 Hz, 2 H, NCH_2), 2.42 (s, 3 H, CH_3), 1.60-1.68 (m, 4 H, CH_2).

***N*-(*tert*-Butoxycarbonyl)-*N*-methyl-3-hydroxypropylamine (4.5a).**[17] A solution of **4.4a** (5.1 g, 57.2 mmol) in triethylamine/MeOH (1:7 v/v, 150 mL) was stirred at 0 °C for 10 min. A solution of di-*tert*-butyldicarbonate (21.2 g, 97.1 mmol) was added dropwise over 10 min. The mixture was stirred for 1 h under a N_2 atmosphere. The temperature was allowed to gradually rise to room temperature and the solution was stirred overnight. The solution was dissolved in CH_2Cl_2 and washed with deionized water. The organic layer was separated, dried over anhydrous Na_2SO_4, filtered, and concentrated to give **4.5a** as a clear oil (9.9 g, 92%). ^{1}H NMR (300 MHz, $CDCl_3$): δ 3.55 (vt, 2 H, OCH_2), 3.39 (vt, 2 H, NCH_2), 2.84 (s, 3 H, NCH_3), 1.68 (br, s, 2 H, CH_2), 1.47 (s, 9 H CH_3).

***N*-(*tert*-Butoxycarbonyl)-*N*-methyl-3-hydroxybutylamine (4.5b).**[18] According to the procedure described for **4.5a**, treatment of **4.4b** (5.0 g, 48.5 mmol) with di-*tert*-butyldicarbonate (15.4 g, 70.5 mmol) gave **4.5b** as a clear oil (9.7 g, 98%) ^{1}H NMR (300 MHz, $CDCl_3$): δ 3.57 (vt, 2 H, OCH_2), 3.16 (t, J = 6.3 Hz, 2 H, NCH_2), 2.76 (s, 3 H, NCH_3), 1.46-1.52 (m, 4 H, CH_2), 1.38 (s, 9 H CH_3).

3-[(*tert*-Butoxycarbonyl)(methyl)amino]propyl methanesulfonate (4.6a).[19] The synthetic procedure of **4.6a** was similar to that reported earlier for the preparation of 3-[(*tert*-butoxycarbonyl)(methyl)amino]propyl methanesulfonate.[12] A solution of **4.5a** (9.5 g, 50.2 mmol) and triethylamine (20.2 g, 0.20 mol) in CH_2Cl_2 (130 mL) was stirred at 0 °C. Methanesulfony chloride (11.5 g, 0.10 mol) was added dropwise over 30 min under a N_2 atmosphere. The reaction mixture was stirred at 0 °C for 1 h, then it was slowly warmed to room temperature and stirred overnight under N_2. The reaction mixture was cooled to 0 °C, then a 4 M NaOH solution (50 mL) was added slowly with vigorous stirring. The organic phase was separated and washed with water (70 mL × 3). It was then dried over anhydrous Na_2SO_4 , and concentrated to give **4.6a** as a yellow oil (12.5 g, 93%). The product was used in the next step without further purification. ^{1}H NMR (400 MHz, $CDCl_3$): δ 4.25 (t, J = 6.0 Hz, 2 H, SCH_2), 3.45 (t, J = 6.8 Hz, 2 H, NCH_2), 3.03 (s, 3 H, CSH_3), 2.86 (s, 3 H, NCH_3), 1.94 - 2.01 (m, 2 H, CH_2), 1.46 (s, 9 H, CH_3).

4-[(*tert*-Butoxycarbonyl)(methyl)amino]butyl methanesulfonate (4.6b). According to the procedure described for **4.6a**, treatment of **5b** (5.0 g, 24.6 mmol) with methanesulfony chloride (5.8 g, 50.6 mmol) gave **4.6b** as a yellow oil (6.3 g, 91%). ^{1}H NMR (400 MHz, $CDCl_3$): δ 4.26 (t, J = 6.4 Hz, 2 H, SCH_2), 3.26 (t, J = 6.8 Hz, 2

H, NCH_2), 3.02 (s, 3 H, SCH_3), 2.84 (s, 3 H, NCH_3), 1.70-1.78 (m, 2 H, CH_2), 1.60-1.68 (m, 2 H, CH_2), 1.46 (s, 9 H, CH_3).

[3-(3-Hydroxypropylamino)propyl](methyl)carbamic acid *tert*-butyl ester (4.8a). The synthetic procedure of **4.8a** was similar to that reported earlier for the preparation of [3-(3-hydroxypropylamino)propyl]carbamic acid *tert*-butyl ester.[12] The mesylate **4.6a** (5.1 g, 19.1 mmol) and **4.2a** (10.0 g, 0.13 mol) were dissolved in acetonitrile (20 mL). The mixture was then stirred at 75 °C under a N_2 atmosphere for 48 h. The solution was concentrated under reduced pressure. The residue was dissolved in CH_2Cl_2 (30 mL) and washed with 10% aqueous Na_2CO_3 (100 mL × 3). The organic layer was separated and dried with anhydrous Na_2SO_4. After concentration in vacuo, the residue was purified by flash column chromatography (SiO_2, 10% MeOH/$CHCl_3$) to afford **4.8a** as light yellow oil (1.6 g, 34%). ^{1}H NMR (300 MHz, $CDCl_3$): δ 3.81 (t, J = 5.1 Hz, 2 H, OCH_2), 3.28 (vt, 2 H, NCH_2), 2.83 (vt, 2 H, NCH_2), 2.83 (s, 3 H, NCH_3), 2.60 (t, J = 6.3 Hz, 2 H, NCH_2), 1.67-1.74 (m, 4 H, CH_2), 1.46 (s, 9 H, CH_3). HRMS (EI) calcd for $C_{12}H_{26}N_2O_3$ $[M]^+$ 246.1938, found: 246.1935.

[4-(3-Hydroxypropylamino)butyl](methyl)carbamic acid *tert*-butyl ester (4.8b). According to the procedure described for **4.8a**, treatment of **4.6b** (5.1 g, 18.1 mmol) with **4.2a** (10.0 g, 0.13 mol) gave **4.8b** as a yellow oil (1.7 g, 36%). ^{1}H NMR (400 MHz, $CDCl_3$): δ 3.81 (t, J = 5.2 Hz, 2 H, OCH_2), 3.21 (vt, 2 H, NCH_2), 2.88 (t, J = 5.6 Hz, 2 H, NCH_2), 2.83 (s, 3 H, NCH_3), 2.63 (t, J = 6.8 Hz, 2 H, NCH_2), 1.67-1.71 (m, 2 H, CH_2), 1.51-1.54 (m, 2 H, CH_2), 1.43-1.47 (m, 2 H, CH_2), 1.46 (s, 9 H, CH_3). HRMS (EI) calcd for $C_{13}H_{28}N_2O_3$ $[M]^+$ 260.2094, found: 260.2093.

{3-[(2-Hydroxyethyl)(methyl)amino](propyl)}(methyl)carbamic acid *tert*-butyl ester (4.8c). According to the procedure described for **4.8a**, treatment of **4.6a** (3.6 g, 13.5 mmol) with **4.7** (3.8 g, 51.1 mmol) gave **4.8c** as a yellow oil (2.0 g, 60%). ^{1}H NMR (400 MHz, $CDCl_3$): δ 3.59 (t, J = 5.2 Hz, 2 H, OCH_2), 3.26 (vt, 2 H, NCH_2), 2.85 (s, 3 H, NCH_3), 2.52 (t, J = 5.2 Hz, 2 H, NCH_2), 2.40 (t, J = 7.2 Hz, 2 H, NCH_2), 2.25 (s, 3 H, CH_3), 1.66-1.73 (m, 2 H, CH_2), 1.46 (s, 9 H, CH_3). HRMS (EI) calcd for $C_{12}H_{26}N_2O_3$ $[M]^+$ 246.1938, found: 246.1935.

{3-[(3-Hydroxypropyl)(methyl)amino](propyl)}(methyl)carbamic acid *tert*-butyl ester (4.8d). According to the procedure described for **4.8a**, treatment of **4.6a** (4.9 g, 18.3 mmol) with **4.4a** (10.0 g, 0.11 mmol) gave **4.8d** as a yellow oil (1.6 g, 33%). ^{1}H NMR (300 MHz, $CDCl_3$): δ 3.80 (t, J = 5.1 Hz, 2 H, OCH_2), 3.23 (vt, 2 H, NCH_2), 2.85 (S, 3 H, NCH_3), 2.59 (t, J = 5.7 Hz, 2 H, NCH_2), 2.34 (t, J = 7.5 Hz, 2 H, NCH_2), 2.25 (s, 3 H, NCH_3), 1.67-1.75 (m, 4 H, CH_2), 1.46 (s, 9 H, CH_3). HRMS (EI) calcd for $C_{13}H_{28}N_2O_3$ $[M]^+$ 260.2094, found: 260.2096.

{4-[(3-Hydroxypropyl)(methyl)amino](butyl)}(methyl)carbamic acid *tert*-butyl ester. (4.8e). According to the procedure described for **4.8a**, treatment of **4.6b** (5.0 g, 17.8 mmol) with **4.4a** (10.1 g, 0.11 mol) gave **4.8e** as a yellow oil (2.4 g, 49%). ^{1}H NMR (400 MHz, $CDCl_3$): δ 3.80 (t, J = 5.2 Hz, 2 H, OCH_2), 3.22 (vt, 2 H, NCH_2), 2.83 (s, 3 H, NCH_3), 2.59 (t, J = 5.6 Hz, 2 H, NCH_2), 2.38 (t, J = 7.2 Hz, 2 H, NCH_2), 2.24 (s, 3 H, NCH_3), 1.67-1.72 (m, 2 H, CH_2), 1.48-1.51 (m, 4 H, CH_2), 1.45 (s, 9 H, CH_3). HRMS (EI) calcd for $C_{13}H_{28}N_2O_3$ $[M]^+$ 274.2251, found: 274.2242.

3-[3-(Methylamino)propylamino]propan-1-ol (4.9a). A solution of Boc-protected **4.8a** (1.5 g, 6.1 mmol) in MeOH (10 mL) was stirred at 0 ^{O}C for 10 min. A 4 M HCl (10 mL) solution was added to the reaction mixture dropwise. The mixture was stirred at 0 ^{O}C for 20 min and then at room temperature overnight. The solution was concentrated under reduce pressure to give a yellow oil. The oil was mixed with aqueous Na_2CO_3 solution (20% w/w, 10 mL) and the solvent was evaporated. The residue was dissolved in CH_2Cl_2. The solution was dried with anhydrous $MgSO_4$, and then concentrated in vacuo to give a clear oil. (0.82 g, 92%). ^{1}H NMR (400 MHz, $CDCl_3$): δ 3.78 (t, J = 5.4 Hz, 2 H, OCH_2), 2.85 (t, J = 5.6 Hz, 2 H, NCH_2), 2.67 (t, J = 7.2 Hz, 2 H, NCH_2), 2.62 (t, J = 7.2 Hz, 2 H, NCH_2), 2.42 (s, 3 H, NCH_3), 1.65-1.71 (m, 4 H, CH_2). ^{13}C{^{1}H} NMR (75.5 MHz, $CDCl_3$): δ 64.1, 50.2, 49.9, 48.1, 36.5, 30.7, 29.9. HRMS (EI) calcd for $C_7H_{18}N_2O$ $[M]^+$ 146.1414, found: 146.1411.

3-[4-(Methylamino)butylamino]propan-1-ol (4.9b). According to the procedure described for **4.9a,** treatment of **4.8b** (1.5 g, 5.8 mmol) with 4 M HCl (10 mL) and then aqueous Na_2CO_3 solution (20% w/w, 10 mL) gave **4.9b** as a clear oil (0.85 g, 91%). ^{1}H NMR (400 MHz, $CDCl_3$): δ 3.80 (t, J = 5.2 Hz, 2 H, OCH_2), 2.87 (t, J = 5.6 Hz, 2 H, NCH_2), 2.63 (t, J = 6.4 Hz, 2 H, NCH_2), 2.57 (t, J = 6.8 Hz, 2 H, NCH_2), 2.42 (s, 3 H, NCH_3), 1.66-1.72 (m, 2 H, CH_2), 1.50-1.53 (m, 4 H, CH_2). ^{13}C{^{1}H} NMR (75.5 MHz, $CDCl_3$): δ 64.6, 51.9, 50.1, 49.7, 36.5, 30.5, 27.7, 27.6. HRMS (EI) calcd for $C_8H_{20}N_2O$ $[M]^+$ 160.1570, found: 160.1567.

2-{Methyl[3-(methylamino)propyl]amino}ethanol (4.9c). According to the procedure described for **4.9a,** treatment of **4.8c** (1.8 g, 7.3 mmol) with 4 M HCl (10 mL) and then aqueous Na_2CO_3 solution (20% w/w, 10 mL) gave **4.9c** as a clear oil

(1.09 g, 93%). ^{1}H NMR (400 MHz, $CDCl_3$): δ 3.61 (t, J = 5.2 Hz, 2 H, OCH_2), 2.69 (t, J = 6.8 Hz, 2 H, NCH_2), 2.48-2.54 (m, 4 H, NCH_2), 2.44 (s, 3 H, NCH_3), 2.26 (s, 3 H, NCH_3), 1.66-1.73 (m, 2 H, CH_2). $^{13}C\{^1H\}$ NMR (100.6 MHz, $CDCl_3$): δ 58.8, 55.1, 50.2, 42.2, 36.1, 26.7. HRMS (ESI) calcd for $C_7H_{19}N_2O$ $[M+H]^+$ 147.1492, found: 147.1489.

3-{Methyl[3-(methylamino)propyl]amino}propan-1-ol (4.9d). According to the procedure described for **4.9a,** treatment of **4.8d** (1.6 g, 6.1 mmol) with 4 M HCl (10 mL) and then aqueous Na_2CO_3 solution (20% w/w, 10 mL) gave **4.9d** as a clear oil (0.83 g, 85%). ^{1}H NMR (300 MHz, $CDCl_3$): δ 3.79 (t, J = 5.1 Hz, 2 H, OCH_2), 2.57-2.63 (m, 4 H, NCH_2), 2.43 (t, J = 7.2 Hz, 2 H, NCH_2), 2.43 (s, 3 H, NCH_3), 2.25 (s, 3 H, NCH_3), 1.66-1.73 (m, 4 H, CH_2). $^{13}C\{^1H\}$ NMR (75.5 MHz, $CDCl_3$): δ 64.2, 58.0, 56.1, 50.1, 41.9, 36.5, 27.8, 27.4. HRMS (EI) calcd for $C_8H_{20}N_2O$ $[M]^+$ 160.1570, found: 160.1576.

3-{Methyl[3-(methylamino)propyl]amino}propan-1-ol (4.9e). According to the procedure described for **4.9a**, treatment of **4.8e** (1.5 g, 5.5 mmol) with 4 M HCl (10 mL) and then aqueous Na_2CO_3 solution (20% w/w, 10 mL) gave **4.9e** as a clear oil (0.66 g, 69%). ^{1}H NMR (400 MHz, $CDCl_3$): δ 3.80 (t, J = 5.2 Hz, 2 H, OCH_2), 2.57-2.61 (m, 4 H, NCH_2), 2.43 (s, 3 H, NCH_3), 2.38 (t, J = 6.8 Hz, 2 H, NCH_2), 2.24 (s, 3 H, NCH_3), 1.68-1.72 (m, 2 H, CH_2), 1.46-1.54 (m, 4 H, CH_2). $^{13}C\{^1H\}$ NMR (100.6 MHz, $CDCl_3$): δ 64.7, 58.5, 58.1, 51.9, 41.9, 36.4, 27.6 (two overlapping signals), 25.0. HRMS (EI) calcd for $C_9H_{22}N_2O$ $[M]^+$ 174.1727, found: 174.1723.

{3-[(3-*tert*-Butoxycarbonyl)(3-hydroxypropyl)amino](propyl)}(methyl)carbamic acid *tert*-butyl ester (4.10). According to the procedure described for **4.5a**, treatment of **4.8a** (5.1 g, 20.7 mmol) with di-*tert*-butyldicarbonate (10.5 g, 48.1 mmol) gave **4.10** as a clear oil (6.5 g, 91%). ^{1}H NMR (300 MHz, $CDCl_3$): δ 3.54 (vt, 2 H, OCH_2), 3.38 (vt, 2 H, NCH_2), 3.22 (vt, 2 H, NCH_2), 3.13 (vt, 2 H, NCH_2), 2.85 (s, 3 H, NCH_3), 1.59-1.80 (m, 4 H, CH_2), 1.46 (s, 18 H, CH_3). HRMS (EI) calcd for $C_{17}H_{34}N_2O_5$ $[M]^+$ 346.2462, found: 346.2460.

3-[{3-[(*tert*-Butoxycarbonyl)(methyl)amino]propyl}(tert-buoxycanbonyl)amino] propyl methanesulfonate (4.11). According to the procedure described for **4.6a**, treatment of **4.10** (5.1 g, 14.7 mmol) with methanesulfony chloride (10.1 g, 88.1 mmol) gave **4.11** as a yellow oil (5.2 g, 83%). ^{1}H NMR (300 MHz, $CDCl_3$): δ 4.25 (t, J = 6.3 Hz, 2 H, OCH_2), 3.29-3.32 (m, 2 H, NCH_2), 3.15-3.23 (m, 4 H, NCH_2), 3.03 (s, 3 H, SCH_3), 2.80 (s, 3 H, NCH_3), 1.95-2.01 (m, 2 H, CH_2), 1.70-1.79 (m, 2 H, CH_2),1.46 (s, 18 H, CH_3).

3-[{3-[{3-[(*tert*-Butoxycarbonyl)(methyl)amino]propyl}(tert-buoxycanbonyl)amino] propyl}(methyl)amino] propan-1-ol (4.12). According to the procedure described for **4.8a**, treatment of **4.11** (5.1 g, 12.0 mmol) with **4.4a** (5.1 g, 57.2 mmol) gave **4.12** as a clear oil (3.0 g, 60%). ^{1}H NMR (400 MHz, $CDCl_3$): δ 3.79 (t, J = 5.2 Hz, 2 H, OCH_2), 3.20 (br, s, 6 H, CH_2), 2.85 (s, 3 H, NCH_3), 2.59 (t, J = 5.6 Hz, 2 H, NCH_2), 2.37 (t, J = 7.2 Hz, 2 H, NCH_2), 2.25 (s, 3 H, NCH_3), 1.68-1.75 (m, 6 H, CH_2), 1.46 (s, 18 H, CH_3). HRMS (EI) calcd for $C_{21}H_{43}N_3O_5$ $[M]^+$ 417.3197, found: 417.3187.

3-[(3-{[3-(Methylamino)propyl]amino}propyl)(methyl)] propan-1-ol (4.13). According to the procedure described for **4.9a,** treatment of **4.12** (1.6 g, 3.8 mmol) with 4 M HCl (10 mL) and then aqueous Na_2CO_3 solution (20% w/w, 10 mL) gave **4.13** as a clear oil (0.69 g, 84%). ^{1}H NMR (400 MHz, $CDCl_3$): δ 3.78 (t, J = 5.2 Hz, 2 H, OCH_2), 2.61-2.68 (m, 6 H, NCH_2), 2.58 (t, J = 5.6 Hz, 2 H, NCH_2), 2.42 (t, J = 7.2 Hz, 2 H, NCH_2), 2.42 (s, 3 H, NCH_3), 2.24 (s, 3 H, NCH_3), 1.65-1.72 (m, 6 H, CH_2). ^{13}C{^{1}H} NMR (100.6 MHz, $CDCl_3$): δ 64.2, 58.0, 56.2, 50,5, 48.4, 48.0, 42.0, 36.5, 30.0, 27.8, 27.6. HRMS (EI) calcd for $C_{11}H_{27}N_3O$ $[M]^+$ 217.2149, found: 217.2153.

Preparation of Phthalocyanine 4.1a. A mixture of silicon(IV) phthalocyanine dichloride (0.20 g, 0.33 mmol), 2-(methylamino)ethanol (0.22 g, 2.93 mmol), and pyridine (0.5 mL) in toluene (30 mL) was refluxed for 4 h. After evaporating the solvent in vacuo, the residue was dissolved in CH_2Cl_2 (100 mL) and then washed with water (100 mL × 3). The organic layer was collected and evaporated under reduced pressure. The crude product was recrystallized from $CHCl_3$/1-hexane (1:4 v/v) to give the product as a blue solid (0.18 g, 79%). ^{1}H NMR (400 MHz, $CDCl_3$): δ 9.63-9.65 (m, 8 H, Pc-H_α), 8.34-8.36 (m, 8 H, Pc-H_β), 0.73 (s, 6 H, NCH_3), -0.38 (t, J = 5.2 Hz, 4 H, CH_2), -2.00 (t, J = 5.2 Hz, 4 H, OCH_2). ^{13}C{^{1}H} NMR (100.6 MHz, $CDCl_3$): δ 149.2, 135.9, 131.0, 123.7, 53.5, 50.1, 34.0. HRMS (FAB) calcd for $C_{38}H_{32}N_{10}O_2Si$ $[M]^+$ 688.2473, found: 688.2459. Anal. Calcd for $C_{38}H_{32}N_{10}O_2Si$: C, 66.26; H, 4.68; N, 20.33. Found: C, 65.80; H, 4.55; N, 19.96.

Preparation of Phthalocyanine 4.1b According to the procedure described for **4.1a**, silicon(IV) phthalocyanine dichloride (0.15 g, 0.25 mmol) was treated with hydroxyamine **4.2a** (0.21 g, 2.36 mmol) and pyridine (0.5 mL) in toluene (30 mL) to

give **4.1b** as a blue solid (0.13 g, 72%). ^{1}H NMR (400 MHz, $CDCl_3$): δ 9.63-9.65 (m, 8 H, Pc-H_α), 8.33-8.35 (m, 8 H, Pc-H_β), 1.16 (s, 6 H, NCH_3), -0.08 (t, J = 6.4 Hz, 4 H, NCH_2), -1.35--1.31 (m, 4 H, CH_2), -2.04 (t, J = 5.6 Hz, 4 H, OCH_2). $^{13}C\{^1H\}$ NMR (100.6 MHz, $CDCl_3$): δ 149.2, 135.9, 131.0, 123.6, 53.9, 47.9, 35.2, 28.6. HRMS (FAB) calcd for $C_{40}H_{37}N_{10}O_2Si$ $[M+H]^+$ 717.2865, found: 717.2863. Anal. Calcd for $C_{40}H_{36}N_{10}O_2Si$: C, 67.02; H, 5.06; N, 19.54. Found: C, 67.00; H, 5.22; N, 19.36.

Preparation of Phthalocyanine 4.1c. According to the procedure described for **4.1a**, silicon(IV) phthalocyanine dichloride (0.15 g, 0.25 mmol) was treated with hydroxyamine **4.2b** (0.25 g, 2.43 mmol) and pyridine (0.5 mL) in toluene (30 mL) to give **4.1c** as a blue solid (0.14 g, 76%). ^{1}H NMR (400 MHz, $CDCl_3$): δ 9.62-9.64 (m, 8 H, Pc-H_α), 8.32-8.34 (m, 8 H, Pc-H_β), 1.61 (s, 6 H, NCH_3), 0.76 (t, J = 7.2 Hz, 4 H, NCH_2), -1.22--1.14 (m, 4 H, CH_2), -1.65--1.58 (m, 4 H, CH_2), -2.09 (t, J = 6.0 Hz, 4 H, OCH_2). $^{13}C\{^1H\}$ NMR (100.6 MHz, $CDCl_3$): δ 149.2, 136.0, 130.8, 123.7, 54.6, 50.1, 35.5, 26.7, 24.1. HRMS (FAB) calcd for $C_{42}H_{41}N_{10}O_2Si$ $[M+H]^+$ 745.3178, found: 745.3195. Anal. Calcd for $C_{42}H_{42}N_{10}O_3Si$ (**4.1c**·H_2O): C, 66.12; H, 5.55; N, 18.36. Found: C, 66.68; H, 5.44; N, 17.93.

Preparation of Phthalocyanine 4.1d. According to the procedure described for **4.1a**, silicon(IV) phthalocyanine dichloride (0.13 g, 0.21 mmol) was treated with hydroxyamine **4.8a** (0.23g, 1.58 mmol) and pyridine (0.5 mL) in toluene (30 mL) to give **4.1d** as a blue solid (0.11 g, 62%). ^{1}H NMR (300 MHz, $CDCl_3$): δ 9.63-9.66 (m, 8 H, Pc-H_α), 8.34-8.37 (m, 8 H, Pc-H_β), 2.25 (s, 6 H, NCH_3), 2.05 (t, J = 7.2 Hz, 4 H, NCH_2), 1.29 (t, J = 7.2 Hz, 4 H, NCH_2), 0.68-0.78 (m, 4 H, CH_2), -0.06 (t, J = 6.3 Hz, 4 H, NCH_2), -1.35--1.31 (m, 4 H, CH_2), -2.06 (t, J = 5.7 Hz, 4 H, OCH_2). $^{13}C\{^1H\}$

NMR (75.5 MHz, $CDCl_3$): δ 149.2, 135.9, 130.9, 123.7, 53.8, 50.0, 47.0, 45.6, 36.3, 29.3, 28.7. HRMS (FAB) calcd for $C_{46}H_{51}N_{12}O_2Si$ $[M+H]^+$ 831.4022, found: 831.4040. Anal. Calcd for $C_{46}H_{52}N_{12}O_3Si$ (**4.1d**·H_2O): C, 65.07; H, 6.17; N, 19.80. Found: C, 65.32; H, 5.90; N, 17.47.

Preparation of Phthalocyanine 4.1e. According to the procedure described for **4.1a**, silicon(IV) phthalocyanine dichloride (0.14 g, 0.23 mmol) was treated with hydroxyamine **4.8b** (0.28 g, 1.75 mmol) and pyridine (0.5 mL) in toluene (30 mL) to give **4.1e** as a blue solid (0.12 g, 61%). ^1H NMR (400 MHz, $CDCl_3$): δ 9.69-9.72 (m, 8 H, Pc-H_α), 8.46-8.48 (m, 8 H, Pc-H_β), 2.29 (s, 6 H, NCH_3), 2.26 (t, J = 7.6 Hz, 4 H, NCH_2), 1.24 (t, J = 7.2 Hz, 4 H, NCH_2), 0.98-1.05 (m, 4 H, CH_2), 0.54-0.61 (m, 4 H, CH_2), -0.11 (t, J = 6.8 Hz, 4 H, NCH_2), -1.26--1.20 (m, 4 H, CH_2), -1.99 (t, J = 5.6 Hz, 4 H, OCH_2). $^{13}C\{^1H\}$ NMR (100.6 MHz, $CDCl_3$): δ 149.2, 135.9, 130.9, 123.6, 53.8, 51.7, 48.7, 45.5, 36.3, 28.6, 27.2, 27.0. HRMS (FAB) calcd for $C_{48}H_{55}N_{12}O_2Si$ $[M+H]^+$ 859.4335, found: 859.4347. Anal. Calcd for $C_{48}H_{56}N_{12}O_3Si$ (**4.1e**·H_2O): C, 65.73; H, 6.44; N, 19.16. Found: C, 65.66; H, 6.34; N, 18.67.

Preparation of Phthalocyanine 4.1f. According to the procedure described for **4.1a**, silicon(IV) phthalocyanine dichloride (0.15 g, 0.25 mmol) was treated with hydroxyamine **4.8c** (0.25 g, 1.71 mmol) and pyridine (0.5 mL) in toluene (30 mL) to give **4.1f** as a blue solid (0.13 g, 64%). ^1H NMR (300 MHz, $CDCl_3$): δ 9.61-9.65 (m, 8 H, Pc-H_α), 8.32-8.35 (m, 8 H, Pc-H_β), 2.06 (s, 6 H, NCH_3), 1.63 (t, J = 6.9 Hz, 4 H, NCH_2), 0.47 (t, J = 6.3 Hz, 4 H, NCH_2), 0.45 (s, 6 H, NCH_3), 0.27-0.37 (m, 4 H, CH_2), -0.79 (t, J = 6.3 Hz, 4 H, NCH_2), -1.97 (t, J = 6.3 Hz, 4 H, OCH_2). $^{13}C\{^1H\}$ NMR (100.6 MHz, $CDCl_3$): δ 149.2, 136.0, 130.8, 123.6, 56.0, 54.3, 53.3, 49.7, 41.1, 36.2,

26.5. HRMS (FAB) calcd for $C_{46}H_{51}N_{12}O_2Si$ $[M+H]^+$ 831.4022, found: 831.4025. Anal. Calcd for $C_{46}H_{52}N_{12}O_3Si$ (**4.1f**·H_2O): C, 65.07; H, 6.17; N, 19.80. Found: C, 65.19; H, 6.24; N, 19.31.

Preparation of Phthalocyanine 4.1g. According to the procedure described for **4.1a**, silicon(IV) phthalocyanine dichloride (0.20 g, 0.33 mmol) was treated with hydroxyamine **4.8d** (0.20g, 1.25 mmol) and pyridine (0.5 mL) in toluene (30 mL) to give **4.1g** as a blue solid (0.18 g, 64%). ^{1}H NMR (400 MHz, $CDCl_3$): δ 9.62-9.64 (m, 8 H, Pc-H_α), 8.32-8.35 (m, 8 H, Pc-H_β), 2.18 (s, 6 H, NCH_3), 1.99 (t, J = 6.8 Hz, 4 H, NCH_2), 1.15 (t, J = 7.2 Hz, 4 H, NCH_2), 1.03 (s, 6 H, NCH_3), 0.68-0.75 (m, 4 H, CH_2), -0.57 (t, J = 7.6 Hz, 4 H, NCH_2), -1.52--1.45 (m, 4 H, CH_2), -2.06 (t, J = 5.6 Hz, 4 H, OCH_2). ^{13}C{^{1}H} NMR (100.6 MHz, $CDCl_3$): δ 149.2, 136.0, 130.8, 123.6, 54.6, 53.2, 52.3, 50.1, 41.3, 36.3, 26.5 (Two overlapping signals). HRMS (FAB) calcd for $C_{48}H_{55}N_{12}O_2Si$ $[M+H]^+$ 859.4335, found: 859.4350. Anal. Calcd for $C_{48}H_{56}N_{12}O_3Si$ (**4.1g**·H_2O): C, 65.73; H, 6.44; N, 19.16. Found: C, 66.16; H, 6.23; N, 18.85.

Preparation of Phthalocyanine 4.1h. According to the procedure described for **4.1a**, silicon(IV) phthalocyanine dichloride (0.25 g, 0.41 mmol) was treated with hydroxyamine **4.8e** (0.41 g, 2.36 mmol) and pyridine (0.5 mL) in toluene (30 mL) to give **4.1h** as a blue solid (0.19 g, 51%). ^{1}H NMR (400 MHz, CD_3OD): δ 9.66-9.68 (m, 8 H, Pc-H_α), 8.43-8.46 (m, 8 H, Pc-H_β), 2.28 (s, 6 H, NCH_3), 2.22 (t, J = 7.2 Hz, 4 H, NCH_2), 1.20 (t, J = 7.6 Hz, 4 H, NCH_2), 1.04 (s, 6 H, NCH_3), 0.96-1.02 (m, 4 H, CH_2), 0.54-0.60 (m, 4 H, CH_2), -0.66 (t, J = 7.6 Hz, 4 H, NCH_2), -1.38--1.31 (m, 4 H, CH_2), -2.00 (t, J = 5.6 Hz, 4 H, OCH_2). ^{13}C{^{1}H} NMR (100.6 MHz, CD_3OD): δ 150.8, 137.1, 132.8, 124.8, 57.4, 54.5, 53.0, 52.2, 41.2, 35.9, 27.8, 26.9, 24.5. HRMS (FAB)

calcd for $C_{50}H_{59}N_{12}O_2Si$ $[M+H]^+$ 887.4648, found: 887.4682. Anal. Calcd for $C_{50}H_{60}N_{12}O_3Si$ (**4.1h**·H_2O): C, 66.34; H, 6.68; N, 18.57. Found: C, 66.40; H, 6.27; N, 18.14.

Preparation of Phthalocyanine 4.1i. According to the procedure described for **4.1a,** silicon(IV) phthalocyanine dichloride (0.19 g, 0.31 mmol) was treated with hydroxyamine **4.13** (0.34 g, 1.57 mmol) and pyridine (0.5 mL) in toluene (30 mL) to give **4.1i** as a blue solid (0.14 g, 45%). ^{1}H NMR (400 MHz, CD_3OD): δ 9.67-9.70 (m, 8 H, Pc-H_α), 8.44-8.46 (m, 8 H, Pc-H_β), 2.46 (t, J = 7.2 Hz, 4 H, NCH_2), 2.33 (t, J = 7.2 Hz, 4 H, NCH_2), 2.30 (s, 6 H, NCH_3), 2.02 (t, J = 7.6 Hz, 4 H, NCH_2), 1.47-1.54 (m, 4 H, CH_2), 1.21 (t, J = 7.2 Hz, 4 H, NCH_2), 1.06 (s, 6 H, NCH_3), 0.74-0.82 (m, 4 H, CH_2), -0.59 (t, J = 7.2 Hz, 4 H, NCH_2), -1.39--1.33 (m, 4 H, CH_2), -1.98 (t, J = 5.6 Hz, 4 H, OCH_2). ^{13}C{^{1}H} NMR (100.6 MHz, CD_3OD): δ 150.8, 137.1, 132.8, 124.8, 55.4, 54.5, 53.4, 50.5, 48.4, 48.3, 41.3, 35.8, 29.3, 27.1, 26.2. HRMS (FAB) calcd for $C_{54}H_{69}N_{14}O_2Si$ $[M+H]^+$ 973.5492, found: 973.5466. Anal. Calcd for $C_{54}H_{72}N_{14}O_4Si$ (**4.1i**·$2H_2O$): C, 64.26; H, 7.19; N, 19.43. Found: C, 66.40; H, 6.69; N, 19.19.

4.4.2 In Vitro Studies

Cell Lines and Culture Conditions. Chinese hamster ovary cell CHO (ATCC No. CCL-61) was cultured in RPMI-1640 medium with 2 mM aminoguanidine, 10% FBS, 100 U/ml penicillin, and 100 μg mL^{-1} streptomycin. The cell cultures were maintained at 37 °C with 5% CO_2, where cells from 5th to 19th passages were used for the study.

Light-dose Dependent Toxicity of Phthalocyanine 4.1b. For the study of light-dose dependent toxicity of **4.1b** on HT29 cells, the cells were incubated with the drug at concentrations of 250, 16 and 1 nM for 2 h. Light energy at various doses was delivered by laser of bandwidth 675 ± 3 nm with a power of 0.2 W (CeramOptec GmbH). The viability of cell was determined as described in Chapter 2.

Flow Cytometric Studies. HT29 cells were seeded on a 35 mm dish at a density of 2.5×10^4 cells mL^{-1} and incubated for 24 h. The cells were then treated with **4.1b** (16 nM) for 2 h in darkness. After washing the cells twice with PBS, 2 mL of fresh DMEM was added to each dish. The plates were then subject to illumination for 20 min by a halogen lamp. After 24 h of incubation, the cells were trypsinized and centrifuged at 664 × g for 3 min at room temperature. The pellet was resuspended in binding buffer (10 mM HEPES-NaOH, 140 mM NaCl and 2.5 mM $CaCl_2$ at pH 7.4) containing annexin V-GFP and PI. After incubation in darkness for 15 min at room temperature, the proportion of viable (1×10^4 cells per sample), necrotic and apoptotic cells were determined by a flow cytometer FACScanto (BD Falcon). Annexin V-GFP and PI were excited by a 488 nm argon laser. The emitted fluorescence at 509 nm for annexin V-GFP and at 562-588 nm for PI was collected. The data collected were analyzed by using WinMDI 2.9.

4.4.3 Animal Tumor Model

Male nude mice were inoculated at the back of the animal subcutaneously with 1×10^7 HT29 cells for growth of tumor. Tumor size was calculated by $d_1 \times d_2 \times d_3 \times \pi/6$ mm^3, where d_1, d_2, and d_3 represent the width, length, and thickness of the tumor measured by using a digital caliper. Only mice bearing tumor of size ranging from 80

to 120 mm^3 were adopted for the experiment. To make a 2.5 mM stock for each phthalocyanines, **4.1e** was dissolved in absolute ethanol and **4.1b** in THF with sonication. The drugs were further diluted by 5% cremophor EL to make a dose of 1 μmol per kg body weight. The phthalocyanines were administrated 24 hours prior to illumination via intravenous injection route. The tumor areas of the treatment groups and the light-only controls were illuminated by a laser of bandwidth 675 ± 3 nm with a power of 0.1 W (CeramOptec GmbH) for 5 min, in order to deliver 30 J cm^{-2} energy. The tumor size of each group of animals was monitored for 2 weeks after PDT.

The in vivo toxicity of phthalocyanines was determined by using plasma enzyme assay. The blood was collected by cardiac puncture and subsequently centrifuged at 2655 × g at room temperature for 5 min with the supernatant collected. The activity levels in serum of hepatic enzymes aspartate aminotransferase (AST) and alanine aminotransferase (ALT) were assaved by using standard kits (Stanbio).

4.5 References

1. Barret, J. M.; Kruczynski, A.; Vispé, S.; Annereau, J. P.; Brel, V.; Guminski, Y.; Delcros, J. G.; Lansiaux, A.; Guilaud, N.; Imbert, T.; Bailly, C. *Caner Res.* **2008**, *68*, 9845.
2. (a) Karigiannism G.; Papaioannou, D. *Eur. J. Org. Chem.* **2000**, 1841. (b) Seiler, N. *Pharmaco. Ther.* **2005**, *107*, 99.
3. (a) Holley, J. L.; Mather, A.; Wheelhouse, R. T.; Cullis, P. M.; Hartley, J. A.; Bingham, J. P.; Cohen, G. M. *Cancer Res.* **1992**, *52*, 4190. (b) Cullis, P. M.; Merson-Davies, L.; Weaver, R. *J. Am. Chem. Soc.* **1995**, *117*, 8033.

4. Holley, J.; Mather, A.; Cullis, P.; Symons, M. R.; Wardman, P.; Watt, R. A.; Cohen, G. M. *Biochem. Pharmacol.* **1992**, *43*, 763.

5. Eiseman, J. L.; Rogers, F. A.; Guo, Y.; Kauffman, J.; Sentz, D. L.; Klinger, M. F.; Callery, P. S.; Kyprianou, N. *Cancer Res.* **1998**, *58*, 4864.

6. Delcros, J. D.; Tomasi, S.; Carrington, S.; Martin, B.; Renault, J.; Blagbrough, I. S.; Uriac, P. *J. Med. Chem.* **2002**, *45*, 5098.

7. Suzuki, I.; Shigenaga, A.; Nemoto, H.; Shibuya, M. *Tetrahedron Lett.* **2004**, *45*, 1955.

8. Battaglia, A.; Guerrini, A.; Baldelli, E.; Fontanna, G.; Varchi, G.; Samorì, C.; Bambrdelli, E. *Tetrahedron Lett.* **2006**, *47*, 2667.

9. Dallavalle, S.; Giannini, G.; Alloatti, D.; Casati, A.; Marastoni, E.; Musso, L.; Merlini, L.; Morini, G.; Penco, S.; Pisano, C.; Tinelli, S.; De Cesare, M.; Beretta, G. L.; Zunino, F. *J. Med. Chem.* **2006**, *49*, 5177.

10. (a) Wang, J.; Xie, S.; Li, Y.; Guo, Y.; Ma, Y.; Zhao, J.; Phanstiel IV, O.; Wang, C. *Bioorg. Med. Chem.* **2008**, *16*, 7005. (b) Wang, C.; Delcros, J.-G.; Biggerstaff, J.; Phanstiel IV, O. *J. Med. Chem.* **2003**, *46*, 2663. (c) Breitbeil III, F.; Kaur, N.; Delcros, J.-G.; Martin, B.; Abboud, K. A.; Phanstiel IV, O. *J. Med. Chem.* **2006**, *49*, 2407. (c) Tsen, C.; Lltis, M.; Kaur, N.; Bayer, C.; Delcros, J.-G.; von Kalm, L.; Phanstiel IV, O. *J. Med. Chem.* **2008**, *51*, 324. (f) Kaur, N.; Delcros, J. G.; Martin, B.; Phanstiel IV, O. *J. Med. Chem.* **2005**, *48*, 3832.

11. Sol, V.; Lamarche, F.; Enache, M.; Garcia, G.; Granet, R.; Guilloton, M.; Blais, J. C.; Krausz, P. *Bioorg. Med. Chem.* **2006**, *14*, 1364.

12. Kaur, N.; Delcros, J. G.; Martin, B.; Phanstiel IV, O. *J. Med. Chem.* **2005**, *48*, 3832.

13. (a) Králová, J.; Bříza, T.; Moserová, I.; Dolenský, B.; Vašek, P.; Poučková, P.; Kejík, Z.; Kaplánek, R.; Martásek, P.; Dvořák, M.; Král V. *J. Med. Chem.* ***2008***, *51*, 5964. (b) Tang, P. M. K.; Liu, X. Z.; Zhang, D. M.; Fong, W. P.; Fung, K. P. *Cancer Biol. Ther.* **2009**, *8*,1.

14. Vermes, I.; Haanen, C.; Steffens-Nakken, H.; Reutelingsperger, C. *J. Immunol. Methods* **1995**, *184*, 39.

15. Koepke, S. R.; Kupper, R.; Michejda, C. J. *J. Org. Chem.* **1979**, *4*, 2718-2722.

16. Asaki, T.; Hamamoto, T.; Sugiyama, Y.; Kuwano, K.; Kuwabara, K. *Bioorg. Med. Chem.* **2007**, *15*, 6692-6704.

17. Vedejs, E.; Stults, J. S. *J. Org. Chem.* **1988**, *53*, 2226-2232.

18. Das, B.; Venkateswarlu, K.; Krishnaiah, M.; Holla, H. *Tetrahedron Lett.* **2006**, *47*, 7551-7556.

19. Yamawaki, K.; Nomura, T.; Yasukata, T.; Uotani, K.; Miwa, H.; Takeda, K.; Nishitani, Y. *Bioorg. Med. Chem.* **2007**, *15*, 6716-6732.

CHAPTER 5

Synthesis, Characterization and in vitro Photodynamic Activities of Cholesterol-Containing Silicon(IV) Phthalocyanines

5.1 Introduction

Cholesterol is a key component of all eukaryotic plasma membranes and is essential for the growth and viability of cells in higher organisms. Hence it is natural that tumor cells and tumor vascular endothelial cells over-express the low-density lipoprotein (LDL) receptor for the demand of increased proliferation membrane turnover.[1] Conjugation of photosensitizers to cholesterol favors their binding to LDL, which in turn promotes the interaction with LDL receptors over-expressed on tumor cells and enhances the selectivity of tumor loading.[1] This strategy has been employed for several photosensitizers such as pyropheophorbide,[2] germanium(IV) phthalocyanine,[3] zinc(II) phthalocyanine,[4] and silicon(IV) phthalocyanine,[5] but only a limited selectivity for tumors has been demonstrated. We report herein the synthesis, characterization, and in vitro photodynamic activities of a new series of silicon(IV) phthalocyanines axially substituted with one or two cholesterol unit(s) via a long ethylene glycol chain. Owing to the presence of oligo hydrophilic ethylene glycol chains and hydrophobic cholesterol anchor(s), these amphiphilic derivatives could be stably intercalated into the phospholipids monolayer of LDL particles as an effective way to deliver photosensitizers into tumor cells.

5.2 Results and Discussion

5.2.1 Synthesis and Characterization

Scheme 5.1 shows the synthetic route used to prepare phthalocyanines **5.1**-**5.6**. Treament of silicon(IV) phthalocyanine dichloride with a large excess of tri- or tetra-ethylene glycol in the presence of NaH in toluene led to the formation of the disubstituted product **5.1** or **5.2**. Displacement reaction of cholesteryl chloroformate with the hydroxyl groups of phthalocyanines **5.1**-**5.2** in the presence of pyridine in

CH_2Cl_2 gave a mixture of mono- and di-substituted products **5.3-5.6**, which were purified by column chromatography. All the new compounds were characterized with various spectroscopic methods and elemental analysis.

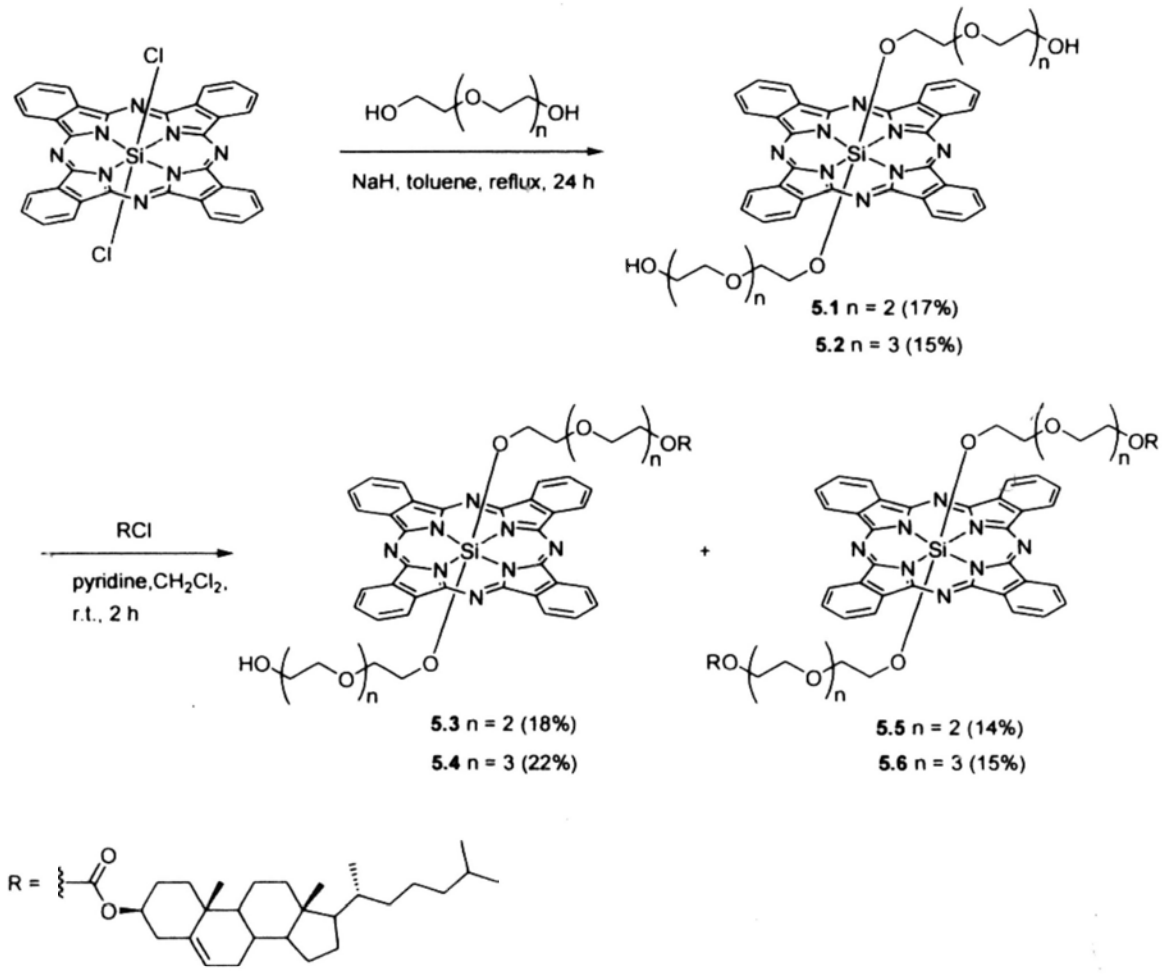

Scheme 5.1. Preparation of phthalocyanines **5.1-5.6**.

The ^1H NMR spectra of all phthalocyanines **5.1-5.6** in $CDCl_3$ showed two typical downfield AA'BB' multiplets (δ = 8-10 ppm) for the α and β protons of the

phthalocyanine ring, and several upfield-shifted signals for the axial substituents due to the shielding by the phthalocyanine ring current. Figure 5.1 shows the ^{1}H NMR spectrum of compound **5.1** in $CDCl_3$ given as an example. The two downfield multiplets at δ 9.65-9.68 and 8.34-8.37 are due to the phthalocyanine α and β ring protons, respectively. In addition, six well-separated triplets are also seen for the methylene protons of the axial chains. Due to the shielding effect by the ring current, these signals are singnificantly shifted upfield (up to δ -1.9).

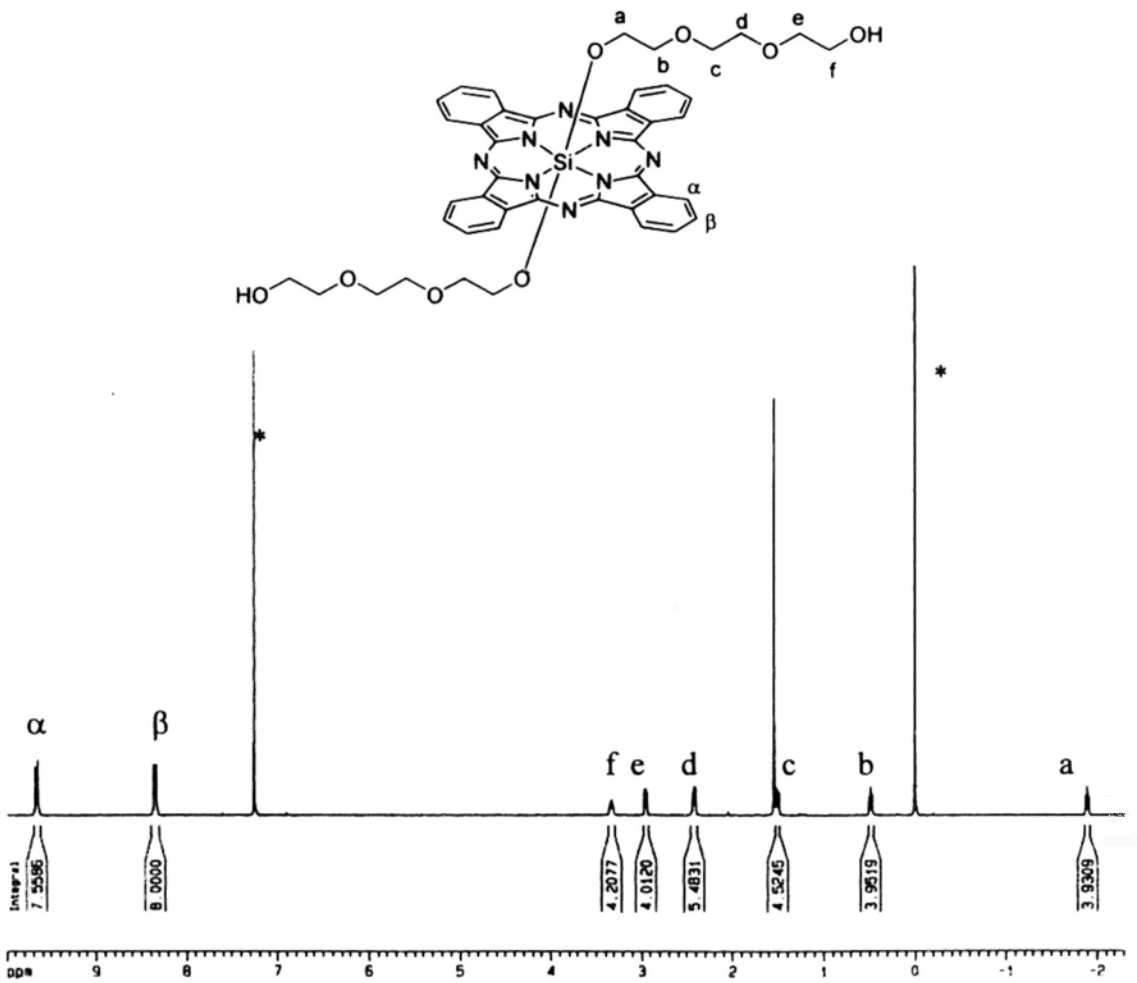

Figure 5.1 ^{1}H NMR spectrum of **5.1** in $CDCl_3$.

A ^{1}H NMR spectrum of compound **5.3** in $CDCl_3$ is given in Figure 5.2. Apart from the signals for the phthalocyanine ring protons and the ethylene groups, the

spectrum also shows a doublet at δ 5.35 (Chol-6-CH), a multiplet at δ 4.35-4.39 (Chol-3-CH), a singlet at δ 0.68 (Chol-18-CH_3), and several multiplets in the region δ 0.87-2.32 for the cholesterol protons.

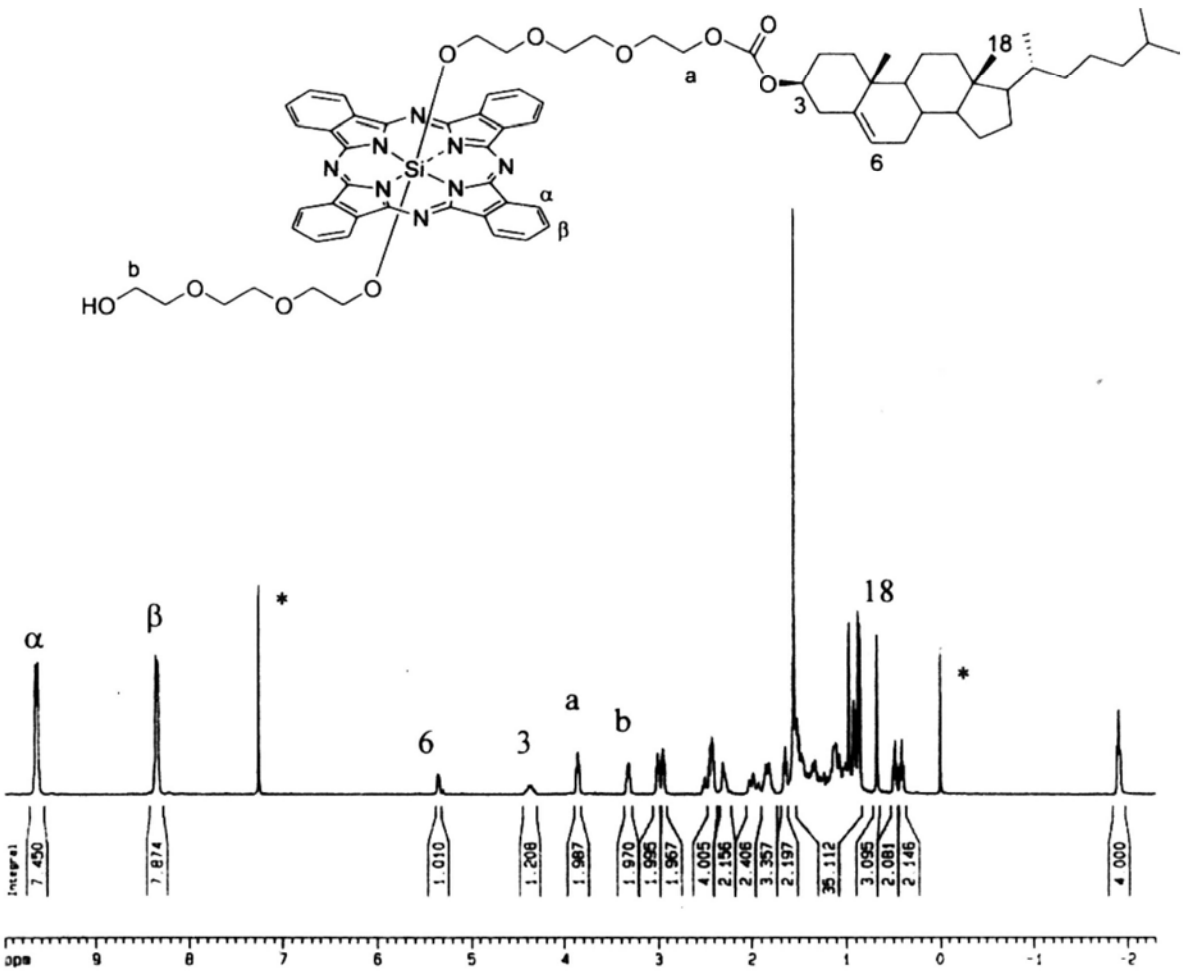

Figure 5.2 ^{1}H NMR spectrum of **5.3** in $CDCl_3$.

Compound **5.1** was also characterized structurally by X-ray diffraction analysis. Single crystals of **5.1** were obtained by slow evaporation of a DMF solution. Figure 5.3 shows a perspective view of the molecular structure of **5.1**, which contains an inversion center (at the silicon atom) relating the two halves of the molecule. The

silicon atom is hexacoordinated with a Si-O bond distance of 1.702 Å and an average Si-N bond distance of 1.920 Å.

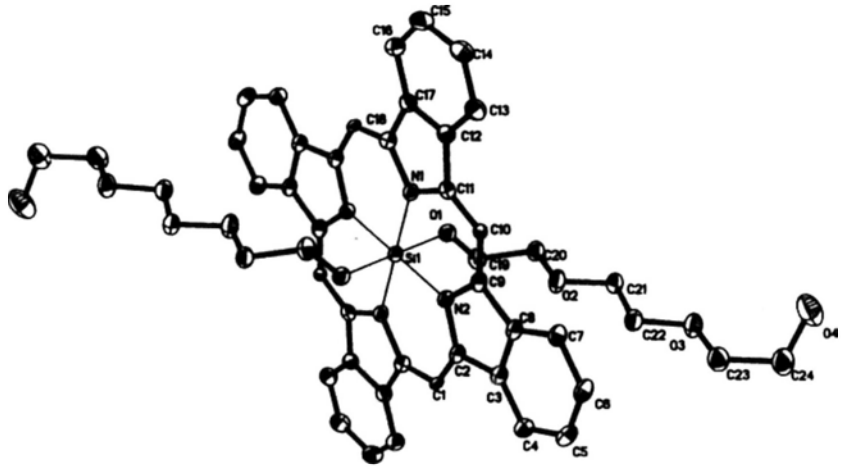

Figure 5.3. Molecular structure of **5.1** showing the 30% probability thermal ellipsoids for all non-hydrogen atoms.

5.2.2 Electronic Absorption and Photophysical Properties

These data for the new phthalocyanines **5.1-5.6** measured in DMF are summarized in Table 5.1. The absorption spectra of **5.1-5.6** in DMF are typical for non-aggregated phthalocyanines, showing a B-band at 356 nm, an intense and sharp Q band at 674 nm, together with two vibronic bands at 606 and 645 nm. The absorption positions of all these compounds are very similar showing that the phthalocyanine π system is not significantly perturbed by the axial substituents. Figure 5.4 shows the absorption spectra of **5.1** in DMF in different concentrations. By plotting the Q-band absorbance versus the concentration, a straight line is obtained indicating that compound **5.1** is essentially free from aggregation under these conditions. Upon excitation at 610 nm, all the compounds **5.1-5.6** show a strong fluorescence emission

at 678 nm with a Stoke shift of 4 nm and a fluorescence quantum yield (Φ_F) of 0.32 to 0.42. To evaluate the photosensitizing efficiency of these phthalocyanines, their singlet oxygen quantum yields (Φ_Δ) were also determined by a steady-state method with 1,3-diphenylisobenzofuran (DPBF) as the scavenger. The concentration of the quencher was monitored spectroscopically at 414 nm against time (Figure 5.5), from which the values of Φ_Δ could be determined. As shown in Table 5.1, all the phthalocyanines generate singlet oxygen efficiently in DMF with Φ_Δ ranging from 0.36 to 0.44.

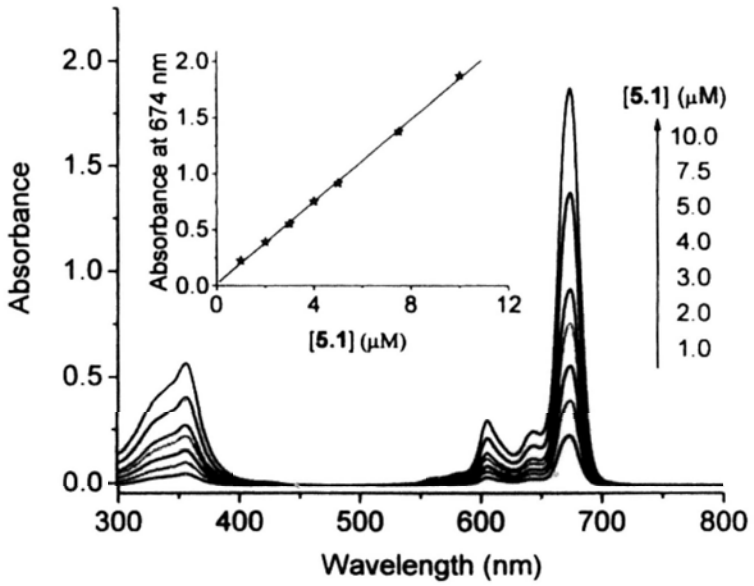

Figure 5.4 UV-Vis spectra of **5.1** in DMF in different concentrations. The insert plots the absorbance at 674 nm versus the concentration of **5.1**.

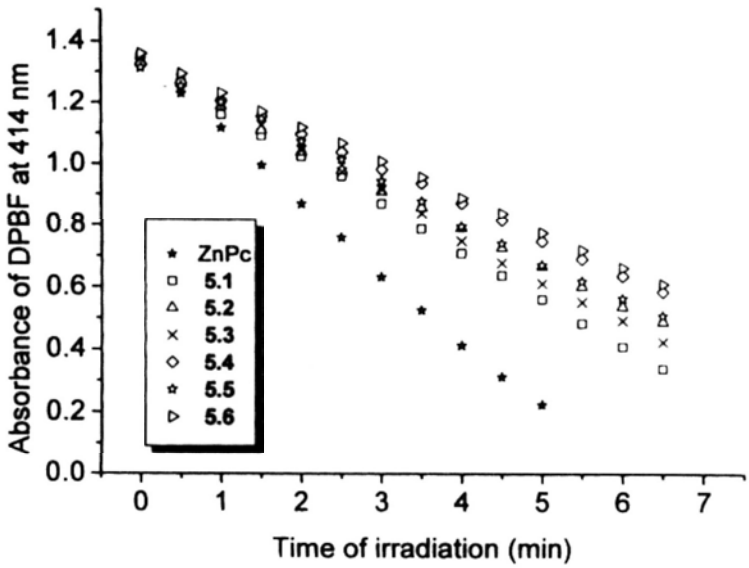

Figure 5.5 Comparison of the rate of decay of DPBF in DMF as monitored spectroscopically at 414 nm, using phthalocyanines **5.1-5.6** as the photosensitizers and ZnPc as the reference.

Table 5.1. Electronic absorption and photophysical data for **5.1-5.6** in DMF.

Compound	λ_{max} (nm) (log ε)	λ_{em} (nm)[a]	Φ_F[b]	Φ_Δ[c]
5.1	356 (4.76), 606 (4.46), 645(4.38), 674(5.26)	678	0.40	0.44
5.2	356 (4.81), 606 (4.52), 645(4.45), 674(5.32)	678	0.38	0.39
5.3	356 (4.86), 606 (4.61), 645(4.53), 674(5.42)	678	0.38	0.40
5.4	356 (4.83), 606 (4.54), 645(4.47), 674(5.34)	678	0.39	0.37
5.5	356 (4.85), 606 (4.57), 644(4.50), 674(5.38)	678	0.32	0.38
5.6	356 (4.87), 606 (4.58), 645(4.51), 674(5.38)	678	0.42	0.36

[a] Excited at 610 nm. [b] Using ZnPc in DMF as the reference (Φ_F = 0.28). [c] Using ZnPc as the reference (Φ_Δ = 0.56 in DMF).

5.2.3 In Vitro Photodynamic Activities

The in vitro photodynamic activities of compounds **5.1-5.6** in Cremophor EL (CEL) emulsions (16 nmol phthalocyanine per mg of CEL) were investigated against HepG2 human hepatocarcinoma cells which are over-expressed with LDL receptors.[6] Due to the fact that the Q band of phthalocyanine appears at a relatively short-wavelength position (ca. 675 nm), a color glass filter cut-on 610 nm was used. Figure 5.6 shows the dose-dependent survival curves for **5.1** on HepG2 cells. It can be seen that while the compound is essentially non-cytotoxic in the absence of light, it

exhibits a very high photocytotoxicity upon illumination. The corresponding IC_{50} values of these phthalocyanines, defined as the dye concentration required to kill 50% of the cells, are summarized in Table 5.2. The cholesterol-free phthalocyanines **5.1** and **5.2** show very high photocytotoxicity with IC_{50} values down to 0.01 μM. However, phthalocyanines **5.3** and **5.4** containing one cholesterol moiety are significantly less photocytotoxic, of which the IC_{50} values are higher by two orders of magnitude than those of compounds **5.1** and **5.2**. Phthalocyanines **5.5** and **5.6** are not photocytotoxic up to 8 μM.

The photocytotoxicities of the cholesterol-containing phthalocyanines **5.3-5.6** in LDL emulsions (80 nmol phthalocyanine per mg of LDL) were also investigated against HepG2 cells. Figure 5.7 compares the effects of compound **5.4** in CEL and LDL emulsions on HepG2 cells both in the absence and presence of light. It can be seen that this compound in LDL emulsion has a slightly higher photodynamic activity compared with the CEL emulsion. Compound **5.3** in CEL emulsion and LDL emulsion shows a similar photoactivity. The results indicate that LDL cannot increase the photodynamic activities of compounds **5.5-5.6** against HepG2 cells.

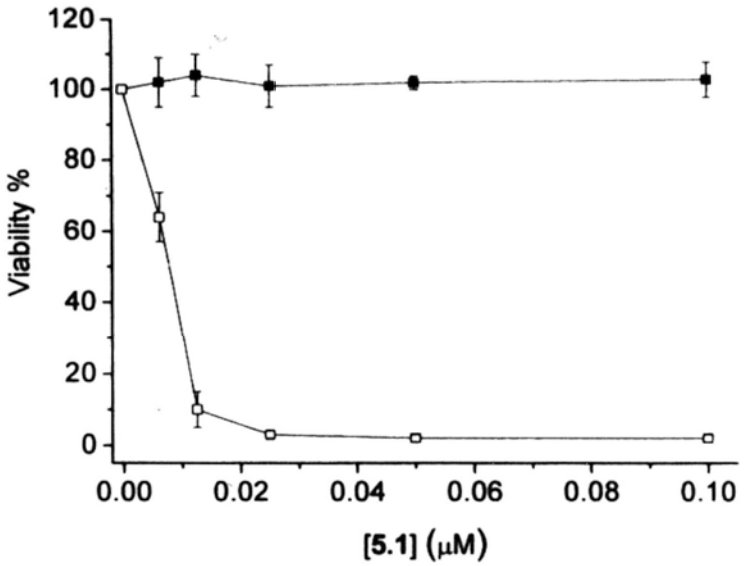

Figure 5.6. Cytotoxic effects of **5.1** in CEL emulsion (16 nmol **5.1** per mg of CEL) on HepG2 cells in the absence (■) and presence (□) of light ($\lambda > 610$ nm, 40 mW cm^{-2}, 48 J cm^{-2}). Data are expressed as mean values ± S.E.M. of three independent experiments, each performed in quadruplicate.

Table 5.2. Comparison of the IC_{50} values of **5.1-5.6** against HepG2 cells.

Compound	IC_{50} (μM)	
	In CEL emulsion[a]	In LDL emulsion[b]
5.1	0.01	
5.2	0.01	
5.3	1.21	1.20
5.4	2.22	1.64
5.5	--[c]	--[c]
5.6	--[c]	--[c]

[a] 16 nmol phthalocyanine per mg of CEL. [b] 80 nmol phthalocyanine per mg of LDL.

[c] non-photocytotoxic up to 8 μM.

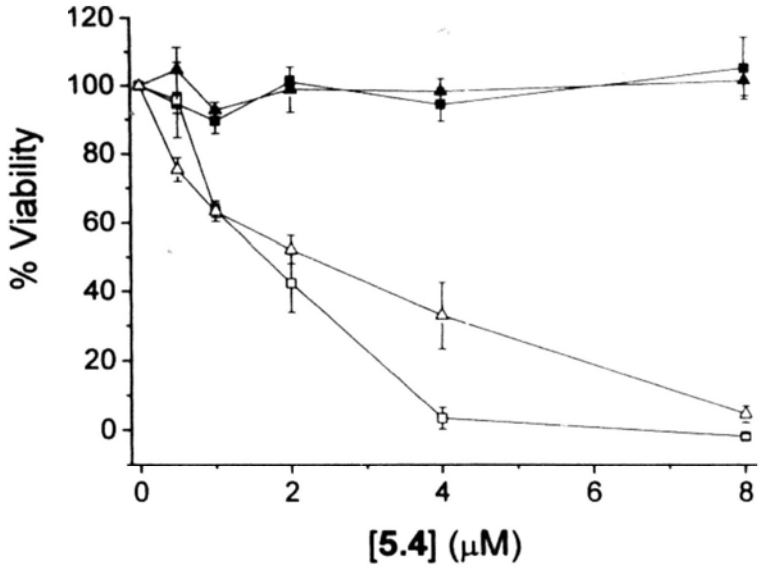

Figure 5.7. Comparison of the effects of **5.4** in LDL emulsion (80 nmol phthalocyanine per mg of LDL, squares) and CEL emulsion (16 nmol phthalocyanine per mg of CEL, triangles) on HepG2 cells in the absence (closed symbols) and presence (open symbols) of light (λ > 610 nm, 40 mW cm^{-2}, 48 J cm^{-2}). Data are expressed as mean values ± S.E.M. of three independent experiments, each performed in quadruplicate.

Figure 5.8 shows the UV-Vis and fluorescence spectra of the cholesterol-free and cholesterol substituted phthalocyanines **5.1-5.6**, formulated with CEL or LDL, in the RPMI culture medium. Compounds **5.1-5.4** formulated with CEL give a sharp Q-band absorption and intense fluorescence emission, showing that these compounds are not significantly aggregated under these conditions. By contrast, compound **5.6** in CEL emulsion gives a broad Q band at 676 nm, which indicates that this compound is slightly aggregated in the medium. Compound **5.5,** which contains shorter ethylene glycol chains, is significantly aggregated under this condition. It can be seen that longer ethylene glycol chains can increase the hydrophilicity of the compounds

effectively. The UV-Vis and fluorescence spectra of compounds **5.3-5.6** in LDL emulsion are shown in Figure 5.8 (c) and (d), respectively. These compounds show weak and broad Q-bands at 710 nm and very weak fluorescence intensities, indicating that they are significantly aggregated in the medium. This may explain the null photodynamic activity of these compounds.

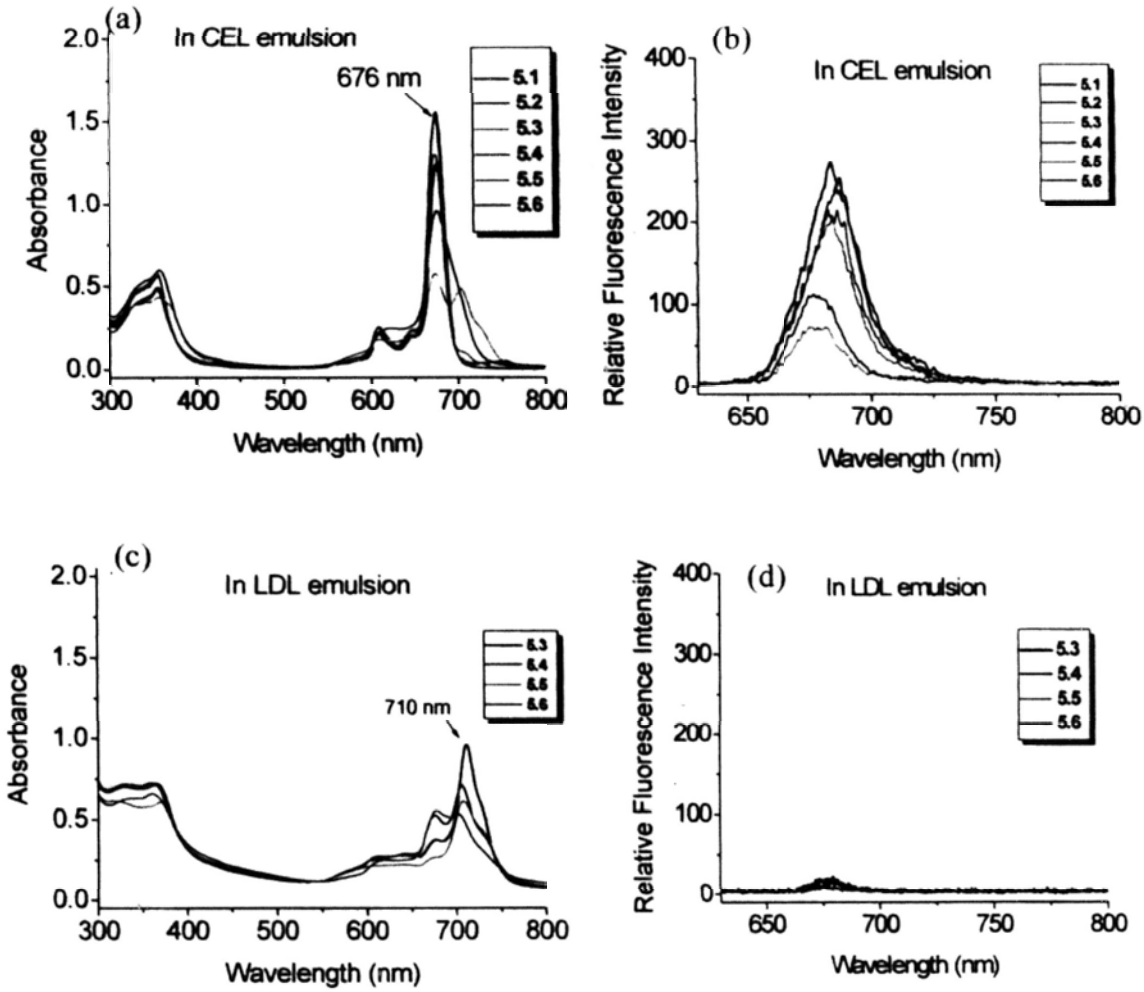

Figure 5.8. UV-Vis and fluorescence spectra of phthalocyanines **5.1-5.6** (8 μM) in the RPMI medium. (a) and (b): in CEL emulsion, 16 nmol phthalocyanine per mg of CEL; (c) and (d): in LDL emulsion, 80 nmol phthalocyanine per mg of LDL.

Figure 5.9 shows the fluorescence microscopic images of HepG2 cells after incubation with phthalocyanines **5.2**, **5.4**, and **5.6** for 2 h. It can be seen that compound **5.2** gives a strong intracellular fluorescence emission at low concentration. By contrast, the images for cholesterol-containing derivatives **5.4** and **5.6** are almost invisible showing that the uptake of this compound is minimal and/or these compounds are highly aggregated within the cells, both of which disfavor the photodynamic action.

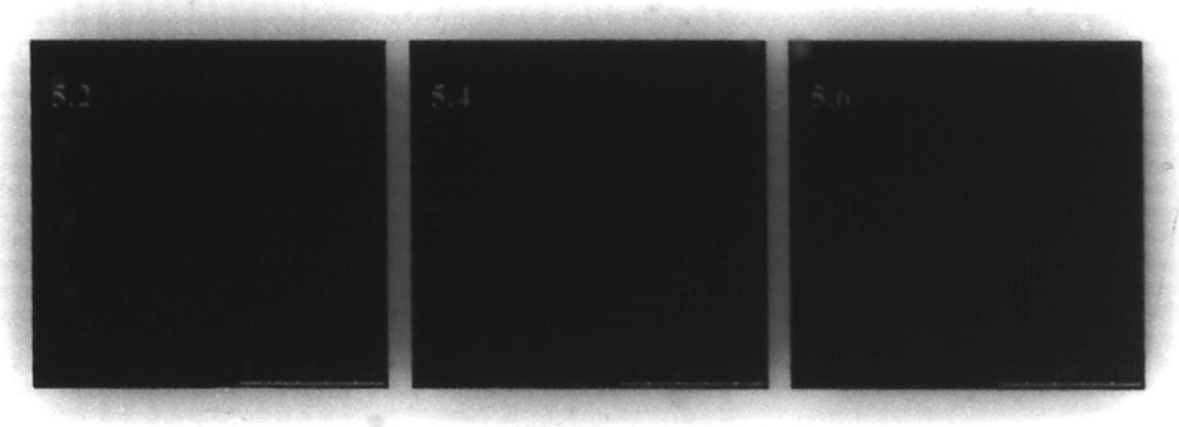

Figure 5.9. Visualization of intracellular fluorescence of HepG2 cells after incubation with **5.2** (0.5 μM), **5.4** (8 μM), and **5.6** (8 μM) for 2 h.

5.3 Conclusions

In summary, we have prepared and characterized a new series of silicon(IV) phthalocyanines axially substituted with one or two cholesterol unit(s) via a long ethylene glycol chain. The mono-cholesterol substituted phthalocyanines **5.3-5.4** in CEL emulsion are relatively non-aggregated in the culture medium, while the di-cholesterol substituted compounds **5.5-5.6** are highly aggregated. The in vitro photodynamic activities of these compounds against HepG2 cells have been evaluated and compared. It has been found that the cholesterol-free compounds **5.1-5.2** in CEL emulsion are highly potent with IC_{50} values down to 0.01 μM. However, conjugation

of cholesterol leads to an adverse effect on the photocytotoxicity, both in CEL and LDL emulsions.

5.4 Experimental Section

Details regarding the purification of solvents, instrumentation, photophysical measurements, and in vitro studies have been described in Chapter 2.

5.4.1 Synthesis

Preparation of Phthalocyanine 5.1. A mixture of silicon phthalocyanine dichloride (0.96 g, 1.57 mmol), triethylene glycol (2.25 g, 14.98 mmol), and NaH (60% in mineral oil, 0.83 g, 20.75 mmol) in toluene (50 mL) was refluxed for 1 day. After evaporating the solvent under reduced pressure, water (2 mL) was added slowly to the residue. The residue was dissolved in CH_2Cl_2 (150 mL) and then washed with water (100 mL × 3). The organic layer was separated, dried over anhydrous Na_2SO_4, and evaporated under reduced pressure. The crude product was purified with silica-gel column chromatography using ethyl acetate as eluent to give the product **5.1** as a blue solid (0.23 g, 17 %). ^{1}H NMR (300 MHz, $CDCl_3$): δ 9.65-9.68 (m, 8 H, Pc-H_α), 8.34-8.37 (m, 8 H, Pc-H_β), 3.31-3.36 (m, 4 H, OCH_2), 2.96 (t, J = 4.5 Hz, 4 H, OCH_2), 2.41-2.45 (m, 4 H, OCH_2), 1.51 (t, J = 4.8 Hz, 4 H, OCH_2), 0.49 (t, J = 5.1 Hz, 4 H, OCH_2), -1.90 (t, J = 5.1 Hz, 4 H, OCH_2); ^{13}C NMR (300 MHz, $CDCl_3$): 149.3, 136.0, 130.9, 123.7, 71.8, 69.4, 69.3, 68.5, 61.4, 55.0 ; MS (ESI): isotopic clusters peaking at *m/z* 861 {100%, $[M+Na]^+$}; HRMS (ESI): *m/z* calcd for $C_{44}H_{42}N_8NaO_8Si$ $[M+Na]^+$: 861.2787, found 861.2797; Anal. Calcd for $C_{44}H_{42}N_8O_8Si$: C 62.99, H 5.05, N 13.36; found: C 62.43, H 5.05, N 13.08.

Preparation of Phthalocyanine 5.2. According to the procedure described for **5.1**, silicon(IV) phthalocyanine dichloride (0.93 g, 1.52 mmol) was treated with tetraethylene glycol (2.83 g, 14.57 mmol) and NaH (60% in mineral oil, 0.95 g, 23.75 mmol) in toluene (50 mL) to give **5.2** as a blue solid (0.21 g, 15%). ^{1}H NMR (300 MHz, $CDCl_3$): δ 9.61-9.65 (m, 8 H, Pc-H_α), 8.32-8.36 (m, 8 H, Pc-H_β), 3.40 (m, 4 H, OCH_2), 3.27 (t, J = 4.8 Hz, 4 H, OCH_2), 3.19 (t, J = 5.1 Hz, 4 H, OCH_2), 2.92 (t, J = 4.8 Hz, 4 H, OCH_2), 2.45 (t, J = 5.1 Hz, 4 H, OCH_2), 1.66 (t, J = 4.8 Hz, 4 H, OCH_2), 0.42 (t, J = 5.4 Hz, 4 H, OCH_2), -1.91 (t, J = 5.4 Hz, 4 H, OCH_2); ^{13}C{^{1}H} NMR:149.3, 136.0, 130.9, 123.7, 72.1, 69.9, 69.8, 69.3 (two overlapping signals), 68.5, 61.4, 54.8; MS (ESI): isotopic clusters peaking at *m*/z 949 {100%, $[M+Na]^+$}; HRMS (ESI): *m/z* calcd for $C_{48}H_{50}N_8NaO_{10}Si$ $[M+Na]^+$: 949.3311, found 949.3315; Anal. Calcd for $C_{48}H_{50}N_8O_{10}Si$: C 62.19, H 5.44, N 12.09; found: C 61.74, H 5.31, N 12.06.

Preparation of Phthalocyanines 5.3 and 5.5. A solution of cholesteryl chloroformate (201.23 mg, 0.45 mmol) and pyridine (2 mL) in CH_2Cl_2 (10 mL) was added to a solution of phthalocyanine **5.1** (101.25 mg, 0.12 mmol) in CH_2Cl_2 (30mL). The mixture was stirred at room temperature for 2 h. After evaporating the solvent under reduced pressure, the residue was subject to column chromatography on neutral alumina using $CHCl_3$ as eluent, followed by gel permeation chromatography using THF as eluent. The first and second green bands were collected respectively. After removing the solvent, the residue of the first band was purified again with silica-gel column chromatography using $CHCl_3$ as eluent to give the product **5.5** (28.45 mg, 14%) as a blue solid. The residue of the second band was purified again with silica-gel column chromatography using ethyl acetate as eluent to give the product **5.3**

(26.67 mg, 18%) as a blue solid. **5.3**: ^{1}H NMR (300MHz, $CDCl_3$): δ 9.63-9.66 (m, 8 H, Pc-H_α), 8.33-8.36 (m, 8 H, Pc-H_β), 5.35 (d, J = 4.5 Hz, 1 H, Chol-6-CH), 4.35-4.39 (m, 1 H, Chol-3-CH), 3.86 (t, J = 4.8 Hz, 2 H, OCH_2), 3.32 (t, J = 4.8 Hz, 2 H, OCH_2), 3.00 (t, J = 4.5 Hz, 2 H, OCH_2), 2.95 (t, J = 4.5 Hz, 2 H, OCH_2), 2.41-2.45 (m, 4 H, OCH_2) , 1.82-2.32 (m, 8 H, Chol), 1.65 (t, J = 4.8 Hz, 2 H, OCH_2), 0.86-1.56 (m, 34 H, OCH_2 and Chol), 0.68 (s, 3H, Chol-18-CH_3), 0.48 (t, J = 4.8 Hz, OCH_2), 0.41 (t, J = 5.1 Hz, OCH_2), -1.91 (t, J = 4.8 Hz, 4 H, OCH_2); MS (ESI): isotopic clusters peaking at *m/z* 1273 {100%, $[M+Na]^+$}; HRMS (ESI): *m/z* calcd for $C_{72}H_{86}N_8NaO_{10}Si$ $[M+Na]^+$: 1273.6128, found 1273.6131; Anal. Calcd for $C_{72}H_{86}N_8O_{10}Si$: C 69.09, H 6.93, N 8.95; found: C 68.50, H 6.94, N 8.93. **5.5**: ^{1}H NMR (300 MHz, $CDCl_3$): δ 9.62-9.64(m, 8 H, Pc-H_α), 8.33-8.35 (m, 8 H, Pc-H_β), 5.35 (d, J = 4.2 Hz, 2 H, Chol-6-CH), 4.35-4.39 (m, 2 H, Chol-3-CH), 3.86 (t, J = 4.5 Hz, 4 H, OCH_2), 3.00 (t, J = 4.8Hz, 4 H, OCH_2), 2.44 (t, J = 4.5 Hz, 4 H, OCH_2), 1.73-2.32 (m, 16 H, Chol), 1.64 (t, J = 4.5 Hz, 4 H, OCH_2), 0.86-1.56 (m, 64 H, Chol), 0.68 (s, 6H, Chol-18-CH_3), 0.40 (t, J = 5.1 Hz, 4 H, OCH_2), -1.92 (t, J = 5.4 Hz, 4 H, OCH_2); MS (ESI): isotopic clusters peaking at *m/z* 1687{100%, $[M+Na]^+$}; HRMS (ESI): *m/z* calcd for $C_{100}H_{130}N_8NaO_{12}Si$ $[M+Na]^+$: 1685.9470, found 1685.9485; Anal. Calcd for $C_{100}H_{130}N_8O_{12}Si$: C 72.12, H 7.87, N 6.73; found: C 71.85, H 7.93, N 6.58.

Preparation of Phthalocyanines 5.4 and 5.6. According to the procedure described for **5.3** and **5.5**, phthalocyanine **5.2** (121.25 mg, 0.13 mmol) was treated with cholesteryl chloroformate (221.53 mg, 0.49 mmol) in the presence of pyridine (2 mL) in CH_2Cl_2 (50 mL) to yield **5.4** (37.55 mg, 22%) and **5.6** (35.89 mg, 15%) both as a blue solid. **5.4**: ^{1}H NMR (300 MHz, $CDCl_3$): δ 9.62-9.66 (m, 8 H, Pc-H_α), 8.33-8.37 (m, 8 H, Pc-H_β), 5.36 (d, J = 4.5 Hz, 1 H, Chol-6-CH), 4.41-4.44 (m, 1 H, Chol-3-

CH), 4.09 (t, J = 5.1 Hz, 2 H, OCH_2), 3.41-3.45 (m, 4 H, OCH_2), 3.27 (t, J = 4.8 Hz, 2 H, OCH_2), 3.18-3.22 (m, 4 H, OCH_2), 2.91-2.97 (m, 4 H, OCH_2), 2.43-2.46 (m, 4 H, OCH_2), 1.82-2.36 (m, 8 H, Chol), 1.66 (t, J = 4.8 Hz, 4 H, OCH_2), 0.85-1.57 (m, 32 H, Chol), 0.68 (s, 3H, Chol-18-CH_3), 0.38-0.44 (m, 4 H, OCH_2), -1.92 (m, J = 4.8 Hz, 4 H, OCH_2); MS (ESI): isotopic clusters peaking at *m/z* 1362 {100%, $[M+Na]^+$}; HRMS (ESI): *m/z* calcd for $C_{76}H_{94}N_8NaO_{10}Si$ $[M+Na]^+$: 1361.6653, found 1361.6639; Anal. Calcd for $C_{76}H_{94}N_8O_{10}Si$: C 68.14, H 7.07, N 8.36; found: C 68.87, H 6.62, N 8.44. **5.6**: ^1H NMR (300 MHz, $CDCl_3$): δ 9.61-9.64 (m, 8 H, Pc-H_α), 8.33-8.36 (m, 8 H, Pc-H_β), 5.36 (d, J = 4.5 Hz, 2 H, Chol-6-CH), 4.40-4.44 (m, 2 H, Chol-3-CH), 4.09 (t, J = 4.8 Hz, 4 H, OCH_2), 3.44 (t, J = 5.1 Hz, 4 H, OCH_2), 3.22 (t, J = 5.1 Hz, 4 H, OCH_2), 2.95 (t, J = 5.1 Hz, 4 H, OCH_2), 2.44 (t, J = 4.8 Hz, 4 H, OCH_2), 1.67-2.36 (m, 16 H, Chol), 1.65 (t, J = 5.1 Hz, 4 H, OCH_2), 0.86-1.56 (m, 64 H, Chol), 0.68 (s, 6H, Chol-18-CH_3), 0.39 (t, J = 5.4 Hz, 4 H, OCH_2), -1.92 (m, J = 5.4 Hz, 4 H, OCH_2); MS (ESI): isotopic clusters peaking at *m/z* 1775{100%, $[M+Na]^+$}; HRMS (ESI): *m/z* calcd for $C_{104}H_{138}N_8NaO_{14}Si$ $[M+Na]^+$: 1773.9994, found 1773.9988; Anal. Calcd for $C_{104}H_{138}N_8O_{14}$: C 71.28, H 7.94, N 6.39; found: C 71.18, H 7.79, N 6.22.

5.4.2 X-ray Crystallographic Analysis of 5.1.

Crystal data and details of data collection and structure refinement are given in Table 5.3. Data were collected on a Bruker SMART CCD diffractometer with an MoKα sealed tube (λ = 0.71073 Å) at 293 K, using a ω scan mode with an increment of 0.3°. Preliminary unit cell parameters were obtained from 45 frames. Final unit cell parameters were obtained by global refinements of reflections obtained from integration of all the frame data. The collected frames were integrated using the preliminary cell-orientation matrix. SMART software was used for collecting frames

of data, indexing reflections, and determination of lattice constants; SAINT-PLUS for integration of intensity of reflections and scaling;[6] SADABS for absorption correction;[7] and SHELXL for space group and structure determination, refinements, graphics, and structure reporting.[8]

Table 5.3. Crystallographic data for **5.1**.

Code	**5.1**
Formula	$C_{48}H_{46}N_4O_8Si$
Mr	834.98
Crystal size [mm^3]	0.30 × 0.20 × 0.10
Crystal system	Monoclinic
Space group	$P2_1/n$
a [Å]	12.190 (2)
b [Å]	9.8182 (17)
c [Å]	15.935 (3)
α [°]	90
β [°]	93.637
γ [°]	90
V [$Å^3$]	1903.3 (6)
Z	2
F (000)	880
ρ_{calcd} [Mg m^{-3}]	1.457
μ [mm^{-1}]	0.129
θ rang [°]	2.04 to 28.05
Reflection collected	12595
Independent reflections	4592 (R_{int} = 0.0563)
Parameters	277
R1 [$I > 2\sigma(I)$]	0.0664
wR2 [$I > 2\sigma(I)$]	0.1683
Goodness of fit	1.038

5.5 References

1. Konan, Y. N.; Gurny, R.; Allémann, E. *J. Photochem. Photobiol. B: Biol.* **2002**, *66*, 89.
2. Zheng, G.; Li, H.; Zhang, M.; Lund-Katz, S.; Chance, B.; Glickson, J. *Bioconjugate chem.* **2002**, *13*, 392.
3. Seglla, A.; Milanesik C.; Jori, G.; Capraro, H. G.; Isele, U.; Schieweck, K. *Br. J. Cancer* **1994**, *69*, 817.
4. Maree, S. E.; Nyokong, T. J. Porphyrins Phthalocyanines **2001**, *5*, 782.
5. Decreau, R.; Chanon, M.; Julliard, M. *Synlett* **1998**, 375.
6. *SMART and SAINT for Windows NT Software Reference Manuals*, Version 5.0, Bruker Analytial X-ray Systems, Madison, WI, 1997.
7. Sheldrick, G. M. SADABS – *A Software for Empirical Absorption Correction*, University of Göttingen, Germany, 1997.
8. *SHELXL Reference Manual*, Version 5.1, Bruker Analytical X-ray Systems, Madison, WI, 1997.

Appendix A-2.1 ^{1}H NMR Spectrum of **2.1** in CD_3OD and $^{13}C\{^{1}H\}$ NMR Spectrum of **2.1** in $CDCl_3$

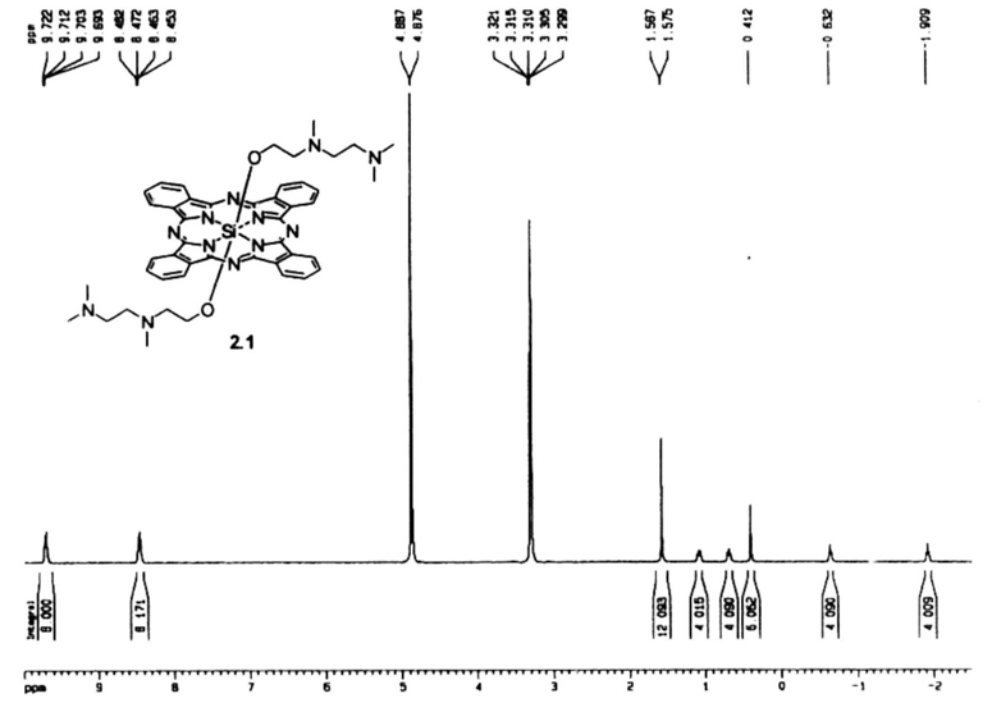

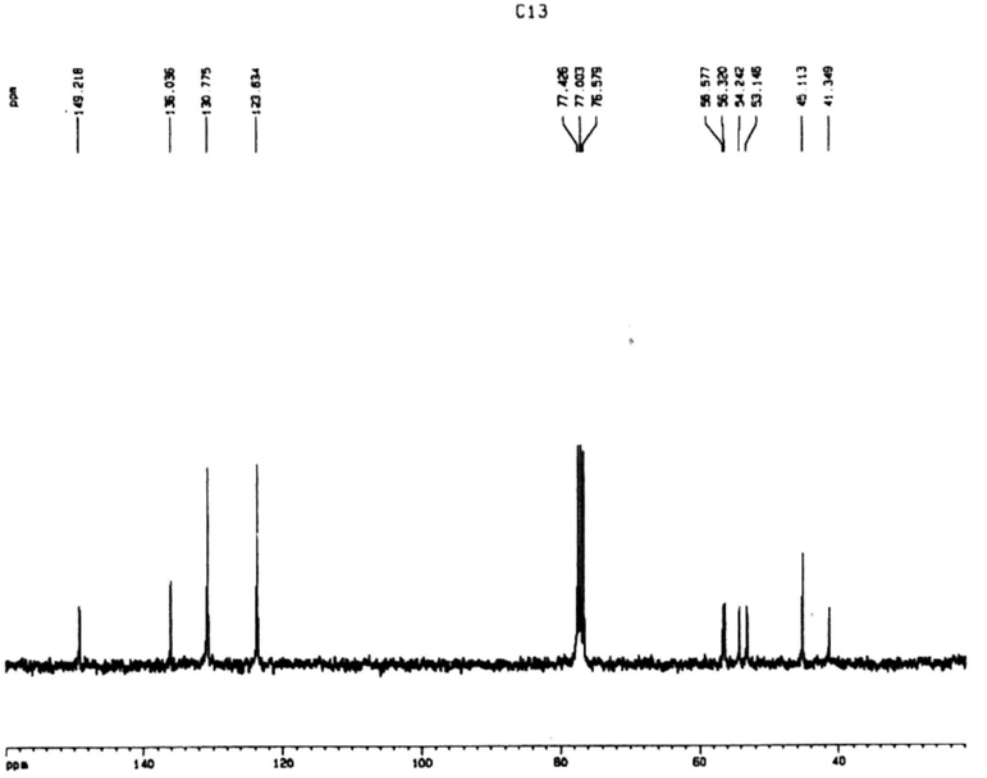

Appendix A-2.2 ^{1}H and $^{13}C\{^{1}H\}$ NMR Spectra of **2.2** in DMSO-d_6

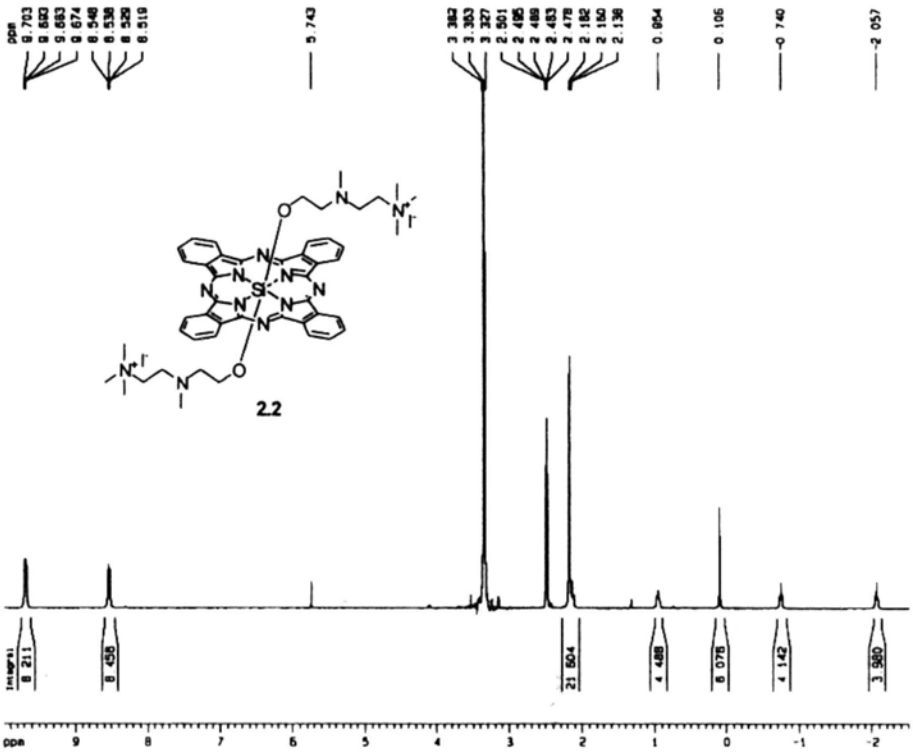

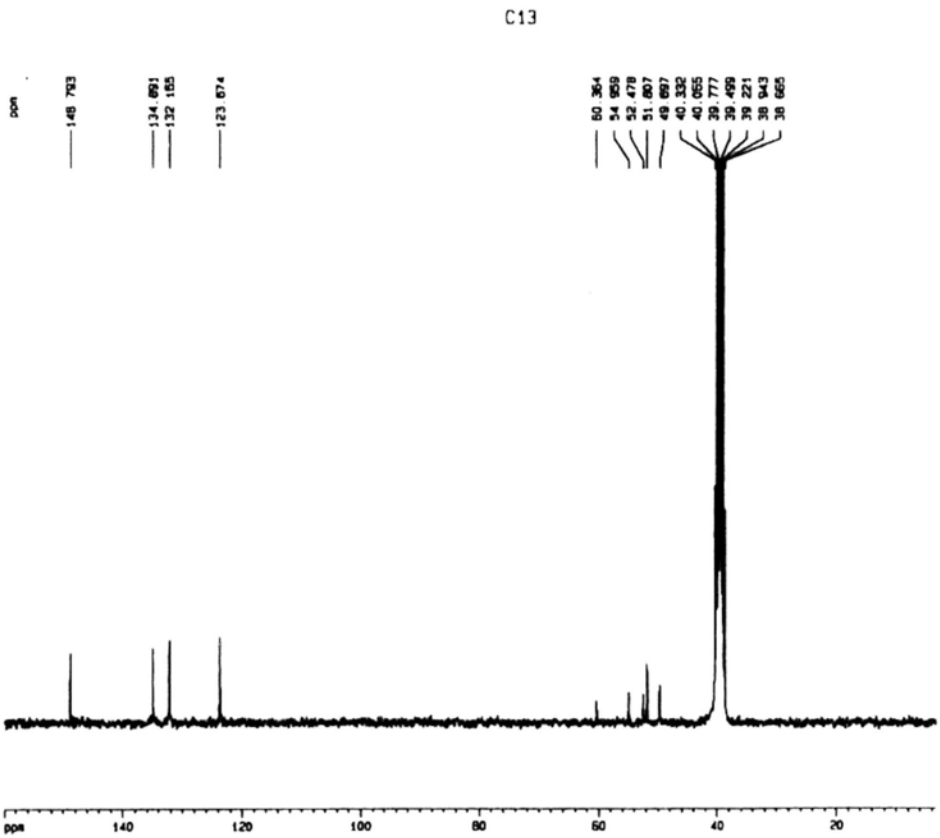

Appendix A-2.3 ^{1}H and $^{13}C\{^{1}H\}$ NMR Spectra of **2.3** in DMSO-d_6

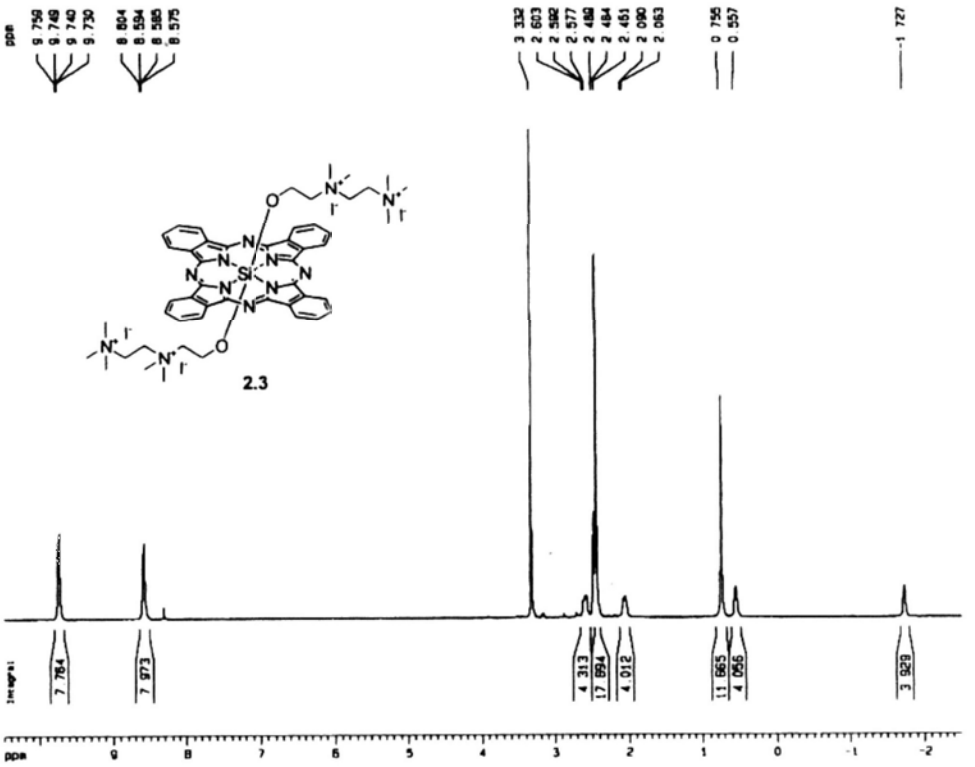

C13

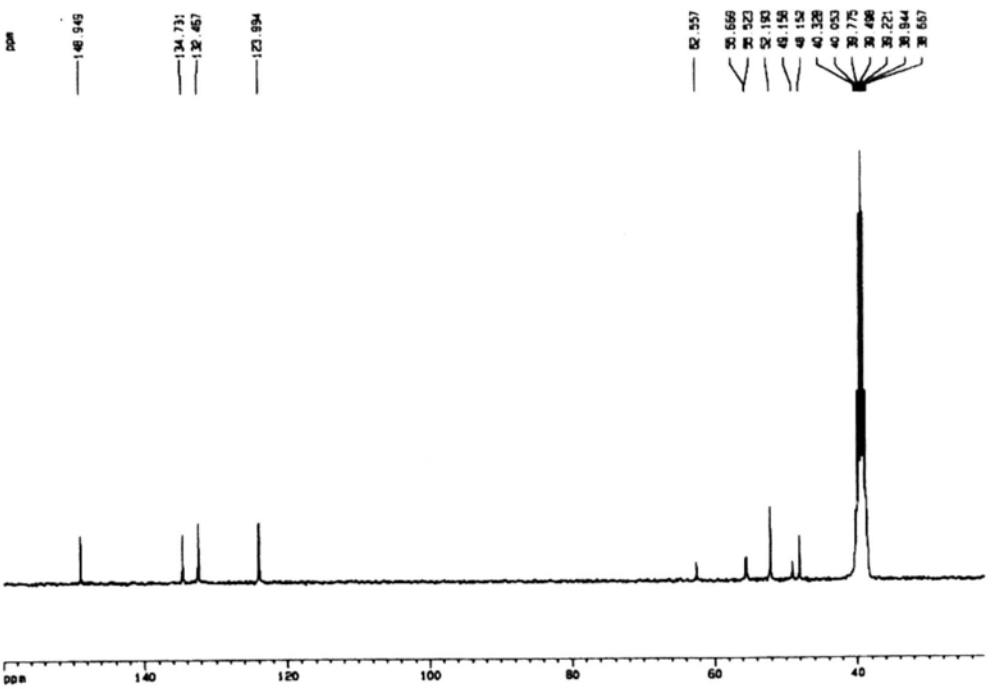

Appendix A-3.1 ^{1}H and $^{13}C\{^{1}H\}$ NMR Spectra of 3.1 in $CDCl_3$

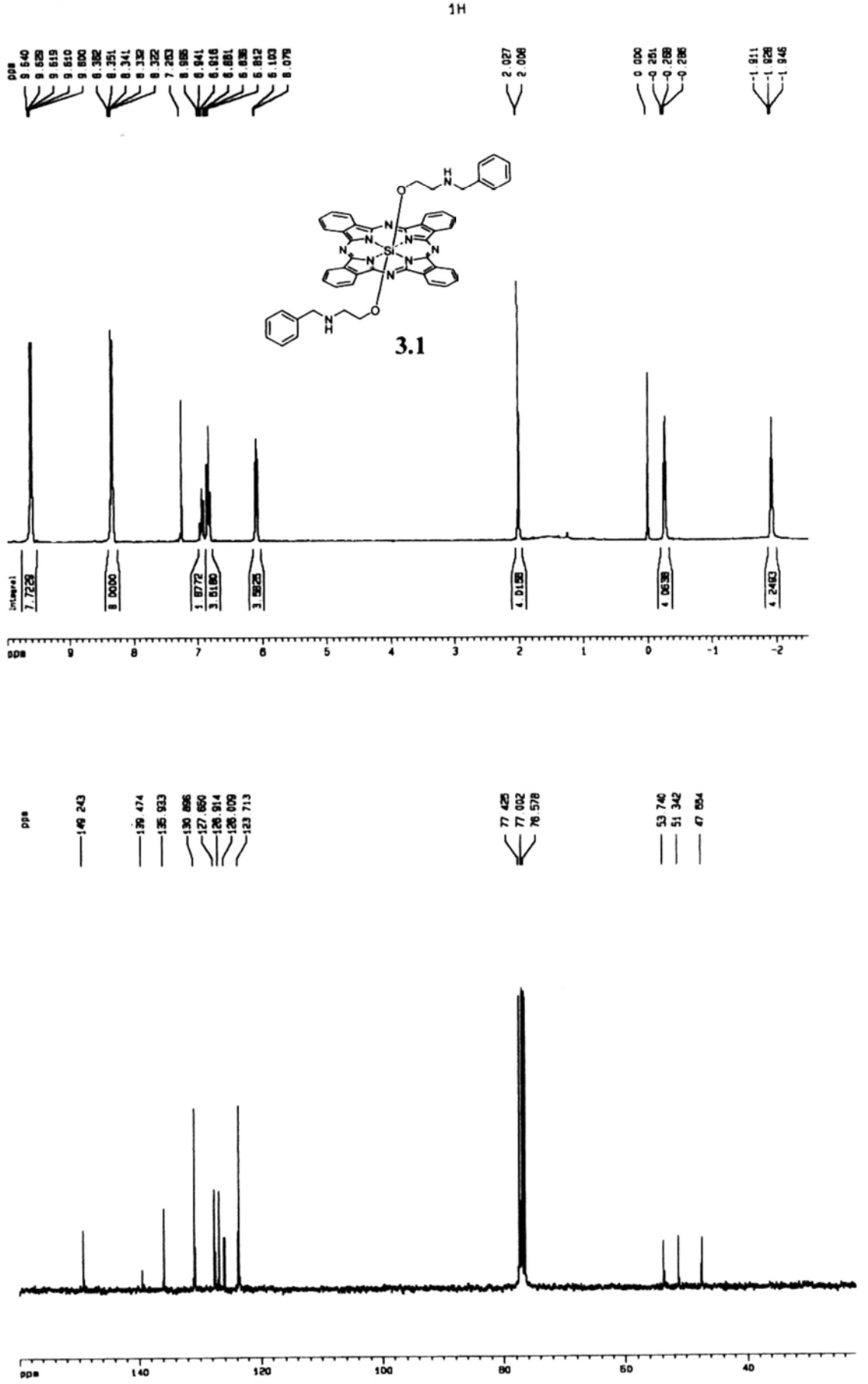

Appendix A-3.2 ^{1}H and $^{13}C\{^{1}H\}$ NMR Spectra of **3.2** in $CDCl_3$

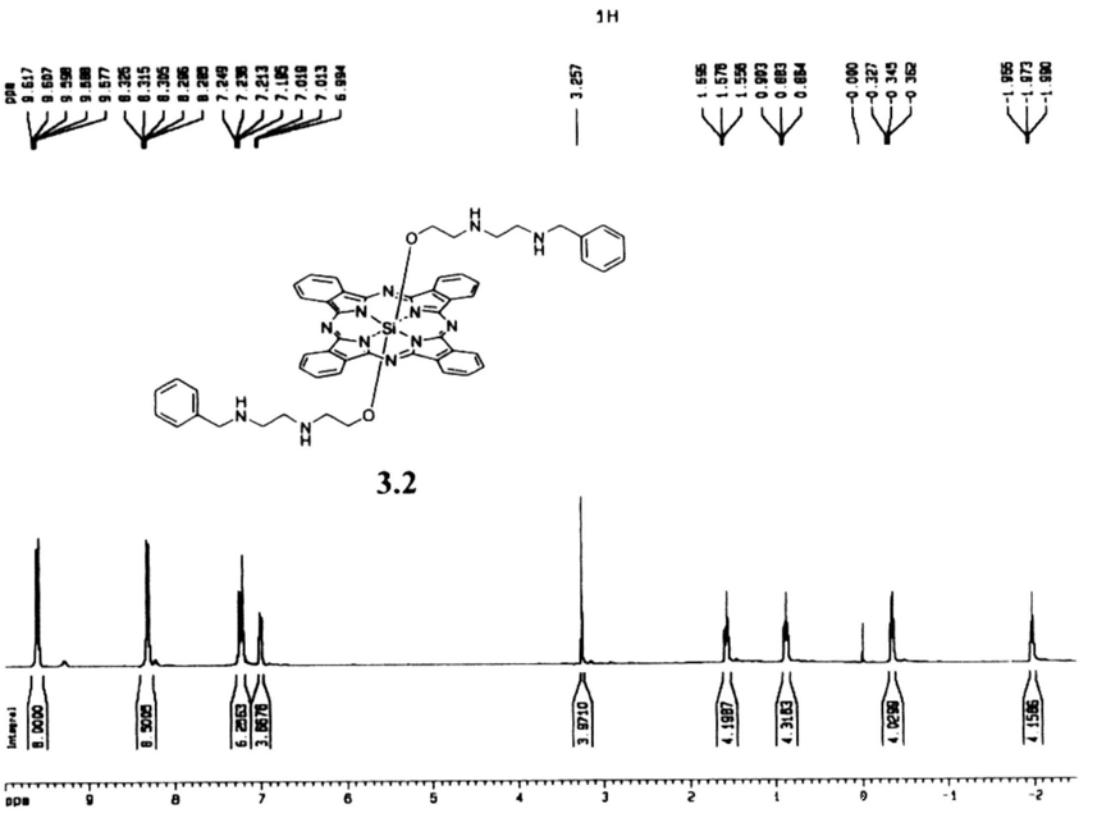

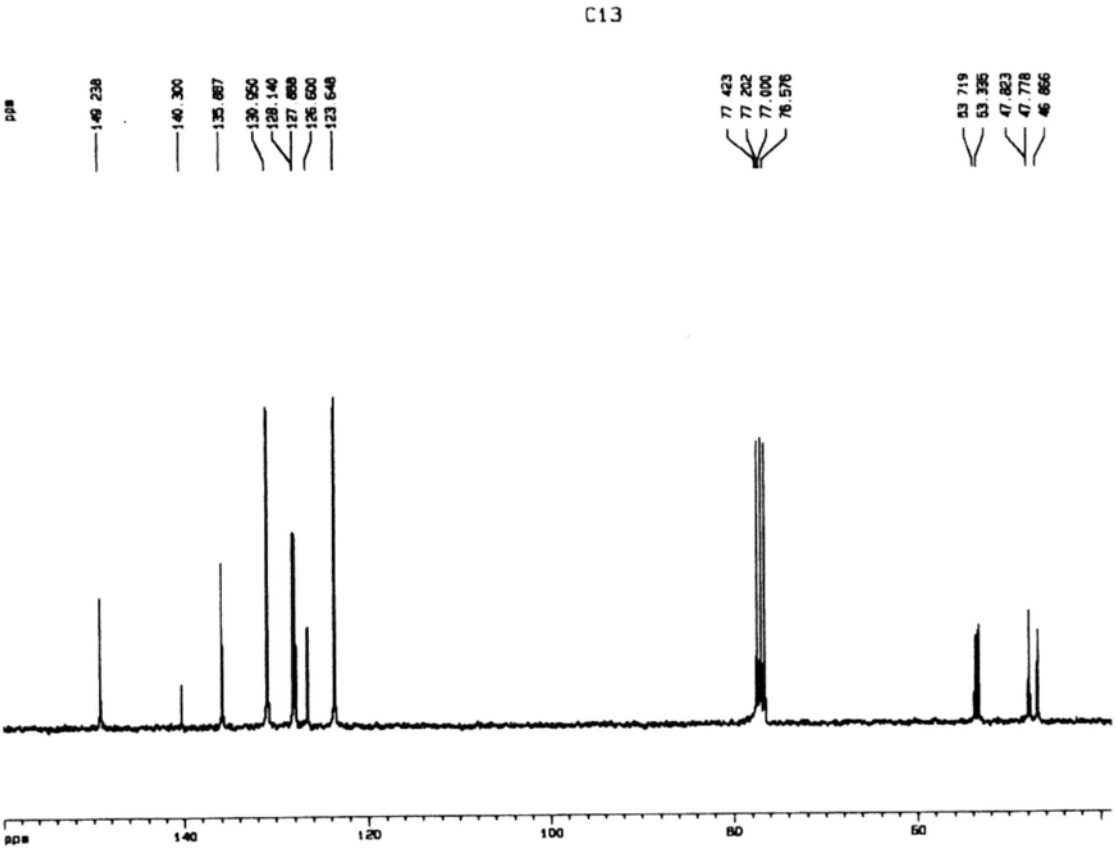

Appendix A-3.3 ^{1}H and $^{13}C\{^{1}H\}$ NMR Spectra of **3.3** in $CDCl_3$

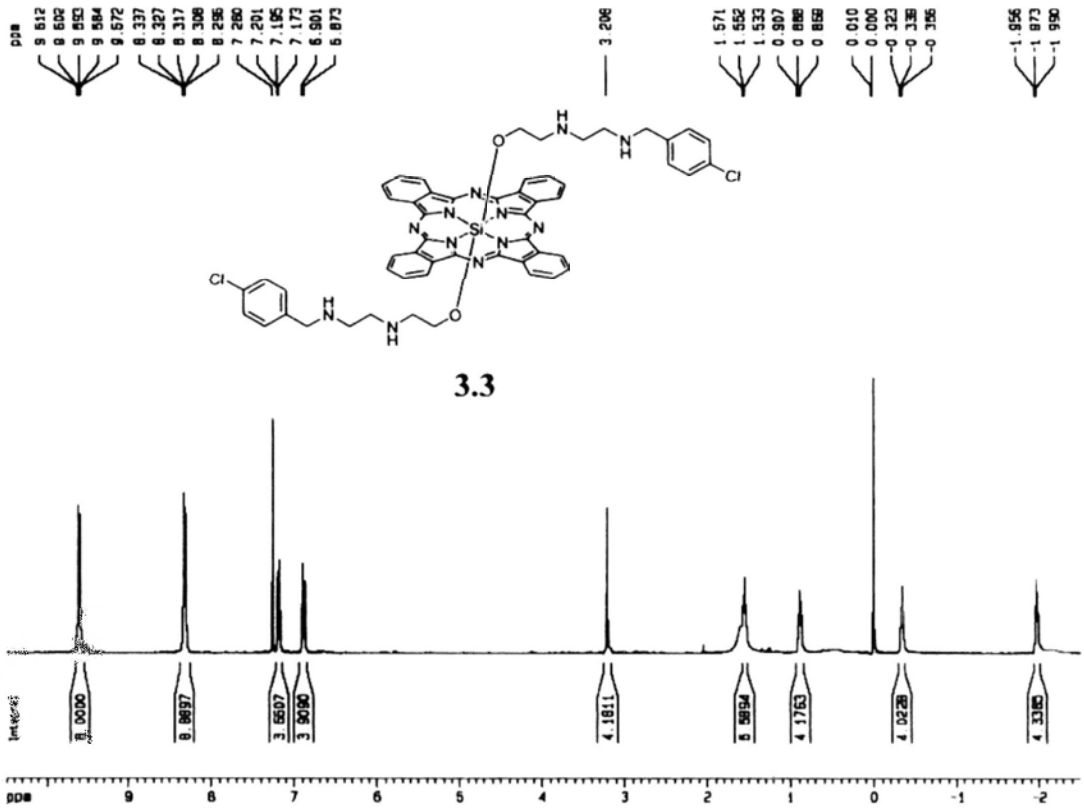

3.3

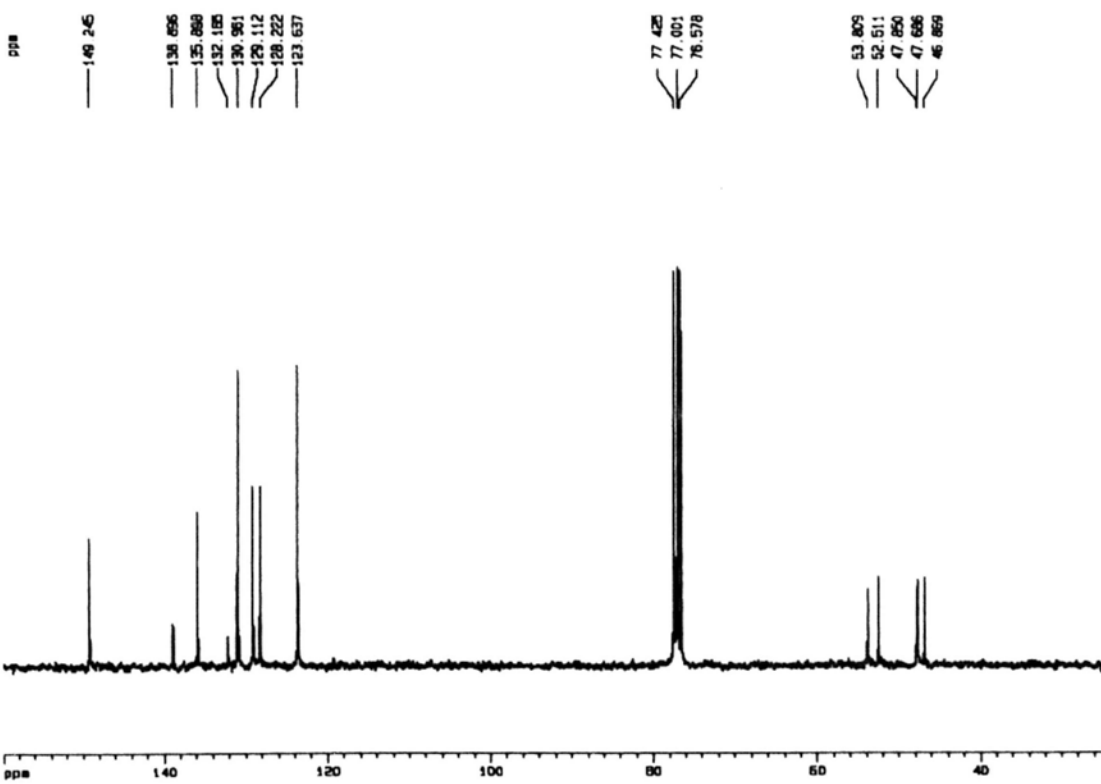

C13

Appendix A-3.4 ^{1}H and $^{13}C\{^{1}H\}$ NMR Spectra of **3.4** in $CDCl_3$

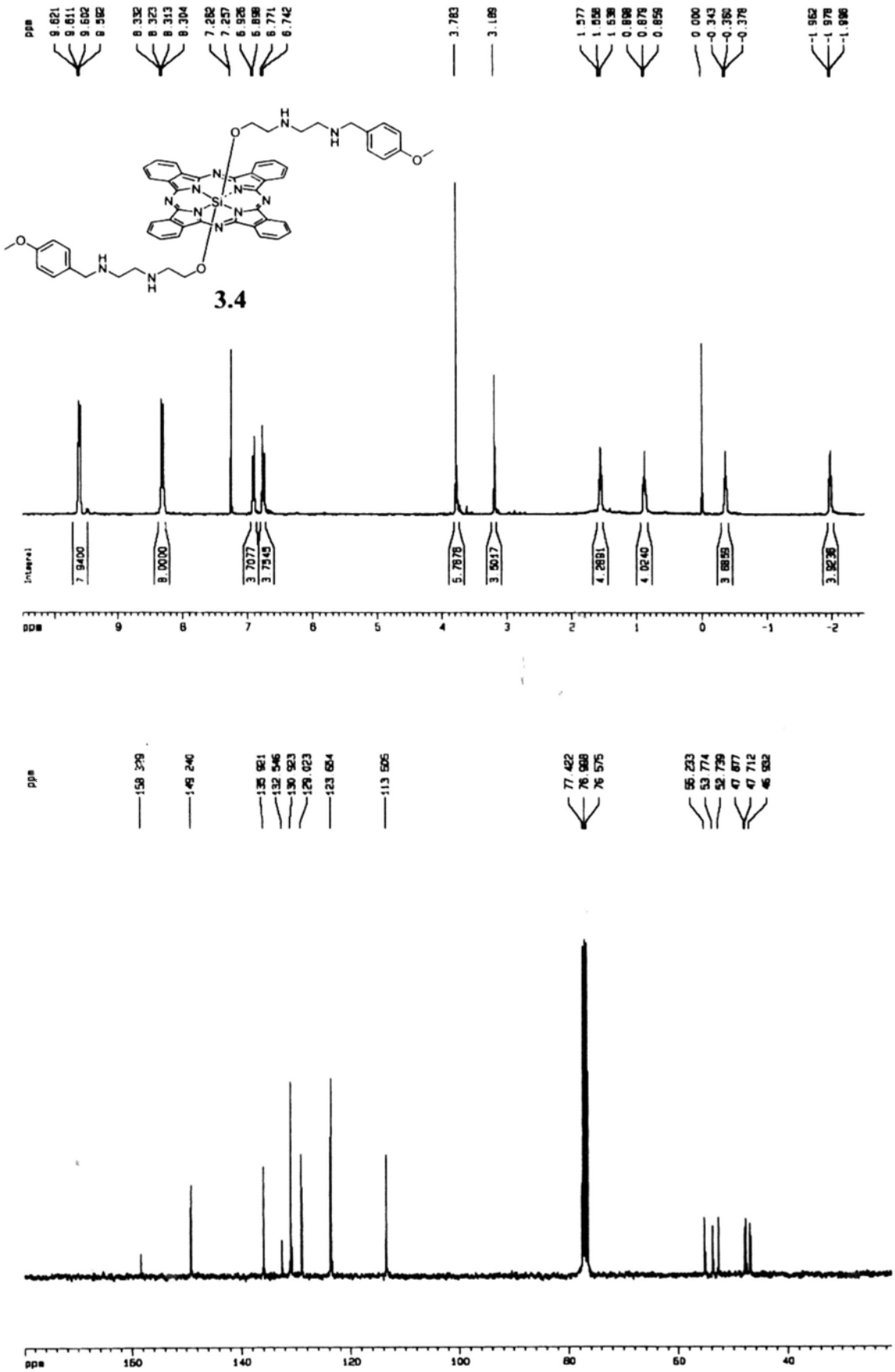

3.4

Appendix A-3.5 ^{1}H and $^{13}C\{^{1}H\}$ NMR Spectra of **3.5** in $CDCl_3$

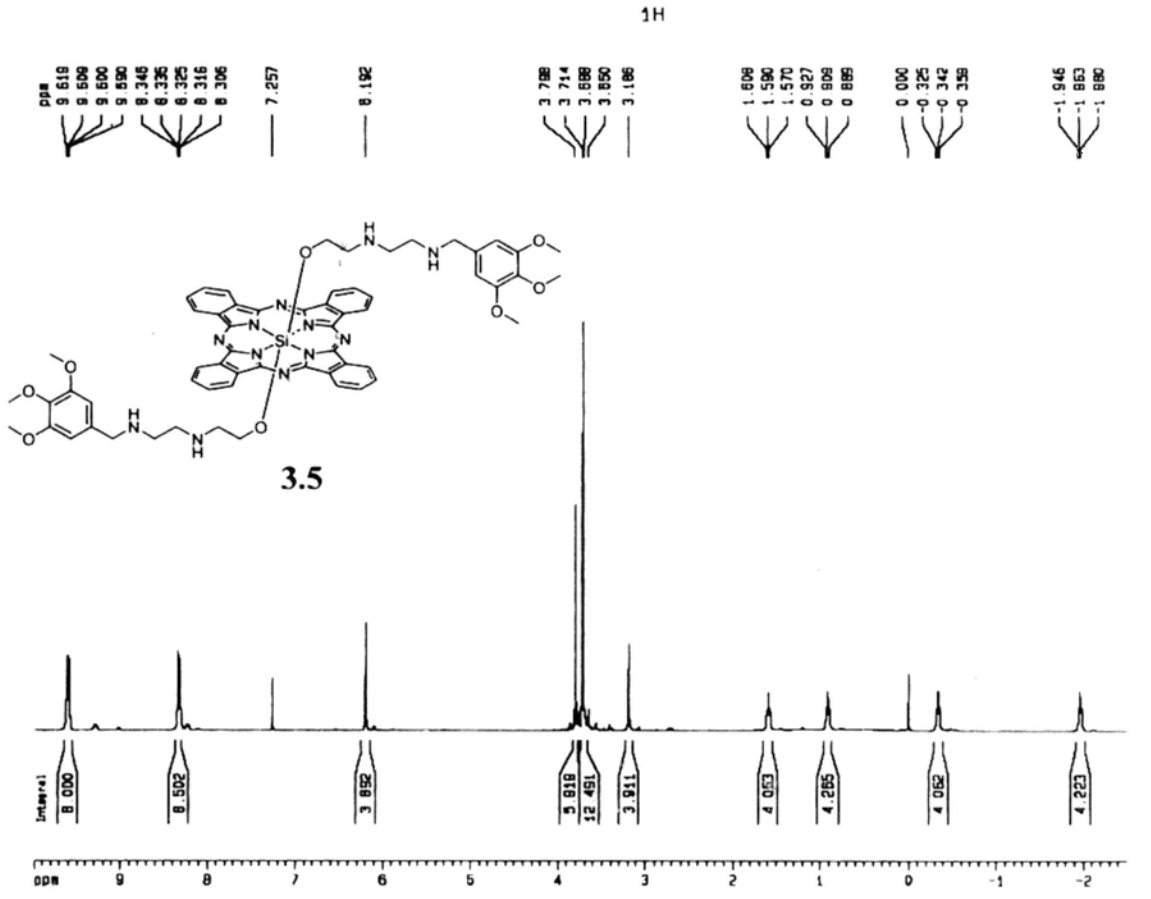

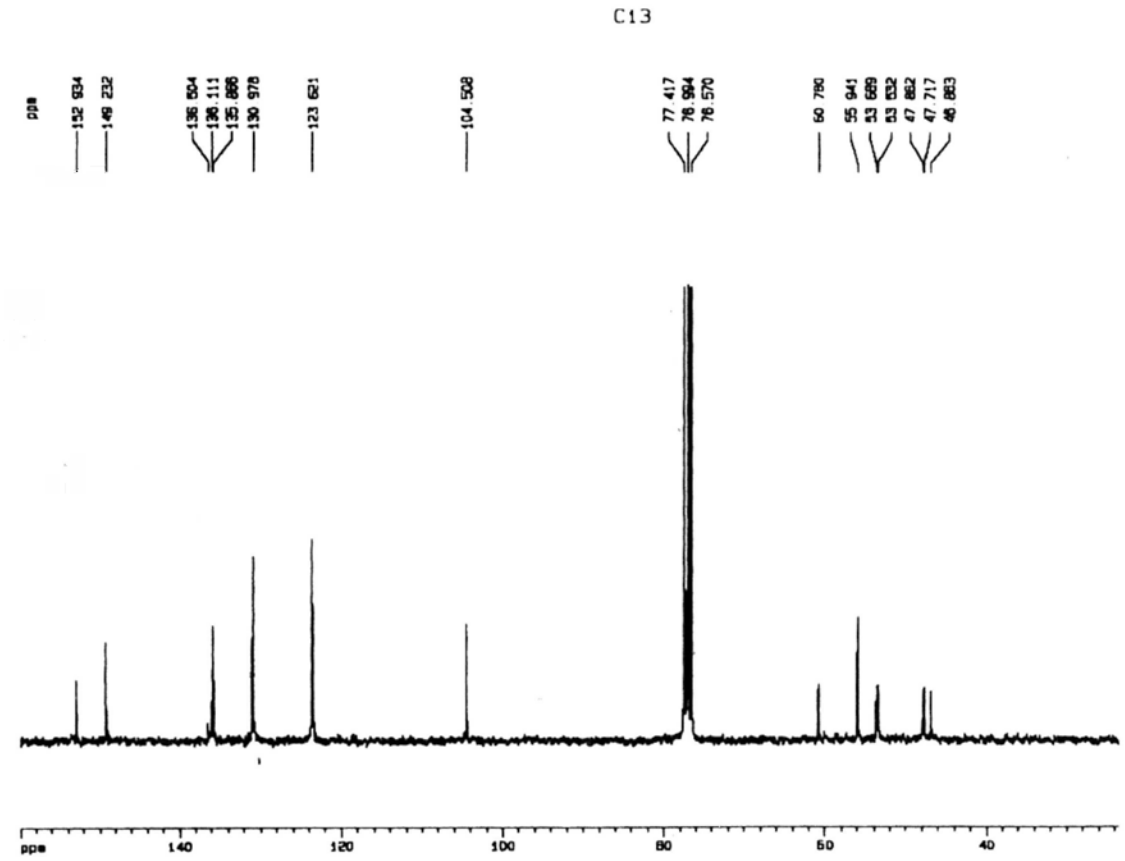

Appendix A-3.6 ^{1}H and $^{13}C\{^{1}H\}$ NMR Spectra of **3.13** in $CDCl_3$

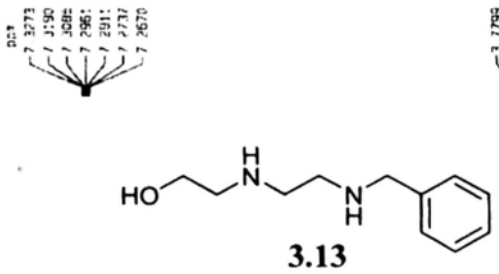

3.13

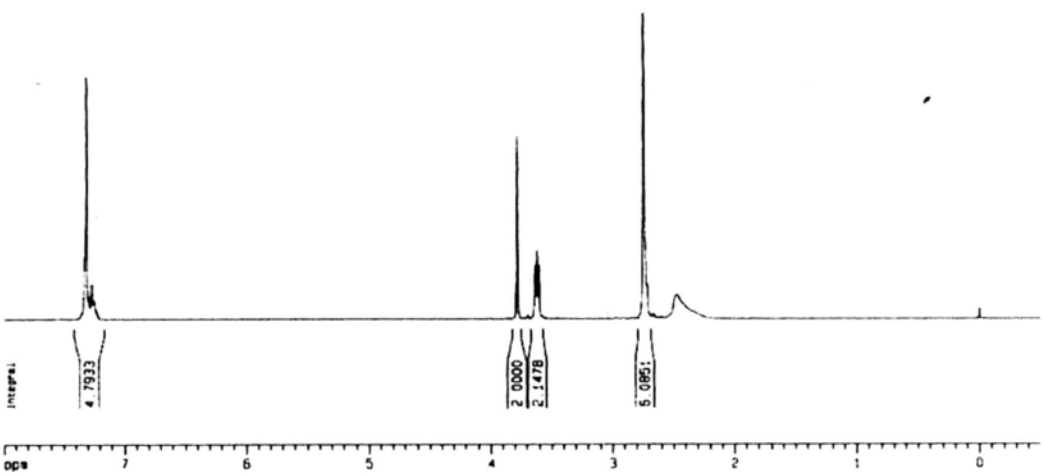

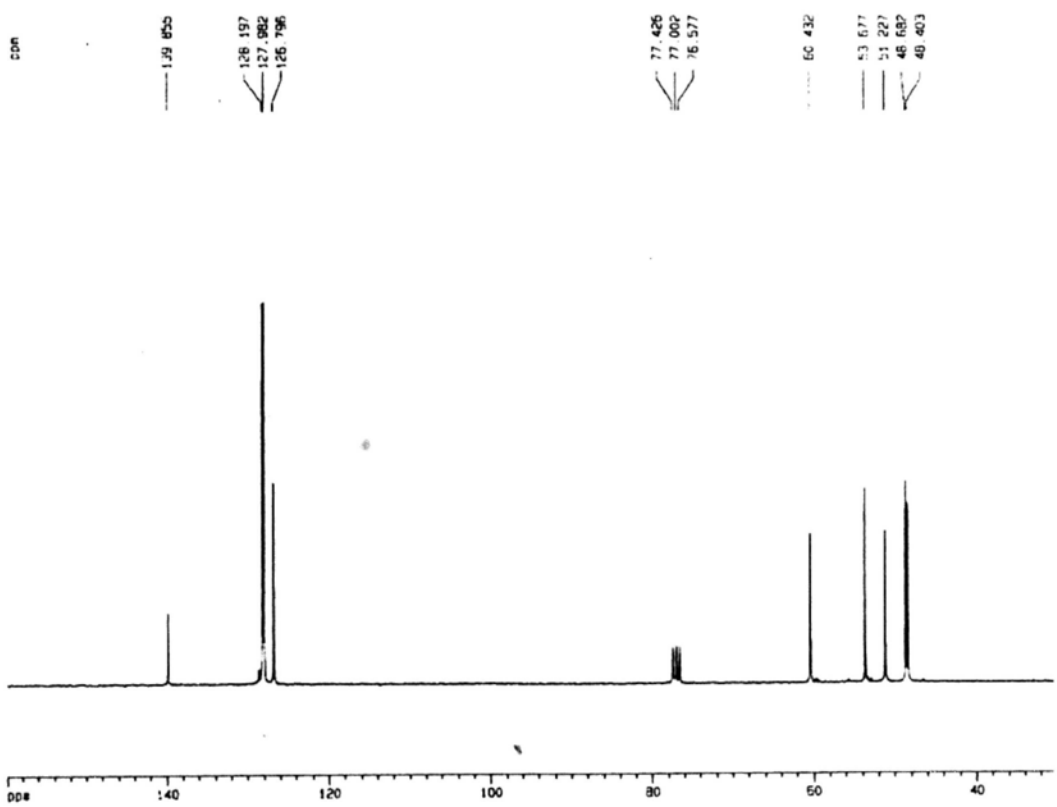

Appendix A-3.7 ^{1}H and $^{13}C\{^{1}H\}$ NMR Spectra of **3.14** in $CDCl_3$

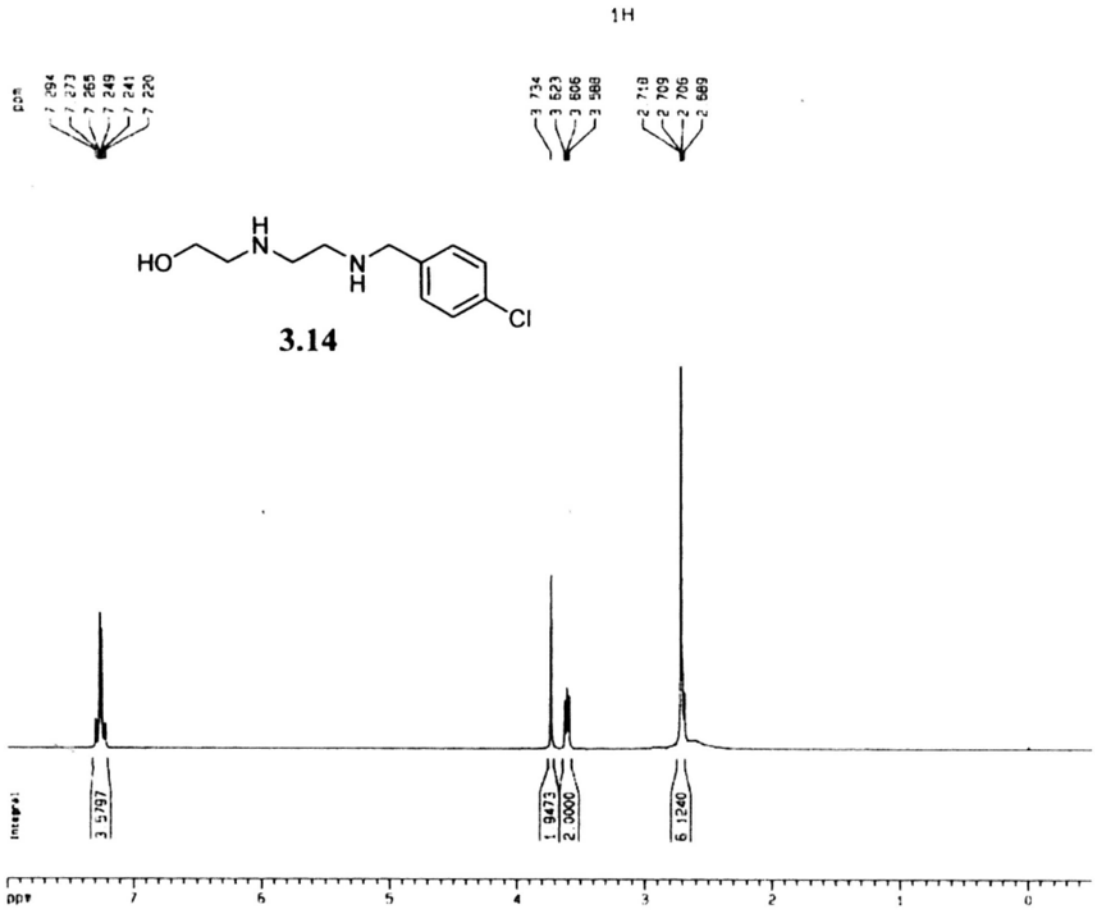

3.14

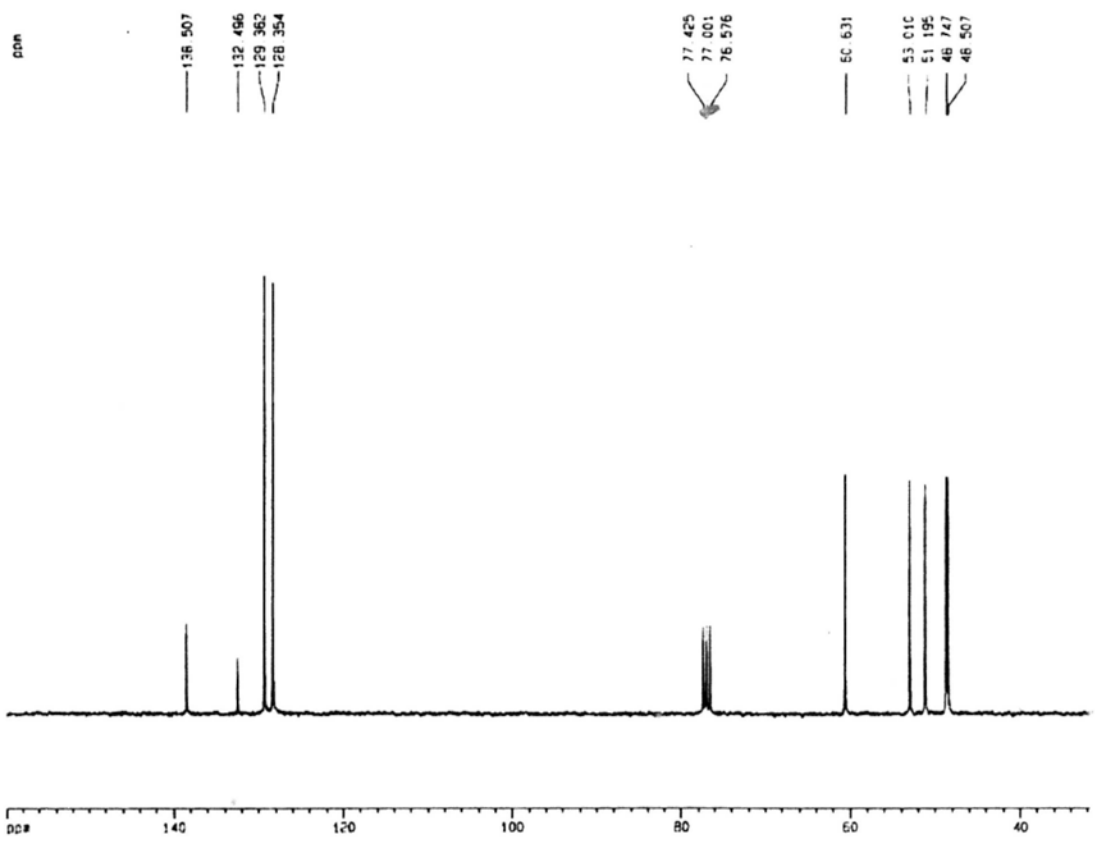

Appendix A-3.8 ^{1}H and $^{13}C\{^{1}H\}$ NMR Spectra of **3.15** in $CDCl_3$

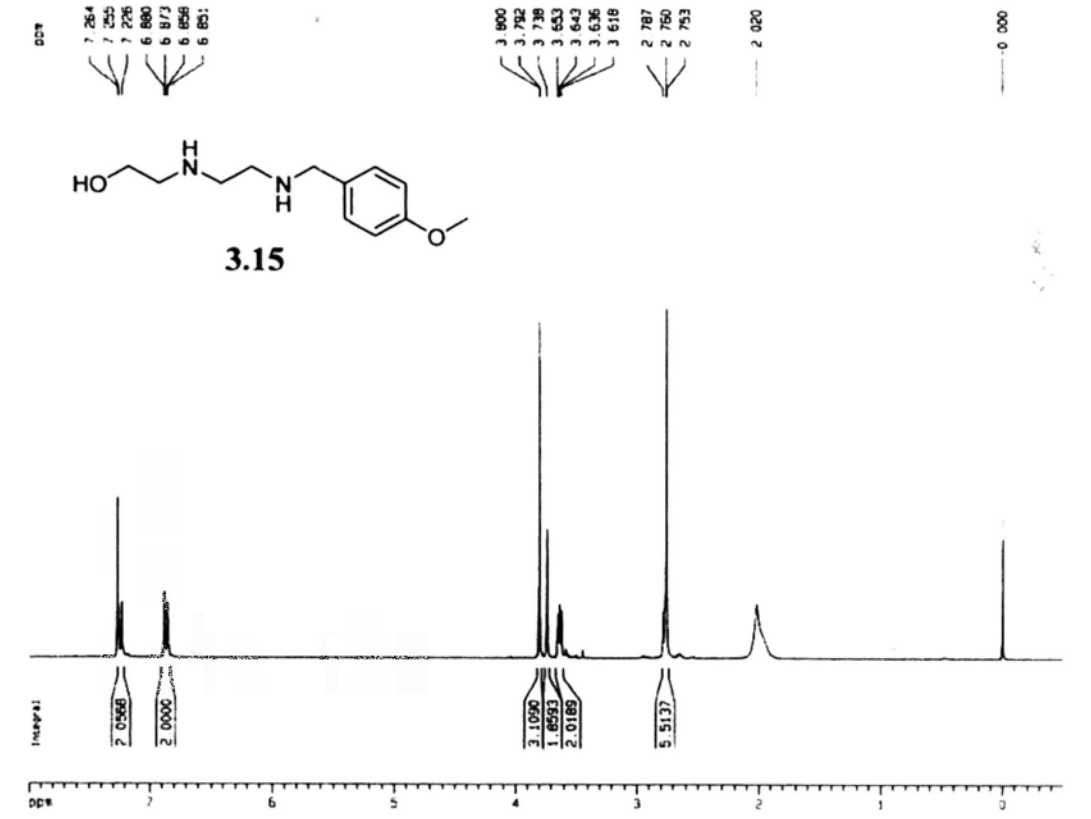

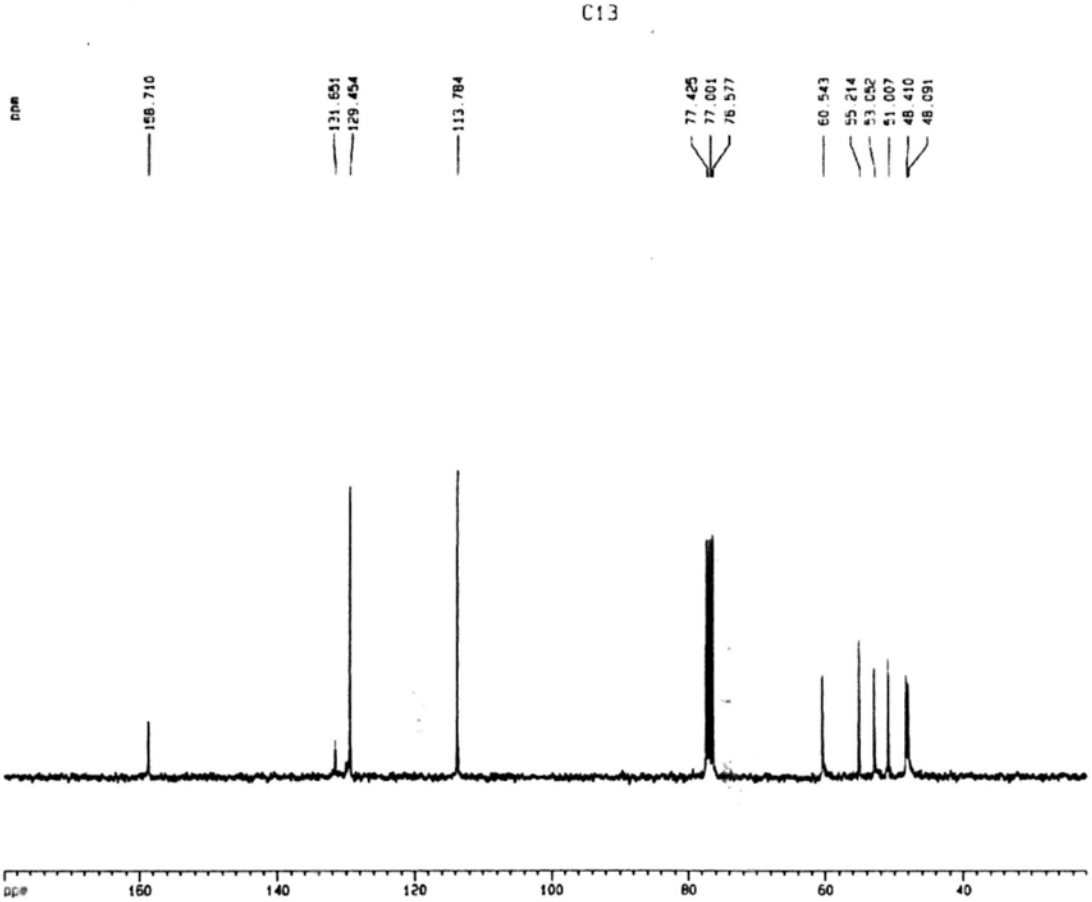

Appendix A-3.9 ^{1}H and $^{13}C\{^{1}H\}$ NMR Spectra of **3.16** in $CDCl_3$

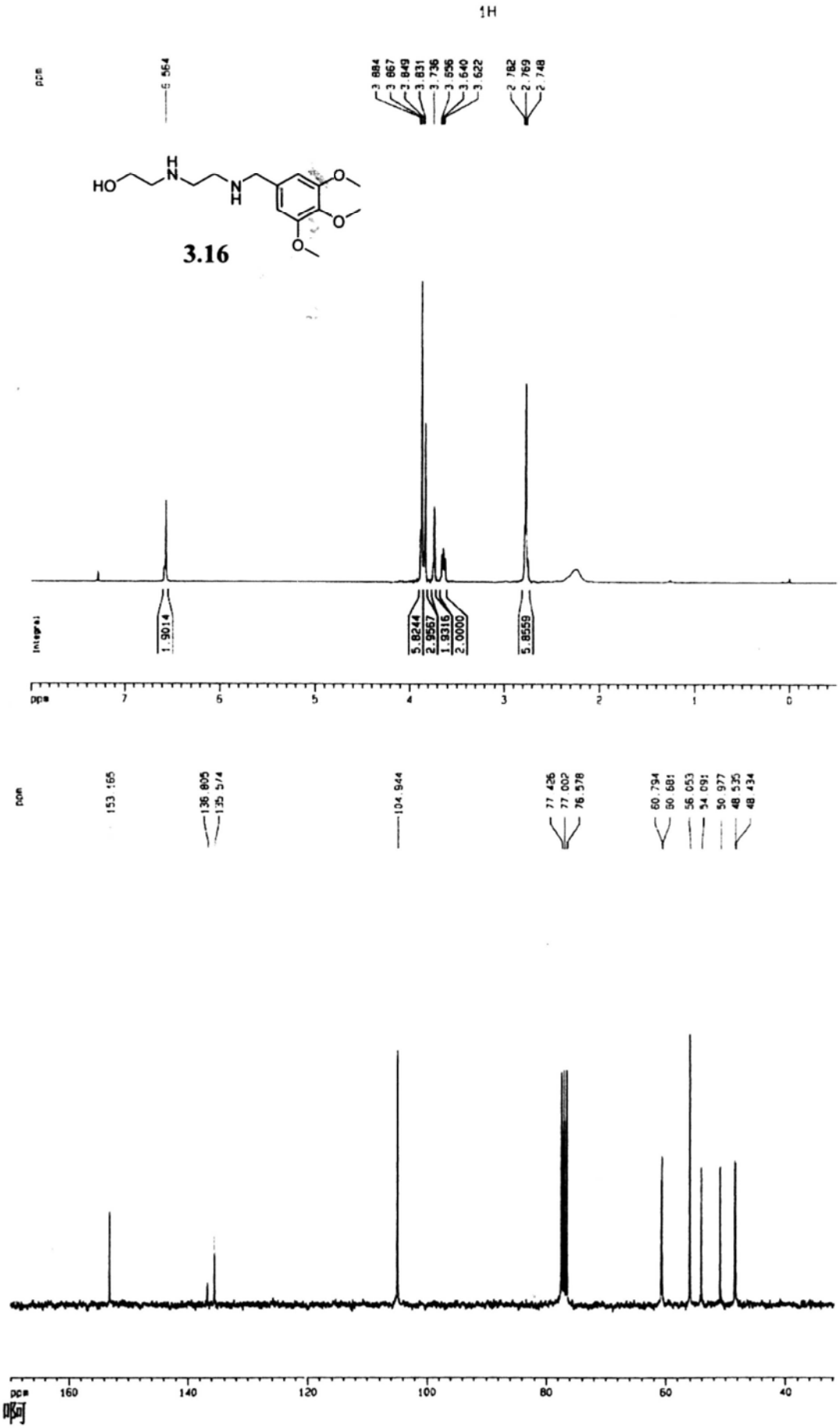

Appendix A-4.1 ^{1}H and $^{13}C\{^{1}H\}$ NMR (300 M Hz) spectra of compound **4.9a** in $CDCl_3$

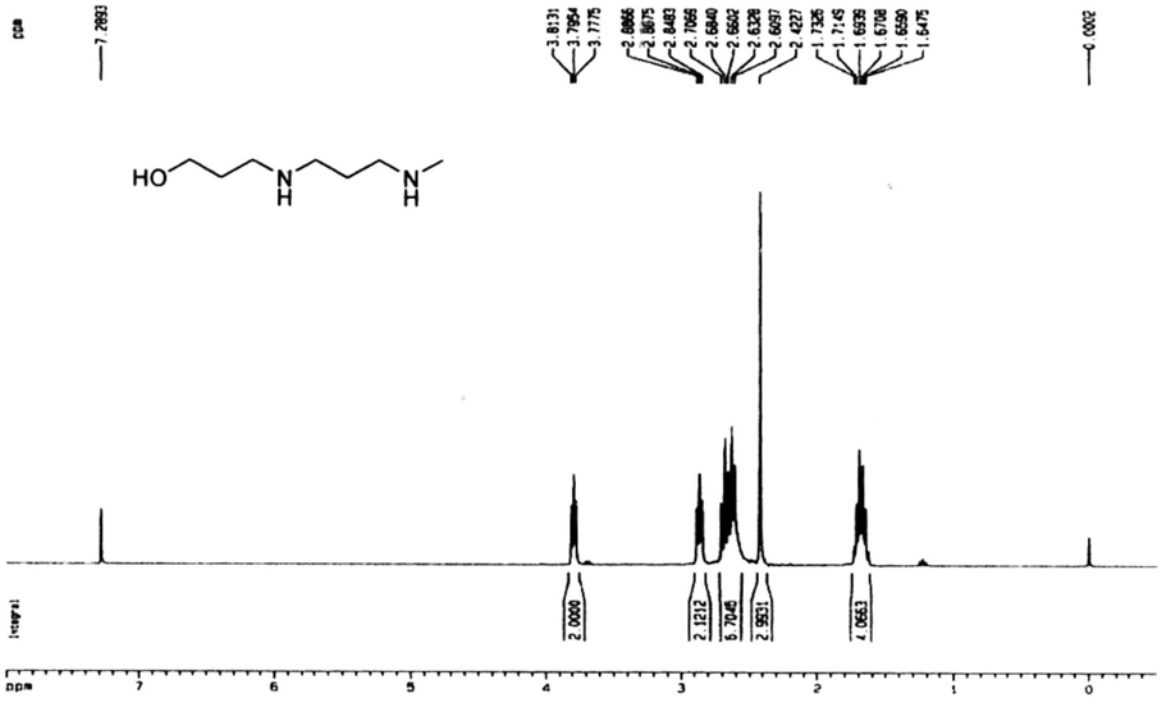

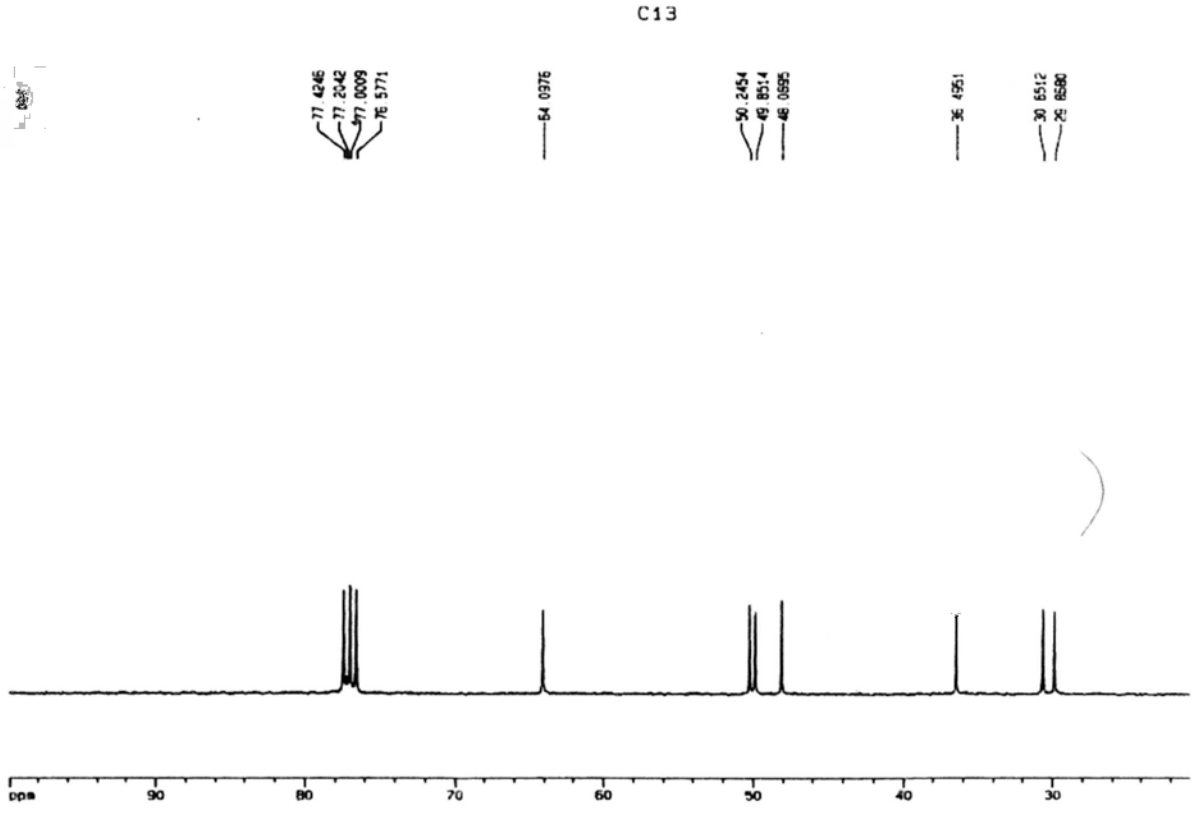

Appendix A-4.2 ^{1}H and $^{13}C\{^{1}H\}$ NMR (400 M Hz) spectra of compound **4.9b** in $CDCl_3$

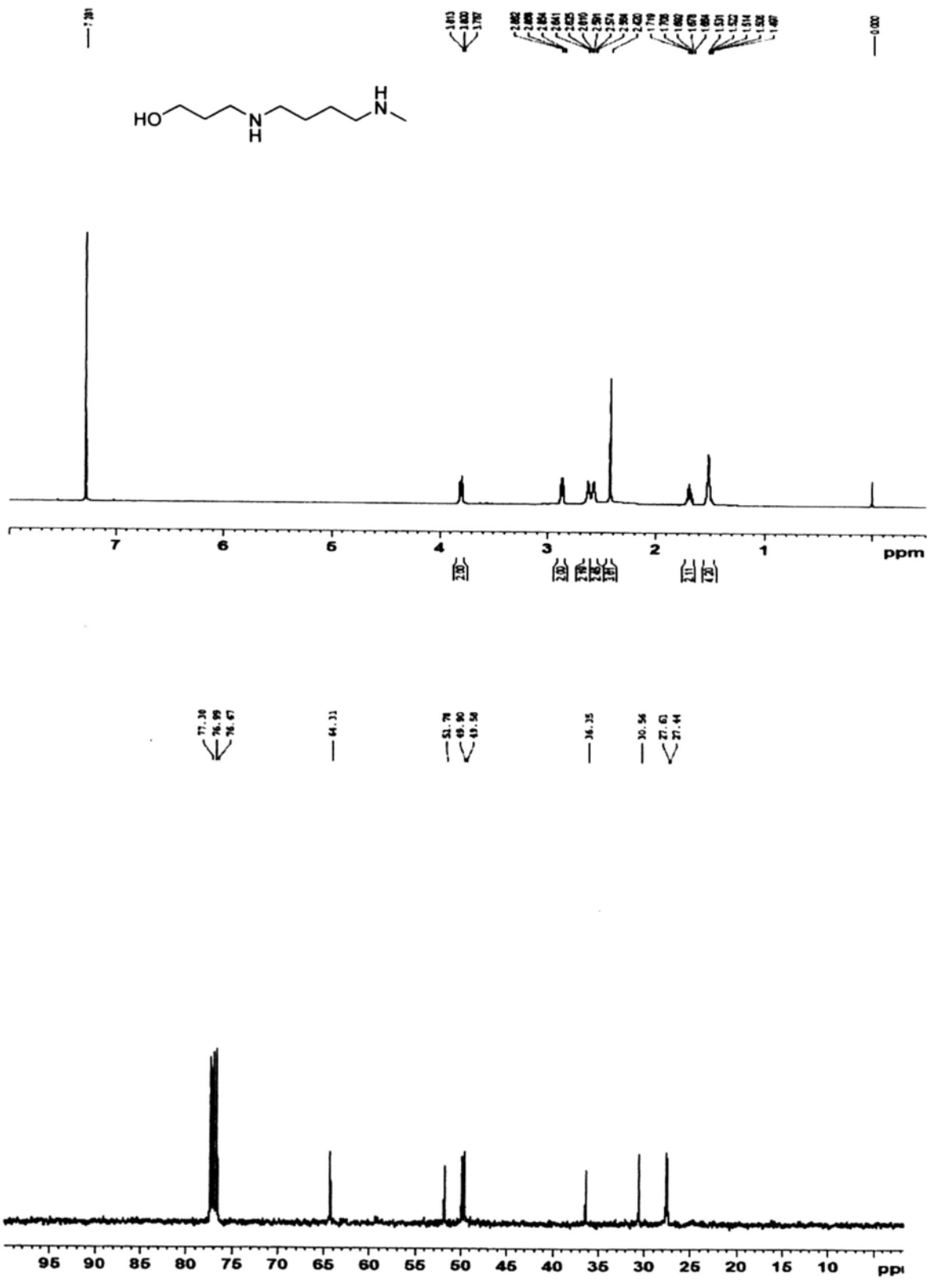

Appendix A-4.3 ^{1}H and $^{13}C\{^{1}H\}$ NMR (400 M Hz) spectra of compound **4.9c** in $CDCl_3$

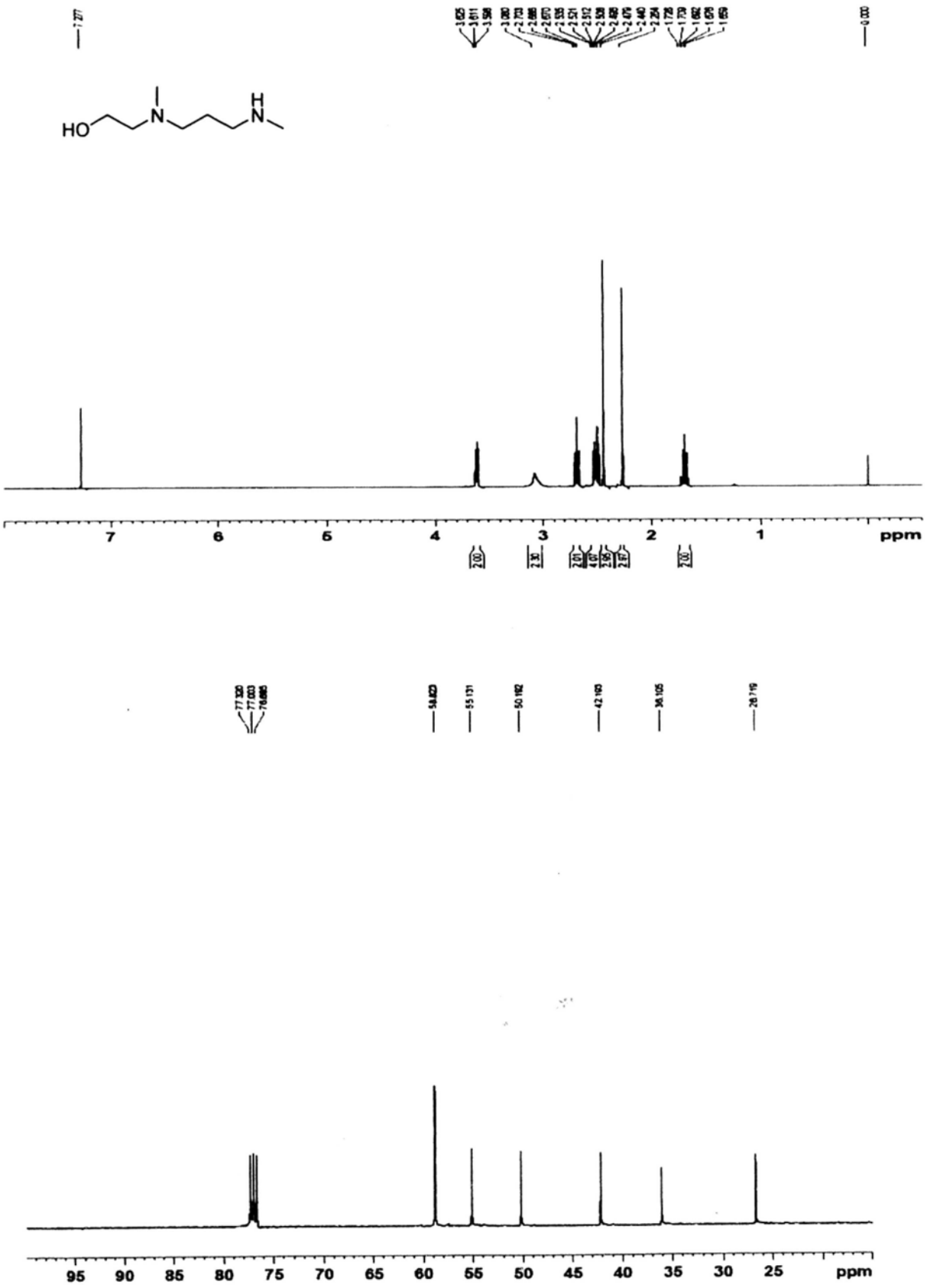

Appendix A-4.4 ^{1}H and $^{13}C\{^{1}H\}$ NMR (300 M Hz) spectra of compound **4.9d** in $CDCl_3$

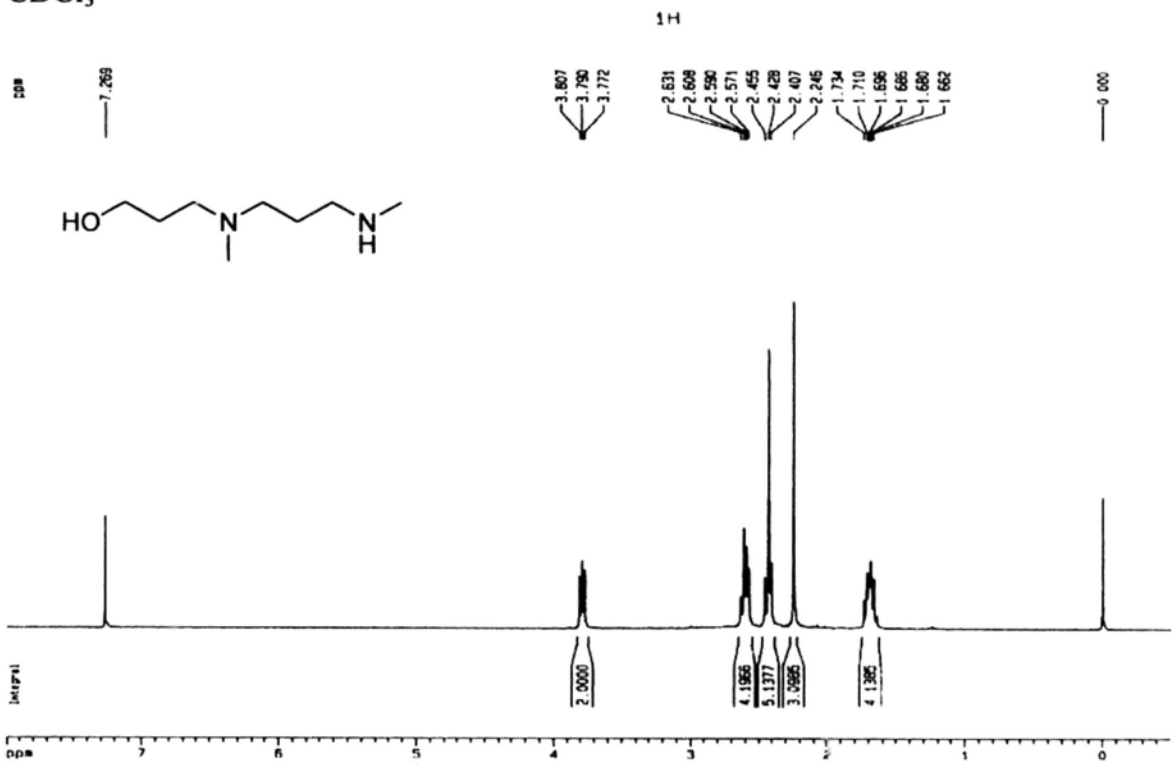

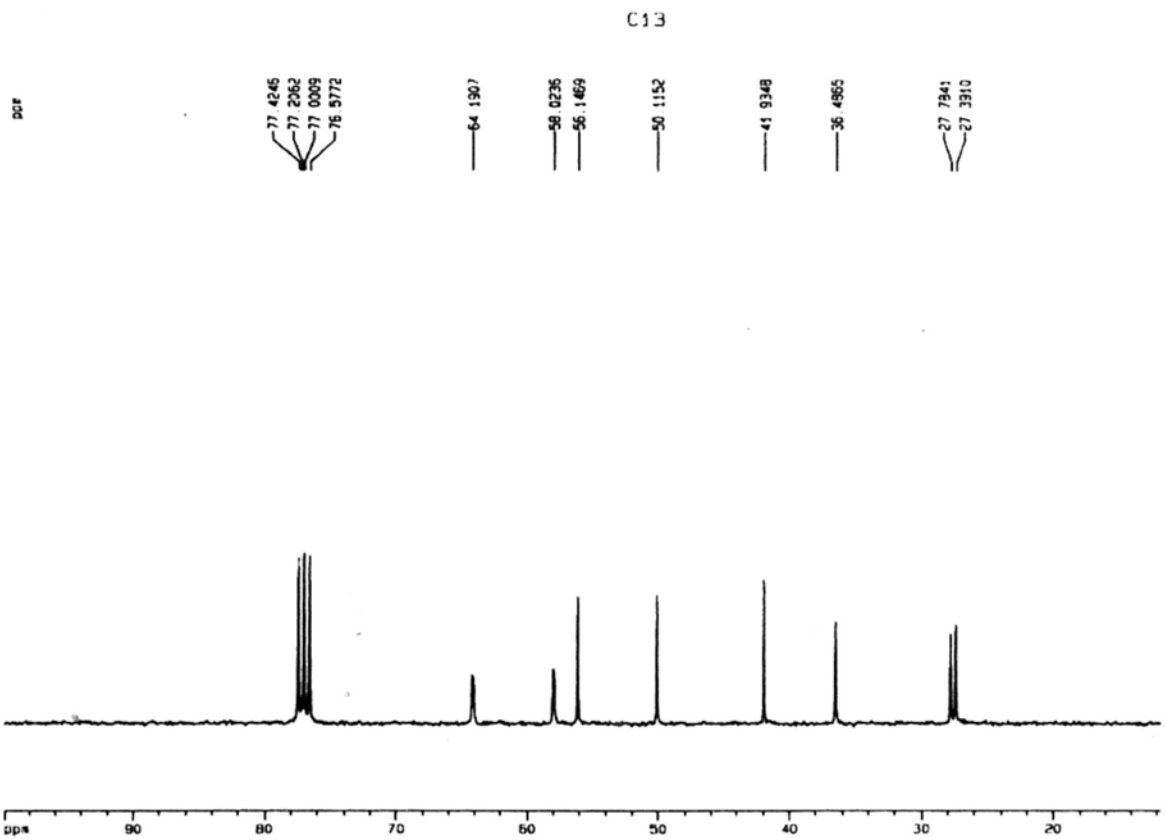

Appendix A-4.5 ^{1}H and $^{13}C\{^{1}H\}$ NMR (400 M Hz) spectra of compound **4.9e** in $CDCl_3$

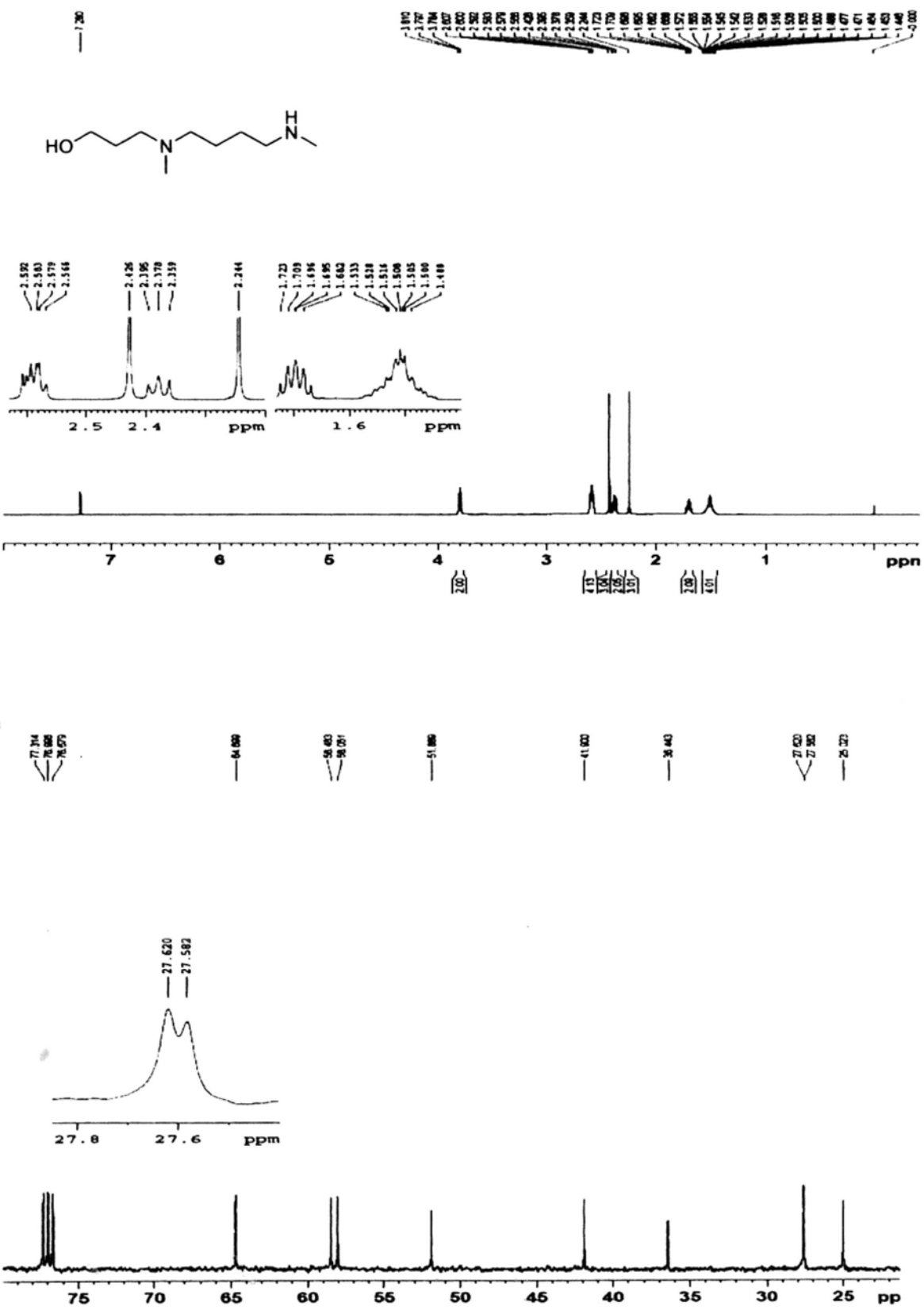

Appendix A-4.6 ^{1}H and $^{13}C\{^{1}H\}$ NMR (400 M Hz) spectra of compound **4.13** in $CDCl_3$

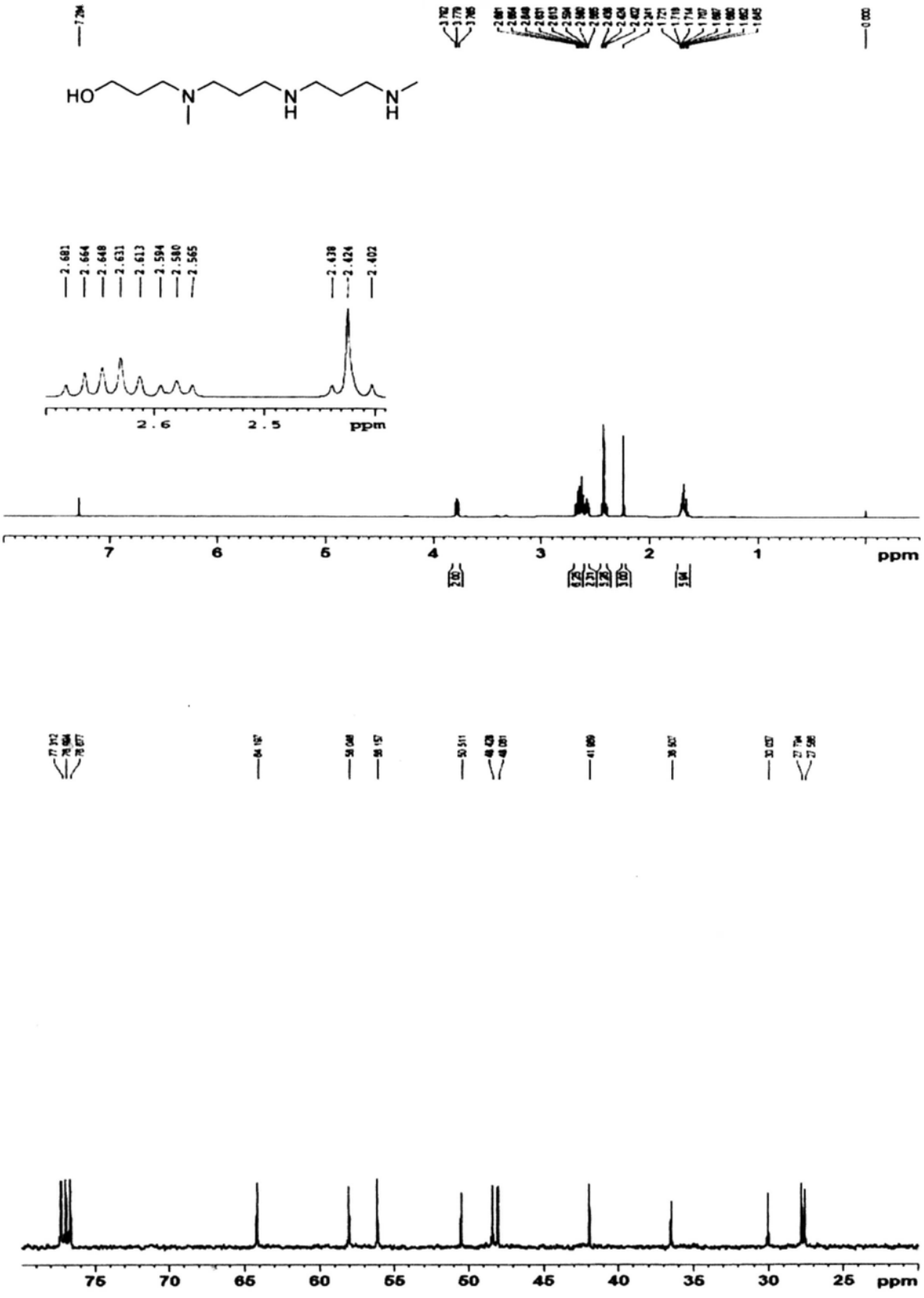

Appendix A-4.7 ^{1}H and $^{13}C\{^{1}H\}$ NMR (400 M Hz) spectra of compound **4.1a** in $CDCl_3$

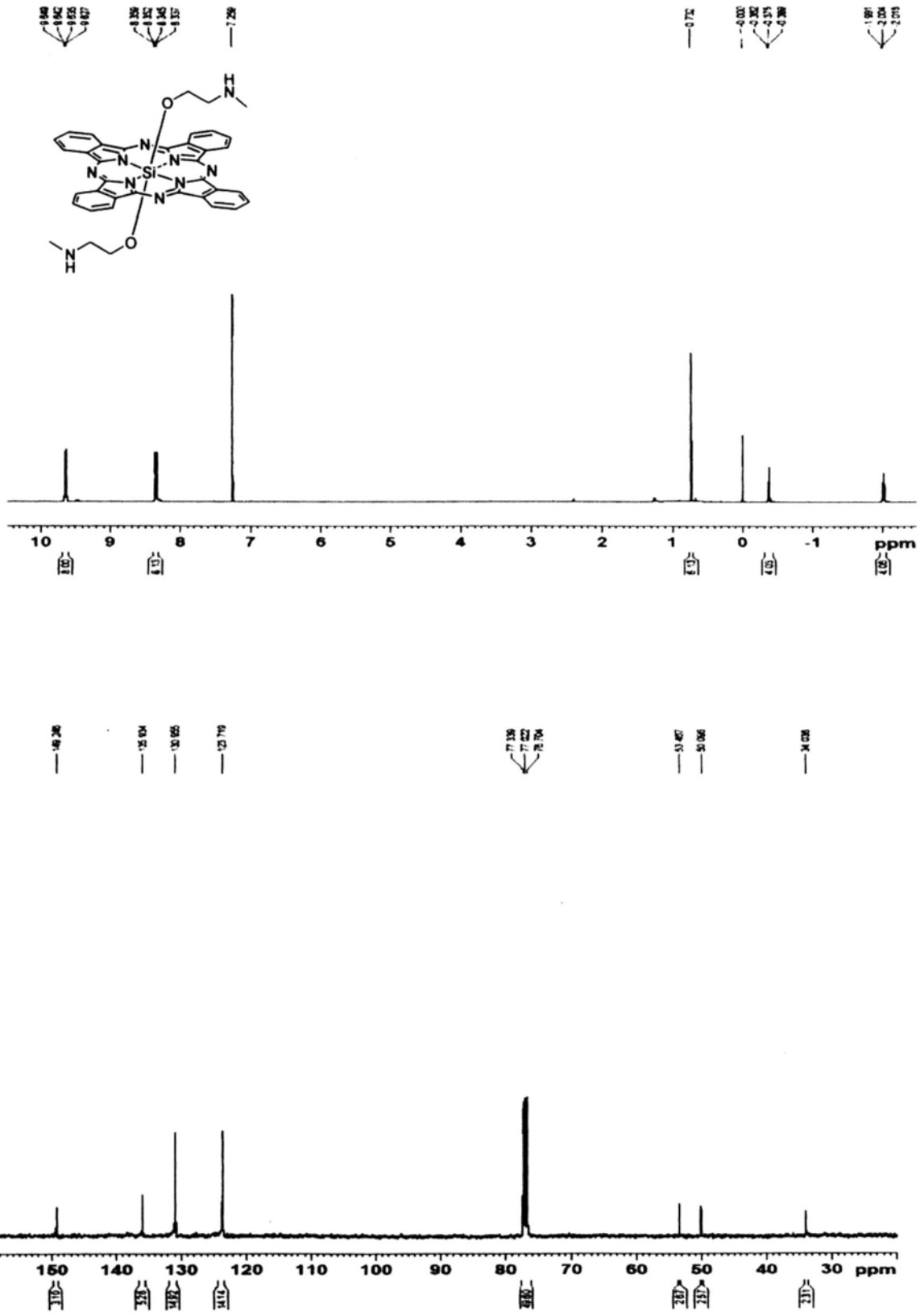

Appendix A-4.8 ^{1}H and $^{13}C\{^{1}H\}$ NMR (400 M Hz) spectra of compound **4.1b** in $CDCl_3$

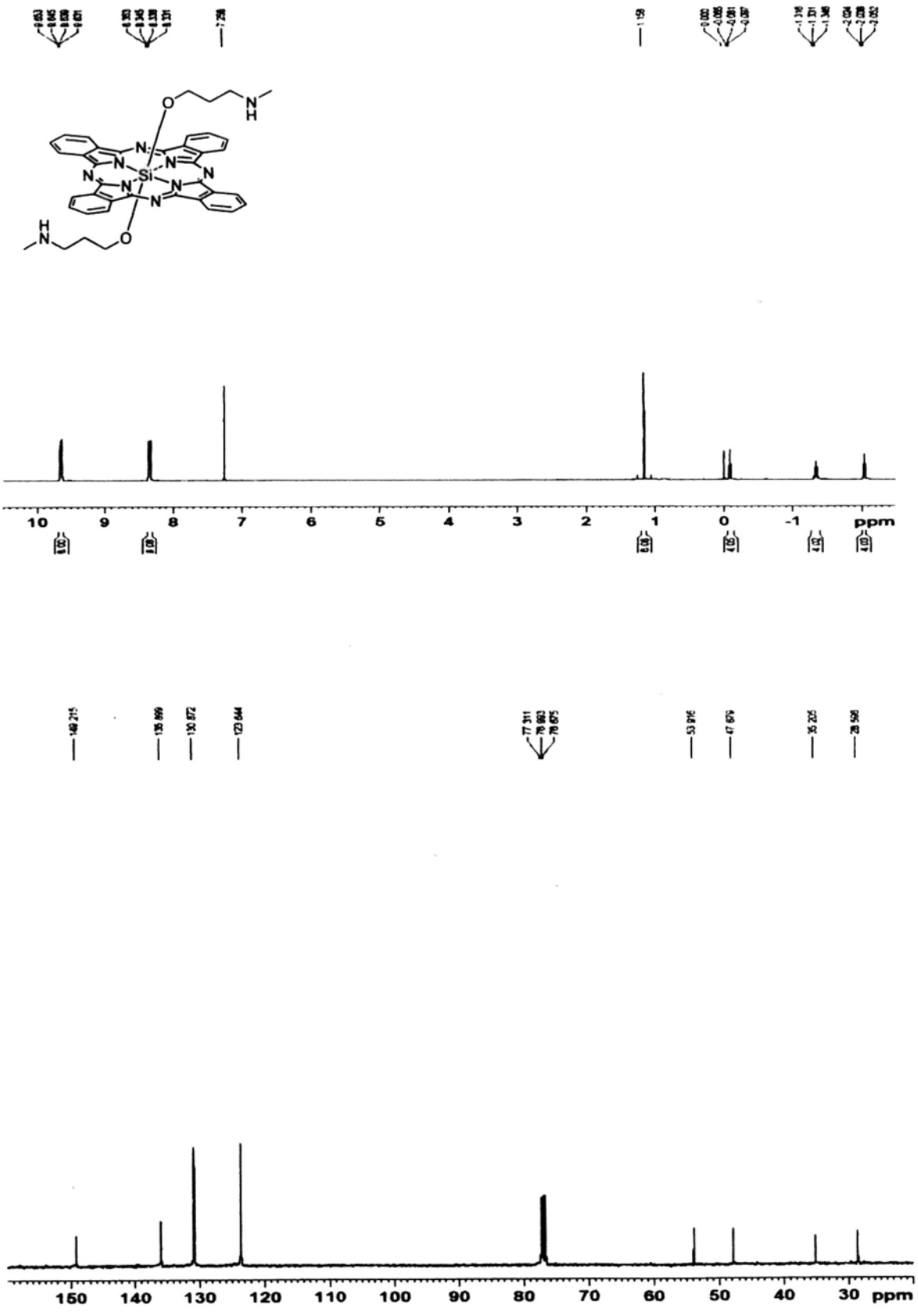

Appendix A-4.9 ^{1}H and $^{13}C\{^{1}H\}$ NMR (400 M Hz) spectra of compound **4.1c** in $CDCl_3$

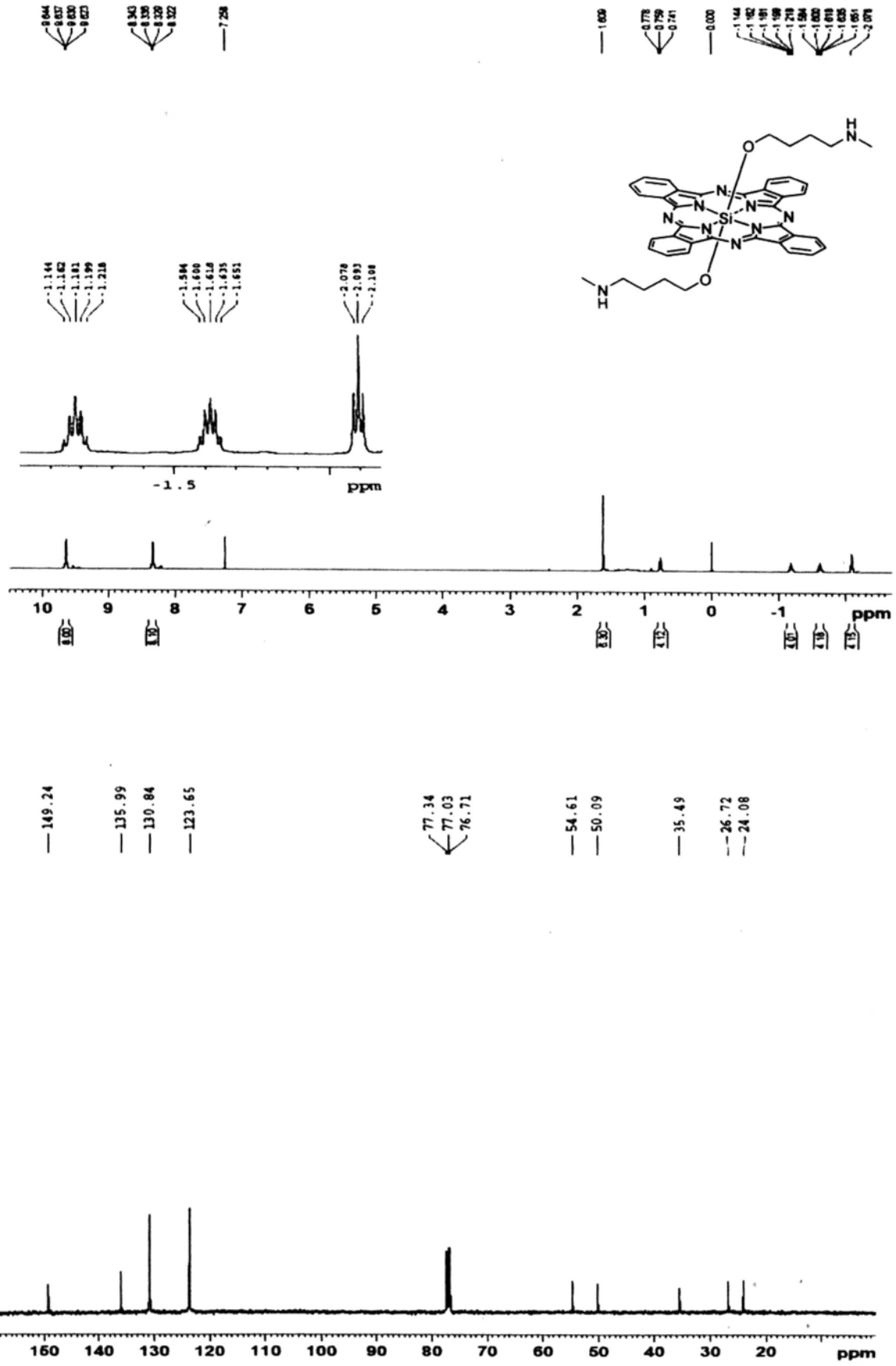

Appendix A-4.10 ^{1}H and $^{13}C\{^{1}H\}$ NMR (300 M Hz) spectra of compound **4.1d** in $CDCl_3$

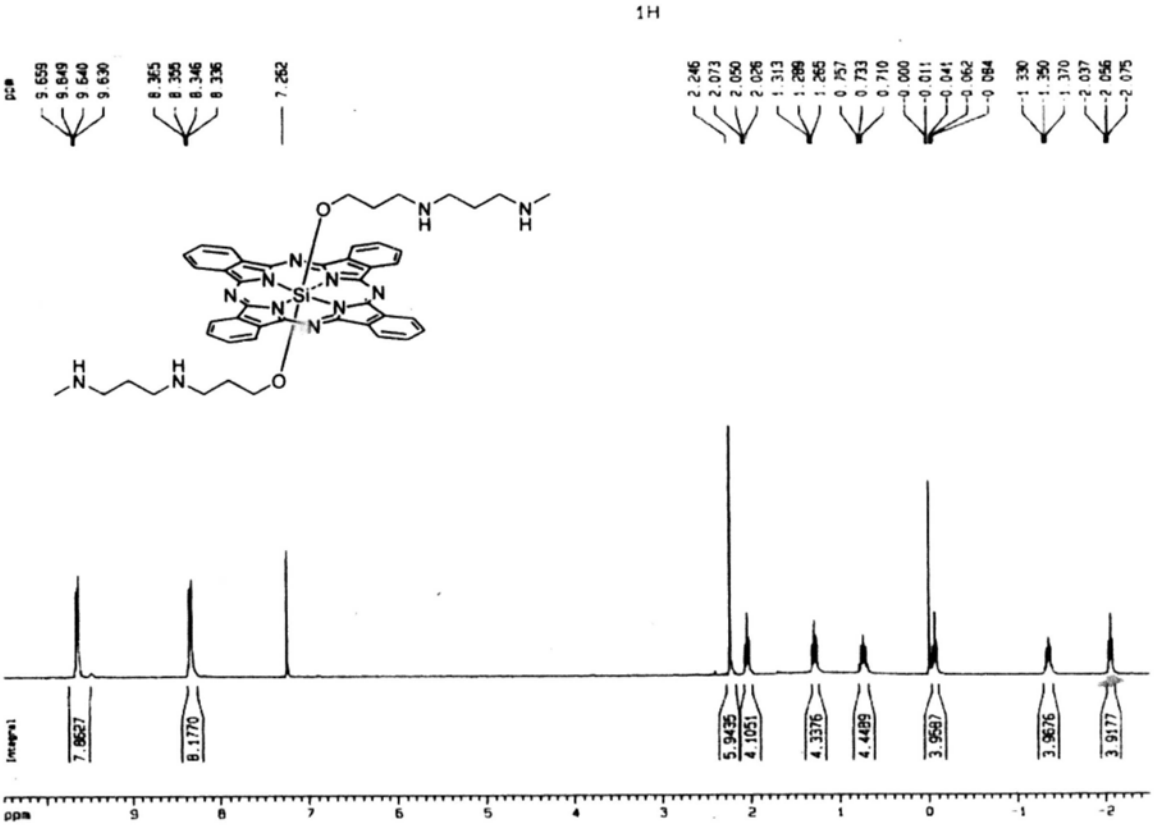

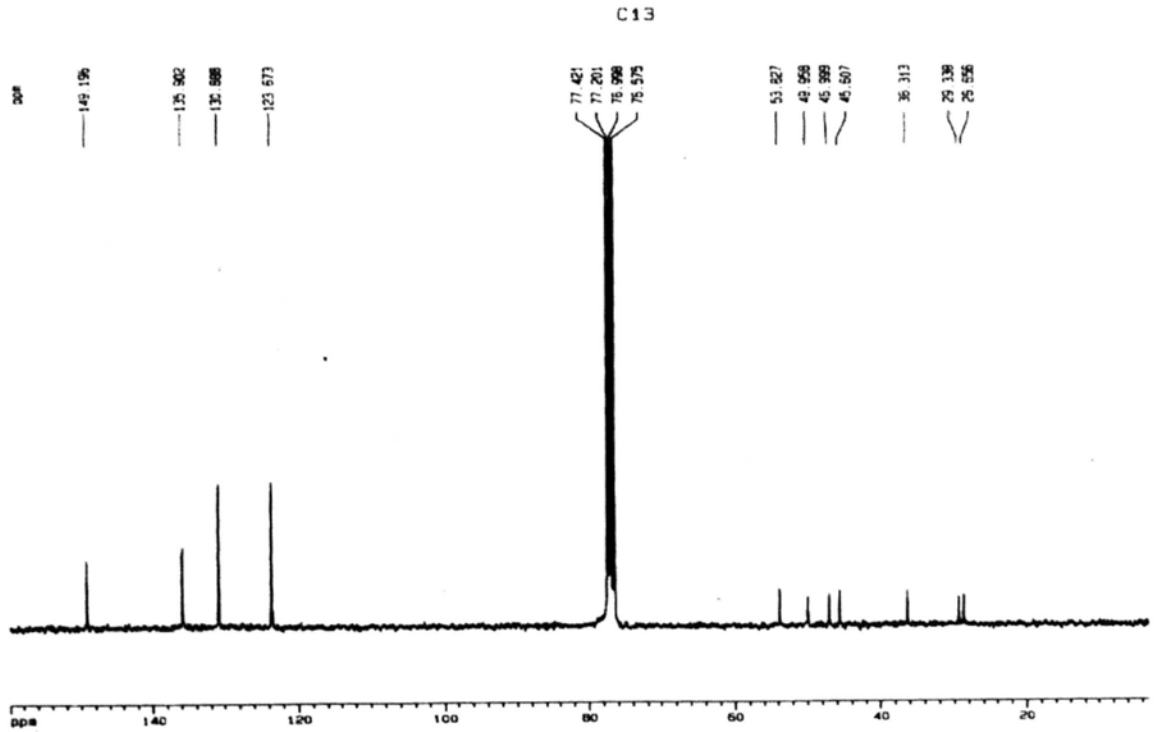

Appendix A-4.11 ^{1}H and $^{13}C\{^{1}H\}$ NMR (400 M Hz) spectra of compound **4.1e** in $CDCl_3$

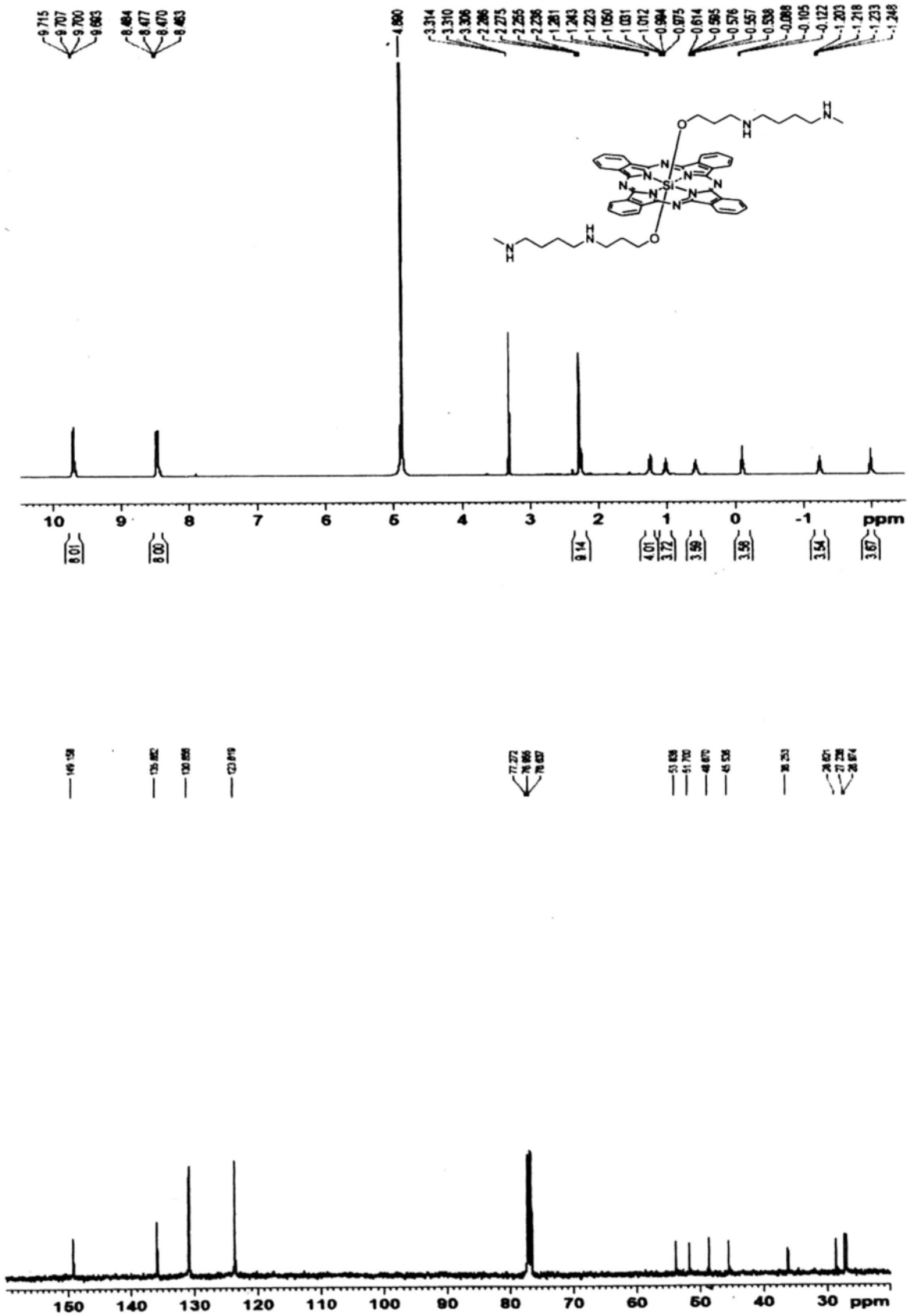

Appendix A-4.12 ^{1}H and $^{13}C\{^{1}H\}$ NMR (300 M Hz) spectra of compound **4.1f** in $CDCl_3$

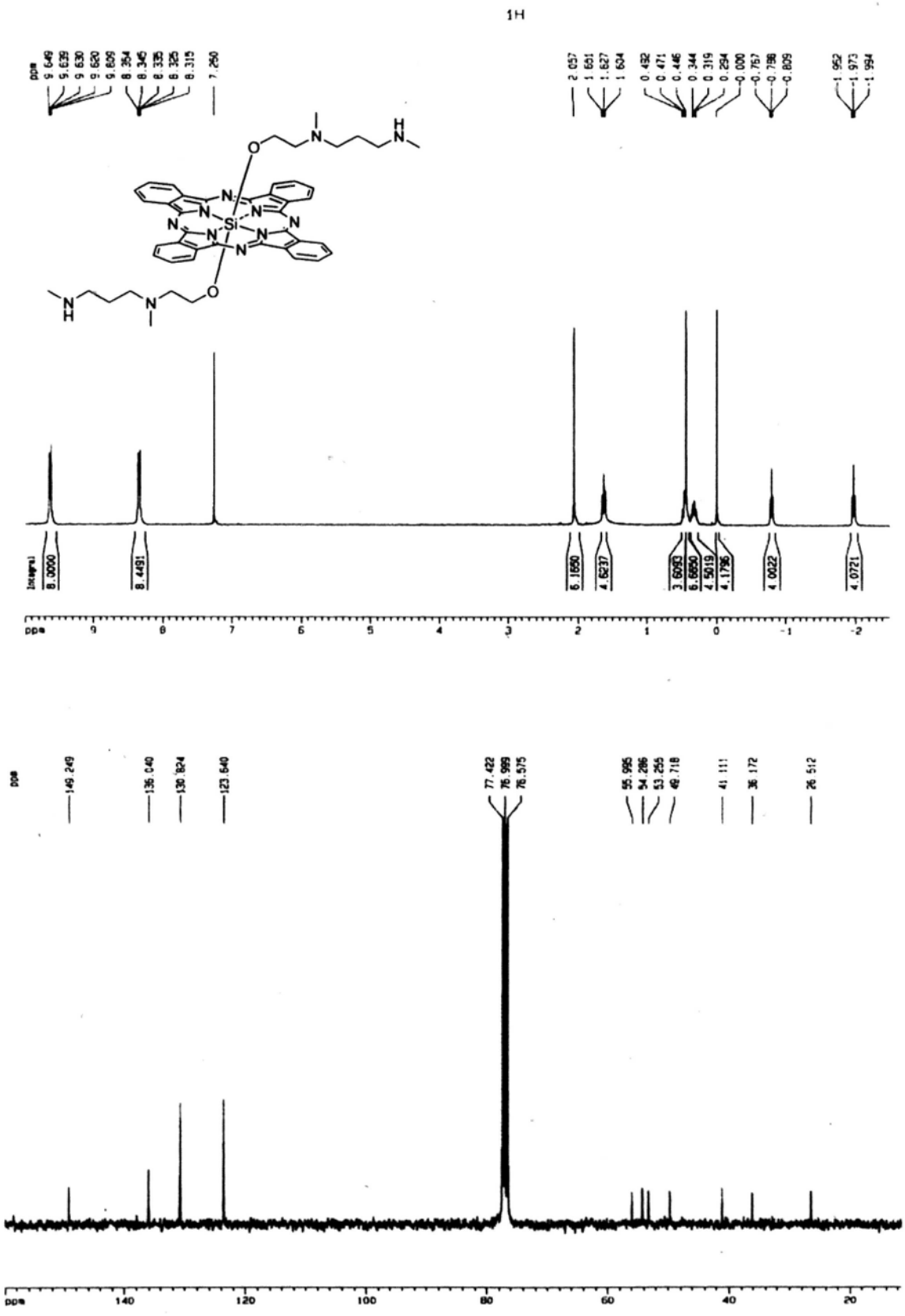

Appendix A-4.13. ^{1}H and $^{13}C\{^{1}H\}$ NMR (300 M Hz) spectra of compound **4.1g** in $CDCl_3$

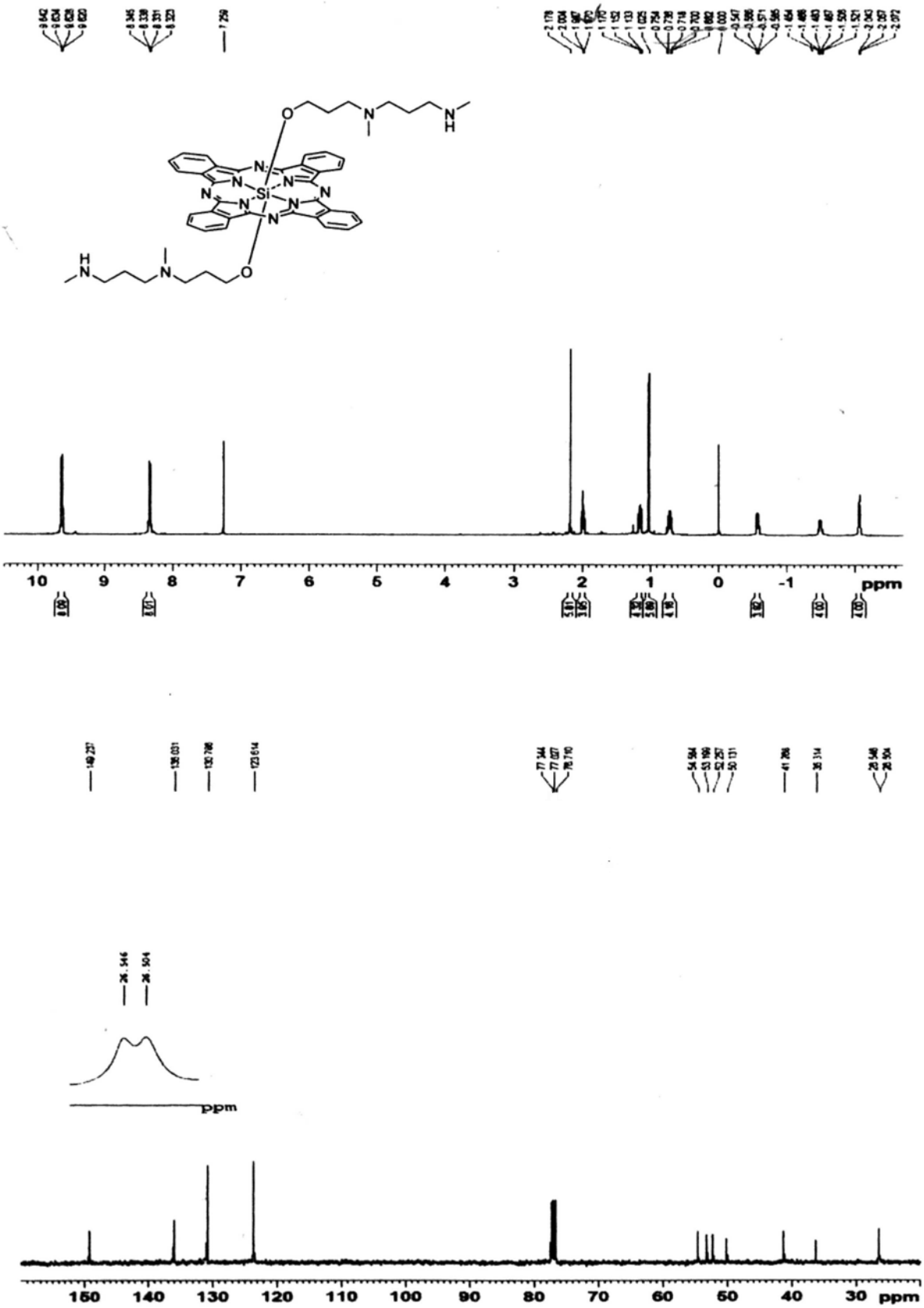

Appendix A-4.14 ^{1}H and $^{13}C\{^{1}H\}$ NMR (400 M Hz) spectra of compound **4.1h** in CD_3OD

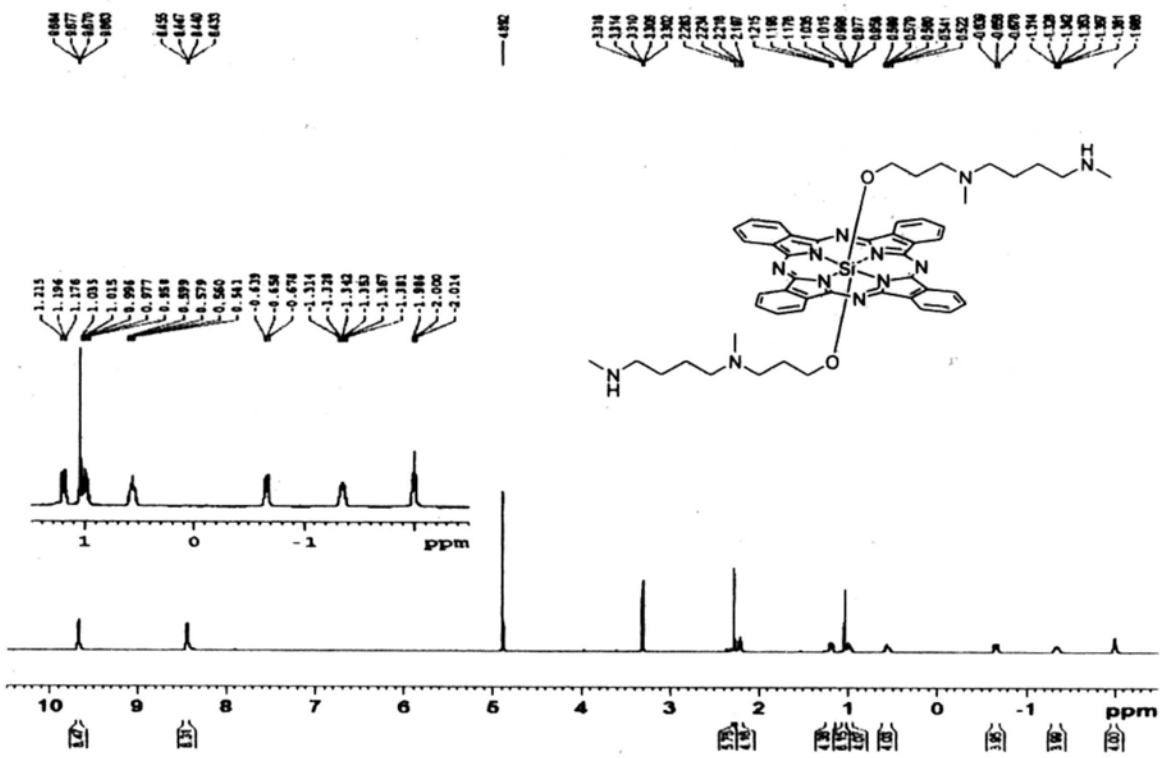

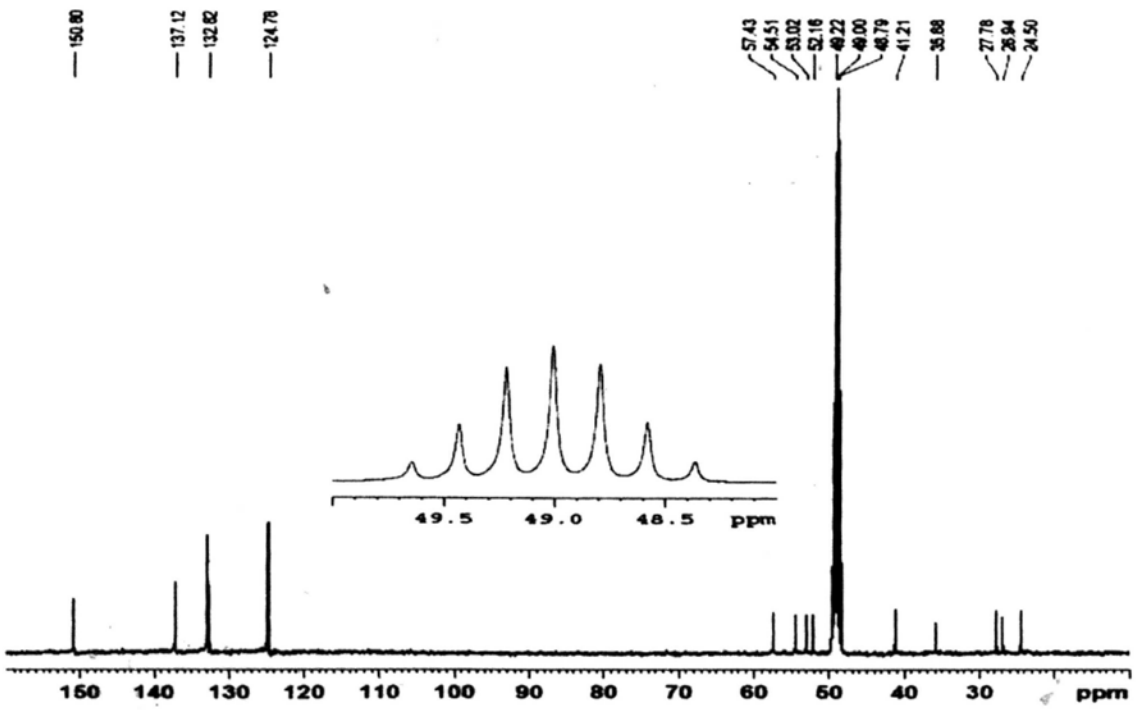

Appendix A-4.15 ^{1}H and $^{13}C\{^{1}H\}$ NMR (400 M Hz) spectra of compound **4.1i** in CD_3OD

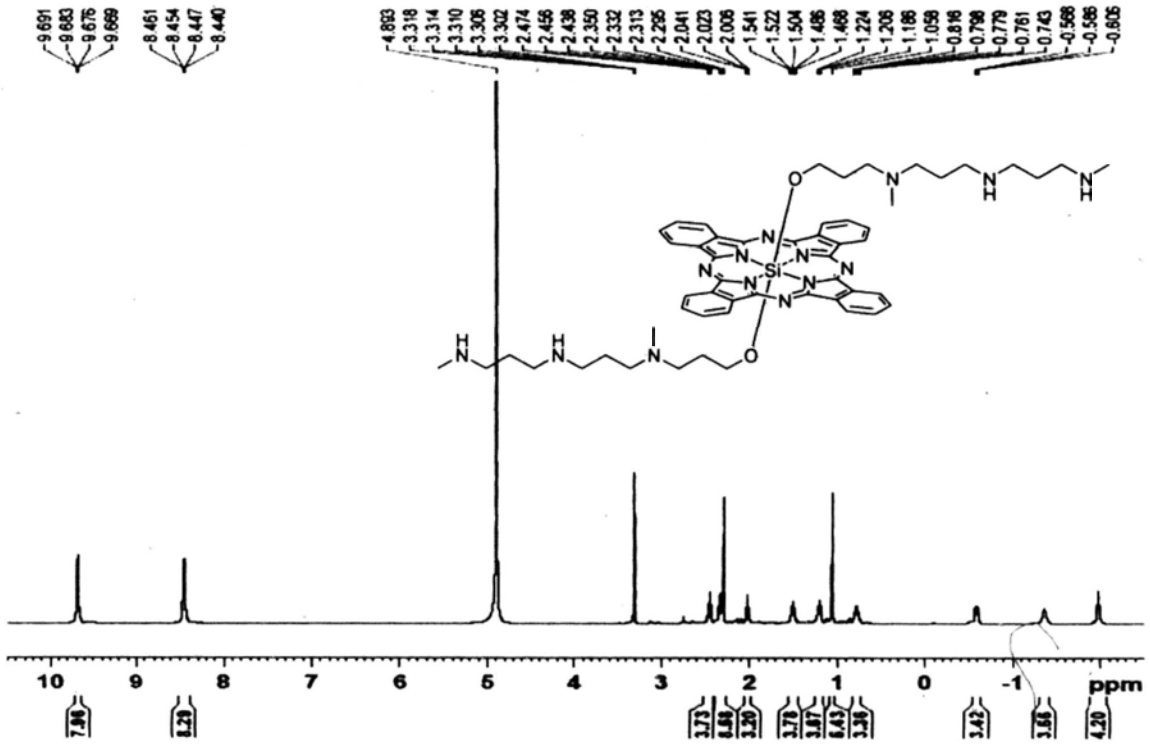

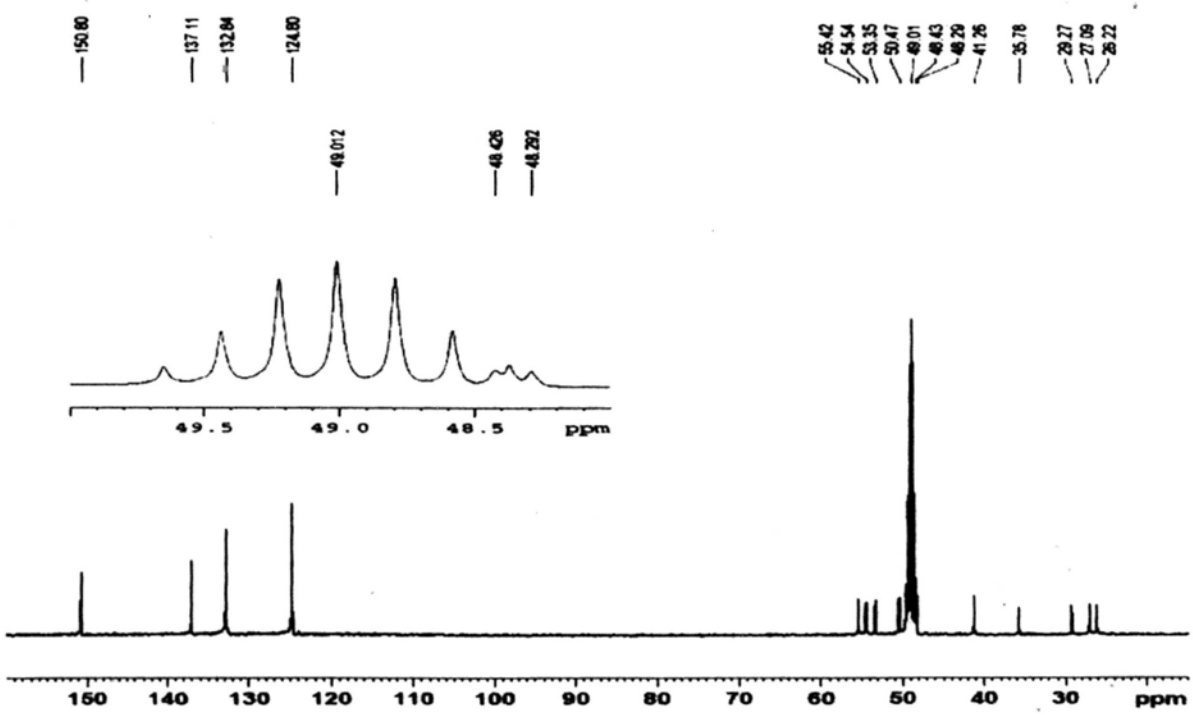

Appendix A-5.1 ^{1}H and $^{13}C\{^{1}H\}$ NMR spectra of compound **5.1** in $CDCl_3$.

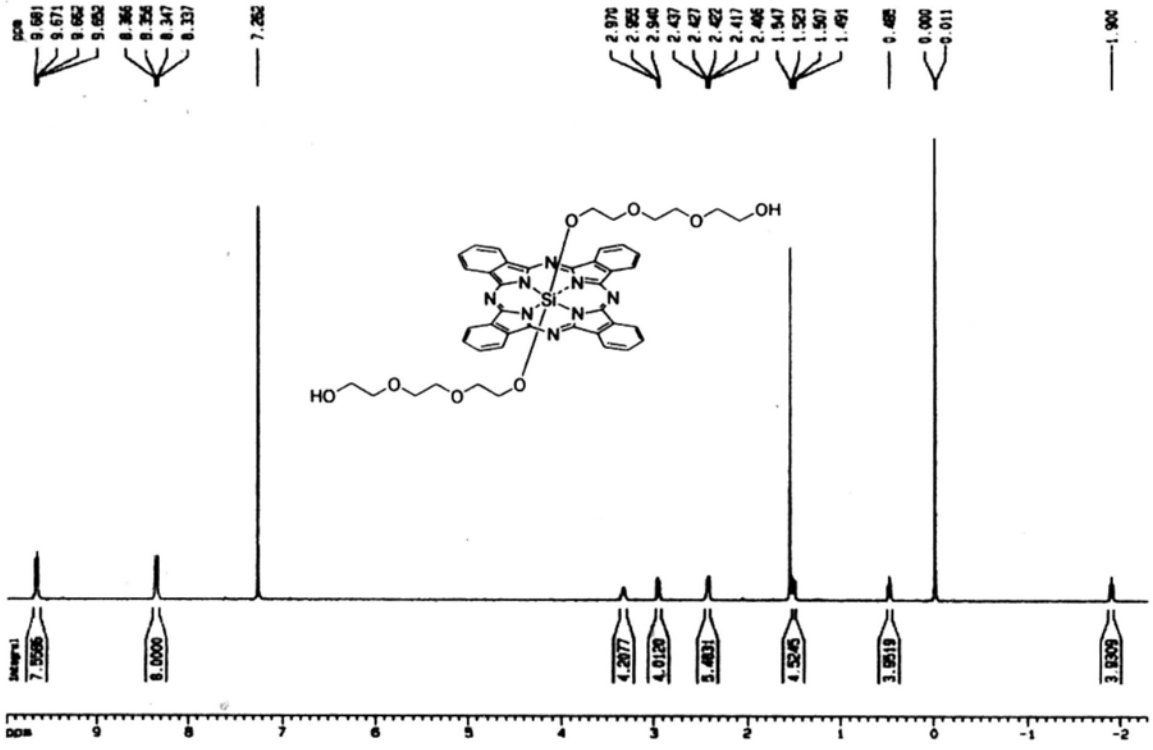

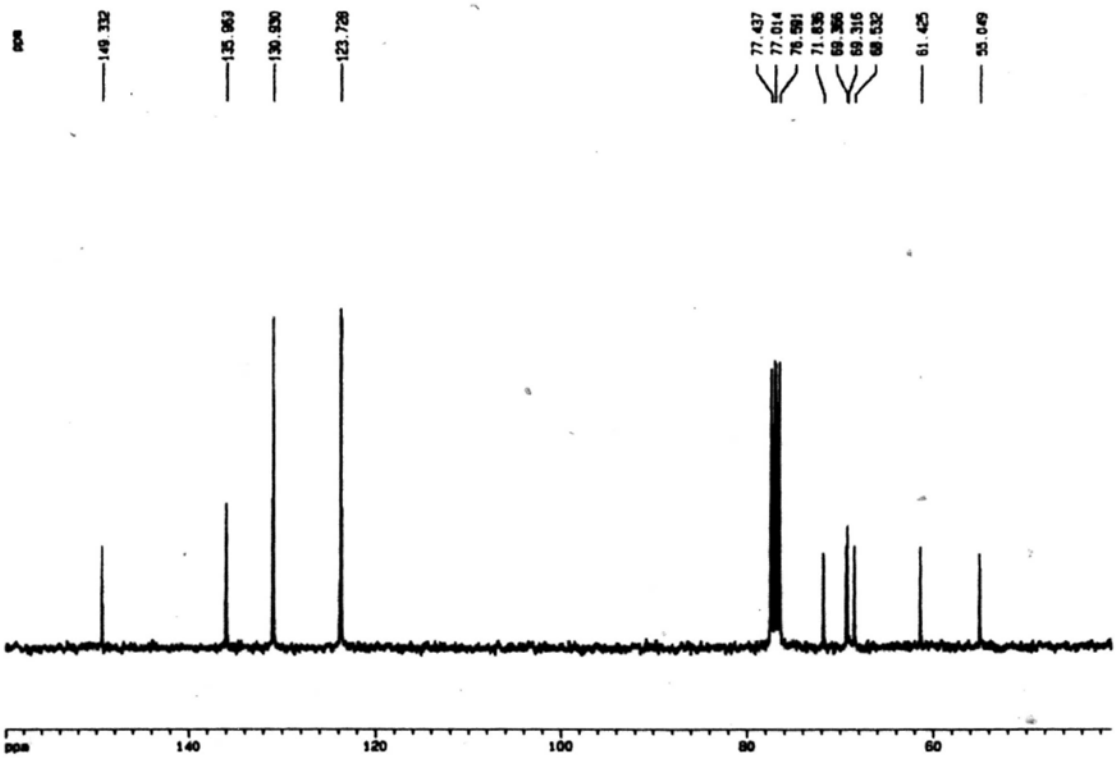

Appendix A-5.2 ^{1}H and $^{13}C\{^{1}H\}$ NMR spectra of compound **5.2** in $CDCl_3$.

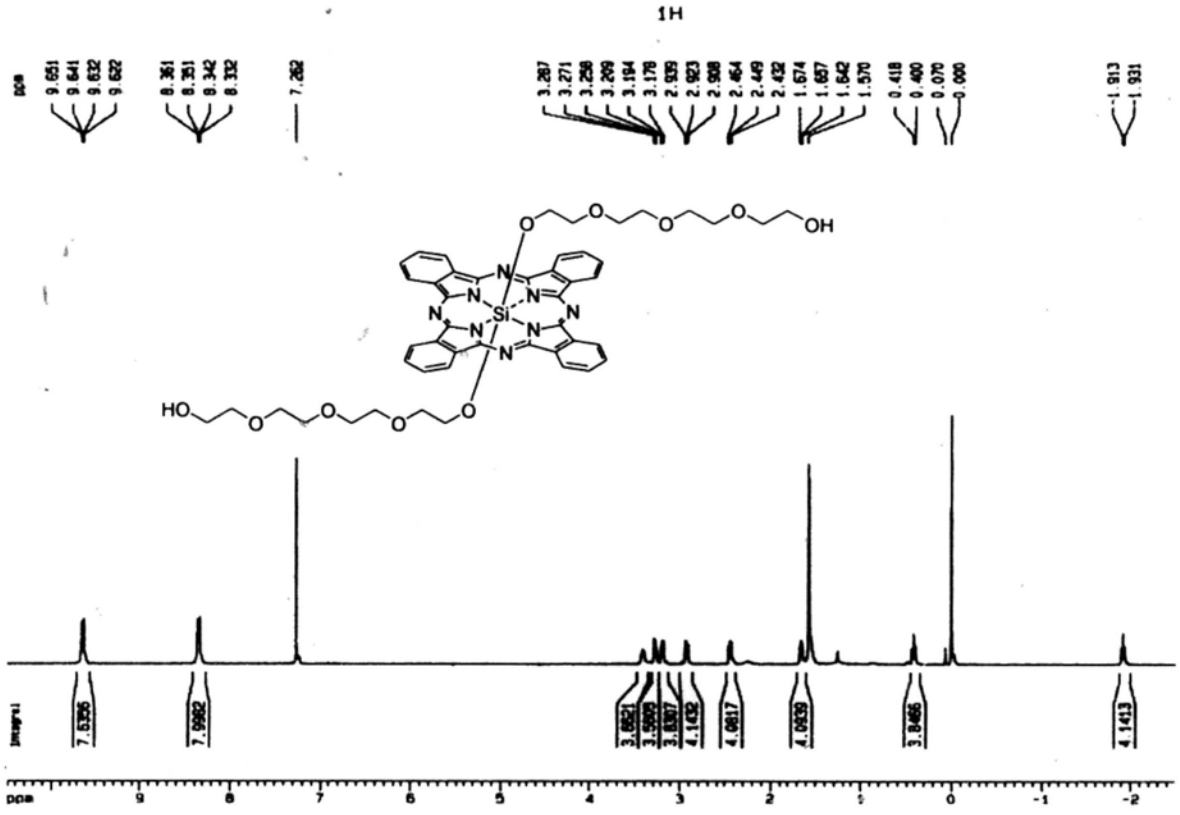

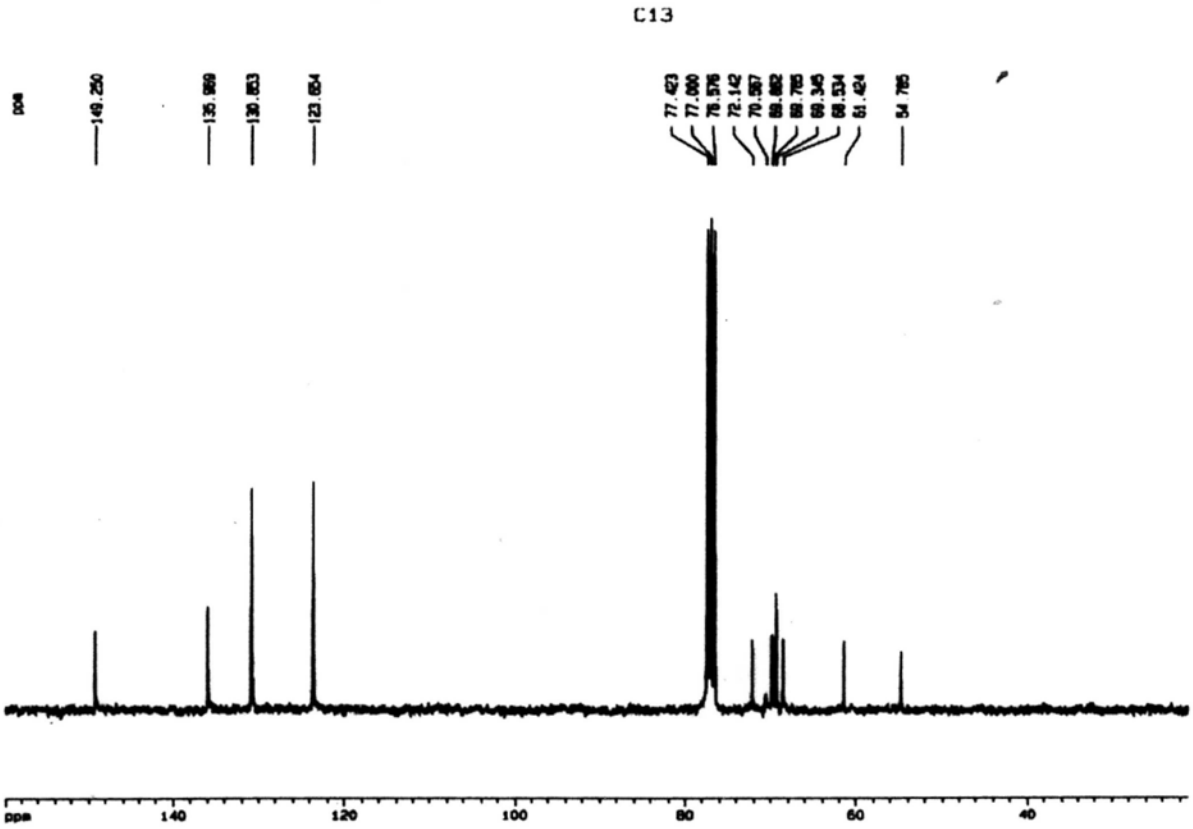

Appendix A-5.3 ^{1}H NMR spectrum of compound **5.3** in $CDCl_3$.

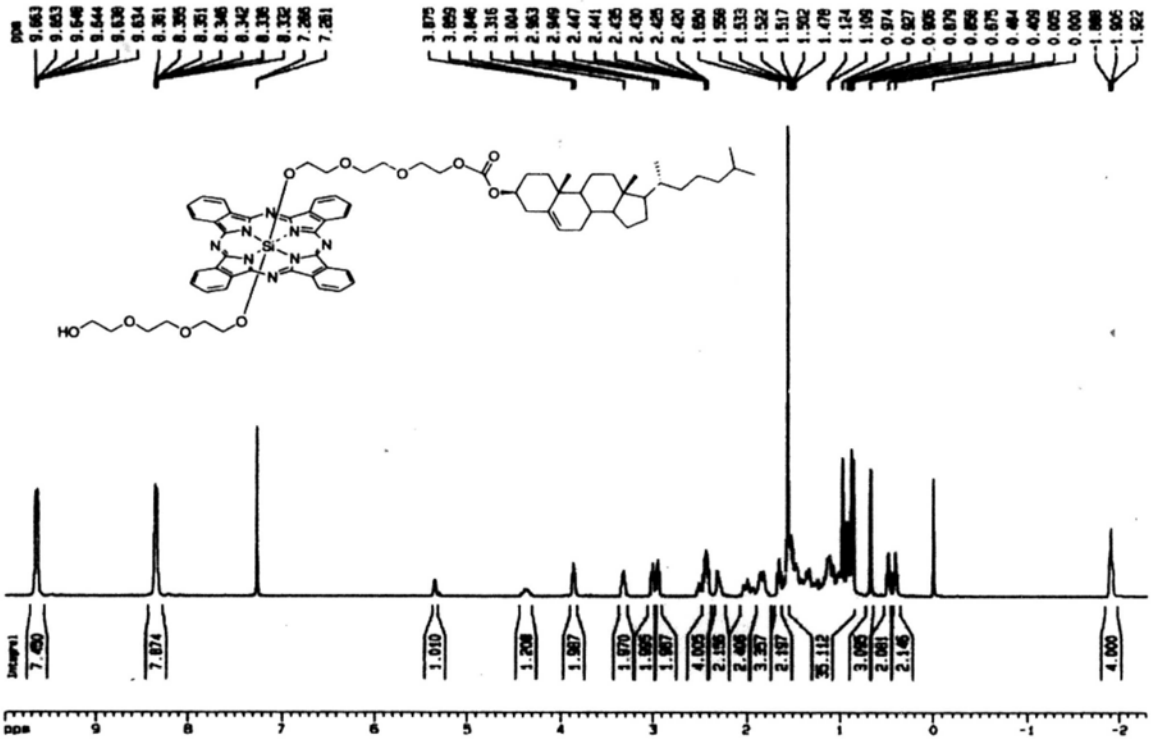

Appendix A-5.4 ^{1}H NMR spectrum of compound **5.5** in $CDCl_3$.

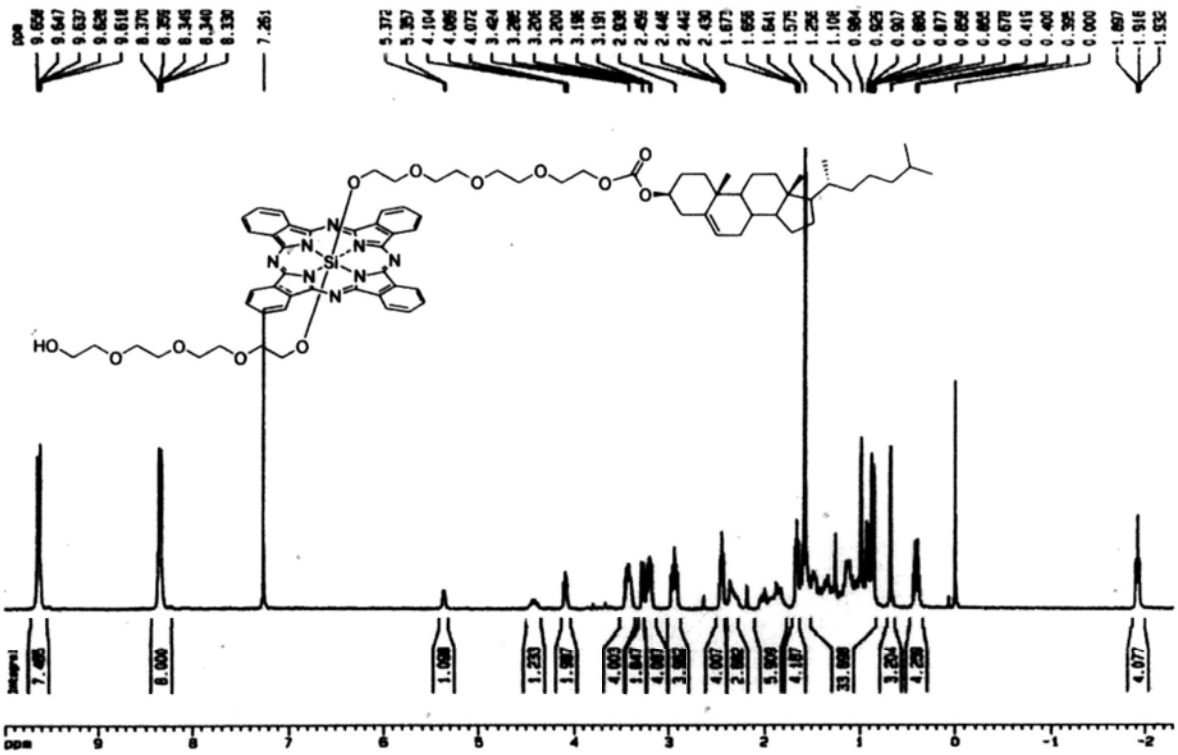

Appendix A-5.5 ^{1}H NMR spectrum of compound **5.4** in $CDCl_3$.

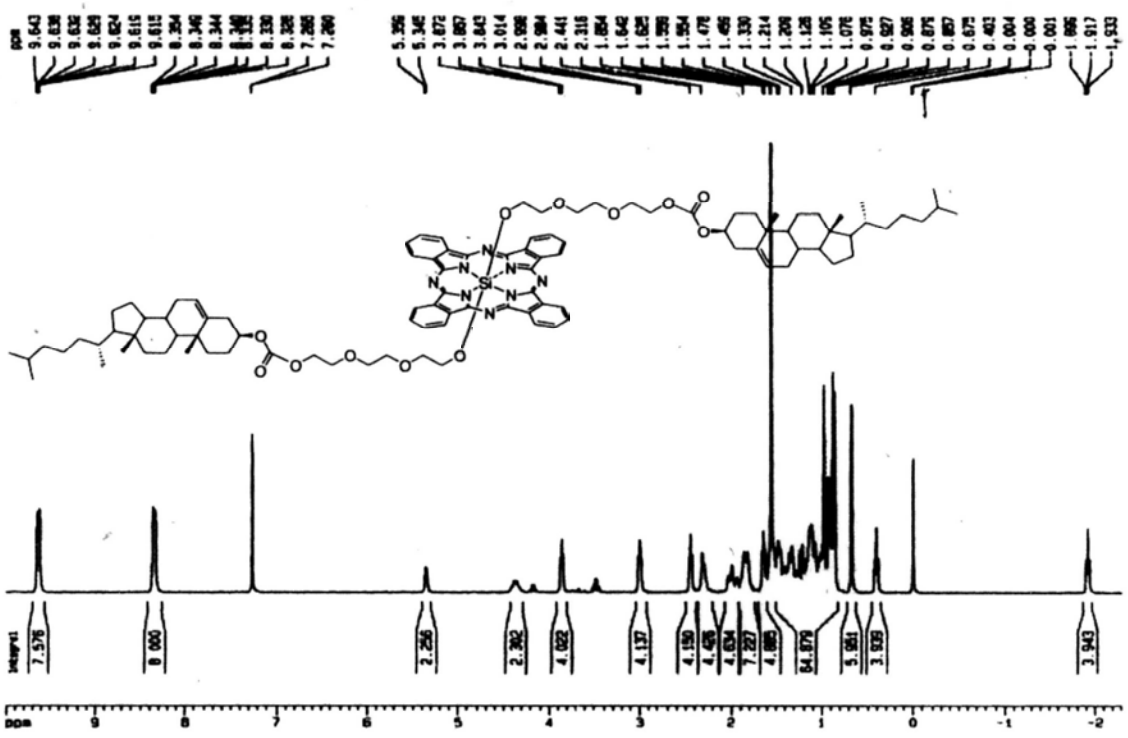

Appendix A-5.6 ^{1}H NMR spectrum of compound **5.6** in $CDCl_3$.

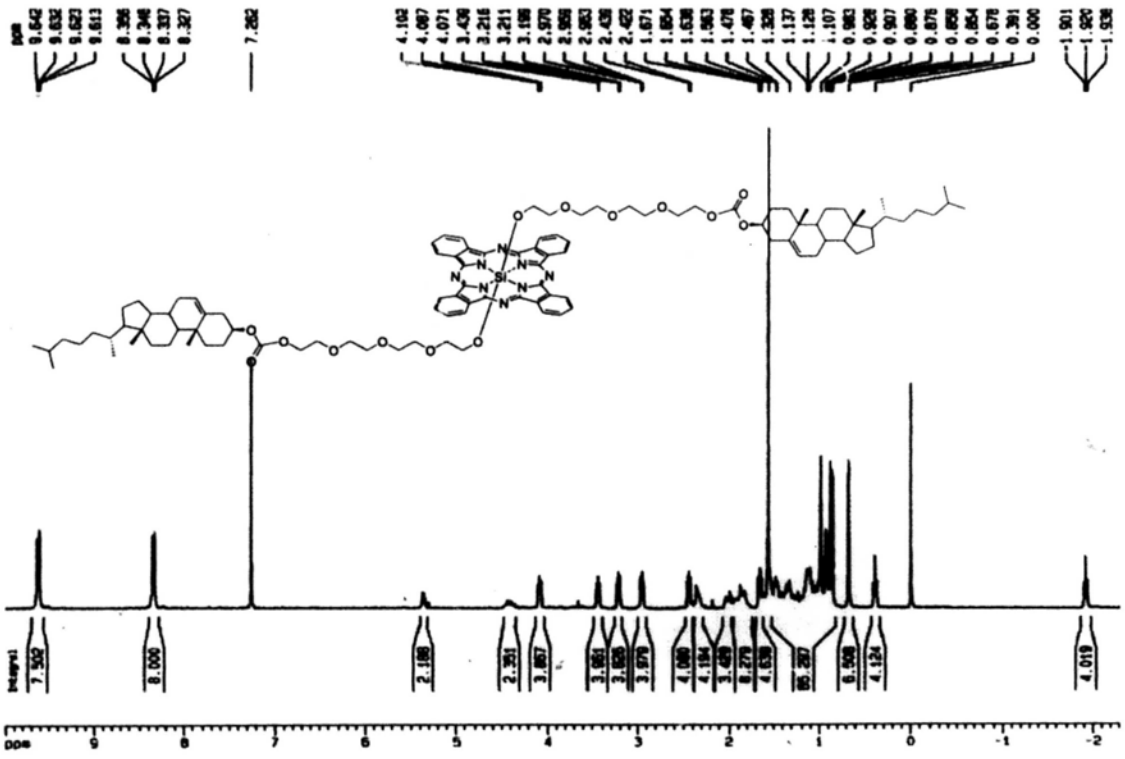

Appendix B-5.1 Crystallographic details of compound **5.1**

Table 1. Crystal data and structure refinement for **5.1** (see section *5.4.2* in Chapter5).

Table 2. Atomic coordinates ($\times 10^4$) and equivalent isotropic displacement parameters ($Å^2 \times 10^3$) for **5.1**. U(eq) is defined as one third of the trace of the orthogonalized U_{ij} tensor.

	x	y	z	U(eq)
Si(1)	5000	5000	0	25(1)
O(1)	4197(2)	6285(2)	333(1)	32(1)
O(2)	4873(2)	7797(3)	1900(2)	49(1)
O(3)	5585(2)	8665(3)	4051(2)	49(1)
O(4)	5300(3)	8479(5)	5875(2)	88(1)
N(1)	4025(2)	3801(3)	535(2)	27(1)
N(2)	5928(2)	5130(3)	1023(2)	26(1)
C(1)	7344(2)	6637(3)	589(2)	20(1)
C(2)	6888(3)	5864(3)	1144(2)	29(1)
C(3)	7341(3)	5690(3)	2001(2)	29(1)
C(4)	8294(3)	6170(4)	2423(2)	35(1)
C(5)	8471(3)	5800(4)	3259(2)	40(1)
C(6)	7750(3)	4971(4)	3656(2)	39(1)
C(7)	6801(3)	4486(4)	3239(2)	34(1)
C(8)	6613(3)	4858(3)	2399(2)	29(1)
C(9)	5735(3)	4510(3)	1772(2)	28(1)
C(10)	4929(2)	3682(3)	1931(2)	18(1)
C(11)	4155(3)	3344(3)	1356(2)	27(1)
C(12)	3293(3)	2385(3)	1518(2)	28(1)
C(13)	3094(3)	1622(4)	2227(2)	36(1)
C(14)	2214(3)	735(4)	2162(2)	42(1)
C(15)	1550(3)	616(4)	1426(2)	44(1)
C(16)	1734(3)	1397(4)	722(2)	40(1)
C(17)	2620(3)	2283(3)	782(2)	31(1)
C(18)	3085(3)	3193(3)	179(2)	31(1)

C(19)	4392(3)	7688(4)	431(2)	38(1)
C(20)	4085(3)	8224(4)	1262(2)	39(1)
C(21)	4744(3)	8467(4)	2675(2)	41(1)
C(22)	5656(3)	7966(4)	3275(2)	44(1)
C(23)	6377(3)	8195(5)	4675(2)	54(1)
C(24)	6244(4)	8925(6)	5488(3)	66(1)

Table 3. Bond lengths [Å] and angles [°] for **5.1**.

Si(1)-O(1)	1.702(2)	O(1)-Si(1)-O(1)#1	180.00(14)
Si(1)-O(1)#1	1.702(2)	O(1)-Si(1)-N(1)#1	93.93(11)
Si(1)-N(1)#1	1.911(3)	O(1)#1-Si(1)-N(1)#1	86.07(11)
Si(1)-N(1)	1.911(3)	O(1)-Si(1)-N(1)	86.07(11)
Si(1)-N(2)	1.928(2)	O(1)#1-Si(1)-N(1)	93.93(11)
Si(1)-N(2)#1	1.928(2)	N(1)#1-Si(1)-N(1)	180.00(13)
O(1)-C(19)	1.405(4)	O(1)-Si(1)-N(2)	90.28(11)
O(2)-C(20)	1.417(4)	O(1)#1-Si(1)-N(2)	89.72(11)
O(2)-C(21)	1.417(4)	N(1)#1-Si(1)-N(2)	89.34(10)
O(3)-C(23)	1.419(5)	N(1)-Si(1)-N(2)	90.66(10)
O(3)-C(22)	1.421(4)	O(1)-Si(1)-N(2)#1	89.72(11)
O(4)-C(24)	1.408(6)	O(1)#1-Si(1)-N(2)#1	90.28(11)
N(1)-C(18)	1.382(4)	N(1)#1-Si(1)-N(2)#1	90.66(10)
N(1)-C(11)	1.383(4)	N(1)-Si(1)-N(2)#1	89.34(10)
N(2)-C(9)	1.374(4)	N(2)-Si(1)-N(2)#1	180.00(16)
N(2)-C(2)	1.377(4)	C(19)-O(1)-Si(1)	131.7(2)
C(1)-C(18)#1	1.311(4)	C(20)-O(2)-C(21)	112.4(3)
C(1)-C(2)	1.315(4)	C(23)-O(3)-C(22)	112.1(3)
C(2)-C(3)	1.450(4)	C(18)-N(1)-C(11)	106.9(3)
C(3)-C(4)	1.388(5)	C(18)-N(1)-Si(1)	127.3(2)

C(3)-C(8)	1.389(4)	C(11)-N(1)-Si(1)	125.8(2)
C(4)-C(5)	1.385(5)	C(9)-N(2)-C(2)	107.5(3)
C(5)-C(6)	1.381(5)	C(9)-N(2)-Si(1)	125.6(2)
C(6)-C(7)	1.381(5)	C(2)-N(2)-Si(1)	126.9(2)
C(7)-C(8)	1.392(4)	C(18)#1-C(1)-C(2)	122.7(3)
C(8)-C(9)	1.457(4)	C(1)-C(2)-N(2)	126.8(3)
C(9)-C(10)	1.311(4)	C(1)-C(2)-C(3)	123.3(3)
C(10)-C(11)	1.315(4)	N(2)-C(2)-C(3)	109.9(3)
C(11)-C(12)	1.447(4)	C(4)-C(3)-C(8)	121.2(3)
C(12)-C(13)	1.389(4)	C(4)-C(3)-C(2)	132.4(3)
C(12)-C(17)	1.392(5)	C(8)-C(3)-C(2)	106.4(3)
C(13)-C(14)	1.380(5)	C(5)-C(4)-C(3)	116.9(3)
C(14)-C(15)	1.388(5)	C(6)-C(5)-C(4)	122.1(3)
C(15)-C(16)	1.389(5)	C(5)-C(6)-C(7)	121.3(3)
C(16)-C(17)	1.385(5)	C(6)-C(7)-C(8)	117.0(3)
C(17)-C(18)	1.453(4)	C(3)-C(8)-C(7)	121.5(3)
C(18)-C(1)#1	1.311(4)	C(3)-C(8)-C(9)	106.7(3)
C(19)-C(20)	1.495(5)	C(7)-C(8)-C(9)	131.8(3)
C(21)-C(22)	1.502(5)	C(10)-C(9)-N(2)	127.8(3)
C(23)-C(24)	1.498(6)	C(10)-C(9)-C(8)	122.7(3)
N(2)-C(9)-C(8)	109.5(3)	C(16)-C(17)-C(12)	121.2(3)
C(9)-C(10)-C(11)	122.4(3)	C(16)-C(17)-C(18)	132.5(3)
C(10)-C(11)-N(1)	127.6(3)	C(12)-C(17)-C(18)	106.2(3)
C(10)-C(11)-C(12)	122.5(3)	C(1)#1-C(18)-N(1)	126.8(3)
N(1)-C(11)-C(12)	109.8(3)	C(1)#1-C(18)-C(17)	123.1(3)
C(13)-C(12)-C(17)	121.5(3)	N(1)-C(18)-C(17)	110.0(3)
C(13)-C(12)-C(11)	131.5(3)	O(1)-C(19)-C(20)	113.2(3)
C(17)-C(12)-C(11)	107.0(3)	O(2)-C(20)-C(19)	109.6(3)
C(14)-C(13)-C(12)	117.1(3)	O(2)-C(21)-C(22)	106.5(3)
C(13)-C(14)-C(15)	121.7(3)	O(3)-C(22)-C(21)	108.1(3)

C(14)-C(15)-C(16)	121.4(3)	O(3)-C(23)-C(24)	110.1(4)
C(17)-C(16)-C(15)	117.2(3)	O(4)-C(24)-C(23)	111.5(4)

Symmetry transformations used to generate equivalent atoms:

#1 -x+1,-y+1,-z

Table 4. Anisotropic displacement parameters ($Å^2 \times 10^3$) for **5.1**. The anisotropic displacement factor exponent takes the form: $-2\pi^2[(ha^*)^2U_{11} + \ldots + 2hka^*b^*U_{12}]$.

	U11	U22	U33	U23	U13	U12
Si(1)	28(1)	29(1)	19(1)	-1(1)	0(1)	-1(1)
O(1)	32(1)	31(1)	34(1)	-4(1)	1(1)	2(1)
O(2)	54(2)	55(2)	36(1)	-17(1)	-4(1)	12(1)
O(3)	53(2)	59(2)	33(1)	-9(1)	-5(1)	14(1)
O(4)	79(2)	134(4)	54(2)	12(2)	18(2)	28(2)
N(1)	30(1)	29(2)	20(1)	-2(1)	0(1)	-1(1)
N(2)	29(1)	28(1)	22(1)	0(1)	-1(1)	-1(1)
C(1)	19(1)	25(2)	16(1)	-2(1)	-3(1)	-6(1)
C(2)	34(2)	30(2)	23(2)	-2(1)	-1(1)	1(1)
C(3)	33(2)	28(2)	26(2)	-2(1)	-2(1)	2(1)
C(4)	36(2)	36(2)	32(2)	0(1)	-2(1)	-2(2)
C(5)	43(2)	40(2)	34(2)	-2(2)	-13(2)	-2(2)
C(6)	51(2)	38(2)	26(2)	0(2)	-10(2)	0(2)
C(7)	42(2)	35(2)	26(2)	0(1)	-1(1)	0(2)
C(8)	36(2)	28(2)	22(1)	-3(1)	-3(1)	4(1)
C(9)	35(2)	28(2)	21(2)	0(1)	-1(1)	5(1)
C(10)	21(1)	22(2)	11(1)	3(1)	-1(1)	0(1)
C(11)	30(2)	29(2)	23(2)	0(1)	5(1)	4(1)
C(12)	31(2)	29(2)	26(2)	2(1)	4(1)	1(1)
C(13)	39(2)	38(2)	31(2)	6(2)	6(1)	1(2)
C(14)	45(2)	41(2)	40(2)	12(2)	10(2)	-3(2)
C(15)	42(2)	40(2)	51(2)	4(2)	11(2)	-12(2)
C(16)	39(2)	43(2)	38(2)	-3(2)	5(2)	-10(2)
C(17)	32(2)	31(2)	29(2)	-1(1)	6(1)	-1(1)
C(18)	31(2)	31(2)	29(2)	-3(1)	2(1)	-1(1)
C(19)	51(2)	31(2)	34(2)	1(1)	6(2)	4(2)
C(20)	42(2)	39(2)	37(2)	-10(2)	1(2)	5(2)
C(21)	48(2)	40(2)	37(2)	-11(2)	5(2)	0(2)
C(22)	46(2)	49(2)	38(2)	-11(2)	1(2)	3(2)

C(23)	50(2)	72(3)	40(2)	-3(2)	-2(2)	13(2)
C(24)	62(3)	98(4)	38(2)	-2(2)	-5(2)	16(3)

Table 5. Hydrogen coordinates ($\times 10^4$) and isotropic displacement parameters ($Å^2 \times 10^3$) for **5.1**.

	x	y	z	U(eq)
H(4A)	4906	9134	5961	133
H(1)	7998	7082	749	24
H(4B)	8791	6715	2156	42
H(5A)	9095	6120	3563	48
H(6A)	7906	4735	4217	46
H(7A)	6311	3934	3507	41
H(10A)	4904	3322	2469	22
H(13A)	3534	1705	2723	43
H(14A)	2063	203	2624	50
H(15A)	968	1	1403	53
H(16A)	1283	1327	231	48
H(19A)	3975	8173	-13	46
H(19B)	5165	7866	370	46
H(20A)	4056	9211	1245	47
H(20B)	3364	7888	1383	47
H(21A)	4035	8250	2885	50
H(21B)	4792	9446	2606	50
H(22A)	5586	6992	3360	53
H(22B)	6362	8142	3048	53
H(23A)	7111	8352	4493	65
H(23B)	6287	7223	4757	65
H(24A)	6888	8768	5865	80
H(24B)	6188	9896	5383	80